

POLITECNICO DI TORINO

**Corso di Laurea Magistrale
In Ingegneria Biomedica**

Tesi di Laurea Magistrale
**Assessment of spinal posture during gait
with inertial sensors**



Relatori

Laura Gastaldi

Stefano Paolo Pastorelli

Elisa Digo

Candidata

Giuseppina Pierro

Matr. 233300

Anno Accademico 2018-2019

Abstract

The work presented in this master thesis aims to describe the spine kinematics during gait using a number of inertial measurement units (IMUs) that allow a denser spinal segmentation. Through these measurements it is possible to trace the role of each segment in the overall trunk motion during walk and thus to maintain balance.

Given the structural complexity of the spine, its segmentation is the result of a compromise identifying the spinal regions that could play a more significant role. From the information derived from literature and from indication of medical team of the Neurorehabilitation Department of the Molinette Hospital, the spine has been modelled by four spinal segments plus the pelvic one. The system consists of five inertial sensors attached C7, T6, T12, L3 and S1 vertebrae. The peculiarity of the developed method is to refer the motion of each sensor, and therefore of each segment, to the one below. The technique can be used in several fields thanks to the intrinsic inertial sensors' characteristics. In fact, accuracy, portability, non-invasiveness, real-time capture data, large capture volume, not prohibitive costs, make inertial sensors a system that can be used in the clinic and beyond. For example, it could have applications in neurological, orthopaedic and rehabilitative fields.

Each inertial sensor provided the orientation matrix instant by instant. Starting from these data, the relative orientation matrix was defined between two sensors and the spherical angles were extracted using the Tilt-Twist Method. These were then transformed into clinically significant parameters of flexion-extension, lateral bending and axial rotation. The planar angles have been associated to the gait phases obtaining the trend and the ROM for each spinal segment. The accuracy of the sensing system was first verified on a subject using Optitrack optical motion capture system and only three inertial sensors positioned at C7, T12 and S1 levels. On each sensor a markers triad has been applied to create a local reference system coinciding with that of the inertial sensor. The patterns obtained with the two motion capture systems were almost completely superimposed and the maximum difference between the ROMs was 1.10° .

The spinal motion technique developed (five IMUs) was applied to healthy young male and female subjects (25.2 ± 0.75 and 25.7 ± 1.03 years respectively), testing three different types of gait on 20 m path. For two of these a metronome was used to mark the step cadence. In the first test the frequency was set to 1.5 steps/s, while in the second test the frequency was set to 2.0 steps/s. In the third test the subjects walked at comfortable self-selected speed. The patterns and ROMs obtained can represent a database on which to make comparisons with subjects

belonging to other categories, such as elderly and subjects affected from neurological or physical disorders. In fact, advanced age or pathology can lead to a trunk inclination that affects its mass distribution and thus its kinematics. The main objective of these tests, however, was to identify differences between the two gender groups in the motion distribution between spinal segments. In the test in which a step frequency of 1.5 steps/s was set, a statistical difference has been found in the frontal plane of lower lumbar segment motion (p-value = 0.02). Here women show a higher ROM than men. The motion in the sagittal plane of the upper thoracic segment is greater for males with a p-value = 0.05. In the 2.0 steps/s walk and in the comfortable walking speed the only statistical difference is in the frontal plane motion of the lower lumbar segment (p-value equal to 0.02 and 0.04 respectively). Overall, males are generally more rigid than females, especially in the lumbar and pelvic segments. From the intra-gender comparison between the different speed tested there are no statistical differences and it is not possible to define a relationship between motion and walking speed.

The thesis structure can be described as follows:

- Chapter 1 was dedicated to the anatomical description of the spine and its importance in maintaining balance in performing typical daily movements. The bibliographic analysis in which inertial systems applied to the trunk were used, but not to verify the locomotion, was described. It was therefore necessary to collect information on trunk kinematics indeed during gait but using a motion capture system based on optical technology. Finally, the most appropriate segmentation with which to model the spinal column was defined.
- Chapter 2 describes the motion capture systems used: Optitrack V120:Trio and Xsens inertial sensors. Furthermore, there is also a description of the software used for data acquisition, i.e. Motive and MT Manager respectively.
- Chapter 3 collects the methods used for data processing, then the Tilt-Twist method, the definition of the spinal segments motion and the definition of gait cycle.
- Chapter 4 focuses on the description of the preliminary tests carried out, from the simplest using only two sensors, to the investigation of spinal segments motion during elementary exercises and during walk. Finally, the test to verify the accuracy of the method using the two motion capture systems together.
- Chapter 5 describes the tests performed on a sample of twelve healthy subjects. In particular, the protocol, the data analysis, the results obtained and the related discussions are reported.

Summary

Summary.....	5
1. Vertebral Column Angles.....	7
1.1 Vertebral Spine Anatomy and Movements.....	7
1.2 Literature Works for the Assessment of the Spine Angles.....	12
1.2.1 Elementary Movements with IMUs	12
1.2.2 Walking Movement with Optoelectronic System	27
1.3 Results Comparison and Sensors Location Definition	36
2. Motion Capture Systems	45
2.1 Optoelectronic System.....	45
2.1.1 V120:Trio	48
2.1.2 Motive Software	51
2.2 Inertial Measurement Units.....	53
2.2.1 Xsens: XBus Kit	56
2.2.2 MTx Motion Tracker	57
2.2.3 Xbus Master.....	59
2.2.4 MT Manager Software.....	61
3. Data Elaboration.....	63
3.1 Tilt-Twist Method.....	63
3.2 Sensors Orientation: Spinal Segments Motion	67
3.3 Gait Analysis: Walk and Gait Cycle.....	69
4. Preliminary Tests.....	73
4.1 Preliminary Test with Magnet	74
4.2 First Preliminary Test with Xsens	84
4.3 Second Preliminary Test with Xsens	86
4.3.1 Elementary Movements	87
4.3.2 Walking Movement	107
4.4 Preliminary Test with Spherical Joint Structure	116
4.5 Preliminary Test with Optitrack and Xsens	121
4.5.1 Elementary Movement: Lateral Bending	126
4.5.2 Walking Movement	133
5. Test on Healthy Subjects.....	143
5.1 Material and Methods	143
5.1.1 Participants	143

5.1.2	Protocol	144
5.1.3	Signal Processing and Data Analysis.....	146
5.2	Results	148
5.2.1	Walking at 1.5 steps/s	148
5.2.2	Walking at 2.0 steps/s	155
5.2.3	Walking at comfortable speed.....	162
5.3	Discussion	169
	References.....	179
	Ringraziamenti	183

1. Vertebral Column Angles

1.1 Vertebral Spine Anatomy and Movements

The spinal column is a structure with several fundamental functions: protection of spinal cord from external forces; structural support of the head and the trunk; mobility of the head, trunk and pelvis; shock absorption. The rachis is a rigid structure thanks to attached muscles contraction, but at the same time, it is flexible. It is subjected to daily compressive and torsional forces and, especially in flexion-extension movement, to shear stresses.

The spine is composed by 33-34 vertebrae divided into five regions. In the cranio-caudal direction, cervical segment, thoracic segment, lumbar segment, sacral and coccygeal segment can be defined (Fig. 1.1-1 a). The spine is characterized, as Fig. 1.1-1 b shows, in the sagittal plane, by curvatures known as lumbar and cervical lordosis, thoracic and sacro-coccygeal kyphosis. Curves have a fundamental role in distributing loads and consequently in maintain balance (El Fagoun, 2005; Schwab, 2006). In the frontal plane, in a column not deformed, there are no curvatures otherwise it would be scoliosis.

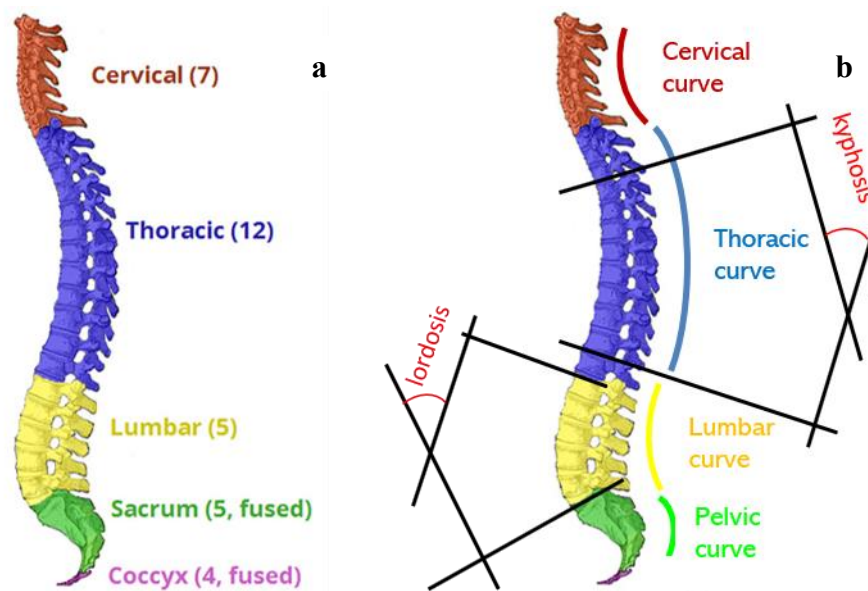


Fig. 1.1-1 a. Spine regions; b. Spine curvature in the sagittal plane.

The cervical segment consists of seven vertebrae (C1-C7) that can be distinguished by anatomy in two further regions: upper region (C1-C2) and lower region (C3-C7). The first segment is represented by only two vertebrae: Atlas and Epistropheus, respectively. The Atlas is a ring (Fig. 1.1-2 **a**) on which the skull rests and it has not spinous process. Differently, the C2 vertebra (Fig. 1.1-2 **b**) has spinous processes like other vertebrae and in addition it is provided with an upward process called odontoid process or dens. The C1 vertebra articulates with the dens and allows head rotation. The lower cervical segment is made up of five vertebrae (Fig. 1.1-1 **c**) that are smaller than those belonging to other spinal regions. They have a very long spinal process and facets that together with ligaments limit the rotation movement (Mow, 1991). In fact, this cervical region allows flexion-extension and lateral bending. Overall, the cervical region reaches 80-90° in flexion, 70° in lateral flexion and 70-90° in axial rotation (Magee, 1987).

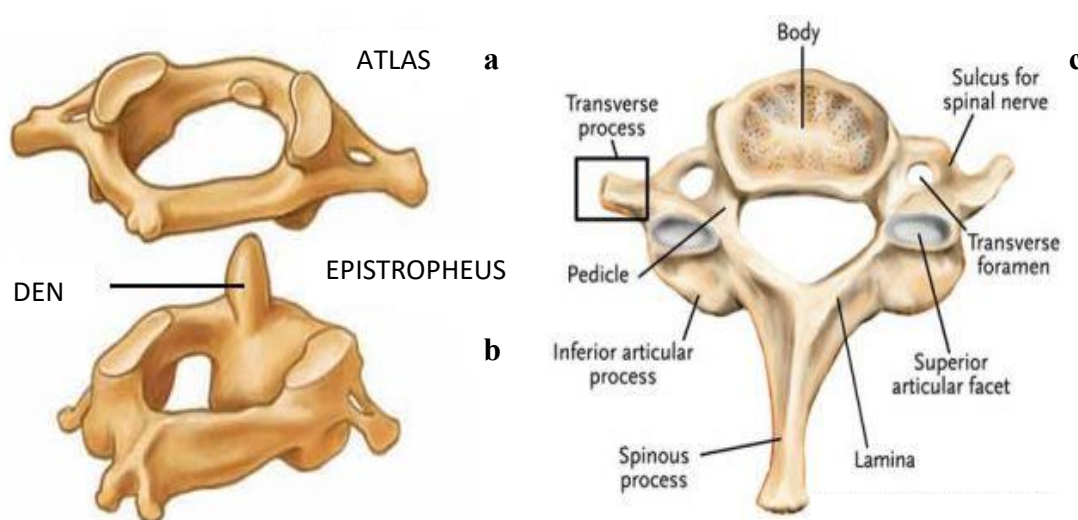


Fig. 1.1-2 **a** Atlas vertebra; **b** Epistropheus vertebra; **c** Lower cervical vertebra.

The thoracic vertebrae (Fig. 1.1-3) are twelve and are connected to the ribs. They have long spinal processes and their size increases in the cranio-caudal direction. The spinal processes extend downwards and together with the angle of facets the axial rotation is limited. The movements are also limited by the connection to the ribs. The ROM in flexion is between 20 and 45°, 25-45° in extension, 20-40° in lateral flexion, 35-50° in axial rotation (Magee, 1987).

The five lumbar vertebrae (Fig. 1.1-4) have a body surface area larger than the other vertebrae and in particular, the vertebra area in the lumbar segment increases from L1 to L5 vertebra. This is in order to support the compressive loads characteristic of this spinal segment. The lumbar spine reaches 40-60° in flexion, 20-35° during extension, 15-20° in lateral bending and 3-18° in axial rotation (Magee, 1987).

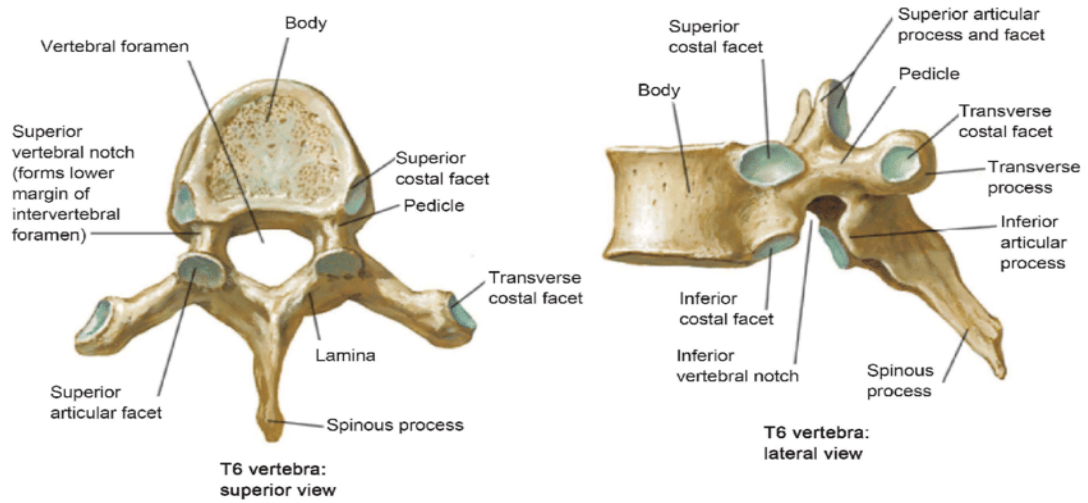


Fig. 1.1-3 Thoracic vertebra in the transversal and sagittal plane.

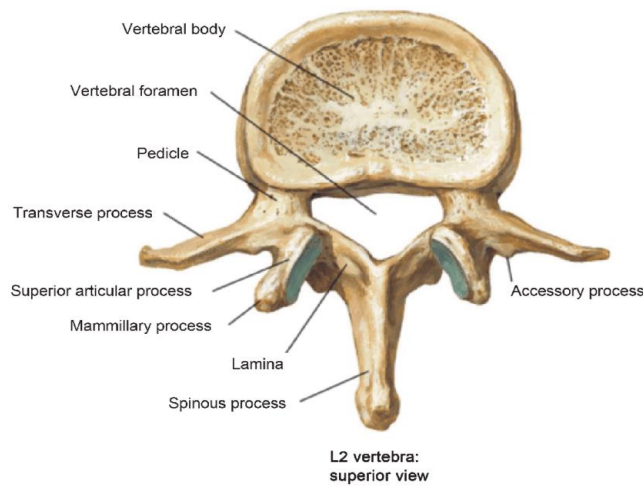


Fig. 1.1-4 Lumbar vertebra in the transversal plane.

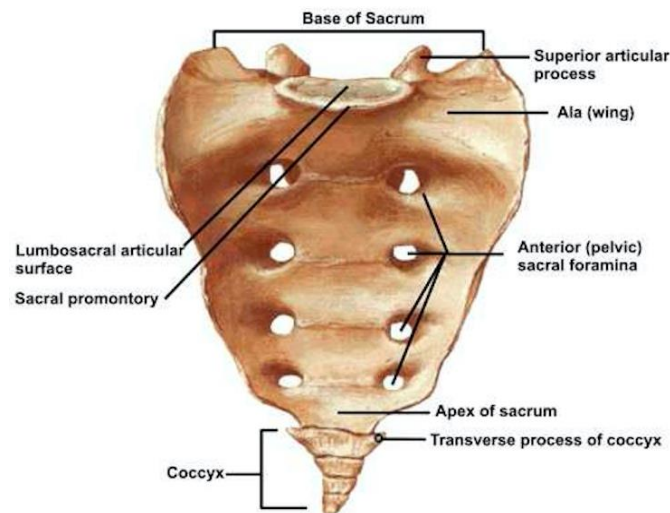


Fig. 1.1-5 Sacrum bone.

The sacrum is made up of five vertebrae that are fused together (Fig. 1.1-5). The sacrum bone, by connecting to the pelvis by lumbosacral disc and ligaments, allows to stabilize it and at same time to discharge the upper body weight on it.

The vertebrae are connected by ligamentous system (Fig. 1.1-6) which includes the anterior longitudinal ligament, the posterior longitudinal ligament, the interspinous ligament, the supraspinous ligament, ligamentum Flavum (yellow ligament) and the intertransverse ligament. The anterior longitudinal ligament connects the entire spine in its anterior part and consists of dense connective tissue. Its role is to limit extension and to support intervertebral discs. The posterior longitudinal ligament starts, as in the case of the anterior longitudinal ligament, from skull base and ends to the sacrum. The difference is in location, size and strength. In fact, the posterior longitudinal ligament is located in the spinal canal, it is narrower than the anterior longitudinal ligament and consequently is less strong. If the anterior longitudinal ligament limits the extension, the posterior longitudinal ligament limits the flexion. The ligamentum Flavum connects one vertebra to another by the lamina. It starts at C2 vertebra and ends at the sacrum. This ligament also limits flexion especially when it occurs abruptly. In fact, unlike other ligaments, it has a higher content of elastin (80%). The supraspinatus ligament connects the apexes of spinous processes from C7 vertebra to the sacrum. The interspinous ligament, on the other hand, connects fully spinal processes and it is less resistant. Both limit flexion. The intertransverse ligament connects the vertebrae transverse processes and it limits lateral flexion (Asher, 2018).

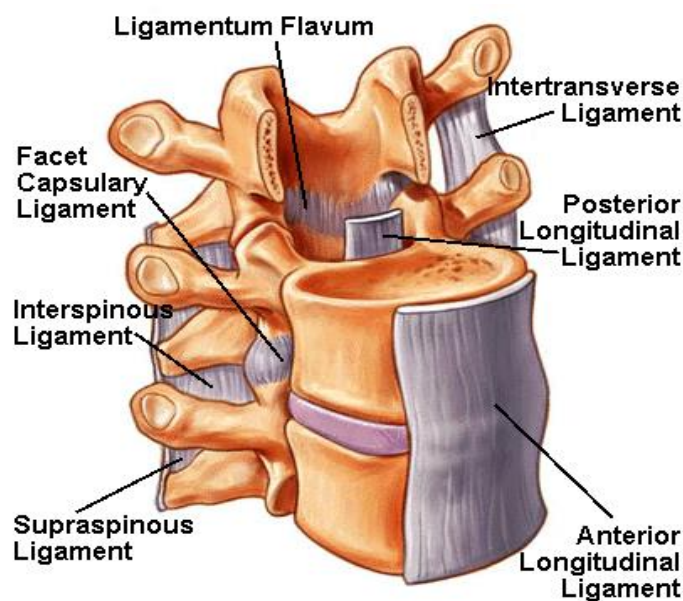


Fig. 1.1-6 Ligamentous system of the vertebral column.

Between two adjacent vertebrae is placed the intervertebral disc (Fig. 1.1-7), formed by nucleus pulposus and anulus fibrosus, which allows them to adapt to static and dynamic conditions. The nucleus pulposus consists of gelatine, water and mucopolysaccharides; the anulus fibrosus ring consists of fibrous lamellae. Intervertebral discs have a fundamental role in dissipating dynamic forces (Voloshin, 1982; Calais-German, 1991), in allowing movement between vertebrae (White, 1978), and maintaining balance (Cyron, 1979). The intervertebral discs in the lumbar region are thicker than those in the other spinal regions. This is because the lumbar region is subjected to higher compression loads due to gravity and muscle forces. With age, the chemical composition of the discs changes, become more rigid and the thickness decreases (Pope, 1991). Degeneration is caused by water reduction and collagen content increased. In addition, degeneration is also caused by lower nutrients supply, in turn caused by the reduced permeability of the endplates. The degeneration of the intervertebral discs causes a shift of the loading area from the vertebral body to the facets and spinal processes that lead to the onset of lower back pain (LBP) (Todd, 1997).

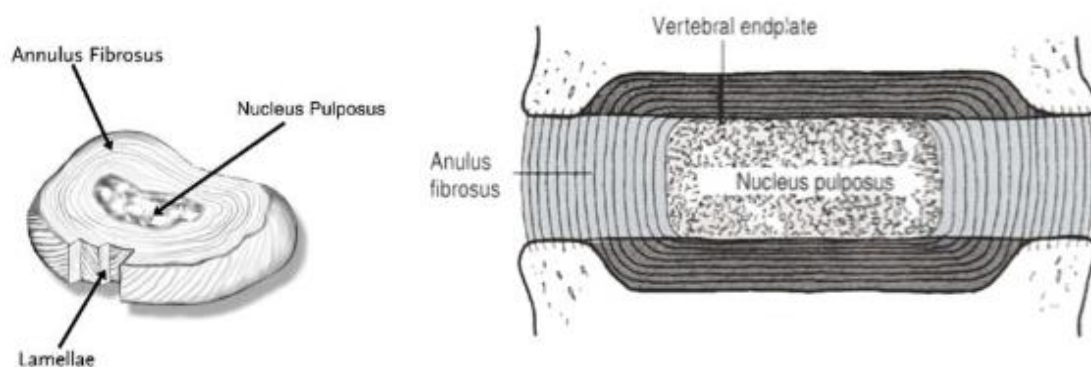


Fig. 1.1-7 Intervertebral disc and its parts.

The alternating curve structure of the spine (kyphosis and lordosis) allows to increase the resistance to the load and to maintain balance. Balance during a static or dynamic condition is maintained by aligning the head to the sacrum (Brindwell, 1997). When the spine is deformed, other strategies must be used to maintain balance, especially during dynamic movements. For this reason, the angular patterns and ROMs will be very different from a normal condition. Often spinal deformities do not allow an optimal balance control or postural changes are not well compensated. The vertebral column is more rigid, and this causes a transmission of the weakly damped forces to the head and therefore difficulties in gait.

1.2 Literature Works for the Assessment of the Spine Angles

1.2.1 Elementary Movements with IMUs

The bibliographic analysis carried out was directed to the search for the positioning of several inertial sensors on the spine, in order to detect the angles of the various segments identified during different tasks. In this way it will be possible to distinguish a healthy posture from a pathological one, to highlight the differences during the movement, and to verify the effectiveness of a treatment. Obviously, the interest lies also in evaluating the inertial system: comparing the obtained values with those of a gold-standard system (optoelectronic system), proving that such results are repeatable.

In 2006 Goodvin et al., with the aim of measuring the three-dimensional motion of column, placed 3 IMUs (MT9, Xsens Technologies B.V.): on the head; torso (at C7/T1 level); and pelvis (at L4/L5 level) (Fig. 1.2.1-1). The sensor outputs were manipulated in order to create a CFP model consisting of 3 segments: pelvis, torso, head. Through a GUI, the vector representation (AVR) (Fig.1.2.2-2) of the model and the pattern of the three-dimensional linear acceleration were shown in order to have real-time information of the spine motion.

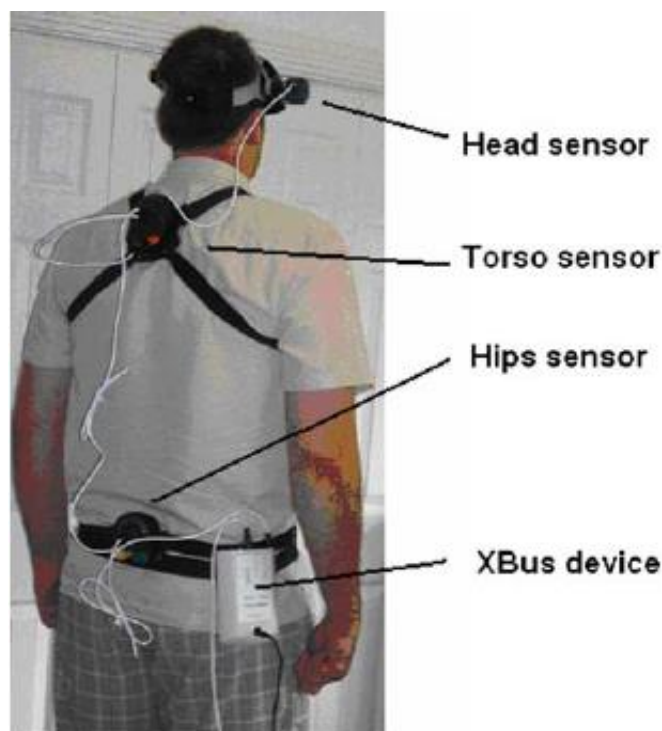


Fig. 1.2.1-1 Sensor location (Goodvin, et al., 2006).

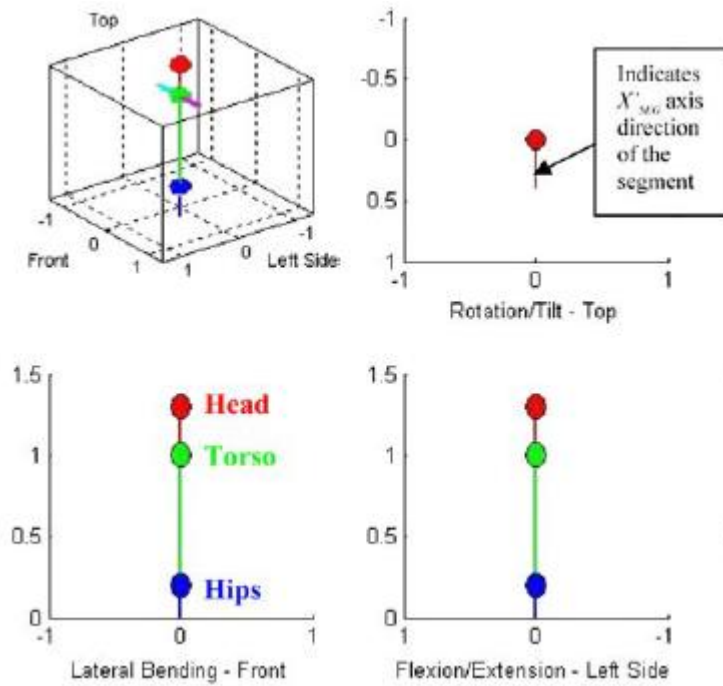


Fig. 1.2.1-2 Animated vector representation (AVR) of the spine (Goodvin, et al., 2006).

For each body segment, the performance of the inertial system implemented was verified with an optoelectronic system (VICON 460). A triad of markers was placed on each IMU. To one of the 5 recruited subjects was asked to perform movements of the individual body segments that covered the entire range of motion in the three main directions. In this way it was possible to evaluate the standard deviation between the two systems (Tab 1.2.1-1). Results showed clearly that measurements with MT9 were accurate compared with the gold-standard technique. Also, to avoid magnetic drift error, the system should be recalibrated after an hour of continuous use.

The authors suggest testing the system in an unhealthy population in order to verify the effectiveness of a rehabilitative or pharmacological treatment. Increasing the number of sensors on the spine and thus increasing the number of segments with which it is represented, more accurate and uniform measurements could be obtained.

	Head	Torso	Hips
Trials	3	2	4
After offset compensation	Roll: 0.1° Pitch:0.42° Yaw: 0.2°	Roll:0.03° Pitch:0.06° Yaw:0.23°	Roll:3.1° Pitch:0.33° Yaw: 1.35°

Tab. 1.2.1-1 Roll, Pitch and Yaw average deviation after offset compensation.

In 2008, Wai Yin Wong and Man Sang Wong developed a system to detect postural changes of the spine in the sagittal and coronal planes. This method involved the construction of three sensor modules, each consisting of tri-axial accelerometer (KXM52-Tri_axis, Kinonix) and three uni-axial gyroscopes (Epson). From acceleration and angular rate data was obtained the sensor orientation, T_{angle} , along the x and y axis. The authors positioned 3 sensor modules at T1/T2 level (upper trunk), at T12 level (middle trunk), and at S1 level (pelvis). The system was then tested with an optoelectronic system (VICON 370) (Fig.1.2.1-3), performing 4 different tasks.

The spine angles with the two measuring systems were determined as follows:

- **Optoelectronic system:** overall change in intersegmental angles formed by 3 consecutive markers (Fig. 1.2.1-4 a, b) belonging to the lumbar or thoracic region;
- **Sensing system:** change in the relative angle between two adjacent sensor modules (Fig. 1.2.1-4 c, d), thus identifying two segments (lumbar and thoracic spine).

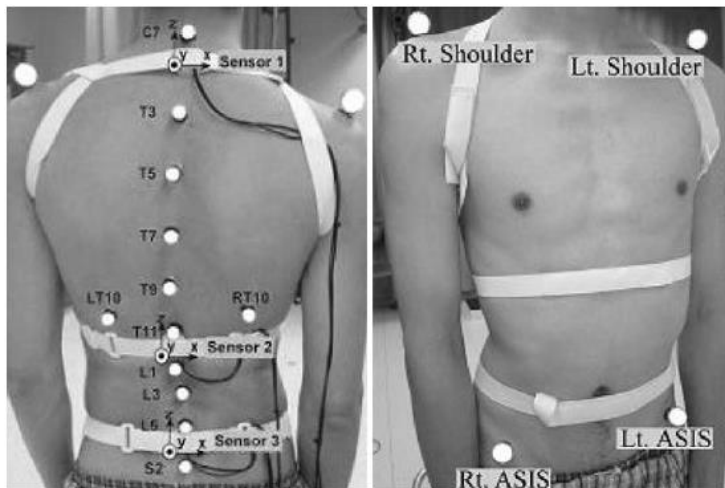


Fig. 1.2.1-3 Position of 16 retro-reflective markers and sensor modules (Wong, et al., 2008).

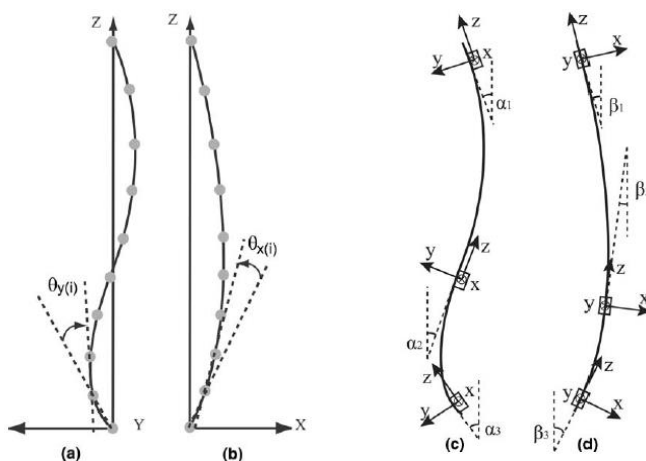


Fig. 1.2.1-4 Trunk postural change calculated with **a** motion analysis system in sagittal plane and **b** in coronal plane; change of inclination of sensor modules **c** in sagittal plane and **d** in coronal plane (Wong, et al., 2008).

The authors developed an auto-reset algorithm in order to derive the tilt angle from the acceleration and angular rate data. The algorithm recognizes whether you are in front of a quasi-static or dynamic condition by analysing the tilt angle resulting from the acceleration data: if the condition is quasi-static the tilt angle is derived from acceleration signals, otherwise, in dynamic condition, the tilt angle is derived from the integration of the gyro signals (Fig. 1.2.1-5).

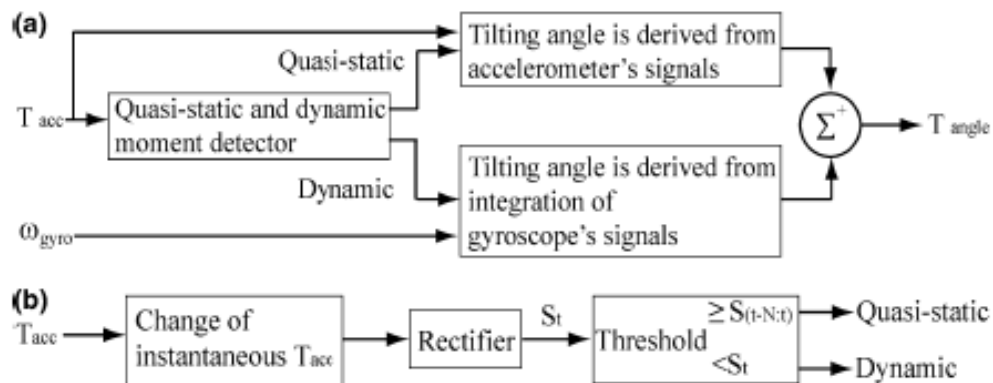


Fig. 1.2.1-5 a auto-reset algorithm with b quasi-static and dynamic moment detector (Wong, et al., 2008).

The results showed average RMS differences between the two systems $< 3.1^\circ$ in the sagittal plane and $\leq 2.1^\circ$ in the coronal plane. In addition it could be seen that the lumbar region is more mobile than the thoracic region.

In view of the above results, the authors found that the three inertial sensors can estimate the change in the spine posture. But the main limitation of the sensor modules done in this way is that they cannot provide information in the transverse plane, instead using commercial sensors such as the MTx of Xsens Technology, also this information can be collected.

Chhikara et al. (2010) tested different algorithms to compensate drift and study the pattern of movement of the lumbar spine and pelvis during lateral flexion. The prototype developed, consisting of a tri-axial accelerometer and two bi-axial gyroscopes, was positioned at L1 spinal process and at L5/S1 spinal process (Fig. 1.2.1-6). From the angular velocity, the sensor orientation was calculated applying the best algorithm found to correct the drift. That is done transforming the gyro data into the frequency domain and eliminate the continuous component and high frequency components. The angular velocity was subsequently integrated over time. Results showed confirmed that the inertial system created gives reliable outputs when compared with an optoelectronic system (mean error: lumbar spine 3.6° , pelvis 1.2°). Furthermore, it is of interest noticing the ratio between the angle of the pelvis and the sum of the angle of the

pelvis and the lumbar spine (R_p), that is how much the pelvis move with respect to the totality of the movement.

$$R_p = \frac{|\theta_p|}{|\theta_p| + |\theta_l|}$$



Fig. 1.2.1-6 Sensors placement on lumbar spine (Quantitative assessment of the motion of the lumbar spine and pelvis with wearable inertial sensors, 2010).

The authors hypothesized that LBP patients may tend to keep the pelvis rigid and use only the lower back to perform lateral flexion. Also, they expect these subjects to show a limited ROM compared to a healthy subject (i.e. lumbar spine ROM: 22.60°, pelvis ROM: 8.33°), a reduced speed, reduced or even negligible pelvic proportional movement.

In 2015, Alqhtani et al. investigated the motion of the spine by dividing it into multiple segments using tri-axial accelerometers (3A Sensor, ThetaMetrix). Linear accelerations can be used to obtain the inclination angles in the sagittal and frontal plane (absolute angles) of the sensors and the regional ROMs or the relative angles between two adjacent sensors. The study was divided in two parts: one to quantify the cervical ROM by placing one sensor on the forehead and another at T1 level (Fig. 1.2.1-7 a) and the other one to quantify the ROM of 5 regions of the spine (Tab. 1.2.1-2). In the latter case, the accelerometers were positioned at T1, T4, T8, T12, and S1 levels (Fig. 1.2.1-7 b). The results showed that LL contributes more during forward flexion than the other segments, while during lateral flexion, several regions of spine (LL, UL, LT) contribute more evenly. During the rotation, the MT region is the one that contributes more. Ultimately, the authors demonstrated that the method is reliable when measuring multiregional ROM and that alteration in this parameter can indicate spine issues.

The same authors, the following year (2016) highlighted the differences in representing the lumbar region or as a single segment or composed of two segments using the same tri-axial

accelerometers (3A Sensor, ThetaMetrix). These were positioned at the S1, L3, T12, and ITB (lateral aspect of thigh) levels (Fig. 1.2.1-8).

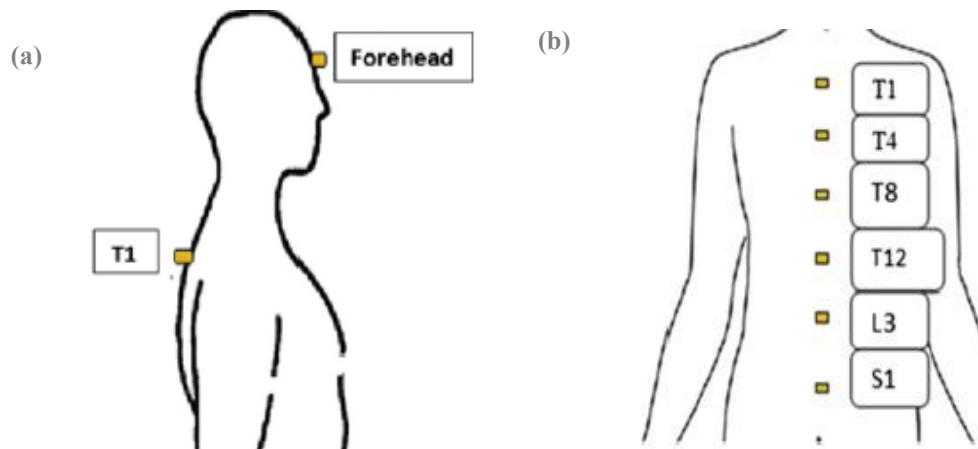


Fig. 1.2.1-7 Accelerometers placement to assess **a** cervical ROM and **b** spine regions ROM (Alqhtani, et al., 2015).

Spinal Regions	Flexion	Extension	Right Lateral Bending	Left Lateral Bending	Right Rotation	Left Rotation
	ROM (SD)	ROM (SD)	ROM (SD)	ROM (SD)	ROM (SD)	ROM (SD)
HC	66.4 (13)	61.7 (11)	41.5 (7)	42.1 (10)	74.4 (10)	80.5 (14)
UT	3.9 (4)	7.1 (4)	6.5 (3)	5.4 (4)	-14.9 (16)	-11.3 (21)
MT	3.5 (4)	11.2 (8)	7.8 (2)	7.1 (3)	34.8 (18)	29.7 (18)
LT	15.0 (8)	7.9 (6)	12.1 (3)	12.4 (4)	21.4 (9)	22.6 (13)
UL	19.4 (7)	5.0 (9)	12.6 (4)	11.3 (4)	6.3 (5)	5.3 (5)
LL	36.8 (6)	21.6 (14)	12.2 (4)	11.6 (3)	9.4 (8)	8.7 (7)

HC, cervical; LL, lower lumbar; LT, lower thoracic; MT, middle thoracic; ROM, range of motion; UL, upper lumbar; UT, upper thoracic.

Tab. 1.2.1-2 Multiregional Mean (SD) ROMs tested on 18 subjects (Alqhtani, et al., 2015).

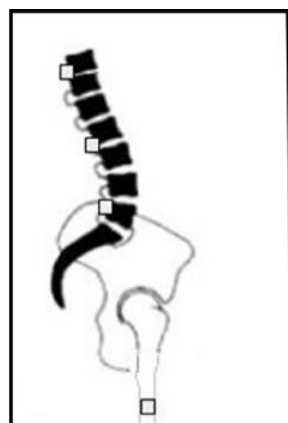


Fig. 1.2.1-8 Sensor positioning (Alqhtani, et al., 2016).

The first model (WLS) considered the regional ROM between S1 and T12 sensors, while the second model identified the ULS (angle between T12 and L3) and LLS (angle between L3 and S1). The sensor on the thigh allowed to quantify the LLS-hip, ULS-hip, and WLS-hip ratios. At First, the LLS-hip ratio was higher than the ULS-hip ratio because it reached higher ROMs.

Then the model with the lumbar region divided into two segments showed that the LLS reached higher rates than the ULS. These factors may explain the appearance of LBP predominantly in the LLS. The WLS model underestimated the LLS motion and overestimated the ULS motion.

The authors suggest testing the system on pathological subjects in order to obtain information confirming these results. The main limitation lies in the kinematic analysis in the sagittal plane only instead of analysing three-dimensional motion.

Again, in 2015, Cafolla et al. used 4 IMUs (InertiaCube BT) (Fig.1.2.1-9 a) at the shoulders (Sensor 1: left shoulder, Sensor 3: right shoulder), at T5 (Sensor 2) and L3 (Sensor 4) spinal processes (Fig. 1.2.1-9 b), to analyse the behaviour of the human torso during typical daily operations. The roll (around X axis), pitch (around Y axis), and yaw (around Z axis) angles were plotted against time. From these plots it was possible to obtain the angular ranges for each sensor and for each movement tested (Tab. 1.2.1-3).

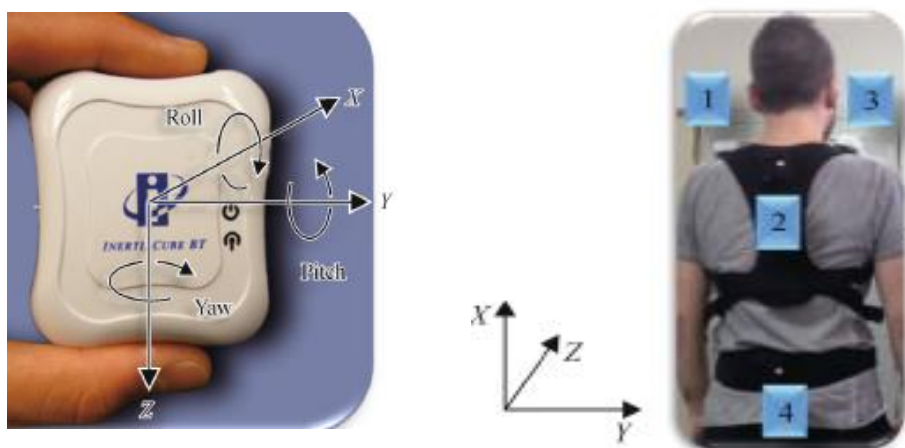


Fig. 1.2.1-9 a InertiaCube axis, b sensor placement (Cafolla, et al., 2015).

Results showed that each movement, while taking place in a certain main direction, had simultaneous presence of motion on the 3 planes. Testing the protocol on different subjects, the authors could observe that the motion of the shoulders was characteristic for each subject, while that of the torso could be generalized. Having also developed a program to evaluate the forces on different points, the authors noted a certain distribution of the forces between trunk and waist and that this could be an indication of the important role of the torso in maintaining balance.

	Range roll angle	Range pitch angle	Range yaw angle
Movement 1 turn right and left slowly, torso in a straight position	Sensor 1: -79.64°÷88.99°	Sensor 1: -26.50°÷11.06°	Sensor 1: -40.56°÷6.00°
	Sensor 2: -72.10°÷66.42	Sensor 2: -77.33°÷6.04°	Sensor 2: -22.16°÷20.32°
	Sensor 3: -78.62°÷89.70°	Sensor 3: -20.14°÷9.65°	Sensor 3: -3.14°÷45.07°
	Sensor 4: -61.28°÷65.40°	Sensor 4: -3.43°÷3.49°	Sensor 4: -20.80°÷35.76°
Movement 2	Data are similar to those during movement 1		
Movement 3 lean forward and then backward slowly	Sensor 1: -39.36°÷9.90°	Sensor 1: -46.01°÷88.97°	Sensor 1: -37.64°÷56.36°
	Sensor 2: -19.94°÷17.18°	Sensor 2: -72.06°÷85.40°	Sensor 2: -18.45°÷15.66°
	Sensor 3: -9.68°÷19.43°	Sensor 3: -37.18°÷89.99°	Sensor 3: -19.73°÷19.78°
	Sensor 4: -19.57°÷3.86°	Sensor 4: -70.89°÷42.30°	Sensor 4: -18.32°÷5.63°
Movement 4	Data are similar to those during movement 3		
Movement 5 lean to the right and left slowly	Sensor 1: -4.35°÷7.95°	Sensor 1: -0.83°÷35.84°	Sensor 1: -45.82°÷53.53°
	Sensor 2: -71.73°÷43.33°	Sensor 2: -68.33°÷40.19°	Sensor 2: -69.11°÷48.09°
	Sensor 3: -15.35°÷6.69°	Sensor 3: -0.73°÷27.93°	Sensor 3: -47.11°÷57.19°
	Sensor 4: -40.10°÷56.01°	Sensor 4: -0.52°÷7.10°	Sensor 4: -40.09°÷56.02°
Movement 6	Data are similar to those during movement 5		
Movement 7 walk forward to reach a marked position and then to turn and walk back to the starting position	Sensor 1: -7.29°÷7.45°	Sensor 1: -4.08°÷4.40°	Sensor 1: -7.17°÷7.45°
	Sensor 2: -5.82°÷19.48°	Sensor 2: -4.18°÷6.35°	Sensor 2: -16.55°÷17.65°
	Sensor 3: -8.68°÷9.50°	Sensor 3: -5.64°÷7.55°	Sensor 3: -6.03°÷5.39°
	Sensor 4: -23.03°÷18.80°	Sensor 4: -4.09°÷4.17°	Sensor 4: -25.03°÷18.51°

Tab. 1.2.1-3 Roll, Pitch and Yaw angular range.

Also in 2015, Bauer et al. used inertial sensors to verify movements of the trunk divided into segments identified by two adjacent sensors. Thus 4 Valedo system (Hocoma AG) were placed at the thigh side (THI), at S2, L1, and T1 spinal processes (Fig. 1.2.1-10). The system was verified with an optoelectronic system by positioning 3 markers for each IMU. It was found

that the deviation between the two systems is acceptable and that therefore IMUs are a valid alternative to measure trunk movements in primary directions.



Fig. 1.2.1-10 Sensor and markers positioning (Bauer, et al., 2015).

It stands out in the bibliographic research conducted the study of Shall at al. (2015). Here sensor positioning had a different configuration. In fact, 12M Motion Tracking System (SXT IMUs series, Nexgen Ergonomics) were located on the sternum and at L5/S1 level. Several methods of signals processing deriving from sensors were tested. That was done in order to compare results from each different method with the system used as a reference (ACUPATH Industrial LMM) (Fig. 1.2.1-11), and thus evaluate which one was the best.

Five methods were defined to obtain angular displacement from inertial sensors:

- Accel 1: Signal of the accelerometer on the sternum;
- Comp 1: Combination of the accelerometer signal and gyroscope on the sternum;
- Accel 2: Difference between acceleration signals from sternum and L5/S1 accelerometers;
- Comp 2: Difference between combined accelerometer and gyroscope signals on sternum and on L5/S1;
- HM Analyzer: combination of accelerometer, gyroscope and magnetometer signals on the sternum and on L5/S1.

All different methods produced a motion profile with similar characteristics, but the angular displacement closest to the signal from LMM reference system was Comp 2 (Fig. 1.2.1-12).



Fig. 1.2.1-11 Industrial Lumbar Motion Monitor (Schall, et al., 2015).

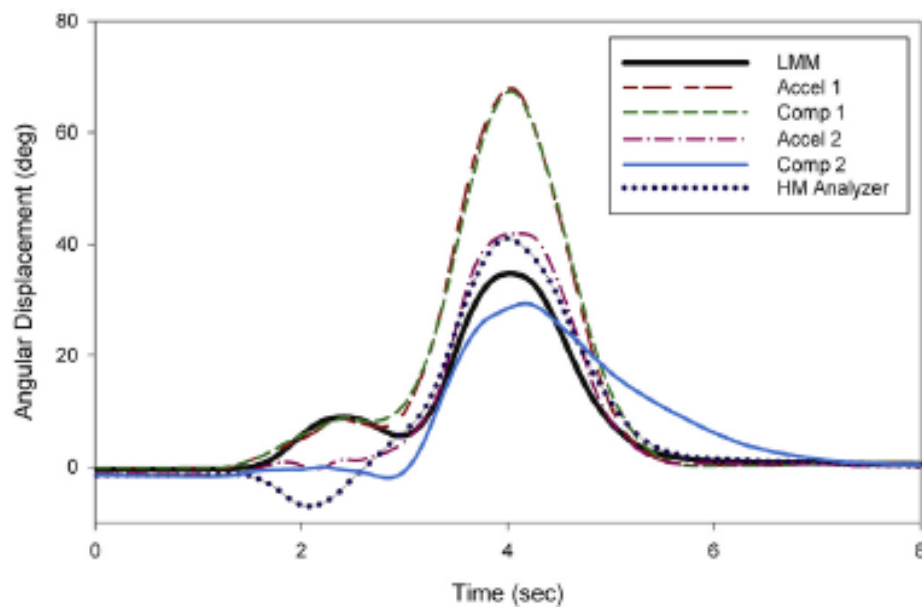


Fig. 1.2.1-12 Averages of the angular displacement waveforms for LMM and the five IMU measurement methods in the flexion/extension motion plane for one participant (Schall, et al., 2015).

However, the protocol developed in this way finds its limitations when comparing the method with LMM, which is not a gold-standard technique. For that reason, results from that method tested could not be consistent when compared with an optoelectronic system. In addition the performance of the HM Analyzer signal was probably influenced by its proximity to the LMM or by ferromagnetic noise.

Antonya, in 2016, by using 5 BNO055 (Bosh Sensotrec) positioned at C6/C7, T5/T6, T10, L3 and Sacrum spinal processes (Fig. 1.2.1-13), developed an algorithm to reconstruct the spine profile. To do this, Antonya collected information from IMUs in the form of pitch angles. From

spine profile it is possible to diagnose postural diseases such as scoliosis, kyphosis and lordosis, and/or to monitor the position and to guide the subject in improving its posture.

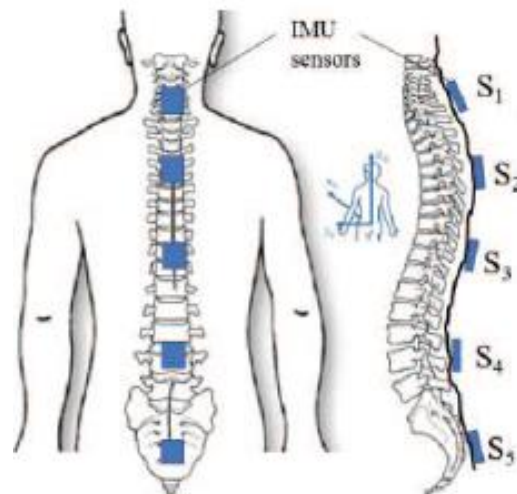


Fig. 1.2.1-13 Sensor positioning to reconstruct spine profile (Real-time representation of the human spine with absolute orientation sensors, 2016).

Very interesting for the purposes of this research is the study done in 2016 by Hajibozorgi and Arjmand, as there was deepened the observation of the ROM of the various segments of the thoracic region in the sagittal plane in a forward flexion, using 4 IMUs of Xsens Technology. The MTx sensors were placed on the T1, T5, T12, and S1 spinal processes (Fig. 1.2.1-14). To determine the relative angles between two adjacent sensors, at each sampling time, before the product between the rotation matrices was calculated and then anatomical angles too.

Results allowed to detect the average bending peaks of the total trunk (orientation of the T1 sensor with respect to the global reference frame), of its different segments (T1-T5 upper

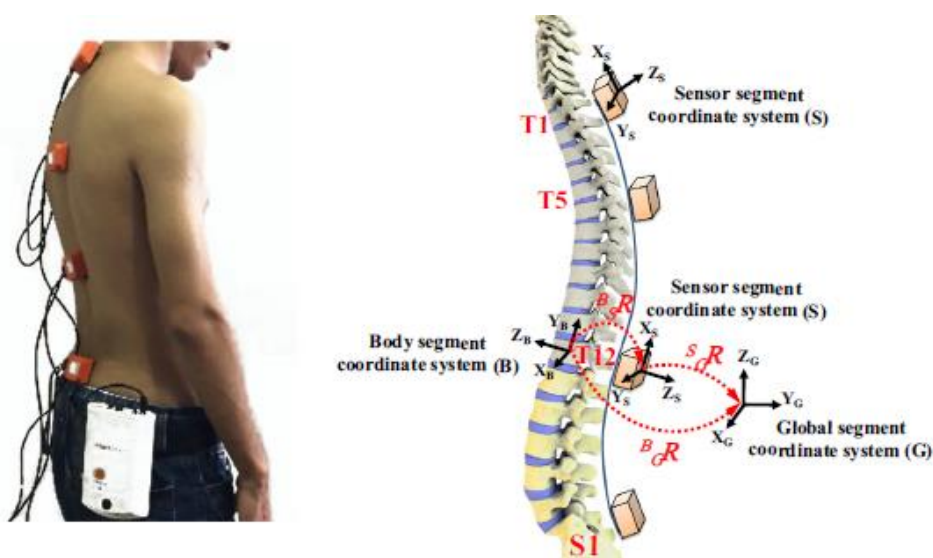


Fig. 1.2.1-14 Position of inertial sensors and a schematic axis definition (Hajibozorgi, et al., 2016).

thoracic, T5-T12 lower thoracic, T1-T12 total thoracic, T12-S1 lumbar spine), and of the pelvis (orientation of the S1 sensor with respect to the global reference frame) (Tab. 1.2.1-4).

Spine region	ROM Mean (SD)	Spine region	ROM Mean (SD)	Spine region	ROM Mean (SD)
Total trunk: T1	118.4° (13.9°)	Thoracic: T1-T12	20.5° (6.5°)	Upper trunk: T1-T5	5.8° (3.1°)
		Lumbar: T12-S1	50.2° (7.0°)	Lower trunk: T5-T12	14.8° (5.4°)
Pelvis: S1	47.8° (6.9°)				

Tab. 1.2.1-4 Mean (SD) ROM in voluntary total flexion.

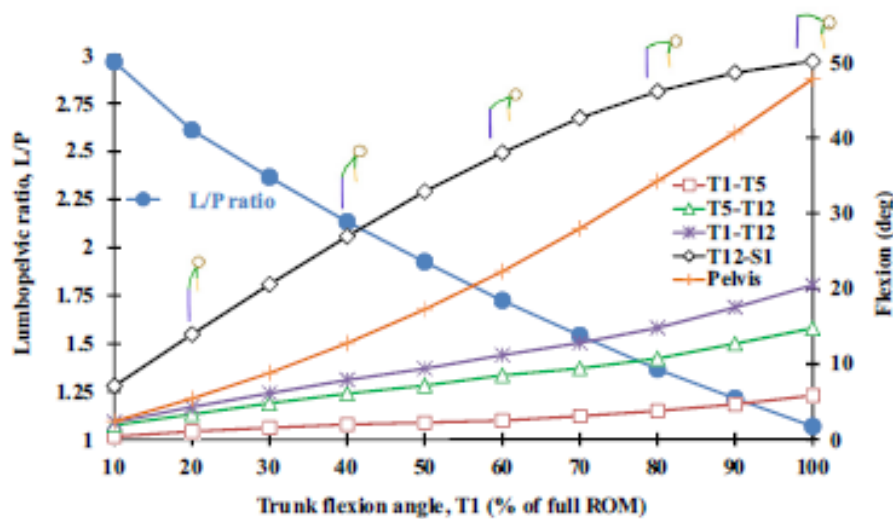


Fig. 1.2.1-15 Sagittal rotations of spine segments and lumbopelvic ratio at different forward trunk flexion angles (Hajibozorgi, et al., 2016).

Throughout the exercise, the ratio between the lumbar spine and pelvis was observed, highlighting that the ratio is reduced when the bending angle increases as the contribution of the pelvis increases, while that of the lumbar spine decreases (Fig. 1.2.1-15). The lower and upper thoracic had almost similar movements and moved simultaneously. The limit detected is

the observation of movement in the sagittal plane only, neglecting those in the coronal and transversal planes.

In conclusion, from literature emerged that an inertial system results reliable when analysing spine movements compared with an optoelectronic system. Indeed, observing the overall results obtained in Goodvin et al. (2006), Wong & Wong (2008), Chhikara et. al (2010) and Bauer et al. (2015), the maximum deviation between the two systems display a value always lower than 4°. Other authors instead verified the repeatability of inertial system outputs. That is done comparing results from several movement repetitions and checking the presence of a consistence among them. Results from those works showed that inertial systems can provide measurements with acceptable differences.

From literature it is also possible to analyse where sensors are positioned. To detect torso angles, all authors, Shall et al. (2015) excepted, chose to locate sensors on the back. That choice is validated from Cafolla et al. (2015). From this work emerged that shoulder movements are individual specific, while back movements are not. This consent to compare results among several subjects and on different kind of subjects, highlighting their distinctive traits. Cafolla et al. (2015), confirmed the importance torso role in balance maintaining, given the force distribution between trunk and waist.

From Hajibozorgi & Arjmand (2016) study emerged that during forward flexion, trunk segments T1-T5 and T5-T12, have similar motion. For that reason, those segments could be considered as a single segment (T1-T12) using two sensors only. The same assumption cannot be done for lumbar spine. In fact, Alqhtani et al. (2015), but also, Wong & Wong (2008), detected that lumbar spine moves more than thoracic spine and so it contributes in a major quantity to the movement to perform. Lately, Alqhtani et al. (2016), splitting lumbar spine in two separate segments, could emphasize that L3-S1 segment achieves higher ROM, velocity and movements pattern respect to the pelvis values, when compared to the T12-L3 segment. Those values would not have been visible if T12-S1 was analysed as a single segment.

At this stage, it is necessary to define whether cervical spine, and therefore the head sensor, it is essential in movement executions. According to Maslivec et al. (2018), during initial phase of walking, elderly subjects met an antero-posterior angular displacement variability of the head higher when compared to young subjects. This instability is due to the elderly subject lag in activation sternocleidomastoid muscle. Therefore, the inability to stabilize the head could lead to impede the balance maintaining.

Thigh could be view as another source of information useful in movements quantification. In fact, in Bauer et al. (2015) and Alqhtani et al. (2016) it is shown that they use a lateral aspect of thigh to evaluate pelvis motion respect to the lumbar spine.

Here, diverse approaches used were summarized, and how different authors relied on different protocols in terms of number of sensors, kind of sensors, movements under observation, position of sensors and measured and calculated parameters. Each approach has some limitations: first, the use of inertial sensors on young subjects and without spinal disorder. For that reason, in Chhikara et al. (2010), regarding to low back pain patients, only hypothesis could be done.

Regarding movements typology exanimated in literature and for the protocol applications on young and healthy subjects, ROM data could be useful to define sensors positioning, and checking that IMUs, and in particular Xsens gave reliable and repeatable outputs when measuring angular trunk data.

The following tables (Tab. 1.2.1-5 and Tab. 1.2.1-6) summarized articles considered in the thesis to extract information regarding the subject posture and it is highlighted the sensors positioning used in each work.

Articles	Head	C6/C7/T1	T1/T2	T4	T5/T6	T8
(Goodvin, et al., 2006)	✓	✓				
(Wong, et al., 2008)			✓			
(Quantitative assessment of the motion of the lumbar spine and pelvis with wearable inertial sensors, 2010)						
(Alqhtani, et al., 2015)	✓		✓	✓		✓
(Cafolla, et al., 2015)					✓	
(Bauer, et al., 2015)			✓			
(Schall, et al., 2015)						
(Real-time representation of the human spine with absolute orientation sensors, 2016)		✓			✓	
(Alqhtani, et al., 2016)						
(Hajibozorgi, et al., 2016)			✓		✓	

Tab. 1.2.1-5 Sensors positioning (from Head to T8) in literature works.

Articles	T10	T12	L1	L3	L4/L5	S1/S2
(Goodvin, et al., 2006)					✓	
(Wong, et al., 2008)		✓				✓
(Quantitative assessment of the motion of the lumbar spine and pelvis with wearable inertial sensors, 2010)			✓			✓
(Alqhtani, et al., 2015)		✓		✓		✓
(Cafolla, et al., 2015)				✓		
(Bauer, et al., 2015)			✓			✓
(Schall, et al., 2015)						✓
(Real-time representation of the human spine with absolute orientation sensors, 2016)	✓			✓		✓
(Alqhtani, et al., 2016)		✓		✓		✓
(Hajibozorgi, et al., 2016)				✓		✓

Tab. 1.2.1-6 Sensors positioning (from T10 to Sacrum) in literature works.

1.2.2 Walking Movement with Optoelectronic system

Crosbie et al. (1997 a) to quantify the movement of spinal segments during walking used an optoelectronic system which markers were positioned as Fig. 1.2.2-1 shows. This markers configuration subdivided the spine in lumbar segment (L5-T12), lower thoracic segment (T12-T6) and upper thoracic segment (T6-T1). Markers were used to define pelvis segment too. Finally, other two markers were located on ankles to determine gait cycle phases. 108 subjects were recruited to test walking movement and their characteristics are in Tab. 1.2.2-1.

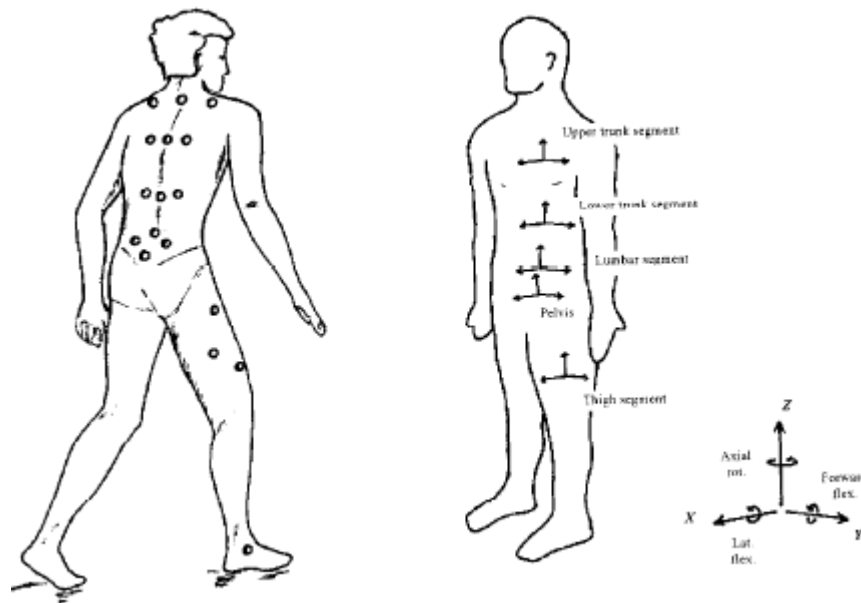


Fig. 1.2.2-1 Markers placement and conventions used to define axes and motions (Crosbie, et al., 1997).

Lumbar segment motion was verified by quantifying lower thoracic motion with respect to pelvis motion. In the same way, lower thoracic motion was verified by quantifying upper thoracic motion with respect to lumbar segment motion. Upper thoracic, lower thoracic and pelvis motion were described with respect to laboratory reference frame. Subjects were asked to walk at comfortable speed and it resulted to be on average 1.3 m/s (S.D. 0.19). In the frontal plane, spinal segments and pelvis showed complementary movement (Fig. 1.2.2-2). Pelvis motion followed lower limb movement. That means that during right heel strike pelvis tilt on the left side, then stabilization phase follows before pelvis tilt on the right side. On the contrary, lumbar region and lower thoracic region shown a pattern that follows stance leg side.

ROM values (Tab. 1.2.2-2) in the frontal plane were higher than those in the sagittal plane. In particular ROM value of lumbar segment is higher than those relative to lower thoracic and pelvis segments.

	Age (years)			Height (m)			Weight (kg)		
	Mean	S.D.	Range	Mean	S.D.	Range	Mean	S.D.	Range
Females	45.24	18.55	20-80	1.61	0.07	1.43-1.8	59.6	9.83	41-95
Males	46.34	18.25	20-82	1.72	0.08	1.57-1.9	73.7	10.5	55-100

Tab. 1.2.2-1 Characteristics of subjects tested.

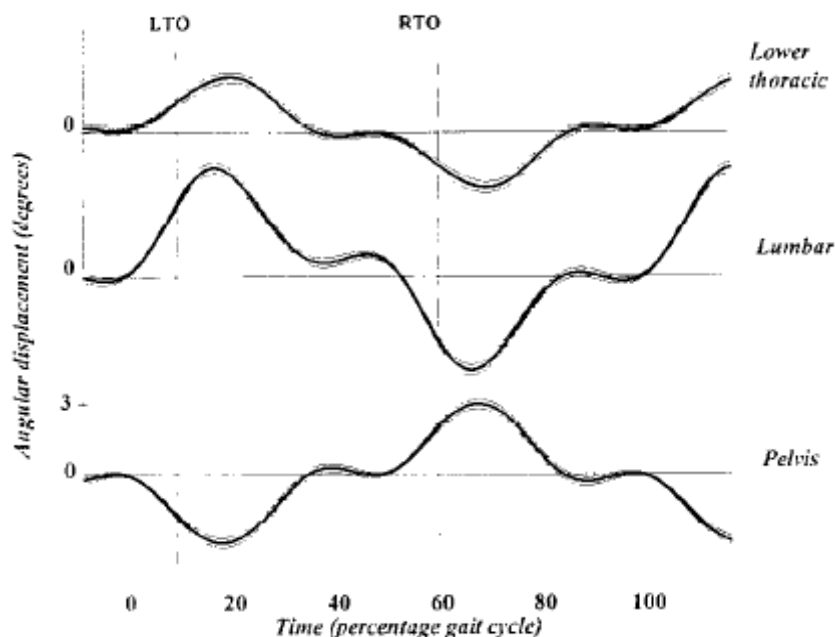


Fig. 1.2.2-2 Patterns in the frontal plane (Crosbie, et al., 1997).

Segment	Lateral flexion	Flexion/extension	Axial rotation
Lower thoracic	7.0 (3.0)	2.5 (1.5)	4.0 (2.5)
Lumbar	9.0 (3.5)	3.5 (2.0)	4.5 (2.0)
Pelvis	6.0 (2.5)	3.5 (1.5)	4.0 (2.5)

Tab. 1.2.2-2 ROMs of lower thoracic, lumbar and pelvis segments in the frontal, sagittal and transversal planes.

Syczewska et al. in 1999 subdivided the vertebral column in seven segments (Fig.1.2.2-3). Markers were positioned at C7, T4, T7, T10, T12, L2, L4 and Sacrum vertebral levels. Spine segment motion, in the frontal and sagittal planes (Fig. 1.2.2-4), was described in relation to its initial inclination during calibration phase: negative angle difference in the sagittal plane indicated that the segment was extended with respect to its reference inclination, on the contrary positive difference indicated a segment flexion; in the frontal plane, negative difference indicated a right lateral flexion and a positive difference indicated a left lateral flexion.

In the frontal plane, higher level spine segments followed lower limb in stance phase, the half-height segment showed little movement, while the other segments belonging to lumbar region and pelvis flexed on the side of swing leg. In the sagittal plane all segments, pelvis excepted, showed little oscillations. The maximum oscillation (ROM about 2°), however, is referred to lumbar region segments.



Fig. 1.2.2-3 Markers placement and difference angle (Syczewska, et al., 1999).

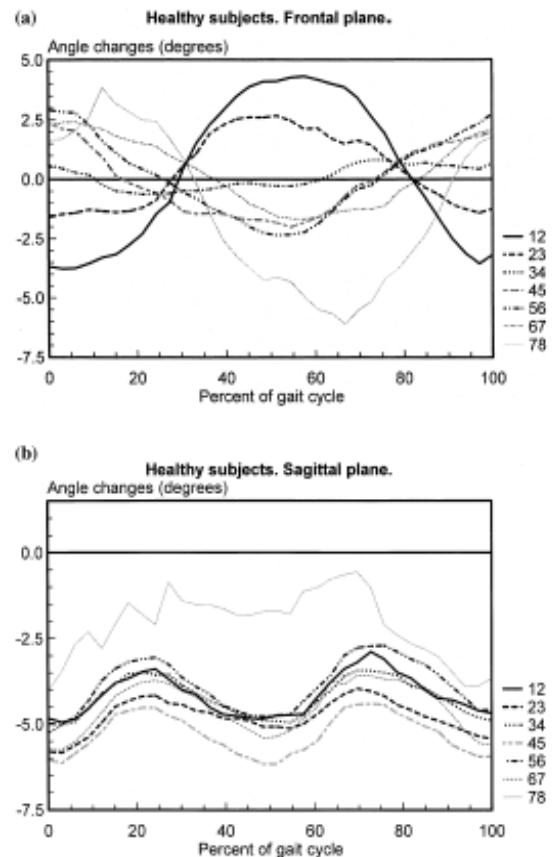


Fig. 1.2.2-4 Angle changes patterns (a) in the frontal plane; (b) in the sagittal plane (Syczewska, et al., 1999).

In 2003, Frigo et al. verified trunk angle patterns during walking with female young subjects. Markers were positioned at C7, T6/T7, L5 and Sacrum vertebral levels (other markers permitted to create a graphic representation of the spine) (Fig. 1.2.2-5). Angles analysed were: lordosis, kyphosis angles in the sagittal plane; in the frontal plane, angles of scoliotic deformities (Fig. 1.2.2-5). Angles of total spine (considered as single segment C7-Sac) were also calculated. ROM values are shown in Tab.1.2.2-3. In the frontal plane higher ROM resulted at T6/T7 vertebral level, while in the sagittal plane resulted that the higher ROM variation is for lordosis angle.

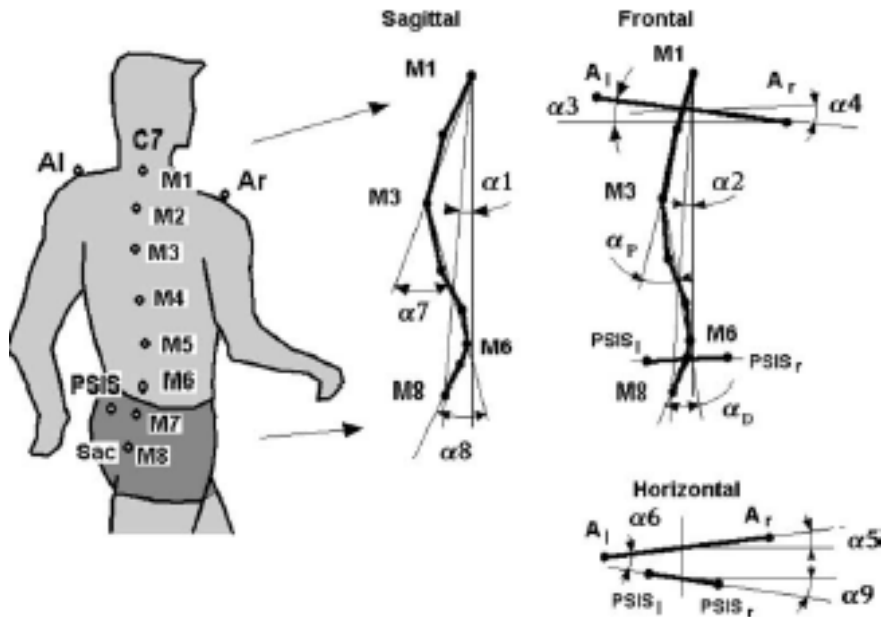


Fig. 1.2.2-5 Markers location and definition of segmental angles. C7=M1; T6/T7=M3; L3=M6; Sac=M8 (Frigo, et al., 2003).

Angle	ROM	ROM
	Sagittal plane	Frontal plane
Total trunk (C7-Sac)	2.0 (2.4)	3.9 (1.5)
C7-T6/T7 vs T6/T7-L3	2.2 (4.4)	7.0 (3.0)
T6/T7-L3 vs L3-Sac	3.8 (4.7)	2.2 (3.2)

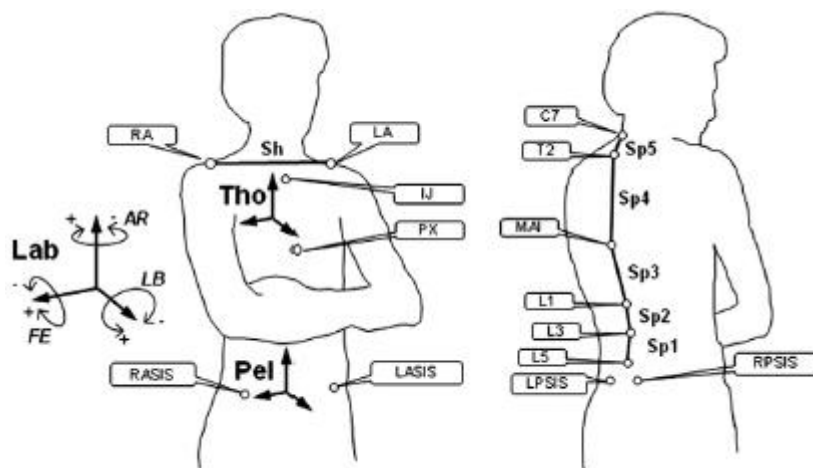
Tab. 1.2.2-3 ROM (degrees) of the angles considered during walking (S.D.).

A kinematic and electromyography analysis was conducted by Ceccato et al. in 2009. The muscle of interest was erector spinae muscle. Markers were located at C7, T3, T7, T12, L3 and S1 vertebral level. These permitted to considerate five spine segments and to verify the angles at T7, T12 and L3 level during gait initiation phase and during level walking. T12-L3 segment motion relative to L3-S1 segment during gait in the sagittal plane showed little oscillations. This characteristic is shown in T7-T12 segment motion relative to T12-L3 segment and in C7-T7 segment motion relative to T7-T12 too. In the frontal plane the oscillations were higher excepted for T12 angle level that showed a more rigid behaviour. All segment motion patterns had opposite phase with respect to pelvis motion.

Leardini et al. (2011) described spinal segments motion not during gait only, but also in the daily activity. For example, stand up and sitting on a chair, step climb/climb down, and elementary exercises in a main plane: flexion-extension, lateral bending and axial rotation. For this purpose, vertebral column was subdivided in five segments. Each segment motion was described relative to adjacent lower one. The authors defined Sp5 (from C7 to T2), Sp4 (from T2 to MAI), Sp3 (from MAI to L1), Sp2 (from L1 to L3), Sp1 (from L3 to L5) and Pelvis segments (Fig. 1.2.2-6). Pelvis is necessary to describe Sp1 segment motion. The mean ROM values and standard deviations over 10 subjects are shown in Tab. 1.2.2-4.

	ROM	ROM
	Sagittal plane	Frontal plane
Sp1-Pel	3.5° (8.0)	6.7° (3.0)
Sp2-Sp1	5.6° (9.4)	4.7° (4.2)
Sp3-Sp2	3.9° (8.3)	4.4° (3.3)
Sp4-Sp3	1.6° (4.3)	8.3° (2.6)
Sp5-Sp4	2.7° (5.4)	8.2° (6.4)

Tab. 1.2.2-4 Spinal segment ROMs over 10 subjects during level walking.



Tab. 1.2.2-6 Markers location on the spine and thorax (Leardini, et al., 2011).

From Tab- 1.2.2-4 it's easy to see that in the frontal plane the values were higher than those in the sagittal plane. The segments more movable in the frontal plane were those belonging to high level vertebral column in agreement to what Syczewska et al. (1999) affirmed. Regardless, all segments did not reach insignificant ROM values. This means that all segments cooperate to execute the tasks.

Needham et al. in 2015 presented a different way to describe spinal segments motion. In fact, on T3, T8 and L3 vertebral level were positioned a marker triad (Fig. 1.2.2-7). Each marker triad identified a spinal segment: upper thoracic segment (UT), lower thoracic segment (LT) and lumbar segment (L) respectively. Marker cluster motion was referred to lower adjacent one. Two test sessions were conducted with a week of time between them.

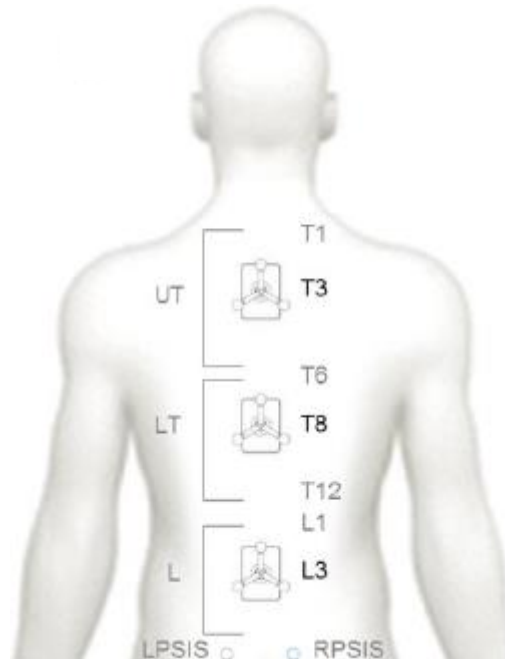


Fig. 1.2.2-7 Clusters of markers placement (Needham, et al., 2015).

ROM values in the three anatomical planes (Tab. 1.2.2-5) showed that upper thoracic segment mainly moved in the transversal plane. Focusing on what happens in the other two planes, it is possible note that ROMs in the sagittal plane were lower than those in the frontal plane. Lumbar region moved more than the other two. Lower thoracic and upper thoracic segments showed almost the same ROM values.

		ROM	ROM	ROM
		Sagittal plane	Frontal plane	Transversal plane
L vs Pelvis	S1	3.22 (0.63)	6.50 (2.11)	7.79 (2.0)
	S2	3.03 (0.81)	5.63 (2.16)	8.24 (2.22)
LT vs L	S1	3.74 (1.74)	5.54 (2.43)	5.50 (1.56)
	S2	3.23 (0.95)	4.81 (1.50)	5.56 (1.45)
UT vs LT	S1	2.21 (0.82)	5.60 (1.93)	11.34 (4.68)
	S2	2.39 (0.70)	4.79 (1.43)	10.77 (3.27)

Tab. 1.2.2-5 ROMs (degree) over 10 subjects.

In Tab. 1.2.2-6 and Tab. 1.2.2-7 markers positioning found in literature are shown. In order to define the optimal positioning of the sensors that can well describe the spine motion during walk tasks, more than one schematic representation of the segmentation adopted by the articles shown in Tab. 1.2.2-6 were used (Fig. 1.2.2-8, Fig. 1.2.2-9, Fig. 1.2.2-10).

Articles	C7	T1	T2	T3	T4	T5	T6	T7	MAI/T8	T9
(Crosbie, et al., 1997)		✓					✓			
(Syczewska, et al., 1999)	✓				✓			✓		
(Frigo, et al., 2003)	✓							✓		
(Rozumalski, et al., 2008)										
(Ceccato, et al., 2009)	✓							✓		
(Leardini, et al., 2011)	✓		✓						✓	
(Needham, et al., 2015)				✓					✓	

Tab. 1.2.2-6 Markers location (from C7 to T9) in literature.

Articles	T10	T11	T12	L1	L2	L3	L4	L5	PSISS	Sac
(Crosbie, et al., 1997)			✓				✓		✓	✓
(Syczewska, et al., 1999)	✓		✓		✓		✓			✓
(Frigo, et al., 2003)						✓				✓
(Rozumalski, et al., 2008)				✓	✓	✓	✓		✓	
(Ceccato, et al., 2009)			✓			✓				
(Leardini, et al., 2011)				✓		✓		✓	✓	
(Needham, et al., 2015)						✓			✓	

Tab. 1.2.2-7 Markers location (from T10 to Sacrum) in literature.



Fig. 1.2.2-10 Spine segmentation in upper, lower thoracic and lumbar regions by articles: C: (Crosbie, et al., 1997), N: (Needham, et al., 2015), L: (Leardini, et al., 2011), R: (Rozumalski, et al., 2008), Cec: (Ceccato, et al., 2009), S: (Syczewska, et al., 1999), F: (Frigo, et al., 2003).

1.3 Results Comparison and Sensors Location Definition

To verify that the different studies found, even if the authors adopted a different rachis segmentation and a different definition motion, have obtained results in agreement each other, a comparison was done. It's important considerate that results can be condition by other factors like the size of the sample recruited, the number of male and female, age and walking speed, and obviously the health status of subject. Regard this last aspect, the studies involved healthy subjects which characteristics are shown in Tab. 1.3-1.

	No. subjects	Age (years)	Height (cm)	Weight (kg)	Walking speed (m/s)
Crosbie	108	F. 58	45.24 (18.55)	161 (7)	59.6 (9.83)
		M. 50	46.34 (18.25)	172 (8)	73.3 (10.5)
Needham	M. 10	22.4 (2.46)	180.3 (7.18)	74.97 (11.02)	1.31 (0.15)
Ceccato	M. 9	27 (6)	179 (7)	70 (6)	1.4 (0.2)
Leardini	10	F. 5	24.7 (0.8)	171.6 (8.1)	62.4 (9.3)
		M. 5			
Syczewska	10	F. 5	Range:		
		M. 5	20-58		Range: 0.8-1.8

Tab. 1.3-1 Characteristics of subjects recruited to evaluate angle patterns and ROMs during walking.

As a whole, the authors subdivided the lumbar region in more segments than upper and lower thoracic segments. Spine angles during walking are not investigated with inertial sensors, so in this phase of thesis it was interested reflected on what inertial sensors could be located to describe spine motion. Thanks to a medical team knowledge, the possible segmentation was in four spine segments: T1/T2-T6, T6-T12, T12-L3, L3-S1. Pelvis motion is considered too.

Focusing firstly on lower lumbar segment (L3-S1), patterns of Needham at al. (2015) and Leardini et al. (2011) were compared. The two research groups defined segment motion in a different way described before (Section 1.2.2). In Fig. 1.3-1 is shown the patterns of two studies in the frontal and in the sagittal plane. Results in the transversal plane are relative Needham et al. (2015) research only. Both groups recruited 10 subjects with about the same age (Tab. 1.3-2), but Needham et al. (2015) recruited all male subjects while Leardini et al. (2011) recruited an equal gender number. Both groups found the principal movement in the frontal plane with similar ROM values. Similar values were observed in the sagittal plane. On the contrary, the angles trends seem poorly matched. This could be depending to motion definition, walking

speed (not specified in Leardini et al. (2011)) and numerosness of gender subjects. Gender factor could be deciding. In fact, plotting the pattern of one subject only (male, 25 years old), this in the frontal plane is almost coinciding. In the sagittal plane, indeed, the patterns even similar, show a 10° shift.

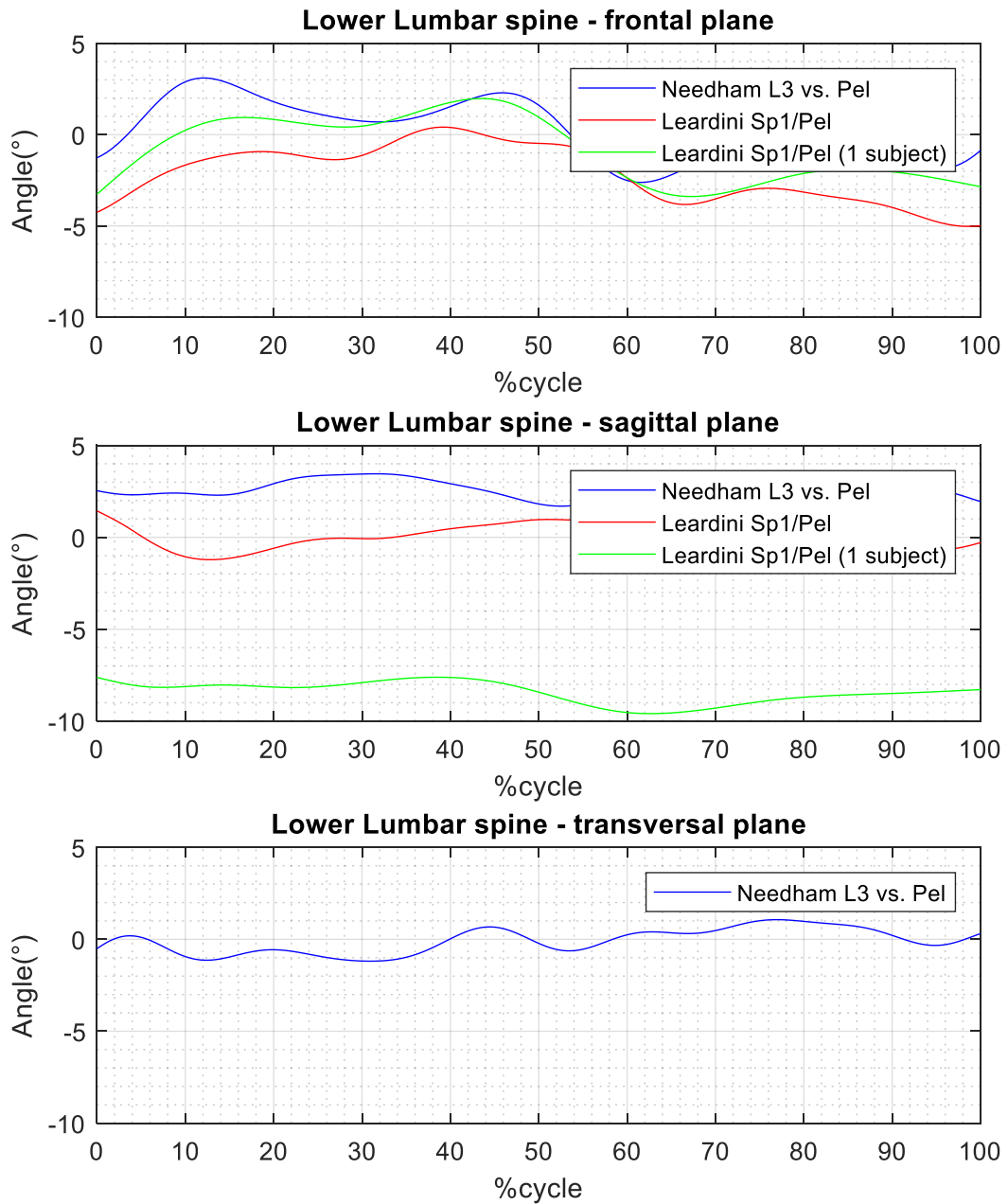


Fig. 1.3-1 Comparison of lower lumbar spine patterns.

	Needham	Leardini
No.Subjects	M.10	M. 5 F. 5
Age (years)	22.4 (2.46)	24.7 (0.8)
Mean walking speed (m/s)	1.31 (0.15)	X
Motion	L3 vs Pel	L3-L5 vs Pel
ROM p.front (°)	6.5 (2.11)	6.7 (3.0)
ROM p.sag (°)	3.22 (0.36)	3.5 (8.0)
ROM p.trans (°)	7.79 (2.00)	X

Tab. 1.3-2 Comparison of subjects group characteristics and ROMs of lower lumbar spine.

The upper lumbar segment, defined from T12 to L3, was investigated by Ceccato et al. (2009) and by Leardini et al. (2011). The segment motions were described almost in the same way, so a more pronounced correspondence was expected. This overlap does not occur either by referring to the ROMs (Tab. 1.3-3) or by evaluating the patterns (Fig. 1.3-2). The difference in patterns and ROM values could depend from specificity of subject movement. In the sagittal plane the patterns seem similar if phase alternation of flexion and extension was considered.

	Ceccato	Leardini
No.Subjects	M. 9	M. 5 F. 5
Age (years)	27 (6)	24.7 (0.8)
Mean walking speed (m/s)	1.4 (0.2)	X
Motion	T12-L3 vs L3-S1	L1-L3 vs L3-L5
ROM p.front (°)	12.32	4.7(4.2)
ROM p.sag (°)	2.08	5.6 (9.4)
ROM p.transv (°)	11.98	X

Tab. 1.3-3 Comparison of subjects group characteristics and upper lumbar spine ROMs.

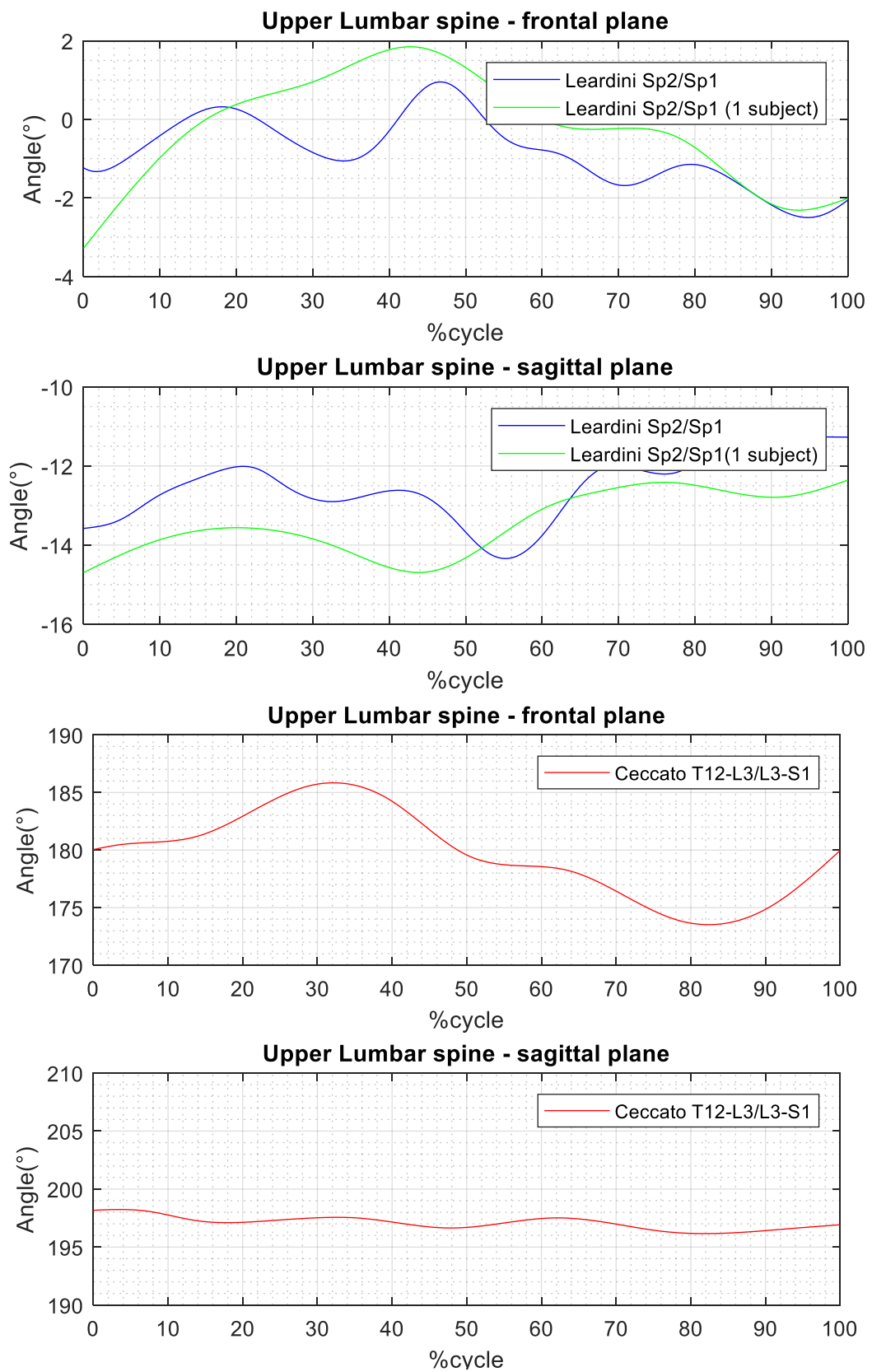


Fig. 1.3-2 Comparison of upper lumbar spine patterns.

The lower thoracic segment (from T6 to T11/T12) was described in Ceccato et al. (2009) and Leardini et al. (2011). In the frontal plane the patterns are similar. In fact, in both patterns it is possible to recognize a lateral flexion on the stance leg side following a stabilization phase and then by lateral flexion on the swing leg side (Fig. 1.3-3). The ROMs values are shown in Tab. 1.3-4.

	Ceccato	Leardini	Crosbie
No. Subjects	M. 9	M. 5 F. 5	M. 50 F. 58
Age (years)	27 (6)	24.7 (0.8)	46.34 (18.25) 45.24 (18.55)
Mean walking speed (m/s)	1.4 (0.2)	X	1.31 (0.19)
Motion	T7-T12 vs T12-L3	MAI-L1 vs L1-L3	T1-T6 vs T12-L5
ROM p.front (°)	2.75	4.4 (3.3)	7.0 (3.0)
ROM p.sag (°)	1.39	3.9 (8.3)	2.5 (1.5)
ROM p.transv (°)	X	X	4.0 (2.5)

Tab. 1.3-4 Comparison of subjects group characteristics and ROMs of lower thoracic segment.

	Ceccato	Leardini	Crosbie	Needham
No. Subjects	M. 9	M. 5 F. 5	M. 50 F. 58	M.10
Age (years)	27 (6)	24.7 (0.8)	46.34 (18.25) 45.24 (18.55)	22.4 (2.46)
Mean walking speed (m/s)	1.4 (0.2)	X	1.31 (0.19)	1.31 (0.15)
Motion	C7-T7 vs T7-T12	T2-MAI vs MAI-L1 C7-T2 vs T2-MAI	T1-T6 vs Lab	T3 vs T8
ROM p.front (°)	8.94	8.3 (2.6) 8.2 (6.4)	7.08	5.60 (1.93)
ROM p.sag (°)	2.98	1.6 (4.3) 2.7 (5.4)	2.23	2.21 (0.82)
ROM p.trans (°)	X	X	4.31	11.34 (4.68)

Tab. 1.3-5 Comparison of subjects group characteristics and ROMs of upper thoracic segment.

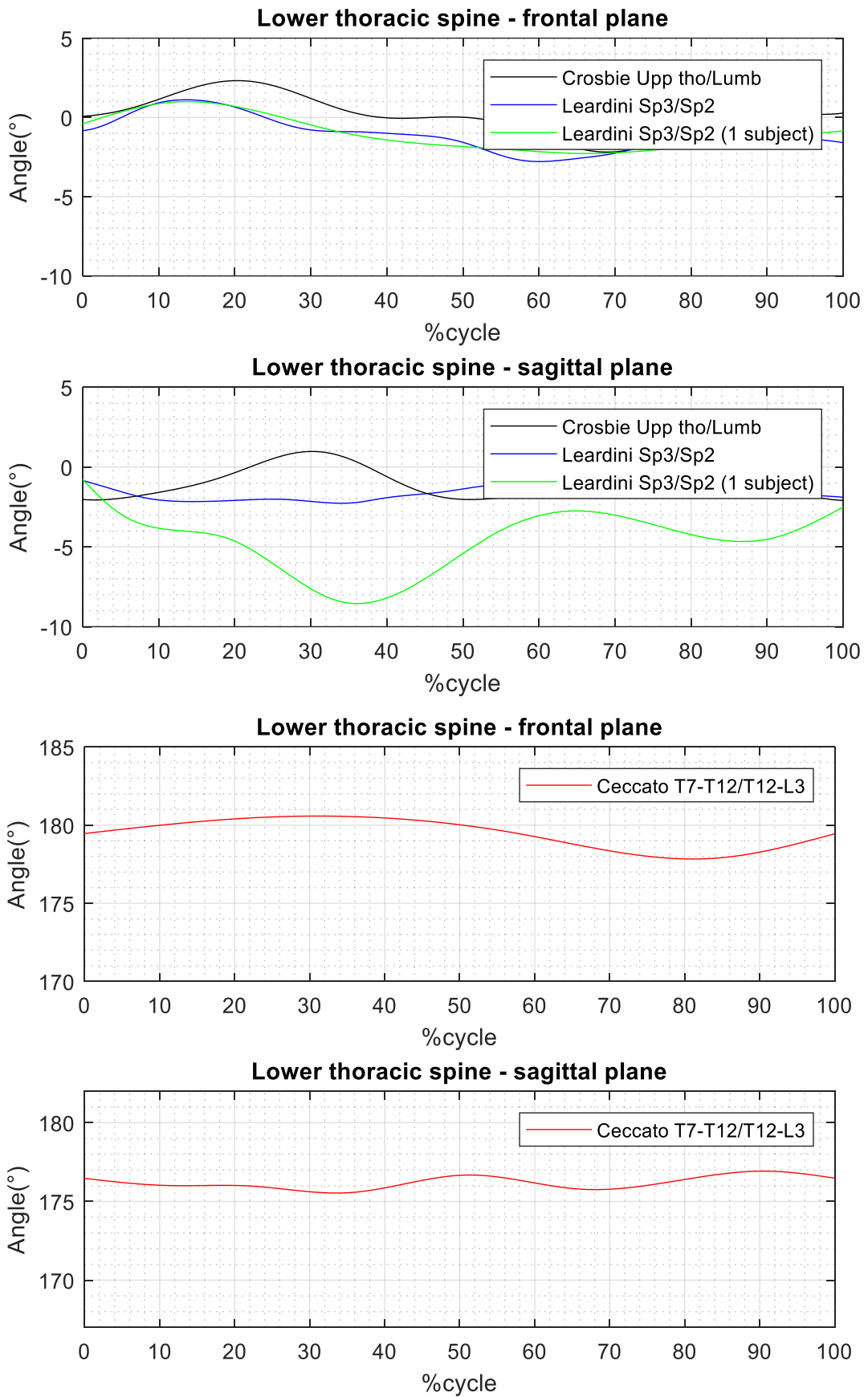


Fig. 1.3-3 Comparison of lower thoracic patterns.

Vertebral Column Angles

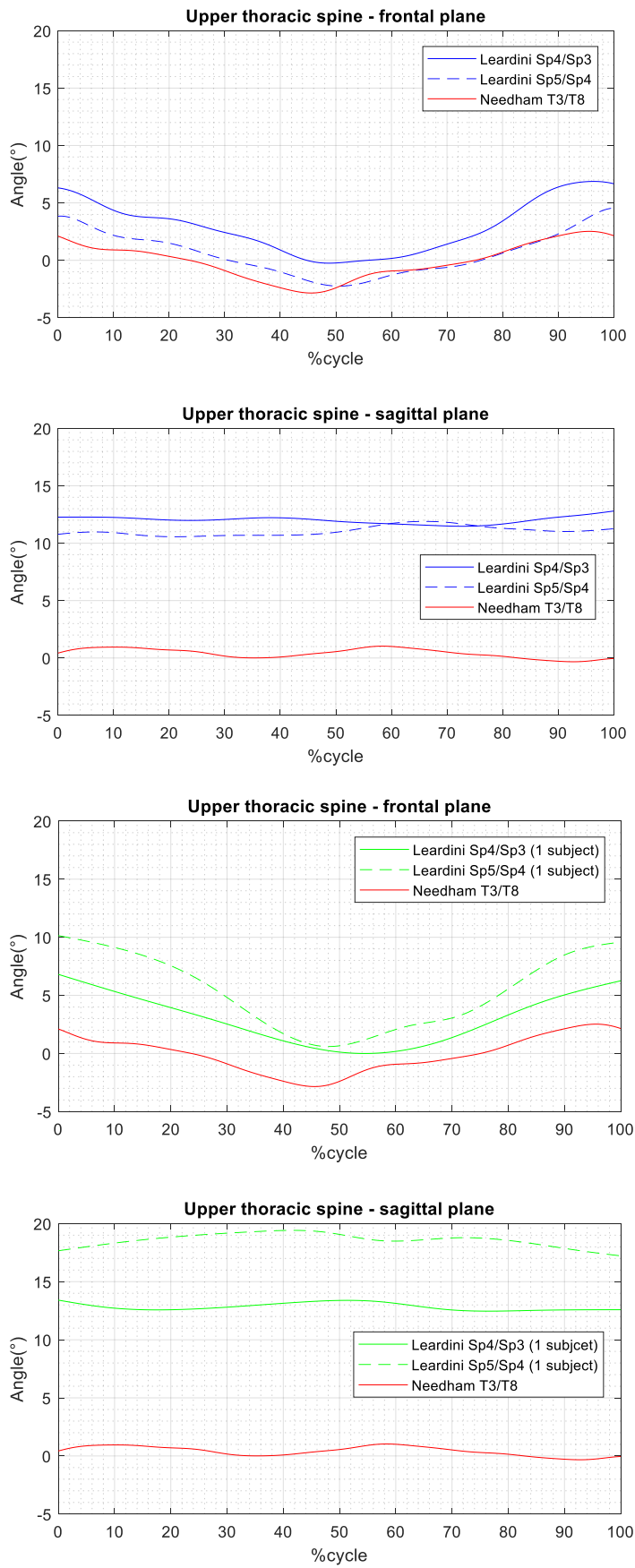


Fig. 1.3-4 Comparison of upper thoracic patterns.

The last segment to examine is the upper thoracic segment (T1-T6). More than two researches could be compared (Crosbie et al.(1997), Ceccato et al. (2009), Leardini et al.(2011), Needham et al. (2015)). For what concerned in Crosbie et al. (1997), the motion described is an absolute motion (with respect to laboratory reference frame). For this reason, patterns are not presented. Leardini et al. (2011) subdivided the segment in other two segments: C7-T2 and T2-MAI. In the frontal plane, patterns of Leardini et al. (2011) and Needham et al. (2015) are similar (Fig. 1.3-4). Also in the sagittal plane, but it could be seen a shift between patterns. In Tab. 1.3-5 ROMs are shown.

The spine segmentation defined before to conduct thesis investigation was changed. In fact, instead to position the sensor at the T1/T2 vertebral level, it was shifted in C7 position as results in these literature works. The final configuration chosen is shown in Fig. 1.3-4.

The follow pattern behaviours in the frontal plane were expected:

- C7-T6 segment relative to T6-T12: initial lateral flexion on stance leg side; maximum contralateral side flexion about 50% gait cycle;
- T6-T12 segment relative to T12-L3: in first single support phase, it flexes on stance leg side; follow a stabilization phase; in the second single support phase it flexes on contralateral side;
- T12-L3 segment relative to L3-S1: initial flexion on opposite stance lag side; around about 50% the angle trends overturned;
- L3-S1 segment relative to S1: initial flexion on opposite stance lag side; between about 10 and 60% it flexes on the contralateral side; from about 60% to 100% it flexes again in the opposite side;
- S1 segment: flexion on stance leg opposite side.



Fig. 1.3-4 Final configuration to divide vertebral column.

2. Motion Capture Systems

Motion capture systems in general provide information on joint angles, orientation between body segments and their movements. This information is combined in order to arrive at an objective assessment of the pathological state of a subject, to define the most appropriate rehabilitation program, to verify the benefits of the rehabilitation identified.

The basic requirements of the systems with which to assess pathological status are:

- Reliability;
- Precision;
- Low cost;
- Easy to use.

Motion capture systems are divided into optical and non-optical systems. The former category is based on the use of cameras, the latter on wearable sensors. In the specific thesis work, for the latter category, inertial sensors were used.

2.1 Optoelectronic System

The systems that represent the gold-standard in motion analysis are optoelectronic systems. This because optoelectronic systems have pronounced characteristics and consequently high performances in comparison with other existing motion capture systems.

Optoelectronic systems require:

- Cameras operating in the infrared field;
- Active or passive markers;
- Software that can join the information coming from each frame recorded by each camera and define its kinematic trajectory.

The markers are positioned according to the movement and therefore verify which body segments investigate (Fig. 2.1-1); they must be as visible as possible to the cameras and there must be no overcrowding.

The markers used can be active (Fig. 2.1-2) or passive (Fig. 2.1-3). Active markers have a LED that is always on or modulated over time, i.e. each marker positioned lights up at a specific time

t so that the camera sees one marker at time. This operation mode solves the problem of identifying two nearby markers, but it makes implementation more difficult due to the need to facilitate synchronization between markers with a radio signal. Regardless of this, the active markers certainly enjoy homogeneous illumination and thus simpler labelling. The negative aspects are the need for a power source to power them, wiring and occlusion problems. Passive markers, on the other hand, have a reflective surface so they do not require wiring, but the disadvantage is that they are not homogeneously illuminated, making it more difficult to recognize their position, and the problem of occlusion persists.

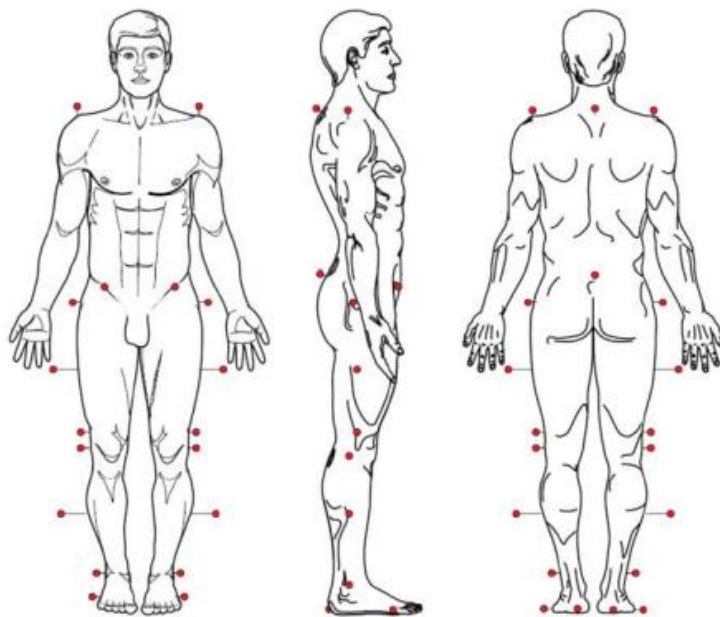


Fig. 2.1-1 Example of Marker set positioning.



Fig. 2.1-2 Active Markers.



Fig. 2.1-3 Passive Markers in different sizes.

Each camera detects the centre of the marker described as a two-dimensional point. In order to reconstruct the three-dimensional position of each marker, whether active or passive, at least two cameras are required, thus exploiting the stereo-photogrammetry: of the same marker, each camera defines the planar coordinates of its centre, then, through the use of the camera parameters, it is possible to reconstruct the marker in its three-dimensionality (Fig. 2.1-4 **a**). The principle is the same that characterizes stereoscopic vision in human being (Fig. 2.1-4 **b**): the brain receives images of the three-dimensional object placed in space with both eyes, combining them to obtain a stereoscopic reconstruction.

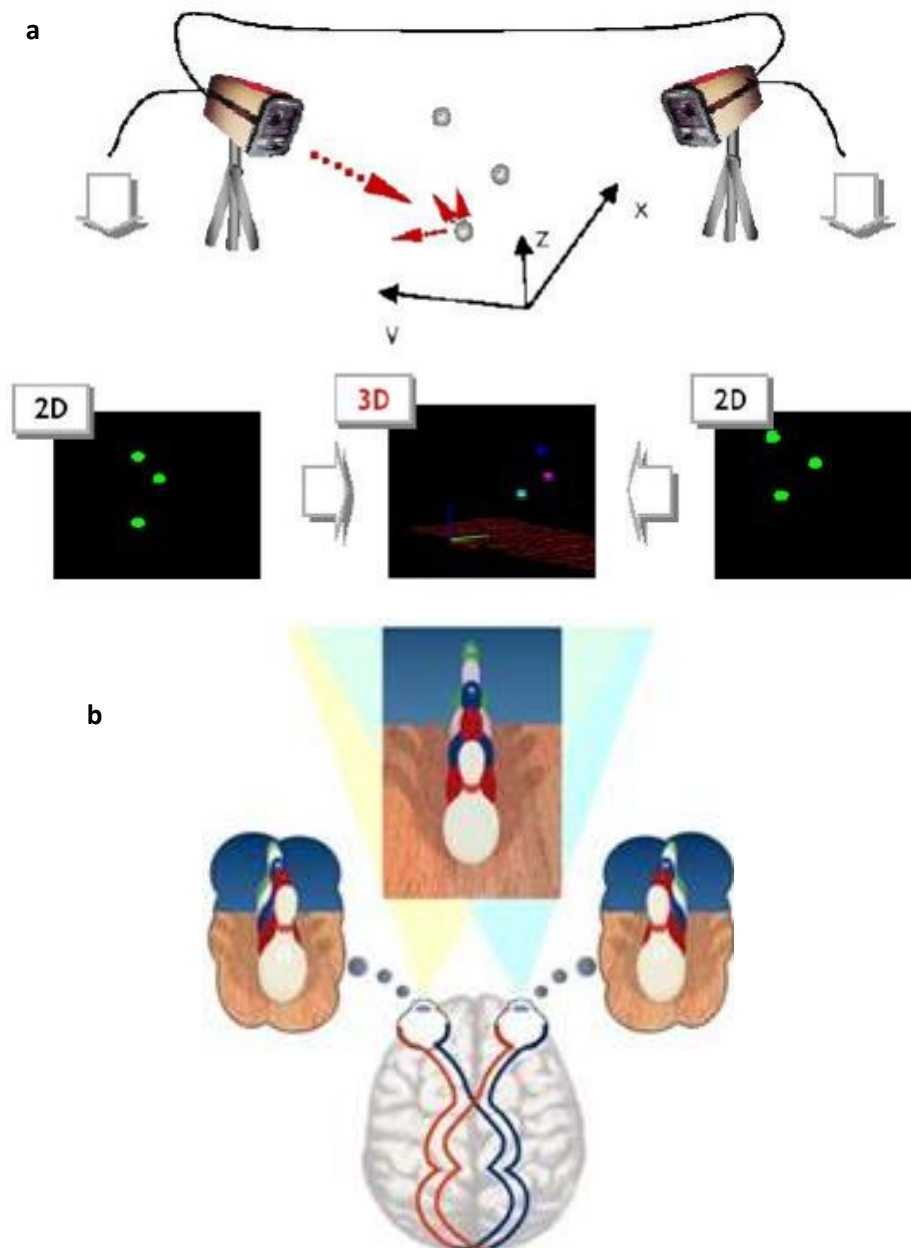


Fig. 2.1-4 **a** Stereophotogrammetry of motion capture system, **b** Stereoscopic vision.

2.1.1 V120:Trio

The V120:Trio tracking system (Fig. 2.1.1-1) is a multi-camera system assembled into a single hardware unit able to track an object un 6 DoF: position and orientation. Made up of three cameras capable of detecting reflected infrared light, the system is easy to use as it is pre-calibrated before package. Despite this, the precision and flexibility characteristics of the technology remain guaranteed. The central camera detects images in the visible spectrum for enhanced quality and flexibility lighting condition. Due to its compactness (Fig. 2.1.1-2), the system is also easy to transport and install in the desired environment. With V120:Trio it is possible to create large capture volumes (Fig. 2.1.1-3) and therefore the possibility of tracing multiple moving objects identified by markers: high accuracy is guaranteed even with the use of sub-millimetre markers. It can capture images at speeds up to 120 FPS.



Fig. 2.1.1-1 V120:Trio tracking system.



Fig. 2.1.1-2 V120:Trio dimensions.

The bar is connected to the power supply by I/O-X box; moreover, this allows its synchronization with other hardware devices (e.g. PC) (Fig. 2.1.1-4).

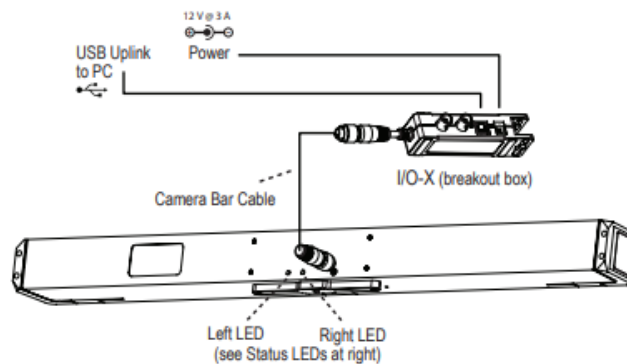


Fig. 2.1.1-4 Hardware Plug in scheme.

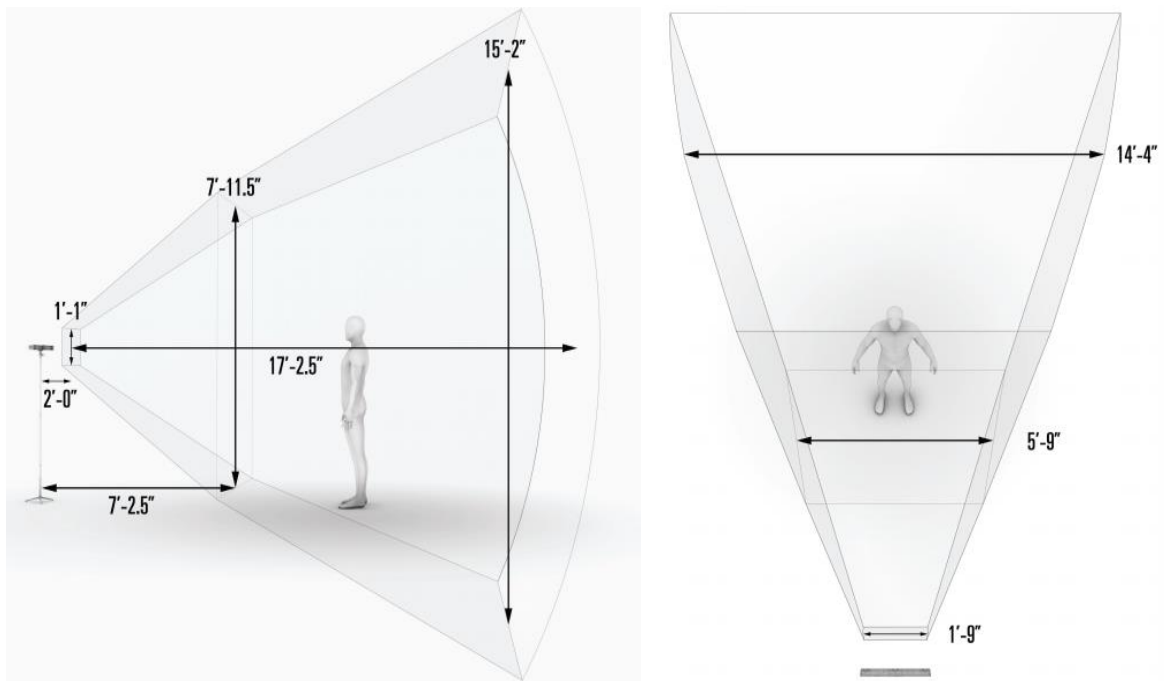


Fig. 2.1.1-3 Capture volume of Optitrack bar.

Optitrack V120:Trio is composed by (Fig. 2.1.1-5):

- 1 bar V120:Trio;
- 1 Quick Start Guide;
- 1 license of Motive: Tracker;
- 1 12V universal power supply;
- 1 USB uplink cable of 5 meters;
- 4 M3 small short marker bases;
- 4 M4 medium short marker bases;
- 4 M4 medium long marker bases;
- 4 M3 7.9mm markers;
- 4 M4 9.5mm markers;
- 8 M4 12.7mm markers;
- 10 Ø3/8 rubber adhesive dots;
- 10 Ø1/2 rubber adhesive dots;
- 1 Hand rigid body.



Fig. 2.1.1-5 Boxed components of Optitrack V120:Trio.

In Tab. 2.1.1-1 technical specifications of the V120:Trio are shown.

Technical Specifications		
Camera Body	Width	23 inches (584.2 mm)
	Height	1.6 inches (40.6 mm)
	Depth	2 inches (50.8 mm)
	Weight	2.8 pounds (1.3 kg)
	Mounting	¼”-20 tripod thread
	Display	128 x 22 OLED
Image Sensors	Imager Resolution	640 x 480
	Frame Rate	30, 60, 120 FPS
	Latency	8.33 ms
Lenses & Filters	Lenses	Standard M12 Lenses
	Left and Right Cameras	800 nm IR long pass filter
	Middle Camera	800 nm IR long pass filter w/Filter Switcher
LED Rings	No. Of LEDs	26 (x3)
	Wavelength	850 nm
	Illumination	Strobe or Continuous
	Brightness	Adjustable
Input/Output & Power	Data	USB 2.0
	Camera Sync	Internal or external (via IO-X)
	Power	12V, 3A

Tab. 2.1.1-1 Technical specifications of V120:Trio bar.

2.1.2 Motive Software

Motive is a software to capture the markers position not only during movement but also in static acquisition to define laboratory reference frame. Before capture starts is necessary crate a new folder in which file is stored in format “TAK”. Once markers are positioned capture can start pressing the red record button. Motive can operate in two different modes: Live Mode and Edit Mode. In the Live Mode the cameras are active, and data can be acquired. To stop the acquisition, the same red button must be pressed. In a folder created, a file (TAK extension) of that capture is saved. The file can be open again to edit and export in different formats the data acquired. In this case Motive is in an Edit Mode and the cameras are not active. In the post-processing phase, thanks to *Data Editing Tool* it’s possible recognize markers and named them with a specific etiquette. This operation named Labelling. A new Markerset Asset must be created (Fig. 2.1.2-1). Each marker will have its own color code. Starting from the first frame, each visible marker is associated with corresponding label: from unlabelled the marker becomes labelled (Fig. 2.1.2-2). Markers can be labelled in two different way: auto-labelling and manual-labelling. The first one can make mistakes and manual-labelling is necessary. At the end of Labelling unlabelled markers can be still present (Fig. 2.1.2-3). These can be removed after exporting file TAK in another format. The two formats available are C3D and CSV. The latter format can be imported in Excel file (Fig. 2.1.2-3) and analysed. For each marker labelled, three coordinates (x, y, z) described it at each sampled time. The coordinates described the markers in a V120:Trio bar reference system.

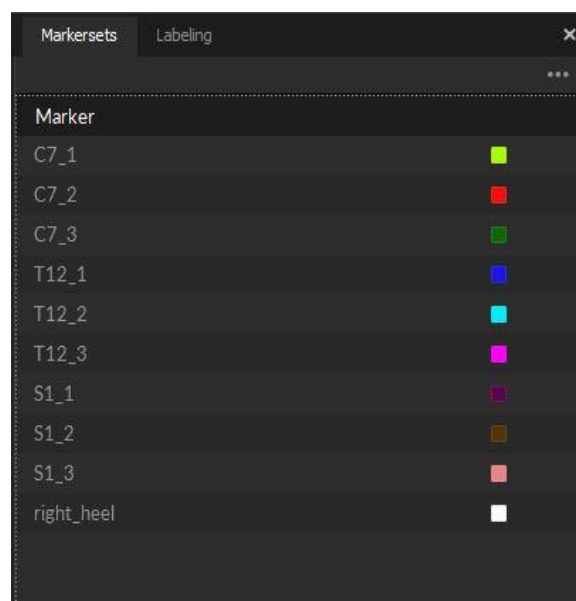


Fig. 2.1.2-1 Markerset crated during Labelling.

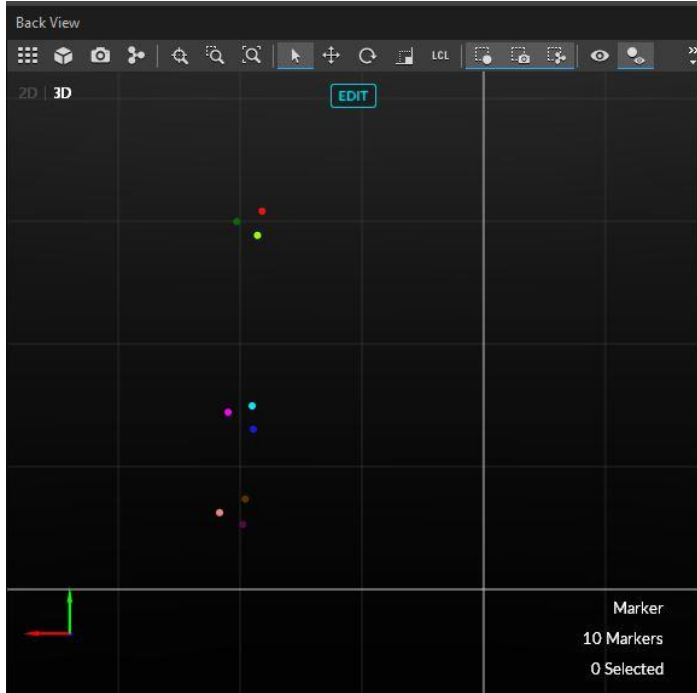


Fig. 2.1.2-2 Marker triads labelled.

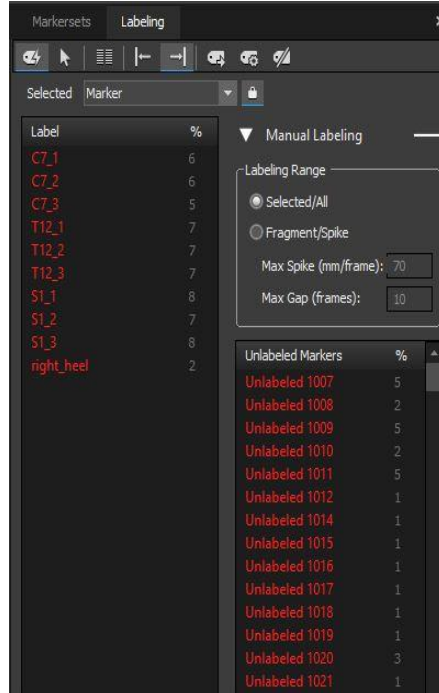


Fig. 2.1.2-3 Unlabeled and labled markers section.

Column9	Column10	Column11	Column12	Column13	Column14	Column15	Column16	Column17	Column18	Column19	Column20	Column21	
Export Frame	120	Capture Start	2019-01-22 11, Total Frames i 8158				Total Exporte	8158	Rotation Type	Quaternion	Length Units	Meters	Coordinate Sp
Marker	Marker	Marker	Marker	Marker	Marker	Marker	Marker	Marker	Marker	Marker	Marker	Marker	
Marker:C7_1	Marker:C7_1	Marker:C7_1	Marker:C7_2	Marker:C7_2	Marker:C7_2	Marker:C7_3	Marker:C7_3	Marker:C7_3	Marker:S1_1	Marker:S1_1	Marker:S1_1	Marker:S1_2	
F2F0B23A1E41	F2F0B23A1E41	F2F0B23A1E41	F2F0B23C1E41	F2F0B23C1E41	F2F0B23C1E41	F2F0B23E1E41	F2F0B23E1E41	F2F0B23E1E41	F8F23F5D1E41	F8F23F5D1E41	F8F23F5D1E41	F8F23F5F1E41	
Position	Position	Position	Position	Position	Position	Position	Position	Position	Position	Position	Position	Position	
X	Y	Z	X	Y	Z	X	Y	Z	X	Y	Z	X	
0,293623	0,740542	2,39929	0,309162	0,779131	2,406429	0,338782	0,750115	2,385704	0,239462	0,296825	2,542861	0,244943	
0,291783	0,739918	2,400912	0,307532	0,7788	2,408662	0,336726	0,749176	2,386291	0,239244	0,297295	2,543837	0,244706	
0,289623	0,739277	2,40191	0,305428	0,777991	2,409232	0,334666	0,748851	2,38821	0,23906	0,29759	2,544657	0,244434	
0,287121	0,739297	2,402586	0,303216	0,778056	2,410383	0,331976	0,748788	2,38808	0,238828	0,297689	2,545054	0,244055	
0,284818	0,740057	2,40403	0,300804	0,77846	2,410934	0,329577	0,749089	2,388468	0,238862	0,297892	2,545546	0,24403	
0,282667	0,740635	2,403841	0,298589	0,779404	2,411367	0,327594	0,750166	2,389616	0,239072	0,298347	2,545286	0,244241	
0,28099	0,742152	2,404797	0,29676	0,780997	2,412452	0,325868	0,751827	2,390301	0,239412	0,299252	2,544618	0,244773	
0,279704	0,744117	2,405852	0,295535	0,782946	2,413562	0,324492	0,753847	2,391134	0,239901	0,300924	2,544559	0,24539	
0,278689	0,746244	2,406772	0,294614	0,784892	2,414341	0,323501	0,755897	2,39222	0,240419	0,302897	2,543618	0,246235	
0,278011	0,748346	2,408328	0,293991	0,78675	2,415223	0,322663	0,757646	2,39265	0,240999	0,305026	2,541711	0,247462	
0,277321	0,749878	2,40868	0,293499	0,78831	2,415602	0,322055	0,75902	2,393425	0,241561	0,307009	2,539521	0,248608	
0,276804	0,751029	2,408967	0,29296	0,789767	2,416472	0,321594	0,760417	2,394565	0,242154	0,309055	2,538787	0,24925	
0,276395	0,75199	2,409616	0,292405	0,790907	2,417545	0,321148	0,7614	2,394699	0,242322	0,310451	2,536862	0,249712	
0,276042	0,752612	2,410097	0,29162	0,791373	2,417342	0,320872	0,762432	2,395679	0,242304	0,311698	2,536077	0,249677	
0,275669	0,753075	2,410318	0,290953	0,792032	2,41797	0,320473	0,763206	2,396283	0,241985	0,312573	2,535749	0,249444	

Fig. 2.1.2-4 Excel File imported from Motive Software.

2.2 Inertial Measurement Units

Inertial sensors represent a tool to detect kinematic quantities such as acceleration, angular velocity, and information related to magnetic field on three orthogonal axes. Thanks to the developing of MEMS (Micro Electro Mechanical System), inertial sensors were made small in order to assemble them in a unique system called IMU (Inertial Measurement Unit) (Xsens, 2000).

Attaching IMUs in different body parts it is possible to obtain information regard their orientation in the space with a minimum encumbrance. They represent a non-invasive system, with high portability, easy to wear and that can be used not only in a clinic environment. Optoelectronic systems are considered gold standards because they ensure accurate information. They are affected though by some limitations related to markers occlusions, high costs, and that they can be implemented exclusively in a laboratory equipped with cameras and consequently a limited volume in which to perform measurements (Xsens, 2000).

Accelerometers can detect accelerations of the object on which they are attached. They can be of various types, but in many cases the operating principle is based on the measurement of the inertia of a mass connected to an elastic element and subjected to an acceleration. An uni-axial accelerometer with a mass-spring system it is shown below (Fig. 2.2-1). The spring, in its linear region, is ruled by the Hooke's law according to which the generated elastic force is proportional to its elongation (positive or negative):

$$F = kx$$

Where k is the spring elastic constant, while x is the displacement.

Furthermore, when the mass is subjected to an acceleration, an inertial force (according to Newton's law) is developed, and it is equal to:

$$F = ma$$

The equilibrium equation of the entire system can be written as:

$$ma = kx$$

Measuring the mass displacement caused by the acceleration, it is possible to describe this as:

$$a = \frac{kx}{m}$$

The concept shown here allows to obtain a unique acceleration, to obtain three different accelerations along three orthogonal axes, the system has to be replicate for each of them. (Xsens, 2000).

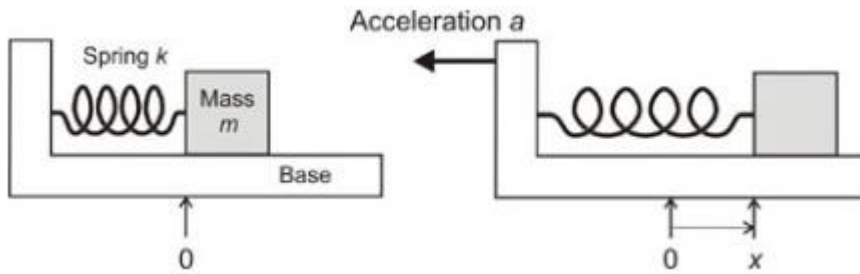


Fig. 2.2-1 Mass-spring system (Xsens, 2000).

Gyroscopes are devices able to detect angular velocity. They are composed by a rotor (internal disk), that rotates around the spin axis (Fig. 2.2-2). The rotor is mounted on a series of cardan joints that allow the axis to assume all possible orientations in space. Therefore, an inner ring is present that allows the rotation around the x axis, an intermediate ring and an external ring that respectively lead the y axis and the z axis. A disk that rotates around its own axis with an angular velocity ω will develop an angular momentum L equal to:

$$L = I \times \omega$$

Where I is the inertial momentum.

At the base of mechanical gyroscopes there is the law of conservation of the angular momentum, meaning that the angular momentum remains constant if no torque τ is applied on it. The torque acting on a system is equal to:

$$\tau = \frac{dL}{dt} = \frac{d(I\omega)}{dt} = I\alpha$$

Where α is the angular acceleration.

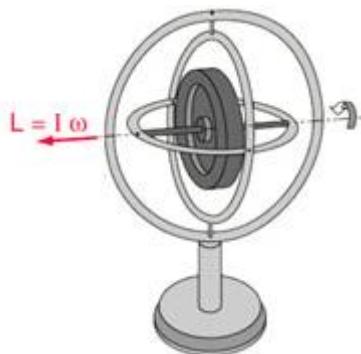


Fig. 2.2-2 Gyroscope with its parts: rotor and rings.

Gyroscopes with vibrating mass represent small systems, not expensive and that need little energy (Xsens, 2000). On the vibrating element, a Coriolis force is developed and because of that it is possible to obtain the angular velocity:

$$\mathbf{F}_C = -2m(\boldsymbol{\omega} \times \mathbf{v})$$

As previously said, an IMU incorporate a tri-axial accelerometer, a tri-axial gyroscope, and as it happens with Xsens sensors, there is the integration of a further element: the magnetometer. That consent to detect the intensity and direction of the earth magnetic field. The three signals typology are combined in order to obtain correct orientation information without drift phenomenon, that is a consequence of the integration of angular velocity to obtain three angles that describe the object orientation. In the Xsens sensors the signals fusion, derived from the gyroscope, accelerometer and magnetometer, it is provided by the Kalman filter. In particular, pitch and roll angles are stabilized by gravity acceleration while yaw angle is stabilized by the earth magnetic field.

2.2.1 Xsens: XBus Kit

Xsens is one of the major developers of inertial technology to detect human movements. Kit (Fig. 2.2.1-1) is composed of:

- 7 MTx Motion Trackers
- 1 Xbus Master
- 1 Xbis Master Cable USB
- 1 Black strap/belt
- 1 Bluetooth Transceiver USB
- 7 Xbus cables
- 1 power adapter

Motion trackers (MTx) are located on segments of interest and they are connected to each other, including also Xbus Master, in order to create a closed kinematics chain. Xbus Master provide energy and samples in a synchronised manner the acquired information relative to the magnetic field, accelerations and angular velocities from MTx. The Xbus Master, powered by 4 AA style batteries or by an external power source, is able to transfer data, via Bluetooth connection or via USB cable, to a PC. On the PC, where the Xsens software is installed, it is possible to visualize all the signal and thus reconstruct the 3D body motions in a real-time (Xsens). The Xbus Kit is used in many fields including rehabilitation, biomechanics, sports and virtual reality.



Figure 2.2.1-1 XBus Kit (Xsens).

2.2.2 MTx Motion Tracker

MTx are miniaturised inertial measurement systems that integrate accelerometers, gyroscopes and magnetometers. Inside them there is a processor that calculate roll, pitch and yaw drift-free angles. Furthermore, they supply accelerations, angular velocities and magnetic field data. They are expressed in the right-handed Cartesian co-ordinate system body-fixed to the device (Fig. 2.2.2-1). The sensor orientation data are described in the Global Reference Frame (G) and can be represented with three methods: as quaternions, Euler angles (roll, pitch and yaw) or as a rotation matrix (direction cosine matrix). Positive angles will occur when rotation is clockwise around the axis of rotation (Fig. 2.2.2-2).

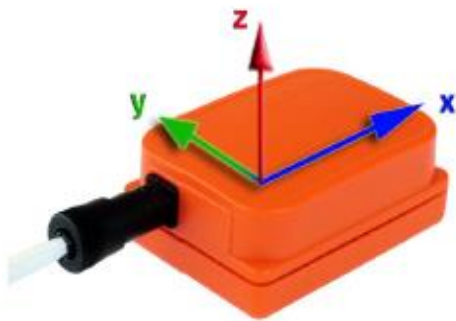


Fig. 2.2.2-1 Co-ordinate system fixed to MTx sensor (S) (Xsens).

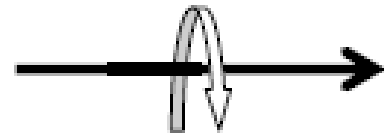


Fig. 2.2.2-1 Rotation according right-handed rule (Xsens).

Calibration outputs (3D linear acceleration, 3D angular velocity, 3D magnetic field data) are expressed with the measurement units shown in Tab. 2.2.2-1.

Vector	Unit
Acceleration	m/s^2
Angular velocity	rad/s
Magnetic field	<i>a.u. (arbitrary units) normalized to earth field strength</i>

Tab. 2.2.2-1 Measurement units of calibration data.

Technical specifications of the MTx sensors are shown in Tab. 2.2.2-2.

Each MTx sensor is equipped with two connectors so that it can be connected to another MTx sensor or to the Xbus Master and form a closed kinematic chain.

Performances		
Orientation Output	Dynamic Range	All angles in 3d
	Angular Resolution	0.05 deg
	Update Rate	Max 256Hz
Angular Velocity Data	Dimension	3 axes
	Full Scale	±1200 deg/s
	Bandwidth	40Hz
Acceleration Data	Dimension	3 axes
	Full Scale	±50 m/s ²
	Bandwidth	30Hz
Magnetic Field Data	Dimension	3 axes
	Full Scale	±750mgauss
	Bandwidth	10Hz
Operating Voltage	4.5-30V	
Temperature Operating Range	-20°C÷60°C	
Power Consumption	350mV	
Weight	30g	
Outline Dimension (W x L x H)	38 X 53 X 21 mm	

Tab. 2.2.2-2 Technical specification of MTx sensor system.

2.2.3 Xbus Master

In Fig. 2.2.3-1 is shown the Xbus Master in the rear and front view.

- Xbus connectors: these can be used to create a chain between the Xbus Master and the Motion Trackers. In addition in this way, the Xbus Master can provide power supply to MTx and receive information about their motion;
- Belt eyelets: these allow the Xbus Master to be attached to a belt and then placed on subject's hip;
- Battery compartment: is the place where the AA batteries are located, which are the energy supply needed to power the MTx and to allow data transmission to the PC;
- Push button: it is the on/off button of the device and it allows you to switch from Bluetooth transmission to serial communication and to restore the information of defaults;
- Sync connector: it permits the synchronization of the Xbus Master with another device or with other devices;
- Host connector: it is the connector for connecting the Xbus Master to a host via USB wiring;
- External power connector: it is the connector used to connect the Xbus Master to an external power source;

Status LED: it allows the recognition of the type of configuration or measurement status of the Xbus Master by a colour code (Tab. 2.2.3-1) and flashing mode (Tab. 2.2.3-2).

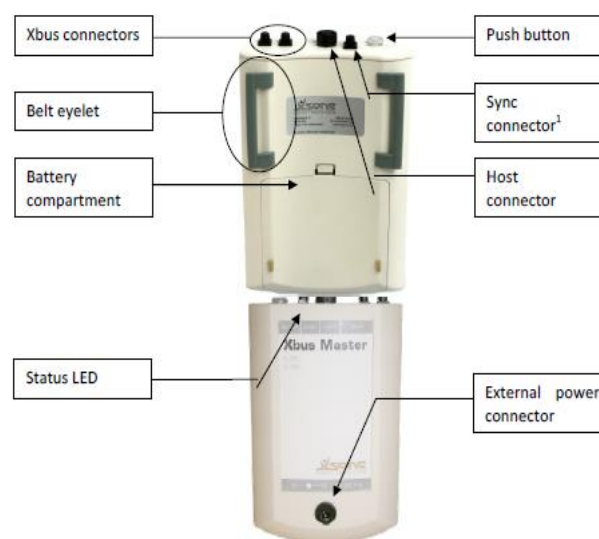


Fig. 2.2.3-1 Xbus Master and its parts (Xsens).

LED flash sequence	Xbus Master current state
Off	Power down
Solid	Config state
Two short flashes	Measurement state-waiting for trigger
One flash	Measurement state-sending data

Tab. 2.2.3-1 Xbus Master status.

LED color	Xbus Master active mode
Off	Power down
Green 	Serial mode
Blue 	Bluetooth mode
Purple 	Bluetooth mode-host not found
Yellow 	Low battery mode
Red 	Fault mode

Tab. 2.2.3-2 Xbus Master flashing mode.

As mentioned a few times, the Motion Trackers are connected each other and with the Xbus Master forming a closed kinematic chain (Fig. 2.2.3-2). It is important not connect a chain of more than 5 MTx to a single connector of the Xbus Master.



Fig. 2.2.3-2 Motion Trackers connected to Xbus Master (Xsens).

2.2.4 MT Manager Software

MT Manager is a software developed specifically to be compatible with Xsens Motion Trackers and Xbus Master. A possible screen that the software can provide is shown in Fig. 2.2.4-1.

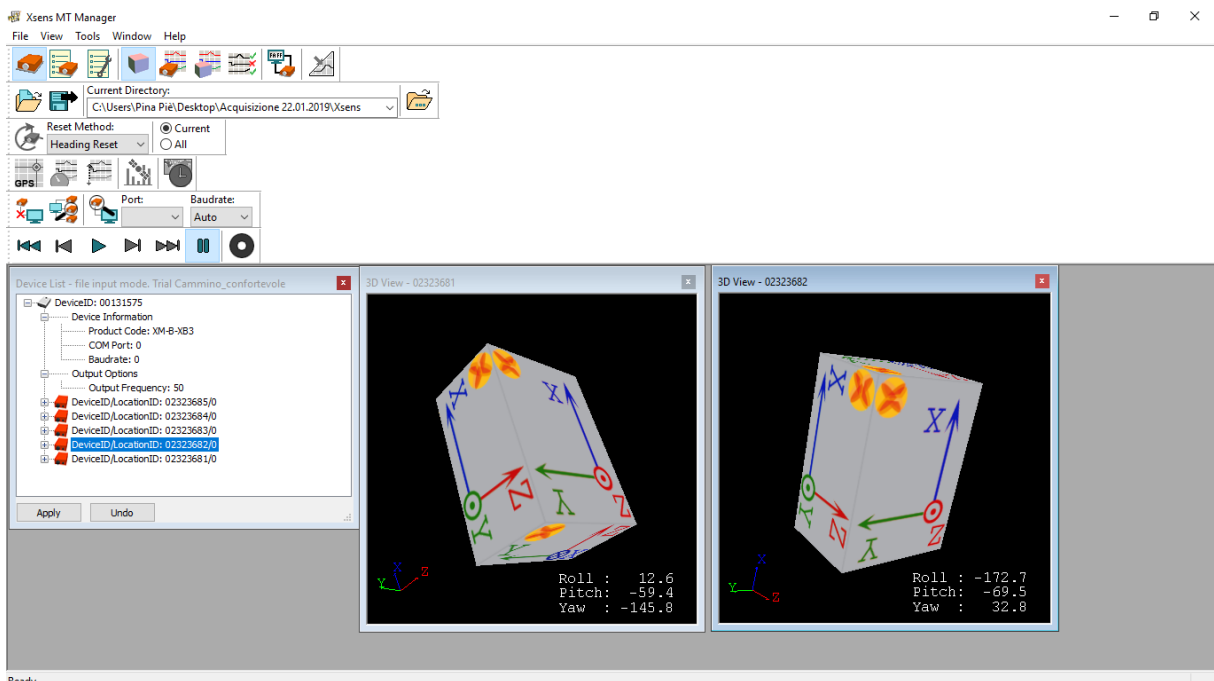


Fig. 2.2.4-1 An example of MT Manager software screen.

Installed on a Windows system, it provides a simple interface in which the 3D orientation as well as calibration data (accelerations, angular velocities, magnetic field) are shown in real-time. When MT Manager starts, a scan is performed so that each individual motion tracker is displayed in the 'Device List'. Each MTx is identified with a specific ID number (Fig. 2.2.4-2). In this phase, but also later, parameters are set: output options (for example sampling frequency, orientation data mode), the filter scenario to which corresponds a different processing in signals fusion operated by the Kalman filter. Once you have ensured that all the Motion Trackers have appeared in the 'Device List', you can record the acquisition.

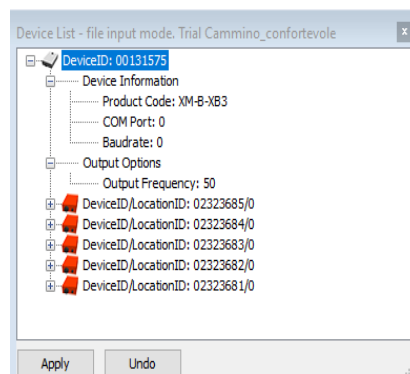


Fig. 2.2.4-2 An example of Device List of MT Manager software.

The software allows to visualize in real-time, for each Motion Tracker, the calibrated data pattern (Fig. 2.2.4-3), but also the 3D view of the sensor and the corresponding Euler angles. The acquisition is saved in a file in “.MTB” (MT Binary Communication Protocol) format. At this point, in order to process the data acquired on a different software, the data can be exported in an ASCII format: a file will be generated for each Motion Tracker belonging to the chain created. The files will contain the information chosen by the user. For this purpose, the user will choose the orientation data convention (Unit normalized Quaternions or Euler parameters, Euler angles, Rotation Matrix).

A file Excel with data imported from MT Manager is shown in Fig. 2.2.4-4.

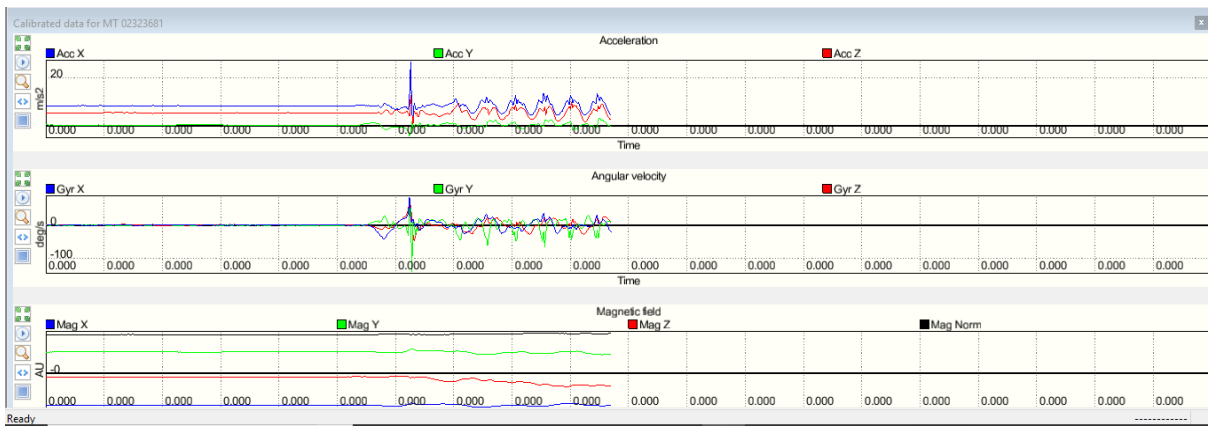


Fig. 2.2.4-3 Real time calibration data (accelerations, angular velocities, magnetic field).

Column1	Column2	Column3	Column4	Column5	Column6	Column7	Column8	Column9	Column10	Column11	Column12	Column13	Column14	Column15	Column16	Column17	Column18
// Start Time: 0																	
// Sample rate: 50,0Hz																	
// Scenario: 5,0																	
// Firmware Version: 2,6,1																	
Acc_X	Acc_Y	Acc_Z	Gyr_X	Gyr_Y	Gyr_Z	Mag_X	Mag_Y	Mag_Z	Mat[0][0]	Mat[0][1]	Mat[0][2]	Mat[1][0]	Mat[1][1]	Mat[1][2]	Mat[2][0]	Mat[2][1]	Mat[2][2]
8,355492	-0,588704	5,165354	0,020987	-0,005078	0,008212	-0,433019	0,329063	-0,737201	0,461671	-0,268421	0,845464	0,582332	0,810689	-0,060606	-0,669141	0,520321	0,530582
8,350413	-0,654564	5,170347	0,022879	-0,010606	0,014547	-0,432356	0,330507	-0,738011	0,462062	-0,268342	0,845276	0,581982	0,810934	-0,060695	-0,669176	0,519980	0,530871
8,374638	-0,644704	5,184670	0,024467	-0,006729	0,002814	-0,431675	0,329894	-0,738091	0,462078	-0,268327	0,845272	0,581722	0,811134	-0,060515	-0,669391	0,519675	0,530859
8,374639	-0,639852	5,199325	0,001528	-0,005098	0,010980	-0,432760	0,329829	-0,737329	0,462215	-0,268142	0,845255	0,581690	0,811137	-0,060770	-0,669323	0,519756	0,530896
8,345163	-0,600864	5,160716	0,012088	-0,001425	0,004694	-0,431936	0,328636	-0,737363	0,462326	-0,268150	0,845193	0,581575	0,811221	-0,060753	-0,669347	0,519630	0,530998
8,359717	-0,600789	5,160512	0,008491	-0,001288	-0,000657	-0,433025	0,330505	-0,738135	0,462378	-0,268194	0,845150	0,581558	0,811235	-0,060737	-0,669326	0,519587	0,531067
8,345675	-0,674098	5,160625	-0,000402	0,000644	-0,005961	-0,431891	0,326187	-0,738219	0,462395	-0,268392	0,845078	0,581701	0,811136	-0,060672	-0,669190	0,519638	0,531189
8,355337	-0,669160	5,158053	-0,010994	0,005931	-0,004096	-0,433526	0,327477	-0,737898	0,462504	-0,268566	0,844963	0,581977	0,810929	-0,060806	-0,668874	0,519872	0,531357
8,330735	-0,615606	5,170657	-0,001328	0,011444	-0,013052	-0,433419	0,329638	-0,738005	0,462575	-0,269003	0,844785	0,582219	0,810768	-0,060631	-0,668615	0,519896	0,531660
8,345335	-0,620423	5,175341	0,006657	0,018538	-0,014843	-0,431492	0,327918	-0,739703	0,462727	-0,269482	0,844549	0,582357	0,810686	-0,060396	-0,668388	0,519776	0,532062
8,360049	-0,639897	5,184879	-0,011114	0,002659	-0,014847	-0,433387	0,328631	-0,739386	0,462665	-0,269848	0,844466	0,582730	0,810426	-0,060295	-0,668106	0,519992	0,532205
8,357657	-0,644792	5,184907	-0,005665	0,004104	-0,002345	-0,432446	0,330220	-0,741018	0,462770	-0,269975	0,844368	0,582918	0,810283	-0,060402	-0,667870	0,520150	0,532348
8,355200	-0,635071	5,199602	-0,021734	0,004459	-0,014785	-0,433562	0,330791	-0,738532	0,462729	-0,270365	0,844266	0,583444	0,809903	-0,060415	-0,667440	0,520537	0,532508
8,340576	-0,630233	5,185162	-0,021622	-0,002968	-0,000516	-0,432589	0,329499	-0,739660	0,462760	-0,270388	0,844242	0,583827	0,809604	-0,060723	-0,667083	0,520991	0,532512
8,338318	-0,664361	5,155855	-0,005561	0,003844	0,008389	-0,431538	0,330079	-0,738441	0,462984	-0,270389	0,844118	0,583910	0,809527	-0,060956	-0,666854	0,521110	0,532681
8,335989	-0,675889	5,160757	-0,002164	0,007773	-0,007700	-0,431808	0,330077	-0,738300	0,463075	-0,270640	0,843988	0,584100	0,809391	-0,060935	-0,666625	0,521191	0,532890
8,355613	-0,698514	5,187315	-0,012742	-0,001227	-0,000547	-0,433192	0,334250	-0,739579	0,463122	-0,270743	0,843929	0,584378	0,809179	-0,061094	-0,666349	0,521467	0,532965
8,326164	-0,649843	5,187783	-0,014422	-0,003247	0,010184	-0,432893	0,332090	-0,739616	0,463274	-0,270589	0,843895	0,584566	0,809012	-0,061506	-0,666078	0,521806	0,532971
8,335743	-0,627848	5,199882	-0,007458	0,000602	-0,003245	-0,431818	0,332239	-0,739770	0,463321	-0,270744	0,843820	0,584778	0,808854	-0,061563	-0,665859	0,521970	0,533084
8,316395	-0,713987	5,200047	-0,007274	0,018057	0,006696	-0,432510	0,336677	-0,739736	0,463716	-0,270869	0,843563	0,584903	0,808742	-0,061840	-0,665474	0,522078	0,533458
8,336421	-0,718210	5,219302	-0,001228	-0,004786	-0,000615	-0,431392	0,331089	-0,740340	0,463720	-0,270926	0,843542	0,585011	0,808662	-0,061875	-0,665376	0,522174	0,533487
8,340433	-0,591387	5,238925	0,017413	0,014668	-0,002396	-0,430750	0,332243	-0,739242	0,463963	-0,271163	0,843392	0,584892	0,808758	-0,061795	-0,665312	0,521901	0,533835
8,320738	-0,549888	5,239247	0,001294	0,009764	-0,016551	-0,431542	0,332240	-0,740321	0,463970	-0,271637	0,843175	0,585126	0,808609	-0,061473	-0,665101	0,521885	0,534113
8,297290	-0,662325	5,249212	-0,005499	0,003778	0,011977	-0,432498	0,332957	-0,739884	0,464237	-0,271529	0,843064	0,585178	0,808545	-0,061819	-0,664869	0,522041	0,534249

Fig. 2.2.4-4 An example of Excel file exported from MT Manager software.

3. Data Elaboration

3.1 Tilt-Twist Method

To trace the movements between two segments connected to the same articulation, it is necessary to derive the planar rotation angles. Various techniques can be used to do this, such as the Euler-Cardan technique, the projection method or the helican angle (Crawford, 1999). All these methods, however, have limitations and it was necessary to develop a new method: Tilt-Twist Method. In fact, this method, differently to what happens in the Euler-Cardan technique, frees the angles from rotations sequence around the axes. Crawford et al. (1999) found that for rotations less than 30° the problem of sequence dependency can be solved with another technique developed, but for angles greater than 30° this technique doesn't solve the issue. In addition a further problem with Euler-Cardan angles is the singularity condition. For example, when the second Euler angle approaches to 90° , singularity condition is achieved.

To describe wider movements with a physiological meaning, Crawford et al. (1999) have formulated a new standard to quantify the planar components of joint rotations. The Tilt-Twist Method describes the joint as two cylinders stacked on top of each other. In this case the two cylinders represent two vertebrae. Each cylinder has its own reference system (Fig. 3.1-1). The upper cylinder rotates, so that, the reference system attached to it will change orientation from time to time. At the beginning, like Fig. 3.1-1 shows, the axes of the two cylinders are aligned. The angles are the calculated from initial and final orientation of unit vectors.

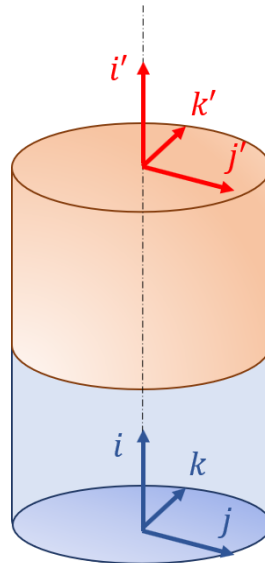


Fig. 3.1-1 Two cylinders with own reference system.

The first angle in consideration is the Tilt angle Φ . The Tilt angle is formed considering the upper cylinder bent downwards and forwards (Fig. 3.1-2). Φ is therefore the angle measured with respect to the X axis, it ranges from 0° to $+180^\circ$ and it is always positive. The Tilt Azimuth angle θ is the angle formed by the projection of i' in the Z-Y plane with respect to the negative Z axis. It ranges from -180° to $+180^\circ$ and it is positive toward the Y axis. The Tilt Azimuth angle is used to measure the direction of bending.

In order to obtain θ the projection i'_{Y-Z} was considered:

$$\begin{cases} i'_Y = i'_{Y-Z} \cdot \sin\theta \\ -i'_Z = i'_{Y-Z} \cdot \cos\theta \end{cases} \Rightarrow \operatorname{tg}\theta = \frac{i'_Y}{-i'_Z}$$

During data processing, the 'atan2' function was used:

$$\theta = \operatorname{atan2}(i'_Y, -i'_Z)$$

Φ was obtained as follows:

$$\begin{cases} i'_X = i' \cdot \cos\Phi \\ i'_{Y-Z} = i' \cdot \sin\Phi = i'_Y \cdot \sin\theta - i'_Z \cdot \cos\theta \end{cases} \Rightarrow \operatorname{tg}\Phi = \frac{i'_{Y-Z}}{i'_X} = \frac{i'_Y \cdot \sin\theta - i'_Z \cdot \cos\theta}{i'_X}$$

Although it is always positive, 'atan2' function was used also for Φ :

$$\Phi = \operatorname{atan2}(i'_Y \cdot \sin\theta - i'_Z \cdot \cos\theta, i'_X)$$

At this point, spherical angles obtained were transformed into planar angles using a sinusoidal relation of θ . In this way flexion-extension and lateral bending have been described:

$$\begin{cases} FE = \Phi \cdot \cos\theta \\ LB = -\Phi \cdot \sin\theta \end{cases}$$

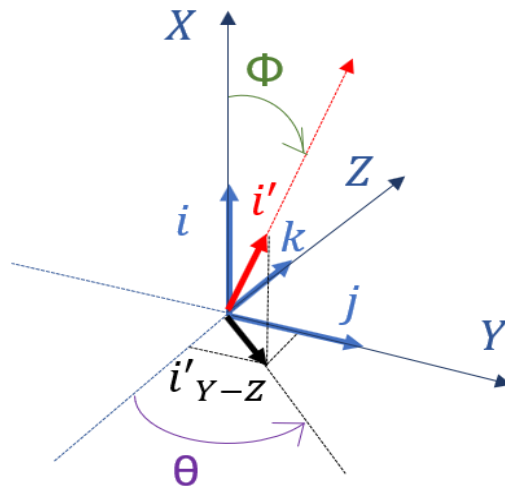


Fig. 3.1-2 Tilt and Tilt Azimuth angles considering upper cylinder bent downwards and forwards.

With Tilt only (Fig. 3.1-3), the intersection plane of the two cylinders (green surface in Fig. 3.1-3) has a normal vector inclined of $\Phi/2$ with respect to the longitudinal axis, while θ is equal to that of the upper cylinder. When both Tilt and Twist are present (Fig. 3.1-4), the vector that identifies the “hatch mark” in the initial position (h_0) and in the final position (h') was used to calculate the Twist angle. h_0 is the intersection of Y-X plane with the intersection plane of the two cylinders. Its projection in the Y-Z plane coincides with the normal vector j :

$$h_0 = k \times i_{\frac{1}{2}}$$

where:

$$i_{\frac{1}{2}} = \begin{bmatrix} \cos \Phi/2 \\ \sin \Phi/2 \cdot \sin \theta \\ -\sin \Phi/2 \cdot \cos \theta \end{bmatrix}$$

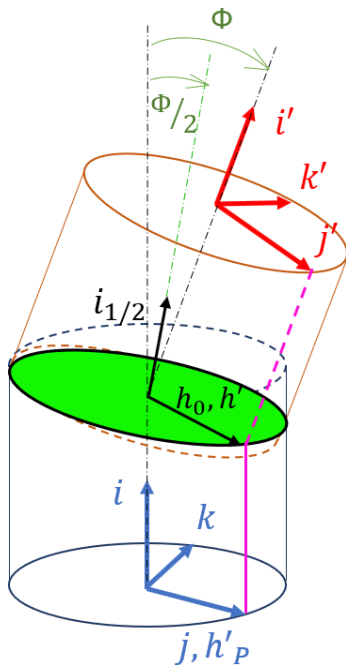


Fig. 3.1-3 Cylinders with tilt and no twist.

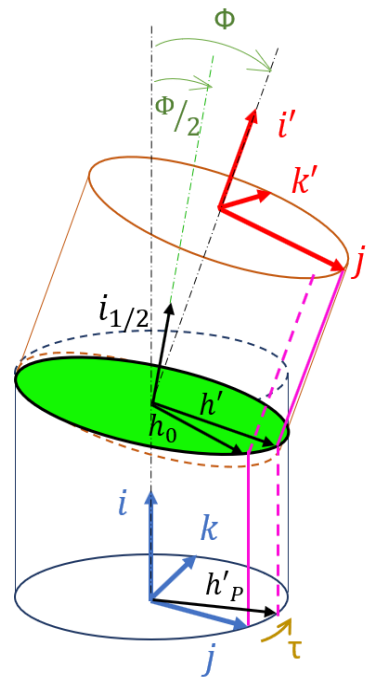


Fig. 3.1-3 Cylinders with tilt and twist.

After Twist, hatch mark moves and it is identified by the vector h' .

$$h' = k' \times i_{\frac{1}{2}} = \begin{vmatrix} i & j & k \\ k'_x & k'_y & k'_z \\ i_{\frac{1}{2}x} & i_{\frac{1}{2}y} & i_{\frac{1}{2}z} \end{vmatrix} =$$

$$= i \left(k'_y \cdot i_{\frac{1}{2}z} - k'_z \cdot i_{\frac{1}{2}y} \right) + j \left(k'_z \cdot i_{\frac{1}{2}x} - k'_x \cdot i_{\frac{1}{2}z} \right) + k \left(k'_x \cdot i_{\frac{1}{2}y} - k'_y \cdot i_{\frac{1}{2}x} \right)$$

Its projection in Y-Z plane is h'_P : from this it is possible obtained the angle τ .

$$\begin{cases} h'_{P,Z} = h'_P \cdot \sin\tau \\ h'_{P,Y} = h'_P \cdot \cos\tau \end{cases} \Rightarrow tg\tau = \frac{h'_{P,Z}}{h'_{P,Y}}$$

Substituting the new formula is:

$$tg\tau = \frac{h'_{P,Z}}{h'_{P,Y}} = \frac{k'_x \cdot i_{\frac{1}{2}y} - k'_y \cdot i_{\frac{1}{2}x}}{k'_z \cdot i_{\frac{1}{2}x} - k'_x \cdot i_{\frac{1}{2}z}} = \frac{k'_x \cdot \sin\frac{\Phi}{2} \cdot \sin\theta - k'_y \cdot \cos\frac{\Phi}{2}}{k'_z \cdot \cos\frac{\Phi}{2} + k'_x \cdot \sin\frac{\Phi}{2} \cdot \cos\theta}$$

The Twist angle ranges from -180° to $+180^\circ$.

The Tilt-Twist Method described reaches a singularity condition when Φ approaches 180° . This singularity is the same reached for 90° in Euler-Cardan method, but Tilt-Twist Method certainly allows in a more satisfactory way to describe wide movements (Crawford, 1999)

In conclusion, considering all three angles, the complete convention is shown in Tab.3.1-1.

	FLEXION- EXTENSION	LATERAL BENDING	AXIAL ROTATION
POSITIVE +	Flexion	Right	Right
NEGATIVE -	Extension	Left	Left

Tab. 3.1-1 Angles convention.

3.2 Sensors Orientation: Spinal Segments Motion

Each sensor, at each sample time (sampling frequency equal to 50 Hz), returns its rotation matrix (r_{SEN}), that is its space orientation, like a vector [1x9].

$$r_{SEN} = [a \ b \ c \ d \ e \ f \ g \ h \ i]$$

his vector is then converted in a rotation matrix [3x3] ${}^G R_{SEN}$ that represents the orientation of sensor SEN attached on to specific spinal segment with respect to the global reference frame (Fig. 3.2-1).

$${}^G R_{SEN} = \begin{bmatrix} a & d & g \\ b & e & h \\ c & f & i \end{bmatrix}$$

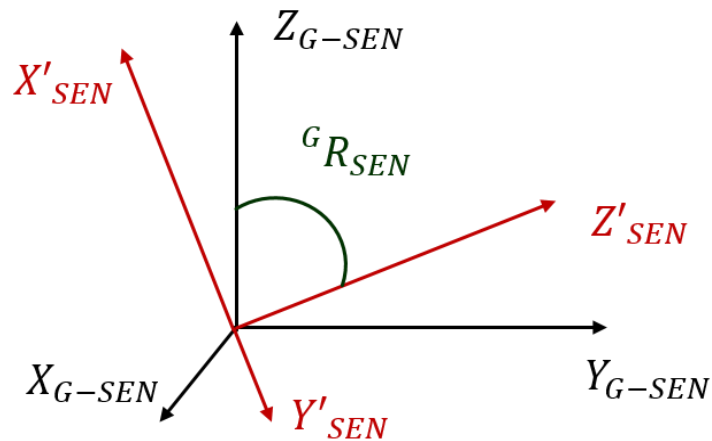


Fig. 3.2-1 Sensor orientation in the global reference frame.

Each column of rotation matrix represents the unit vector of the sensor local reference frame (indicated by “'”). Frame by frame, the columns change because the orientation of sensor local reference frame changes with respect to the global reference frame.

$${}^G R_{SEN} = [{}^G X'_{SEN} \quad {}^G Y'_{SEN} \quad {}^G Z'_{SEN}]$$

Before starting each test, the subject was asked to stand in upright posture for a few seconds. This was necessary to obtain calibration data from each sensor then used to define the neutral position or the initial sensor orientation.

$${}^G r_{SEN-neutral} = \text{mean}({}^G r_{SEN}(\text{calibraion samples})).$$

The row vectors of rotation matrix belonging to calibration time were averaged and converted in a [3x3] rotation matrix (${}^N R_{SEN}$). Focus was taken to check that calibration matrices obtained

were orthogonal and normal matrices. This means that the unit vectors of rotation matrix were orthogonal each other and their absolute value was equal to one.

Each sample time during dynamic movements were reported with respect to the neutral rotation matrix:

$${}^N R_{SEN} = {}^G R_N^{-1} \cdot {}^G R_{SEN}$$

Each sample time, relative rotation matrix between two consecutive and adjacent sensors was calculated like this:

$${}^{s_inf} R_{S_sup} = {}^N R_{S_inf}^{-1} \cdot {}^N R_{S_sup}$$

Through this mathematical operation, the reference system of a superior sensor is expressed in the local reference system of inferior inertial sensor (Fig. 3.2-2).

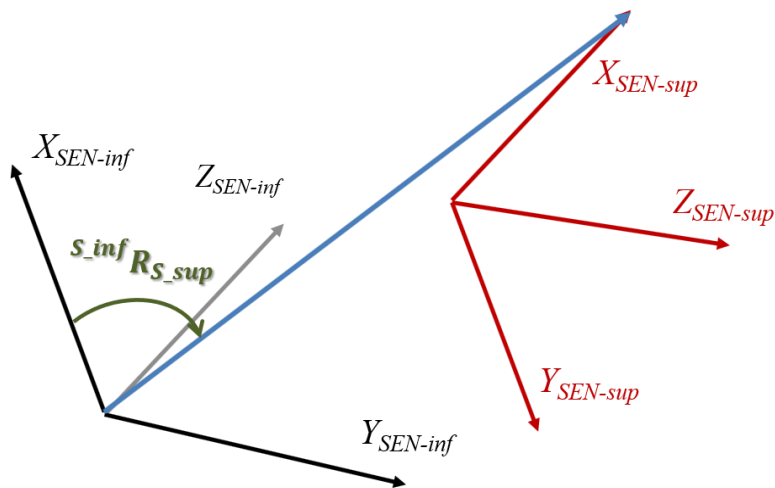


Fig. 3.2-2 Orientation of the upper sensor reference system relative to lower sensor reference system.

Rotational matrices calculated are:

- C7 expressed in T6: ${}^{T6} R_{C7} = {}^N R_{T6}^{-1} \cdot {}^N R_{C7}$;
- T6 expressed in T12: ${}^{T12} R_{T6} = {}^N R_{T12}^{-1} \cdot {}^N R_{T6}$;
- T12 expressed in L3: ${}^{L3} R_{T12} = {}^N R_{L3}^{-1} \cdot {}^N R_{T12}$;
- L3 expressed in S1: ${}^{S1} R_{L3} = {}^N R_{S1}^{-1} \cdot {}^N R_{L3}$;

From rotation matrices were obtained spherical angles (Φ , θ , τ) and then planar angles of Flexion-Extension (FE), Lateral Bending (LB) and Axial Rotation (ROT) were obtained using the Tilt-Twist Method described in Section 3.1.

3.3 Gait Analysis: Walk and Gait Cycle

Walking represents one of the main daily activities and for this reason its analysis is of fundamental importance. Gait analysis has several aims: understand the relationship between movement and control movement, understand the mechanisms that generate movement, analyse the pathological state of the subject in order to identify the right clinical treatment and ultimately to improve sports performance. The gait control occurs through the succession of a series of events: command generation from the central nervous system, signal transmission to the peripheral nervous system, specific muscles contraction, forces and moments generation in the joints, segments limb movement, movement coordination between segments and interaction with external environment. Walking is a repetitive movement consisting of two main phases: stance and swing phases. The stance phase covers 60% of the gait cycle, while the swing phase represents 40% of it. In general, the stance phase starts when one heel impacts the ground and ends when the same foot detaches from the ground; the swing phase starts from the detachment of the foot from the ground and ends with its new impact to the ground. Each of the two macro-phases of the gait cycle can be divided into subphases (Jacquelin, 1992) (Fig. 3.3-1):

- Initial contact (0%): the heel impacts the ground;
- Loading response (0-10%): phase in which the sole of foot is all in contact with the ground;
- Mid-stance (10-30%): phase in which the contralateral limb exceeds the stance leg;
- Terminal-stance (30-50%): the heel rises from the ground;
- Pre-swing (50-60%): phase in which the foot is completely detached from the ground and ends the stance phase;
- Initial swing (60-70%): the leg is accelerated forward;
- Mid-swing (70-85%): the foot overcomes the body;
- Terminal swing (85-100%): it is the deceleration phase that ends with the heel impact on the ground.

In order to determine if a subject is affected by pathologies that involved walking, temporal and geometric parameters were measured. The time taken by the limb is measured both in the stance phase and in the swing phase: if for both limbs the time is the same than the subject is not affected by any pathology. Geometric parameters are: step length (distance between two heel-strikes of the same foot); semi-step length; step width; foot angle.

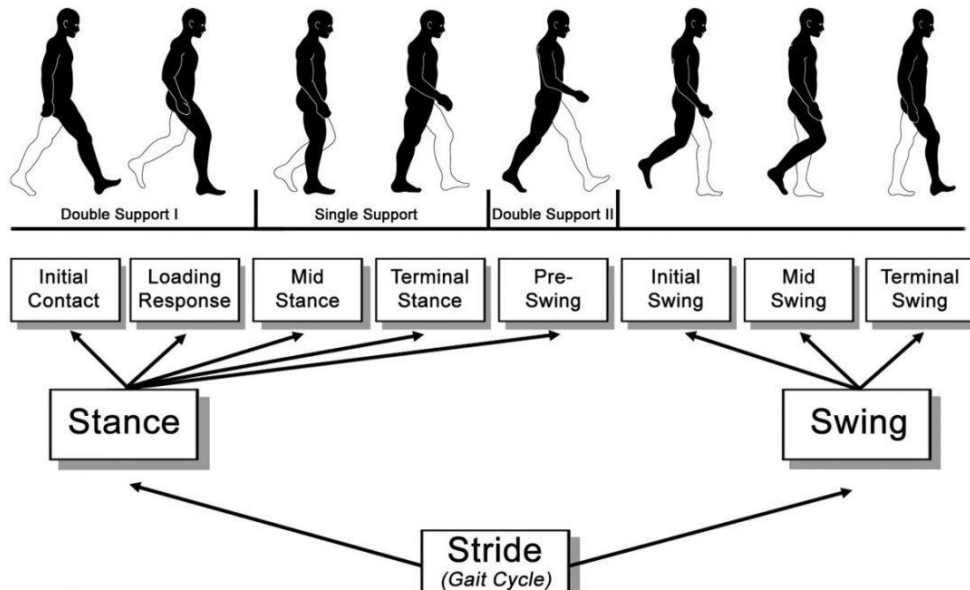


Fig. 3.3-1 Gait cycle: Macro phases and subphases.

In according to (Comparison of Different Motion Capture Setups for Gait Analysis Validation of spatio-temporal parameters estimation, 2018) the information about gait cycle were extracted by acceleration Z of inertial sensor at T12 level. In particular, in correspondence of positive peaks of antero-posterior acceleration were identified the heel-strikes, while the negative peaks represent the toe-rises. It was used the information of angular velocity around Y axis of the same sensor too. If between two consecutive heel-strike, the angular velocity mean was negative then the gait cycle was referred to left leg, otherwise the gait cycle was referred to right leg. Conclusively a gait cycle was identified between two heel-strike of the same leg. In Fig. 3.3-2 is shown the acceleration Z overturned and the angular velocity Y filtered with a low pass Butterworth filter of fourth order and with a cut-off frequency of 15 Hz.

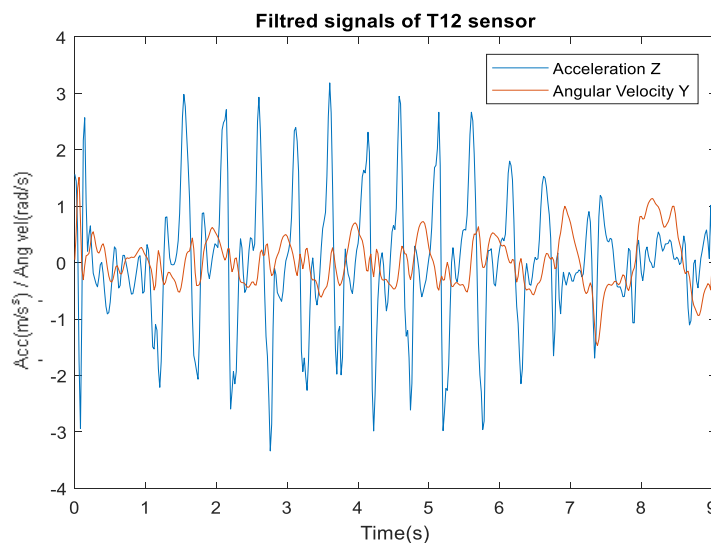


Fig. 3.3-2 Acceleration and angular velocity from T12 sensor vertebral level.

Fig. 3.3-3 and Fig. 3.3-4 show the same trends but with an identification of left and right heel strike, left and right toe-off. In the first graph is possible appreciate that the gait considered starts with a left leg cycle, while the second graph starts with a right leg cycle.

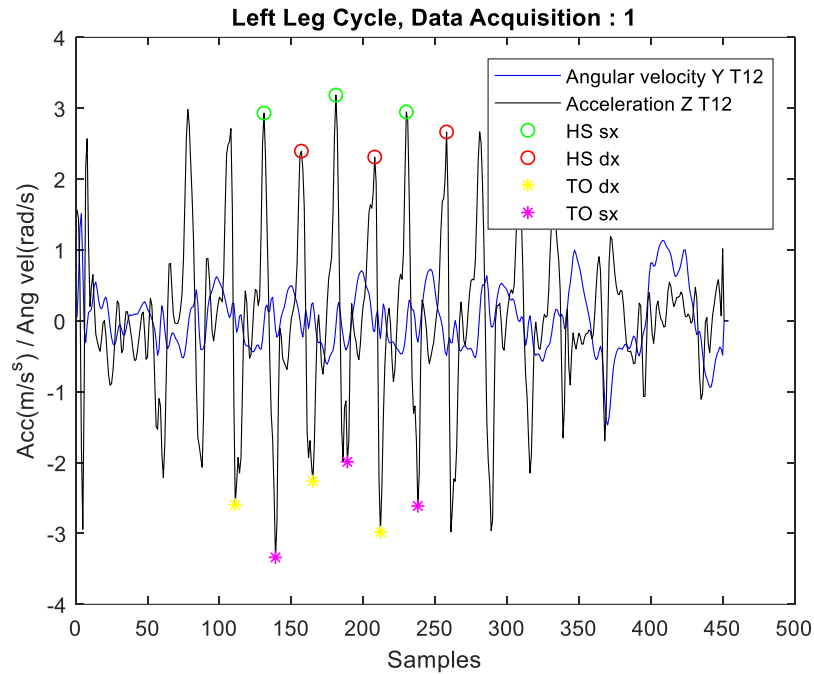


Fig. 3.3-3 An example of left leg cycle sequence.

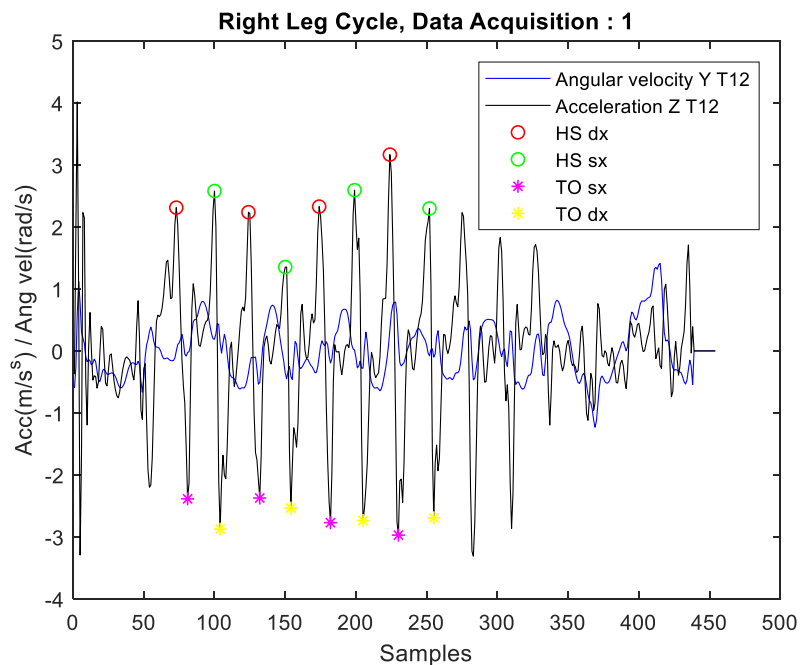


Fig. 3.3-4 An example of right leg cycle sequence.

4. Preliminary Tests

The spinal column is considered formed by a series of rigid segments connected to each other by joints. To obtain a complete description of the column movements, it would be necessary to have a number of inertial sensors equal to the number of vertebrae that constitute it. Since this is obviously not possible, it was decided to position the sensors strategically. In fact, from the literature analysis, and thanks to the collaboration with medical team, it was decided to position the sensors on five vertebral levels: C7, T6, T12, L3 and S1. Each sensor is considered attached to the corresponding spinal segment, in other words, the sensor positioned on the specific vertebra represents the segment between this and the next sensor (Fig. 4-1). More in detail:

- The sensor on C7 identifies the C7-T6 segment;
- The sensor on T6 identifies the T6-T12 segment;
- The sensor on T12 identifies the T12-L3 segment;
- The sensor on L3 identifies the L3-S1 segment;
- The sensor on S1 identifies the Pelvis segment.

The movements of the identified spinal segments can be described with a reference system in accordance with the adopted angles convention. Thus, the Z-axis is perpendicular to the frontal plane and directed forward, the Y-axis is perpendicular to the sagittal plane and directed to the left of the subject, the X-axis perpendicular to the transverse plane and directed downwards.

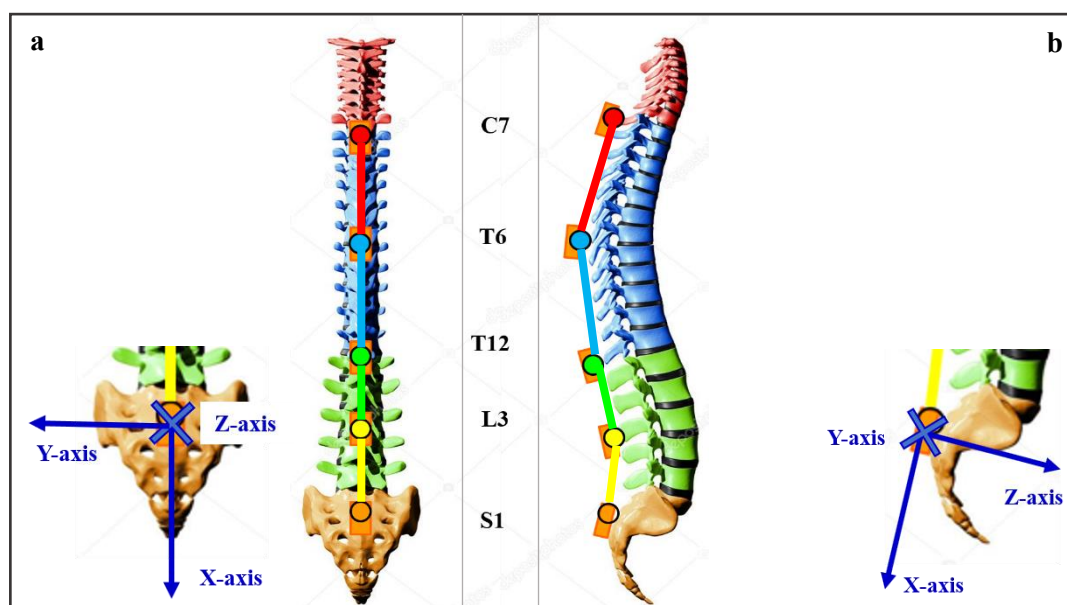


Fig. 4.4-1 Representation of segment by each sensor: **a** frontal plane view and reference system description, **b** sagittal plane view and reference frame description.

4.1 Preliminary Test with Magnet

In order to become familiar with inertial sensors used later, with MT Manager software and with a possible manipulation of the data obtained, a test was performed with only two MTx sensors (Xsens Technologies). For this purpose, a circumference subdivided into 12 sections was drawn on a cardboard (Fig. 4.1-1): each section had an amplitude of 30° (from 0° to 360°). Test was performed in an environment where there were no metallic materials that could act as a disturbance to the magnetometer inside the Xsens sensors.

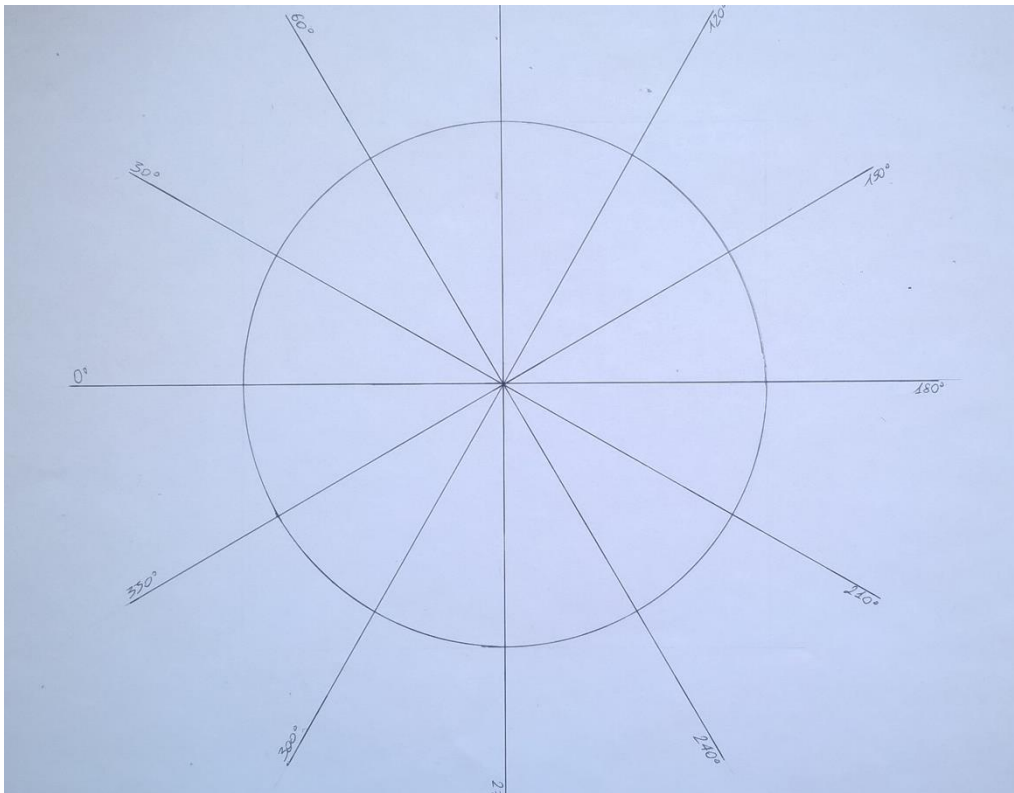


Fig. 4.1-1 Circumference with twelve section drawn.

As already mentioned, only two sensors were used: one fixed and the other movable. These, together with XBus Master, formed the kinematic chain to analyse. The fixed IMU (n° 681) has been positioned inside the drawn circumference (Fig. 4.1-2) and, to guarantee its immobility, a double-sided adhesive tape has been used to keep it anchored to the cardboard. The second sensor represented the mobile inertial sensor (n°682): this was moved along the circumference from section to section (Fig. 4.1-2). Due to the intertwining of the cables, it was only possible to complete the entire circumference twice.

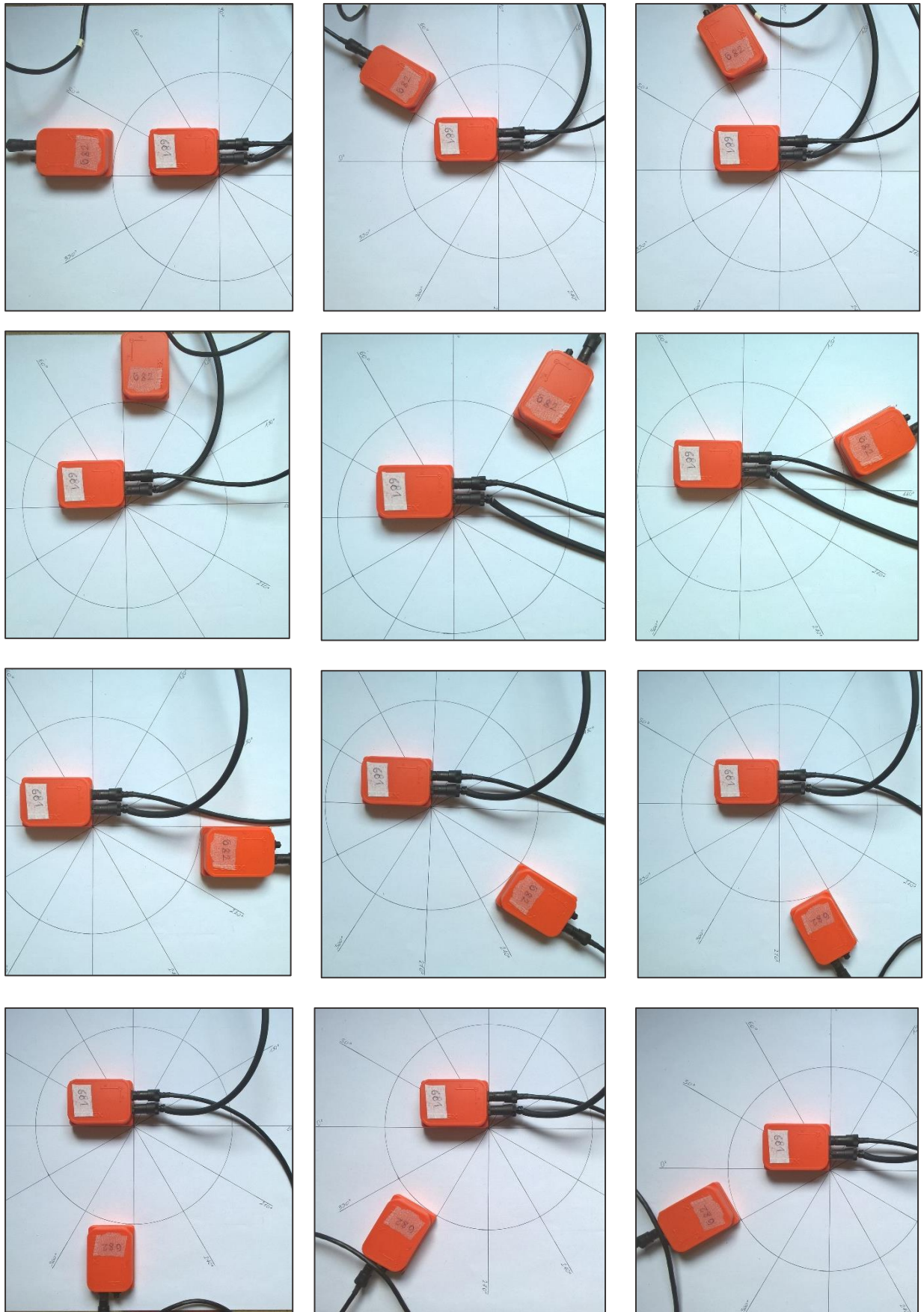


Fig. 4.1-2 Fixed IMU (n° 681) inside the circumference, Moveable IMU (n° 682) along circumference sections.

In Fig. 4.1-3 patterns of the 3 angles relative to each sensor have been reported. The angles shown represent one of the possible outputs of MT Manager software. These patterns are not related to one sensor relative to the other, but to a sensor relative to itself. In fact, the patterns of fixed sensor remain almost constant except for a few peaks probably due to sudden movements of the sensor itself. For the movable sensor, the Yaw angle is the one with the most constant variations. Remembering that the Yaw angle is the angle around Z axis of the Xsens sensor, this result is plausible. In fact, mobile sensor, moving along the circumference, rotates mainly around its Z axis. The circumference was travelled clockwise and this implies a negative rotation of the sensor around its Z axis and this again justifies the pattern of Yaw angle of movable sensor.

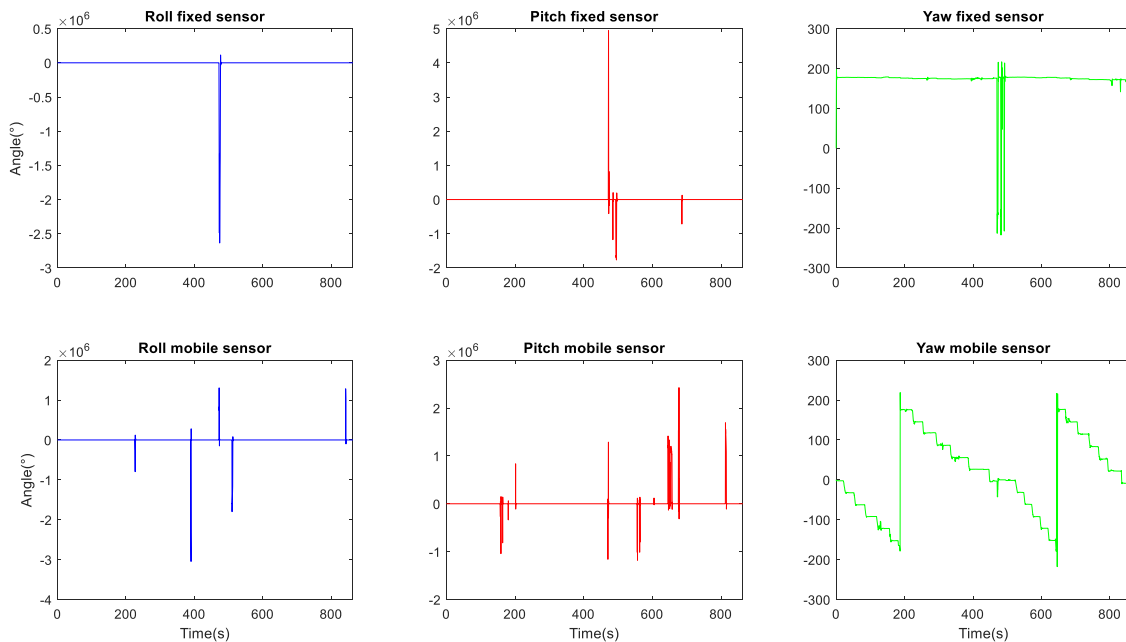


Fig. 4.1-3 Roll, Pitch and Yaw angles of two sensors (up row fixed sensor, down row moveable sensor).

Since the objective is to obtain relative orientation between the two sensors, it is necessary handle rotation matrices data. After acquisition (sampling frequency $f_c=50\text{Hz}$), the data were exported to an Excel file and then manipulated in Matlab.

When movable sensor reached the mark indicating the section, a magnet was brought closer to it. During data processing it was easier recognize the increase orientation of 30° between the two sensors. The sensor was maintained in that position for about 10 s.

In Matlab, first of all, the files related to the two IMUs have been filtered low pass with a suitable cut-off frequency identified with parametric spectral estimation. Subsequently, the

magnetic peaks that correspond to the proximity of the magnet were identified: the parts of signal between two peaks were examined to obtain orientation information. The absolute value of magnetic field (Fig. 4.1-4) of mobile sensor was used to search for magnetic peaks:

$$|Mag| = \sqrt{Mag_X^2 + Mag_Y^2 + Mag_Z^2}$$

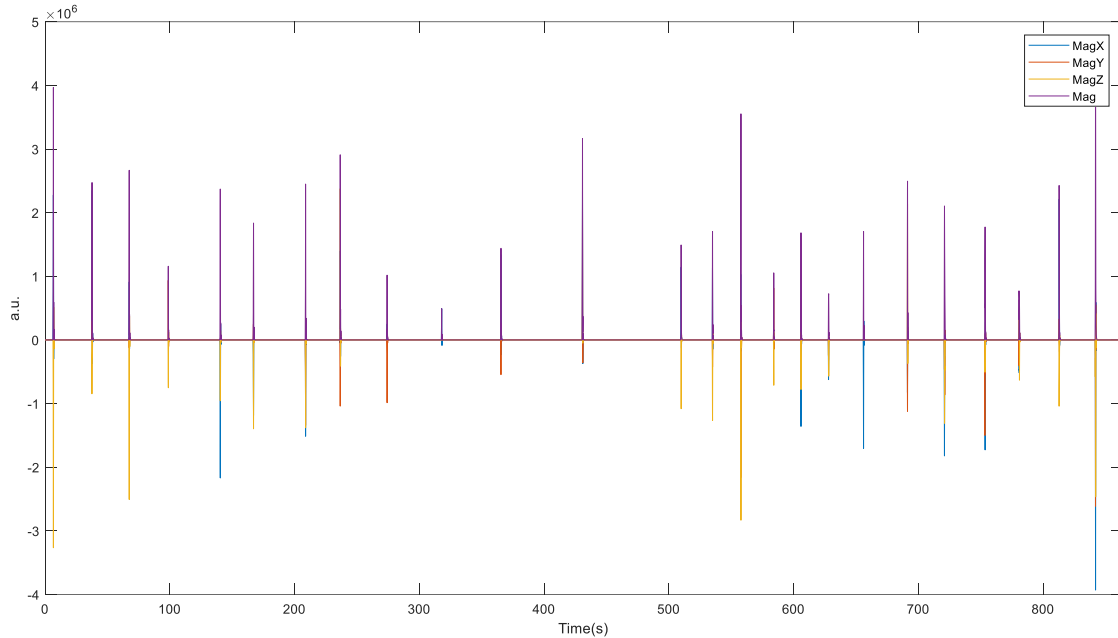


Fig. 4.1-4 Magnetic field in X, Y and Z directions of moveable sensor and absolute magnetic field (purple signal).

To define the orientation of one sensor with respect to the other, the rotation matrices provided by the software are used. For each sensor and for each sample time, a row matrix was obtained. This matrix represents the rotations of sensor respect with global reference frame:

$$R_{GS} = R_{\psi}^z R_{\theta}^y R_{\phi}^x$$

By mathematical operation rotation matrix of movable sensor (S2) was described respect with fixed sensor (S1) reference frame:

$${}^{S1}R_{S2} = {}^{S2}R_G \bullet {}^G R_{S1} = inv({}^G R_{S2}) \bullet {}^G R_{S1}$$

This relative matrix provided the information to obtain Euler angles. It was used a Matlab function “*rotm2eul*”. This function requires the sequence to calculate the angles and it has been set “XYZ” sequence. This means that sensor 2, the mobile one, to be expressed in the local reference system of sensor 1, the fixed one, requires a rotation around the X axis, followed by

a rotation around the Y axis and finally around the Z axis. In other words, they are the rotations necessary for the local reference frame of sensor 2 to align with the local reference system of sensor 1. Fig. 4.1-5 shows the trends on the angles thus obtained and transformed into degrees. In addition the start and the end indices of the magnetic peak were indicated on the trend of the Yaw angle. From the image several aspects can be noted: the first one is that the mobile sensor repeats the same motion twice (at the middle of the acquisition the trend repeats itself); this because the circumference has been crossed twice; the second most important aspect is that, when sensors are aligned on the same mark section circumference, but with the opposite X axis (Fig. 4.1-6), the corresponding rotation shifts repeatedly in the range $[-180^{\circ} \div +180^{\circ}]$.

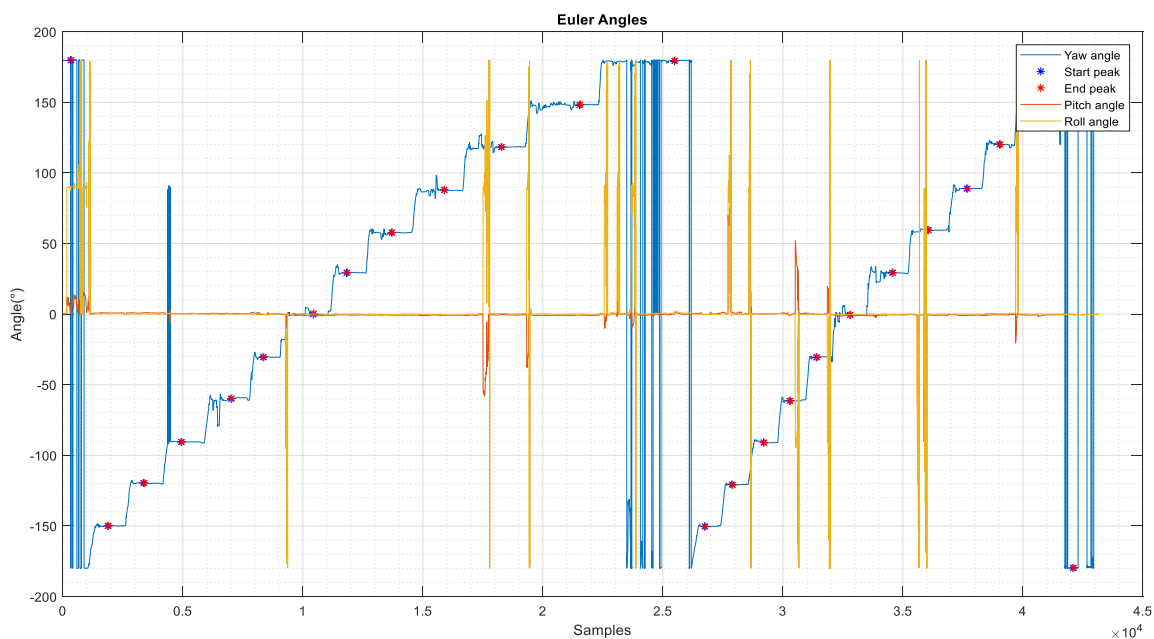


Fig. 2.2.4.1-5 Angle patterns of relative matrix.

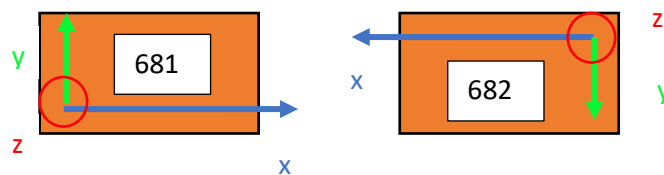


Fig. 2.2.4.1-6 Axis of the two sensors aligned on the same sector mark.

At this point accuracy of the method identified was tested considering the 200 samples at the end of the magnetic peak, obtained the boxplot of which in Figs from 4.1-7 to 4.1-18 are reported those relating to the first rotation.

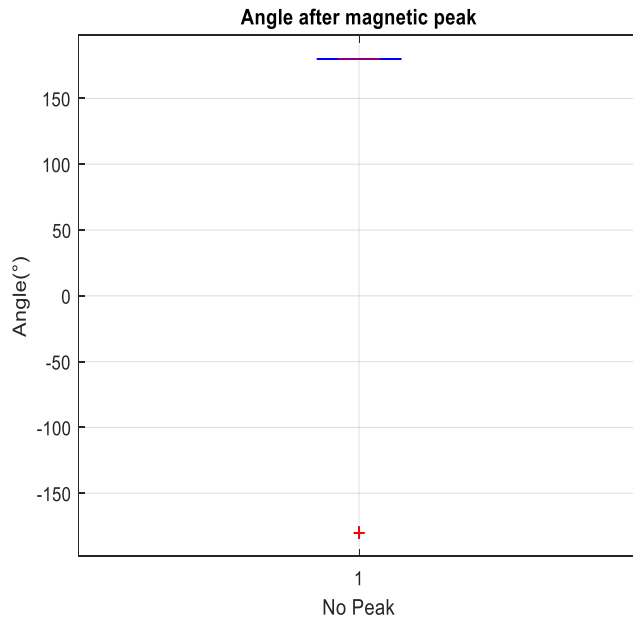


Fig. 4.1-7 Boxplot of 180° rotation.

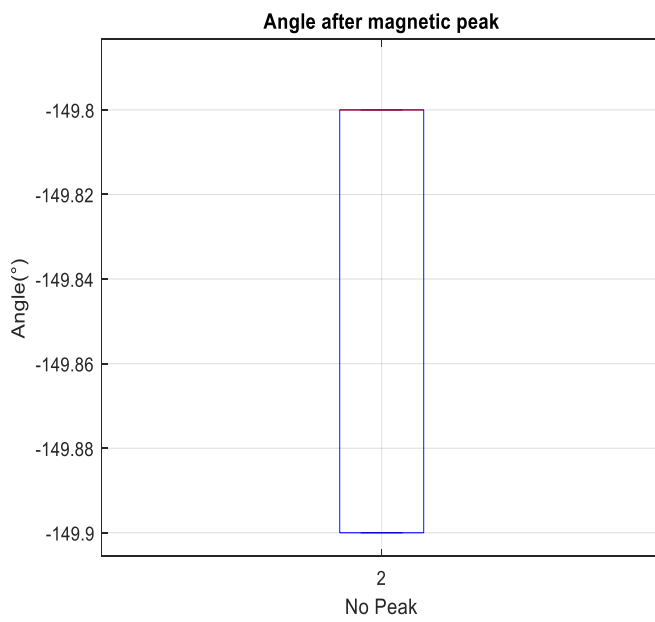


Fig. 2.2.4.1-8 Boxplot of -150° rotation.

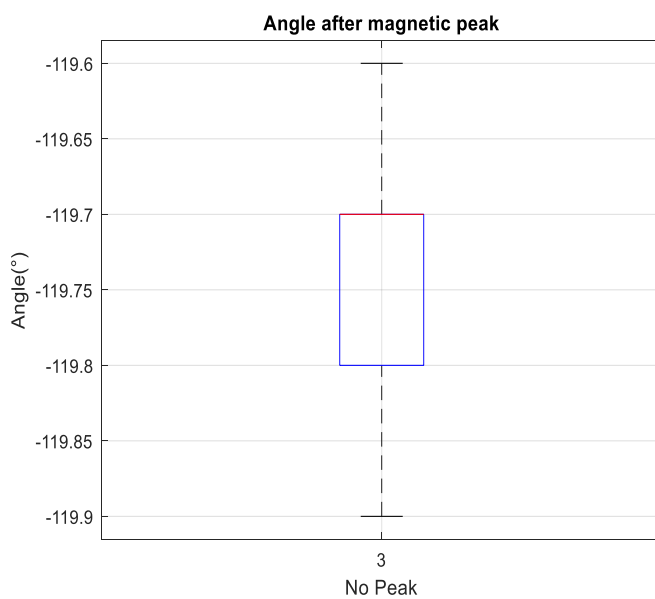


Fig. 2.2.4.1-9 Boxplot of -120° rotation.

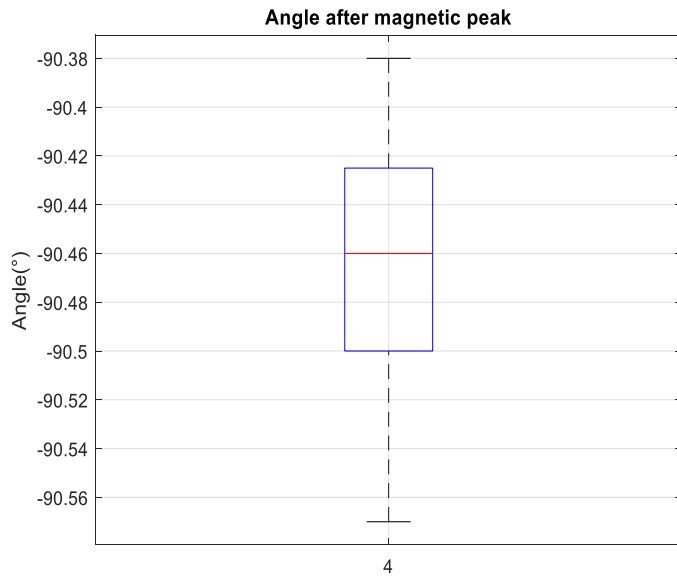


Fig. 2.2.4.1-10 Boxplot of -90° rotation.

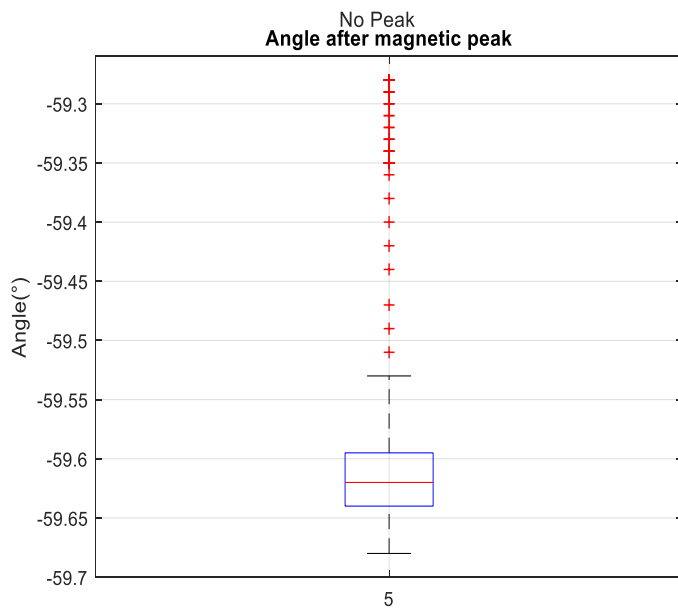


Fig. 2.2.4.1-11 Boxplot of -60° rotation.

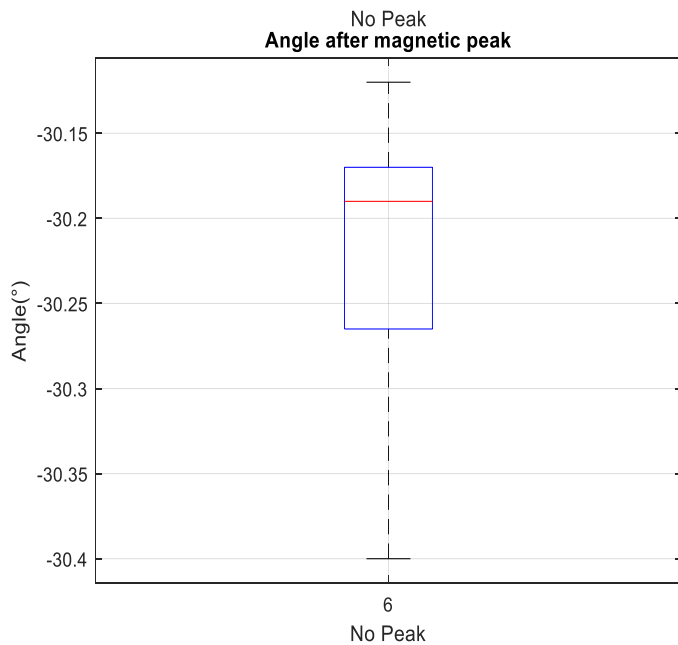


Fig. 2.2.4.1-12 Boxplot of -30° rotation.

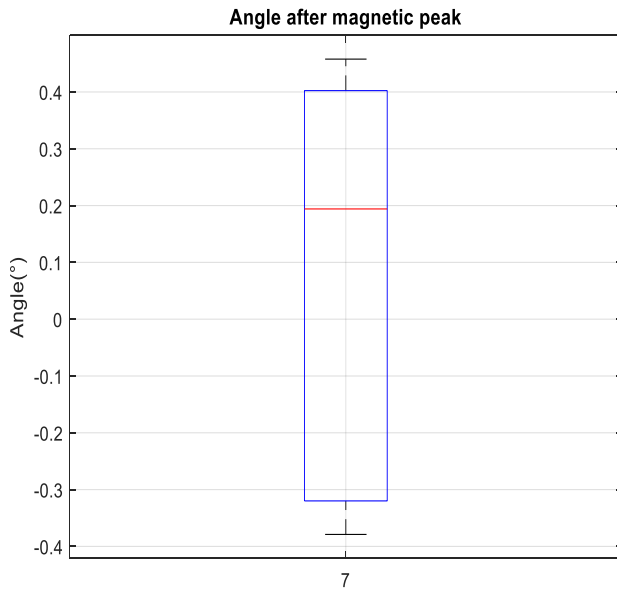


Fig. 2.2.4.1-13 Boxplot of 0° rotation.

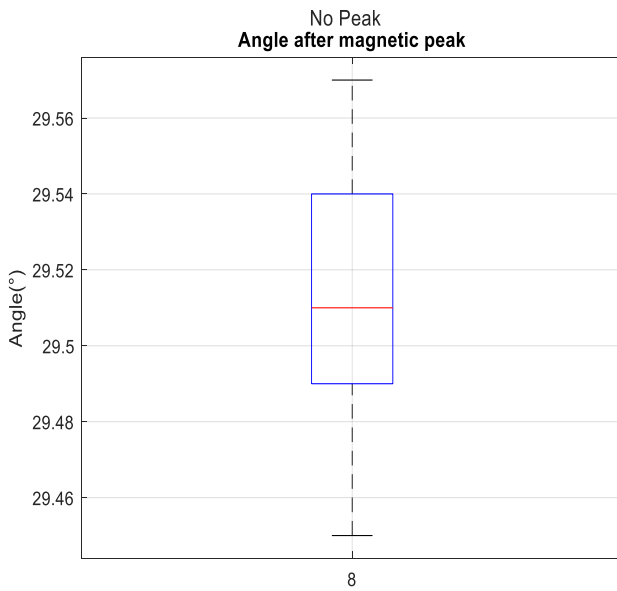


Fig. 2.2.4.1-14 Boxplot of 30° rotation.

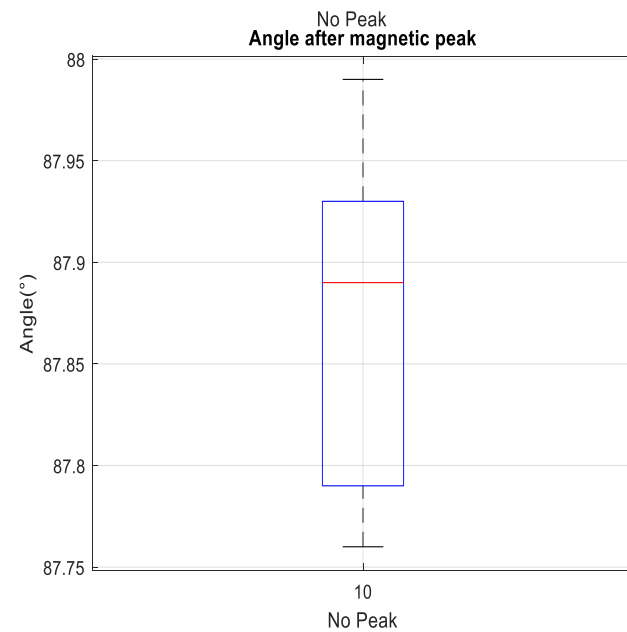


Fig. 2.2.4.1-15 Boxplot of 90° rotation.

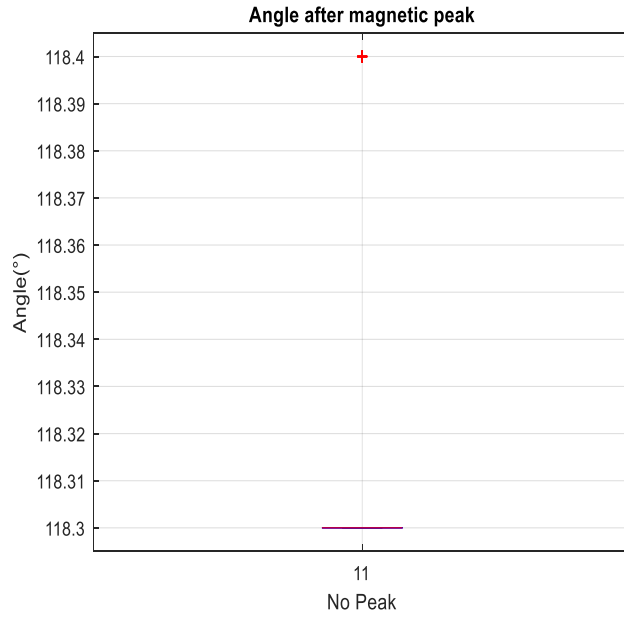


Fig. 2.2.4.1-16 Boxplot of 120° rotation.

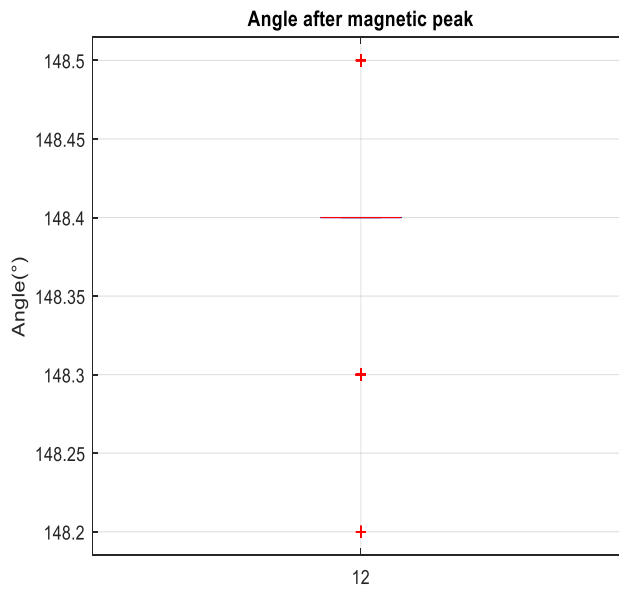


Fig. 2.2.4.1-17 Boxplot of 150° rotation.

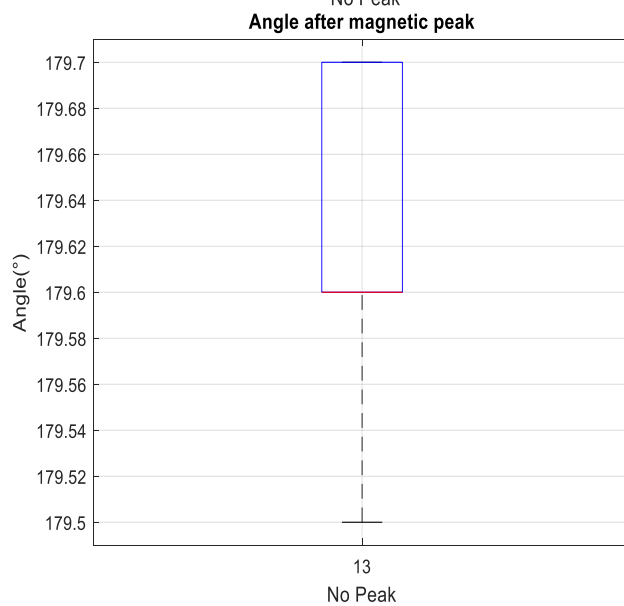


Fig. 2.2.4.1-18 Boxplot of 180° rotation.

Tab 4.1-1 shows the average values of the angles in the 200 samples following the end of the magnetic peak and the corresponding standard deviations.

Section Angle (°)	Mean Rotation Angle (°)	Standar deviation (°)
0	163.74	74.80
	179.62	0.0559
30	-149.85	0.0501
	-150.45	0.0501
60	-119.74	0.096
	-120.91	0.0802
90	-90.462	0.0485
	-91.137	0.0859
120	-59.558	0.128
	-61.386	0.0368
150	-30.221	0.0716
	-30.314	0.0894
180	0.0551	0.345
	-0.4693	0.0702
210	29.514	0.0349
	29.268	0.0407
240	57.865	0.0263
	59.385	0.0655
270	87.865	0.0678
	88.844	0.0509
300	118.30	0.0218
	120.02	0.0875
330	148.38	0.0578
	150.08	0.7410

Tab. 2.2.4.1-1 Mean and standard deviations of rotation angle.

As Tab. 4.1-4 shows, the values of the rotations obtained are not equal to the amplitude of the sectors of the circumference that divide the two sensors, but the consideration to be made concerns the rotation, positive or negative, necessary that the mobile sensor must make around its own axes to aligned with those of the fixed sensor. For example, taking into consideration the case in which the mobile sensor is positioned on 300° mark section, the average rotation, considering the first turn, is $118.30^\circ \pm 0.0218$. This means that the mobile sensor must make a positive rotation around Z axis equal to that value.

4.2 First Preliminary Test with Xsens

Once the optimal positioning of sensors to describe spine movements was identified (Fig 4-1), this configuration was tested on a young healthy female subject, not affected from any neurological or physical problems. The characteristics of the subject are shown in Tab. 4.2-1.

Subject Gender	Age (years)	Height (cm)	Weight (kg)
Female	24	151	45

Tab. 4.2-1 Characteristics of subject recruited.

5 MTx sensors (Xsens Technologies B.V.) were fixed to the subject's spine using double-sided adhesive tape. To ensure greater adherence of sensors to the skin, especially during movement phases, additional reinforcements with scotch and elastic bands have been used. The positioning of the sensor on S1 vertebra was facilitated by the use of the elastic band with Velcro closures supplied by Xsens group. The sensors at level of L3 and T12, due to interference issues, the proximity between the vertebrae in question and the size of the sensor themselves, were positioned in a different orientation from the other sensors at C7, T6 and S1 levels. For this reason, during the data processing phase, the rotation matrices of the two sensors were rotated clockwise by 90° (negative rotation around Z-axis) (Fig. 4.2-1).

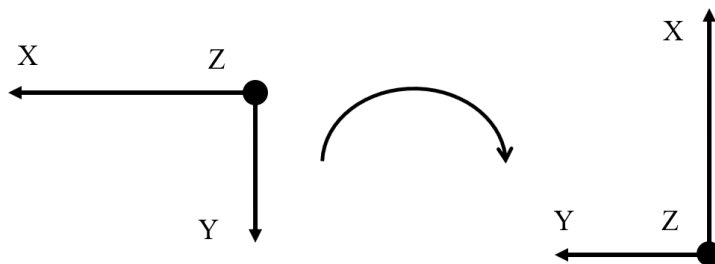


Fig. 4.2-4.2 Rotation of sensors reference frame by 90° around Z-axis.

The IMUs were connected to each other and to the Xbus Master by cables so as to form a continuous and closed chain. The subject was asked to perform a series of tests in order to verify the motion between the spinal segments:

- Elementary exercises in the main planes: Lateral Bending in the frontal plane, Flexion-Extension in the sagittal plane, Axial Rotation in the transverse plane;
- Walking at comfortable self-selected speed;
- Walking at higher self-selected speed.

In the case of walking at the two different speeds, the subject was asked to walk barefoot along a path of 6.60 m bordered by two indicators drawn on the floor. When each indicator was

reached, the subject made a characteristic movement so as to allow its recognition during the post-processing phase. At first the movement required was to subject lift onto the tips. However, from the acceleration trends displayed in real time on the MT Manager software, this movement did not have any strong characteristics. For this reason, the characteristic movement chosen was the impact of one foot on the ground (Fig.4.2-2).



Fig. 4.2-3Foot impact to the ground when indicator was achieved.

In order to correlate the profiles of the spinal angles and their ROMs to the walking speed, this was calculated using an indirect method: the length between the two indicators (6.60 m) was divided by the time necessary to cover this path.

In the case of walking at comfortable self-selected speed, there are two test sessions: between one session and the next, in fact, the sensors are removed and then repositioned. In this way, the variability in the sensors positioning is evaluated.

The choice to add the elementary movement tests was to verify the correctness of data elaboration. Moreover, elementary movement tests could be interesting if executed by Parkinson's subject. In fact, the Parkinson's disease usually produces a reduced mobility of spine caused by muscle weakening and reduced ability to maintain balance. Instead, during walking a Parkinsonian subject is flexed with the torso forward more than a healthy subject. In some cases, the spine is laterally bend and this condition names Pisa Syndrome. These inclinations could represent a reason for instability during gait and consequently one of major cause of falling. Furthermore, lumbar region must facilitate the axial rotation of pelvis and, in the same time, absorb lateral flexion that origins from pelvis (Rozumalski, et al., 2008).

4.3 Second Preliminary Test with Xsens

In the first preliminary test, tasks were tested in a laboratory whose spaces allowed a not very long walk (6.60 m). In addition, there were same instruments in the environment that could have been a source of disturbance for inertial sensors. First preliminary test highlighted the need to keep trunk sensors more fixed. In fact, even if adhesive tape has been used to reinforce the adherence, MTx sensors were moving blatantly. Then elastic bands with Velcro have been specially developed for T12 and L3 level sensors and they were used in the second preliminary test (Fig. 4.3-1). This session test was conducted in a different environment that permitted longer walk and no electronic instruments around. The subject involved was the same of that involved in first preliminary test, but this time tasks were performed wearing shoes. Moreover, this time the subject was instructed, in the elementary movements, not to force the achievement of the maximum flexion in the sagittal and frontal planes and the maximum rotation in the transversal plane. This is to prevent the sensors, despite the best anchorage, from moving from the starting position.

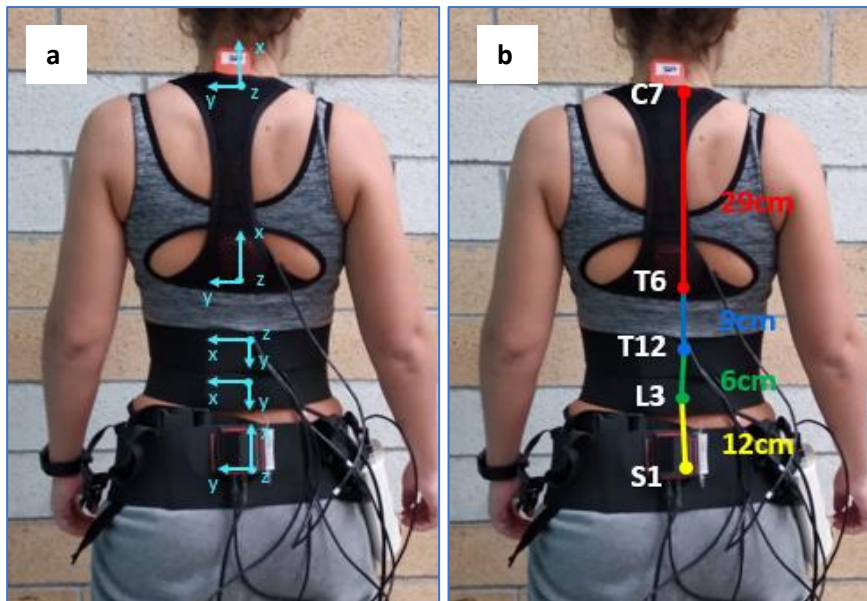


Fig. 4.3-1 a reference systems orientation of IMUs; b spinal segments length.

4.3.1 Elementary Movements

The subject was asked to execute a series of ten repetitions, each in every anatomical plane. The velocity of execution movement was self-selected by the subject recruited. Also, it was asked to hold pelvis to keep the lower limbs constantly in contact with the ground and to execute the movement purely in the plane selected. Before starting the data acquisition, the subject remained for few seconds in upright posture to extract data calibration.

Flexion-Extension in the Sagittal Plane

The subject was asked to execute a series of ten flexion-extension in the sagittal plane. The movement can be described as follows: it starts from the upright posture, follows a forward flexion of the torso without reaching the maximum; the torso returns to the starting position; it extends backwards; movement ends in an upright position. In post-elaboration phase, the entire data acquisition was subdivided between two consecutives extensions (Fig. 4.3.1-1). Flexion and extension peaks were recognised on Pelvis sagittal plane pattern. In particular, at positive peaks corresponded the maximum flexions, while negative peaks corresponded maximum extensions.

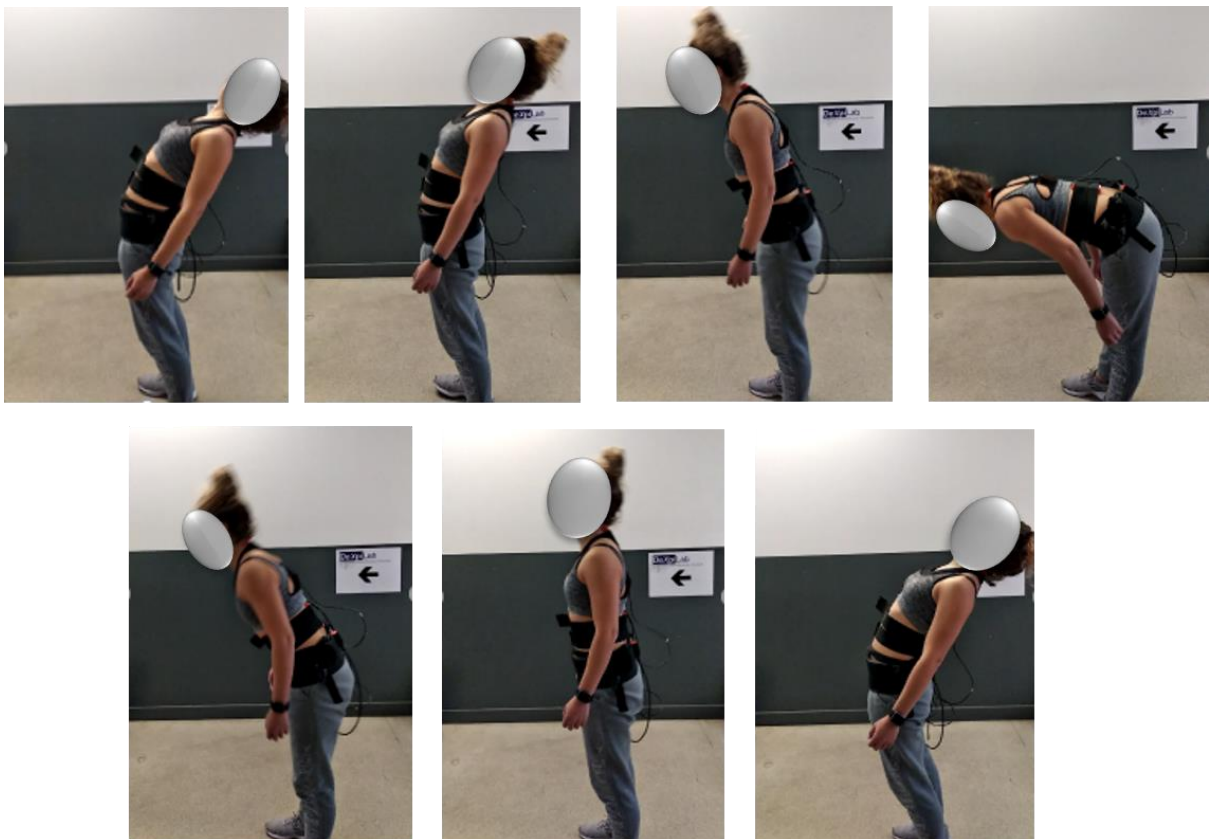


Fig. 4.3.1-1 Frame sequence to describe flexion-extension movement.

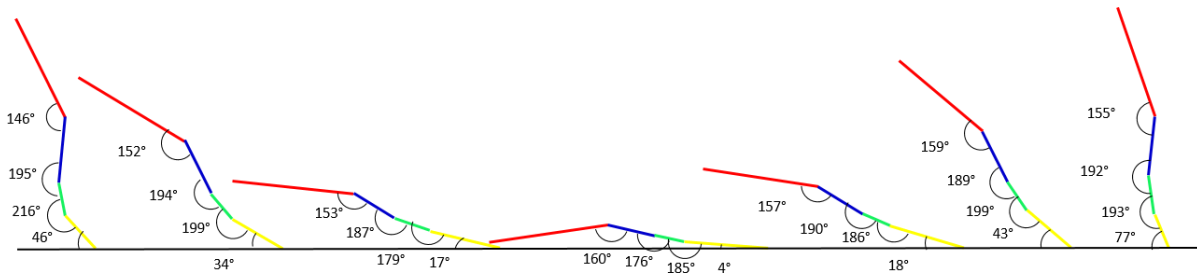


Fig. 4.3.1-2 Stick diagram between two consecutive upright posture.

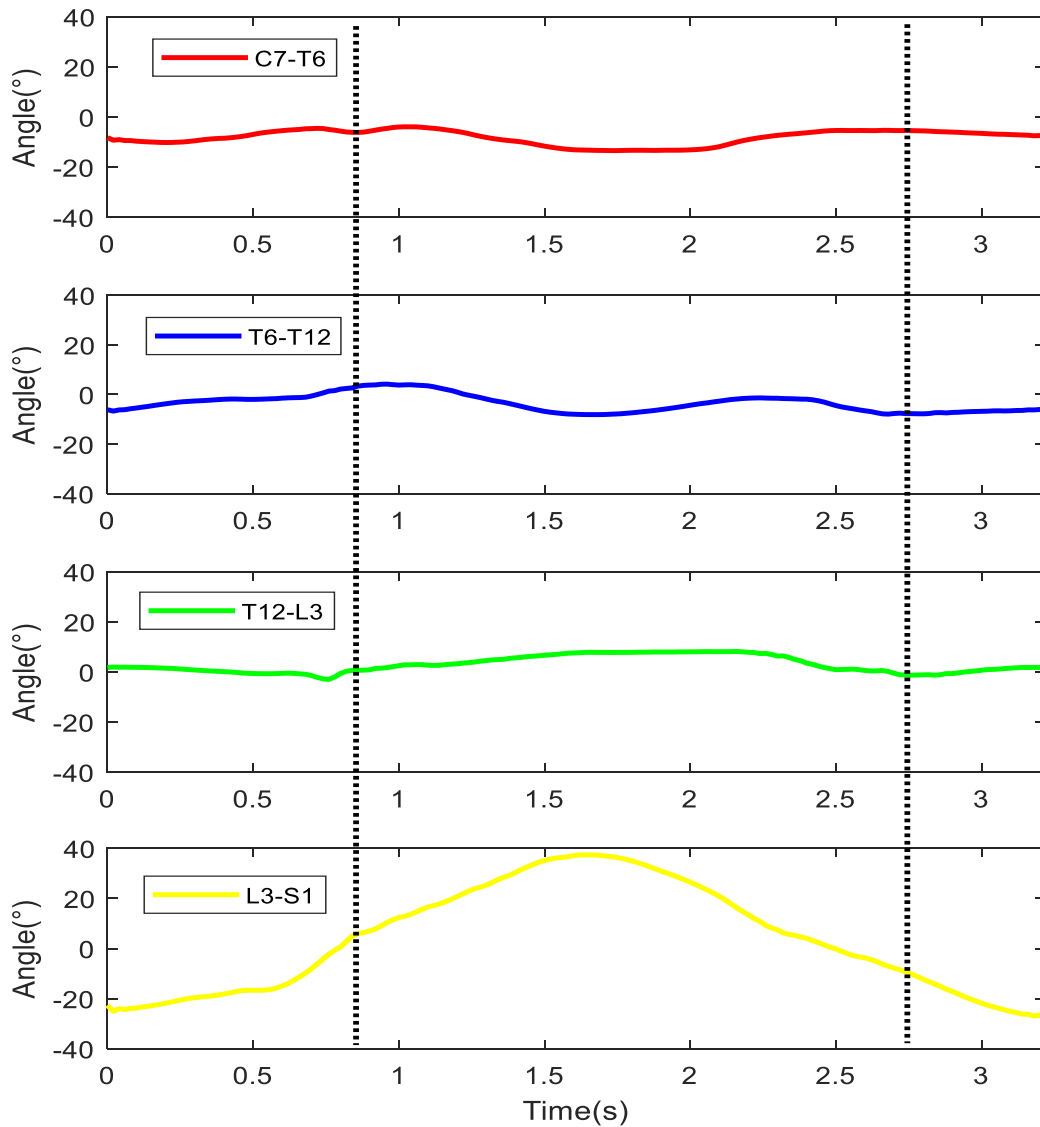


Fig. 4.3.1-3 Segments patterns between two consecutive extensions. Black dashed lines indicate upright posture.

To check that the angles obtained with the data elaboration described in Chapter 3 – Section 2 were right, one repetition was isolated. For each frame belonging to that repetition a stick diagram was drawn on it. Then the angles between segments were manually measured (Fig. 4.3.1-2). This was compared with the relative angles between the two dashed vertical line (Fig. 4.3.1-3). The angles shown in Fig. 4.3.1-2 are not perfectly equal to those shown in angles

trends (Fig. 4.3.1-3). This because the angles to realize the stick diagram were measured manually and inevitable errors were made.

For each segment the average pattern and standard deviation in three planes have been calculated. The Fig. 4.3.1-4 shows the mean trend in the sagittal plane. The segments that flex most (50% of the cycle) are the Pelvis and the L3-S1 segment with respect to S1. When these reach their maximum flexion, the T6-T12 segment tends to extend compared to T12-L3 segment. Moreover, when the maximum extension occurs, once again the segments that most extend are the Pelvis and the L3-S1 segment compared to S1.

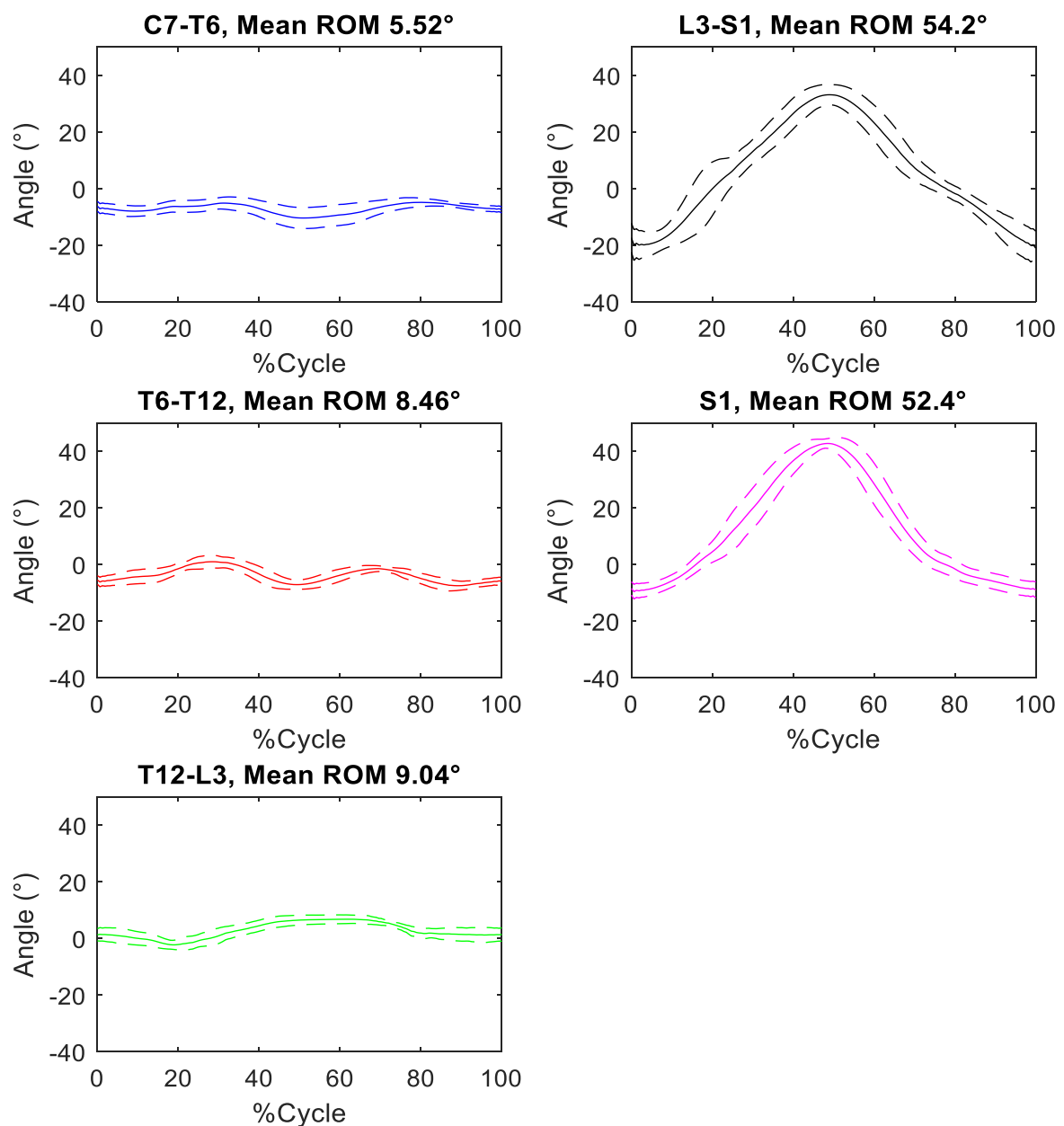


Fig. 4.3.1-4 Mean pattern and deviation of spinal segments in the sagittal plane during Flexion-Extension elementary exercise.

In Tab. 4.3.1-1 the mean ROMs in the three anatomical planes and their standard deviations are reported. The maximum values are reached in the Sagittal plane, but not for all segments considered. In fact, if the movements in the other two planes (Frontal and Transversal plane) are not negligible, for some segments (trunk segments) they are even greater than those occurring in the main plane of the elementary movement.

	ROM (SD) degree		
	Sagittal Plane	Frontal Plane	Transversal Plane
C7-T6	5.52 (5.65)	11.10 (4.79)	28.00 (3.19)
T6-T12	8.46 (4.11)	20.40 (2.80)	29.40 (3.55)
T12-L3	9.04 (3.47)	7.74 (2.57)	20.40 (2.85)
L3-S1	54.20 (11.39)	4.26 (2.01)	13.00 (3.13)
Pelvis	52.40 (4.64)	5.43 (0.65)	2.83 (2.84)

Tab. 4.3.1-1 ROMs in the three anatomical planes during flexion-extension exercise.

Lateral Bending in the Frontal Plane

The lateral bending movement is described as follows: from the upright posture the subject bends the torso to the left keeping the pelvis rigid, the maximum flexion is reached and the subject returns to the upright position; the same happens on the other side (Fig. 4.3.1-5). To divide data acquisition patterns between two upright consecutive postures, pelvis trend relative to frontal plane was analysed. Positive peaks identified maximum right lateral bending on the contrary negative peaks identified maximum left lateral bending. In Fig. 4.3.1-6 is shown a

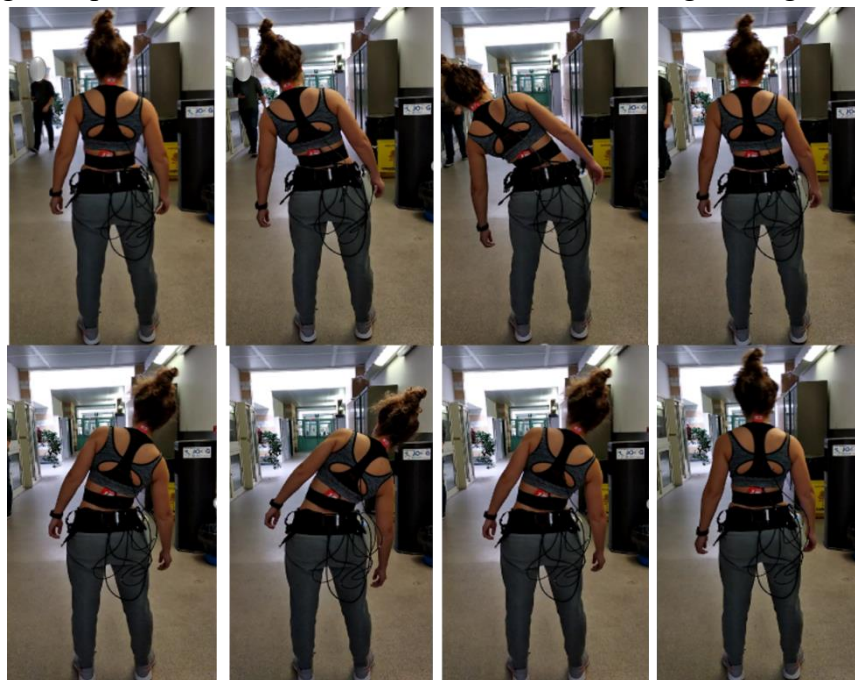


Fig. 4.3.1-5 Frame sequence to describe lateral bending movement.

stick model of one lateral bending movement between two consecutive upright posture. This was compared with the relative angles (Fig. 4.3.1-7).

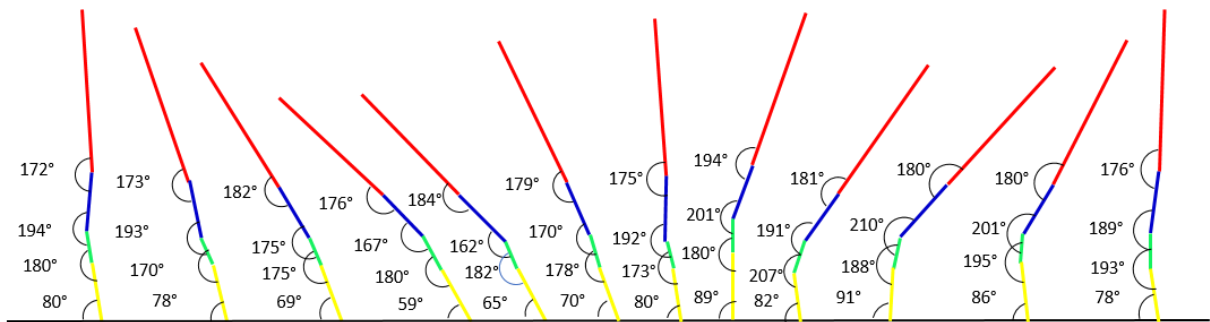


Fig. 4.3.1-6 Stick diagram between two consecutive upright posture.

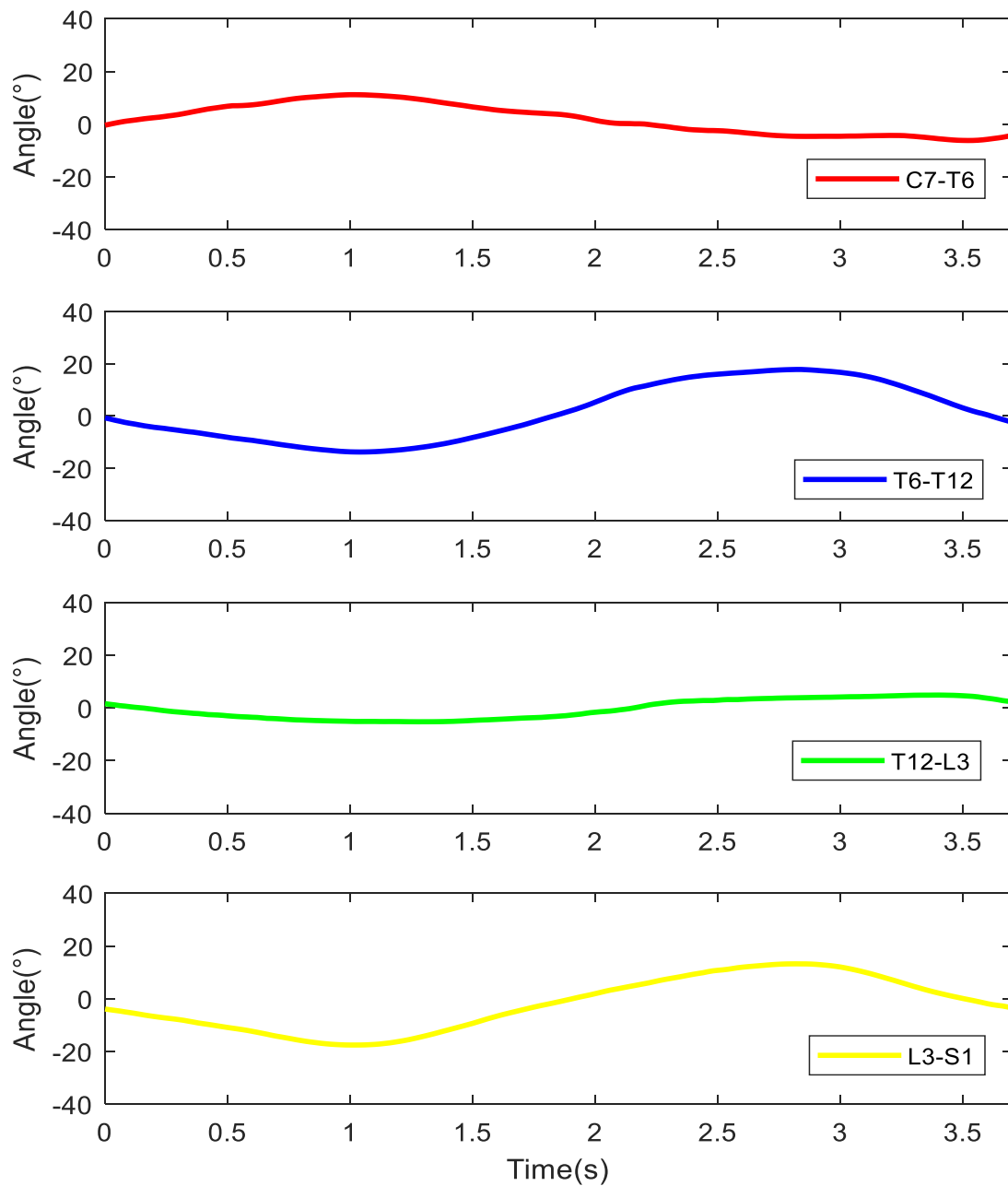


Fig. 4.3.1-7 Segments patterns between two consecutive upright posture.

For each segment the average pattern and standard deviation in three planes were calculated. The Fig. 4.3.1-8 shows the mean trend in the frontal plane.

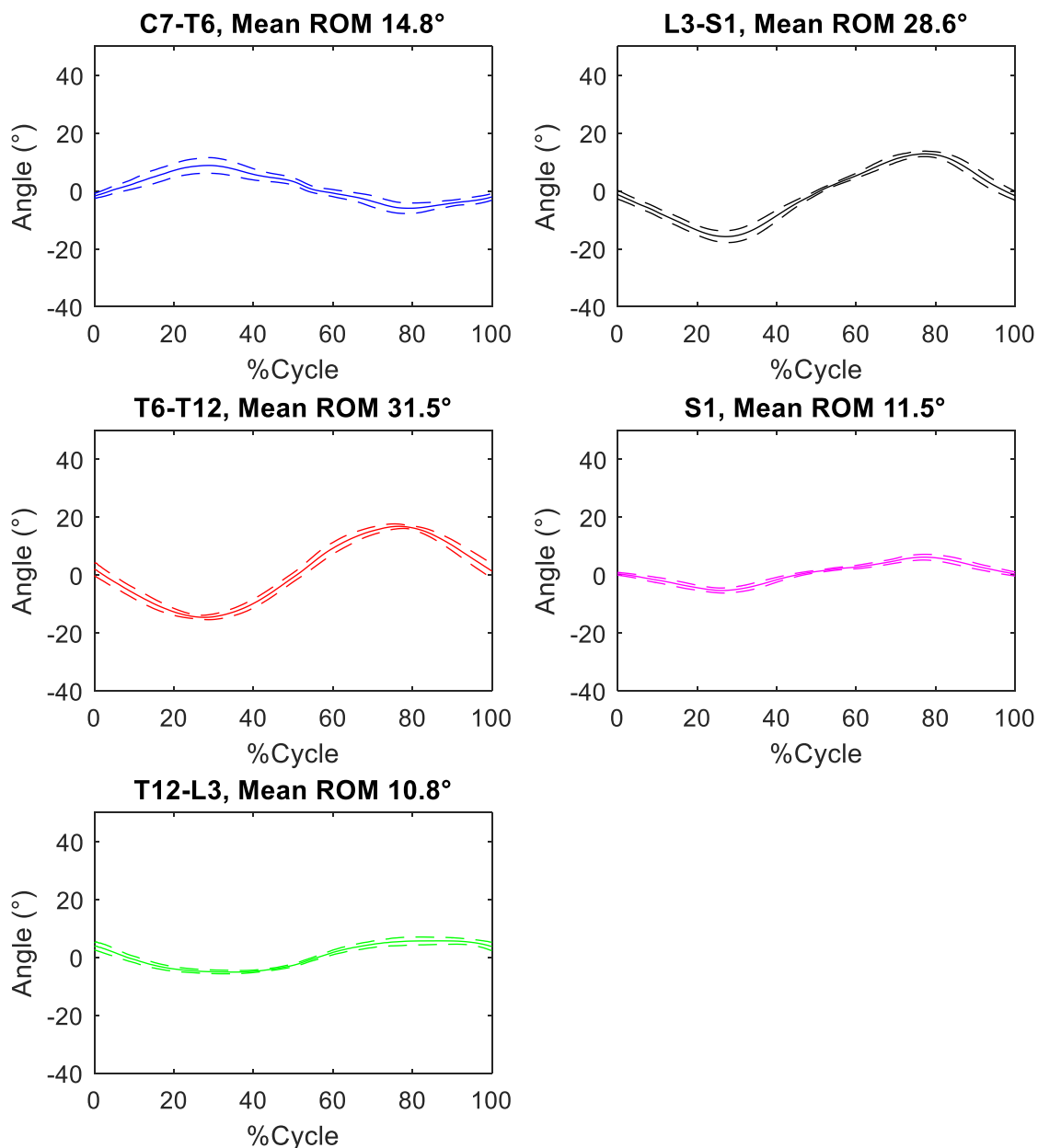


Fig. 4.3.1-8 Mean pattern and deviation of spinal segments in the frontal plane during Lateral Bending elementary exercise.

From the graphs it is possible to observe how the C7-T6 segment with respect to the T6-T12 segment has a different motion with respect to that of the other segments taken into consideration. In fact, when the lateral flexion takes place on the left side, the C7-T6 segment tends to flex on the opposite side with respect to segment below. Vice versa when the movement develops on the right side.

In Tab. 4.3.1-2 the mean ROMs in the three anatomical planes and their standard deviations are reported. The lateral bending movement, as can be seen from ROM values, is characterized by movements obviously in the frontal plane but also especially in the transversal plane. Looking at the C7-T6 segment in particular, it is possible to see how the largest movement occurs not in the frontal plane. The segment to which the largest ROM in the frontal plane is assigned is the T6-T12 segment, which, however is accompanied by greater axial rotation, while L3-S1 segment has the main movement in the frontal plane.

	ROM (SD) degree		
	Sagittal Plane	Frontal Plane	Transversal Plane
C7-T6	15.40 (3.68)	14.80 (4.52)	61.70 (4.82)
T6-T12	6.16 (5.20)	31.50 (1.61)	23.60 (0.03)
T12-L3	5.84 (6.31)	10.80 (1.92)	14.60 (3.87)
L3-S1	2.83 (4.59)	28.60 (3.00)	3.22 (2.30)
Pelvis	3.49(2.28)	11.50 (1.87)	17.80 (5.14)

Tab. 4.3.1-2 ROMs in the three anatomical planes during lateral bending exercise.

Axial Rotation in the Transversal Plane

Subject was asked to rotate torso around longitudinal axis. Once again, to divide data acquisition patterns, S1 information was used. In this case axial rotation trend was analysed. The subject rotates from upright posture to right side and then returns to upright posture. The same movement was repeated on the left side (Fig. 4.3.1-9). In this case it is not possible to construct a stick model and measure the angles between segments. To do this, it was necessary to film the movement perpendicular to transversal plane.

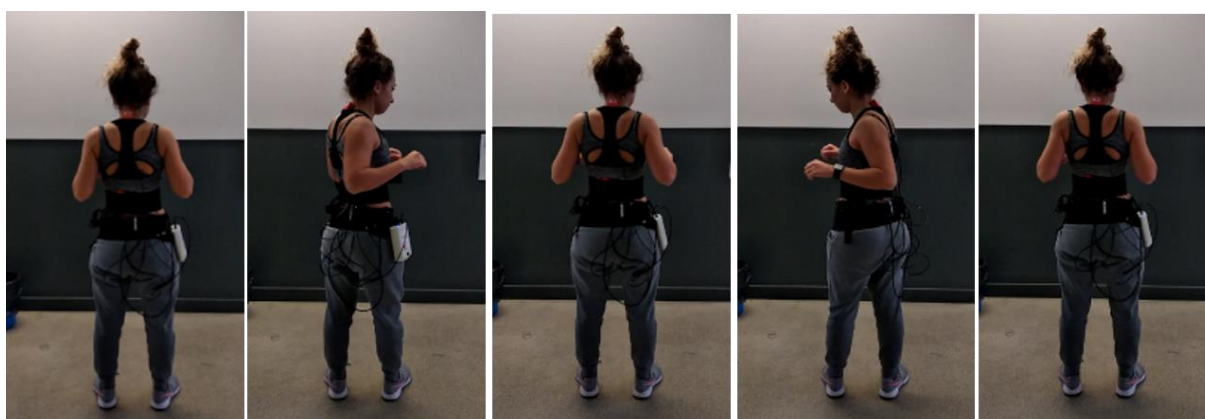


Fig. 4.3.1-9 Frame sequence to describe lateral bending movement.

For each segment the average pattern and standard deviation in three planes have been calculated. The Fig. 4.3.1-10 shows the mean trend in the transversal plane.

Both patterns and ROMs (Tab. 4.3.1-3) show that the segment to which the movement is most due is the pelvis.

	ROM (SD) degree		
	Sagittal Plane	Frontal Plane	Transversal Plane
C7-T6	39.00 (3.79)	117.0 (5.45)	22.70 (4.51)
T6-T12	39.50 (2.44)	15.00 (4.36)	19.10 (5.45)
T12-L3	21.30 (2.49)	28.30 (2.75)	3.62 (6.38)
L3-S1	16.20 (3.37)	20.00 (2.24)	11.90 (4.89)
Pelvis	6.54(2.77)	26.70 (3.09)	101.0 (7.56)

Tab. 4.3.1-3 ROMs in the three anatomical planes during axial rotation exercise.

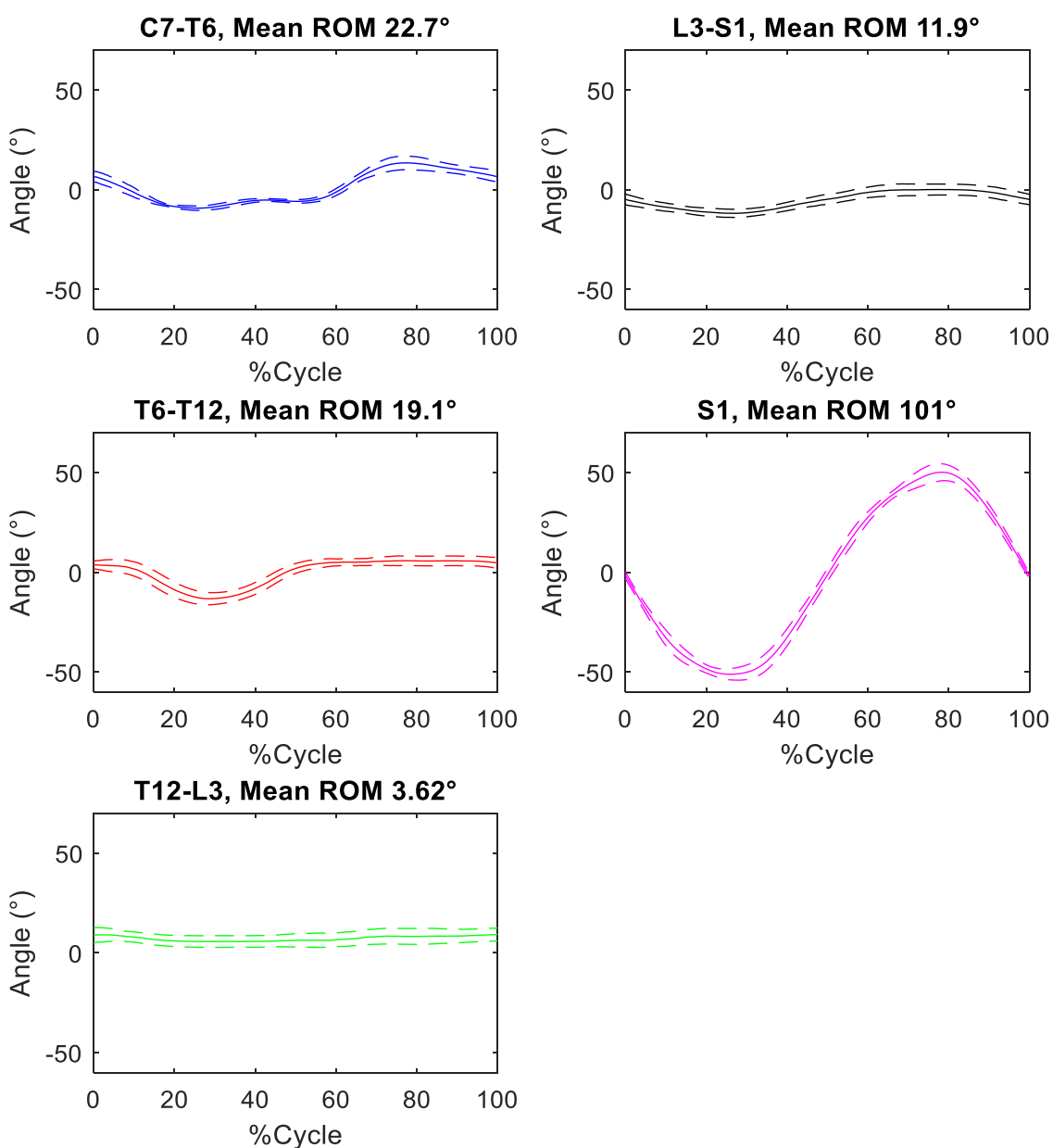


Fig. 4.3.1-10 Mean pattern and deviation of spinal segments in the transversal plane during Axial Rotation elementary exercise.

4.3.1.1 Sensor motion with respect to its neutral orientation

Since during the execution of the elementary movements some segments have greater ROM in the non-main planes of motion, a different description of movement was investigated to verify, from another point of view, the correctness of the developed algorithm. The pattern this time was obtained by referring the orientation of each sensor taken at any given time to its neutral orientation:

$${}^N R_{SEN} = {}^G R_N^{-1} \cdot {}^G R_{SEN} .$$

Flexion-Extension in the Sagittal Plane

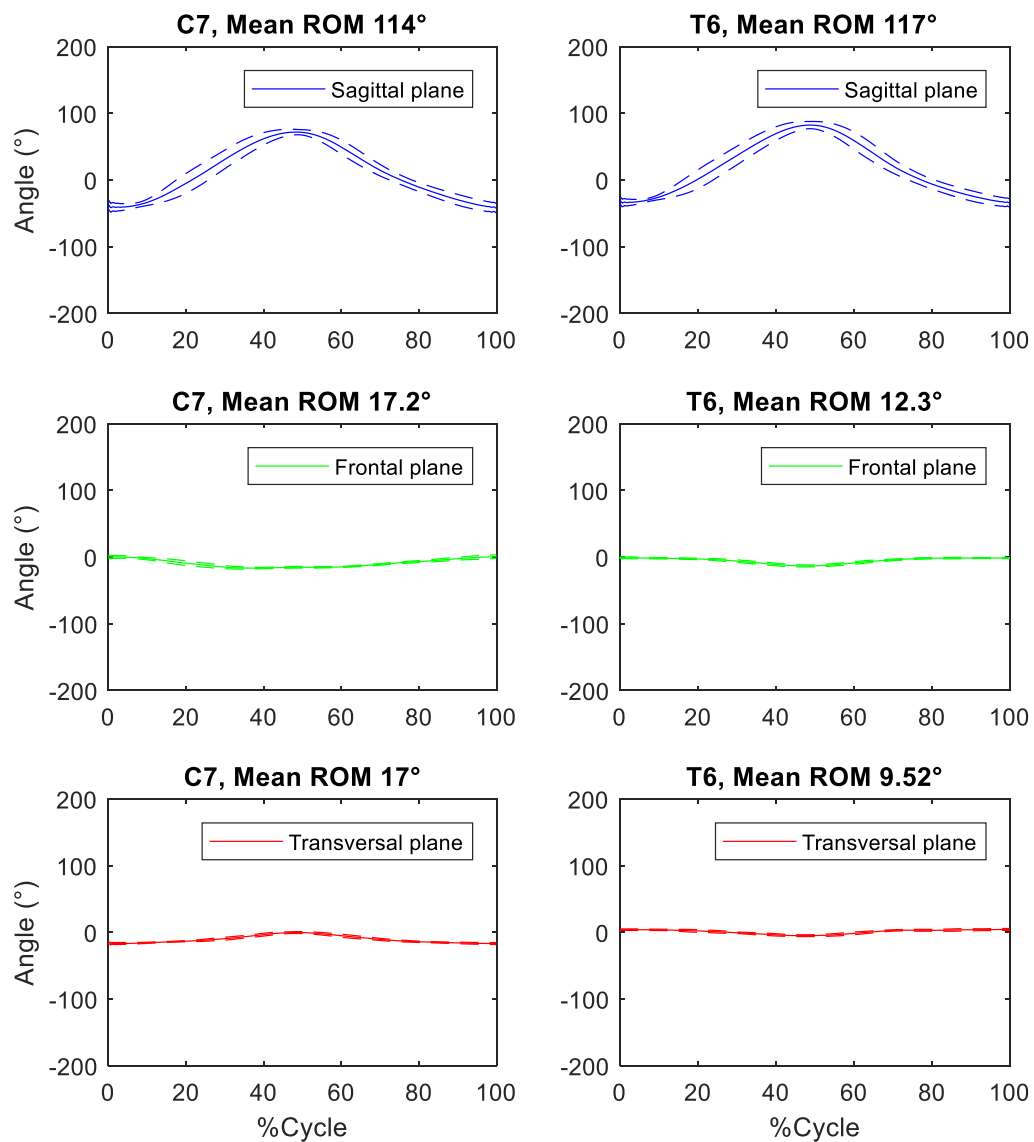


Fig. 4.3.1.1-1 Mean pattern and deviation of upper spinal segments in the three anatomical planes during Flexion-Extension elementary exercise.

From the patterns and the relative ROMs shown in Fig. 4.3.1.1-1 it is possible to confirm that for the sensors positioned on the upper spinal segments, the main movement is in the sagittal plane. During the maximum extension, both sensor C7 and sensor at T6 level are extended with respect to the neutral position obtained in the acquisition part in which the subject remained stationary. At the maximum flexion, on the other hand, reached at 50% of cycle, both sensors are flexed with respect to their neutral position. Moreover, from the patterns in the sagittal plane is possible to see that the two sensors reach almost the same ROM. In the other two planes there are certainly less ROM than those obtained for the main plane of motion. It is possible to notice that in the maximum extension and in the frontal plane, both segments considered have no

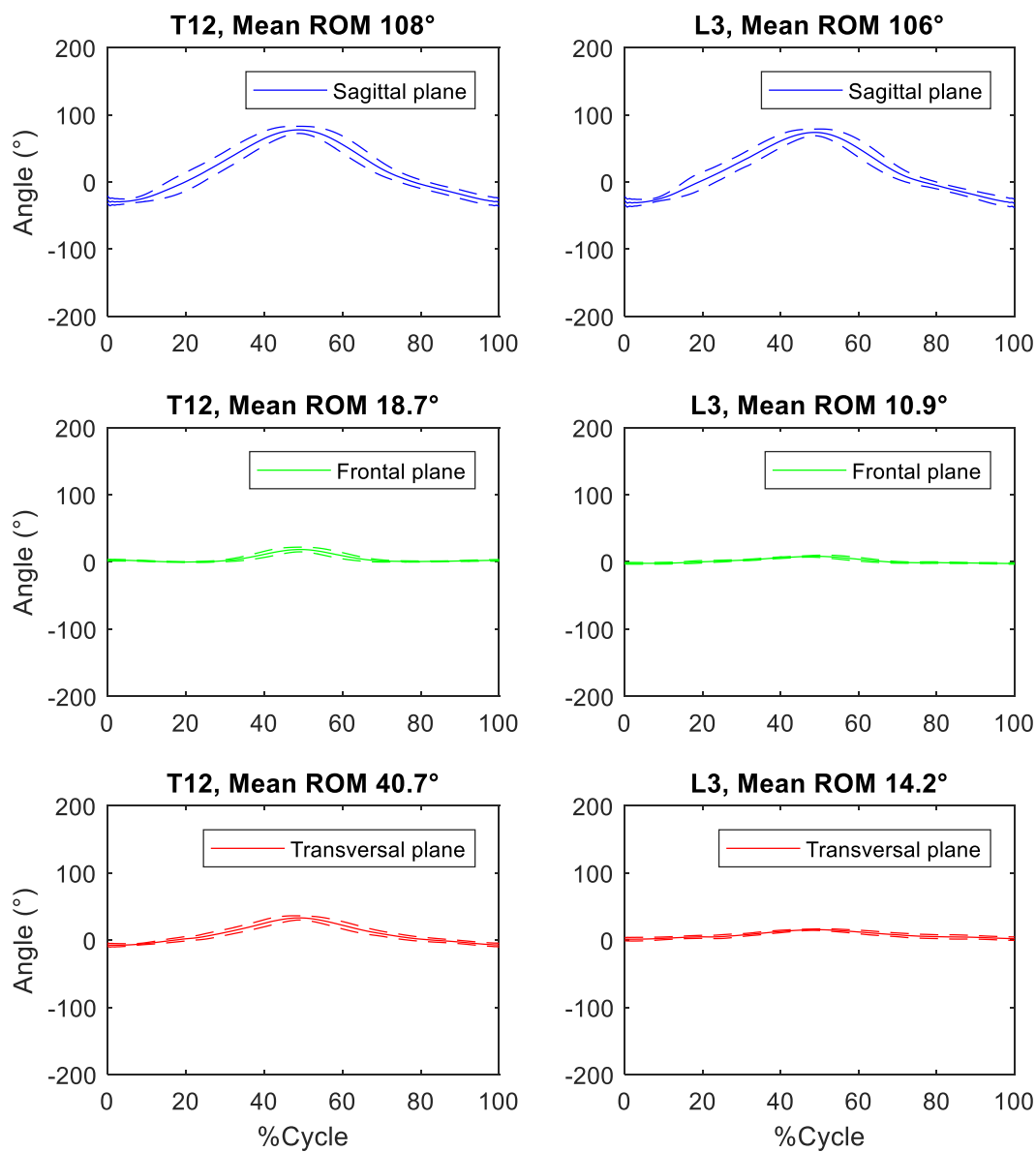


Fig. 4.3.1.1-2 Mean pattern and deviation of lower spinal segments in the three anatomical planes during Flexion-Extension elementary exercise.

lateralisation with respect to their neutral position, but that during the maximum flexion this appears with a slight propensity to the left for both. In the transverse plane, a maximum extension results in a slight negative rotation for C7 sensor and a slight right rotation for T6 sensor; a maximum flexion results in a positive rotation for C7 sensor and a negative rotation for T6 sensor.

In Fig. 4.3.1.1-2 the patterns of the segments belonging to the lumbar region of the spinal column is shown. Also in this case the same considerations made for the upper segments are valid, but it should be underlined that the T12 sensor in the transversal plane reaches a not negligible ROM (40.7°). This may lead one to suspect that this value is dictated by a movement

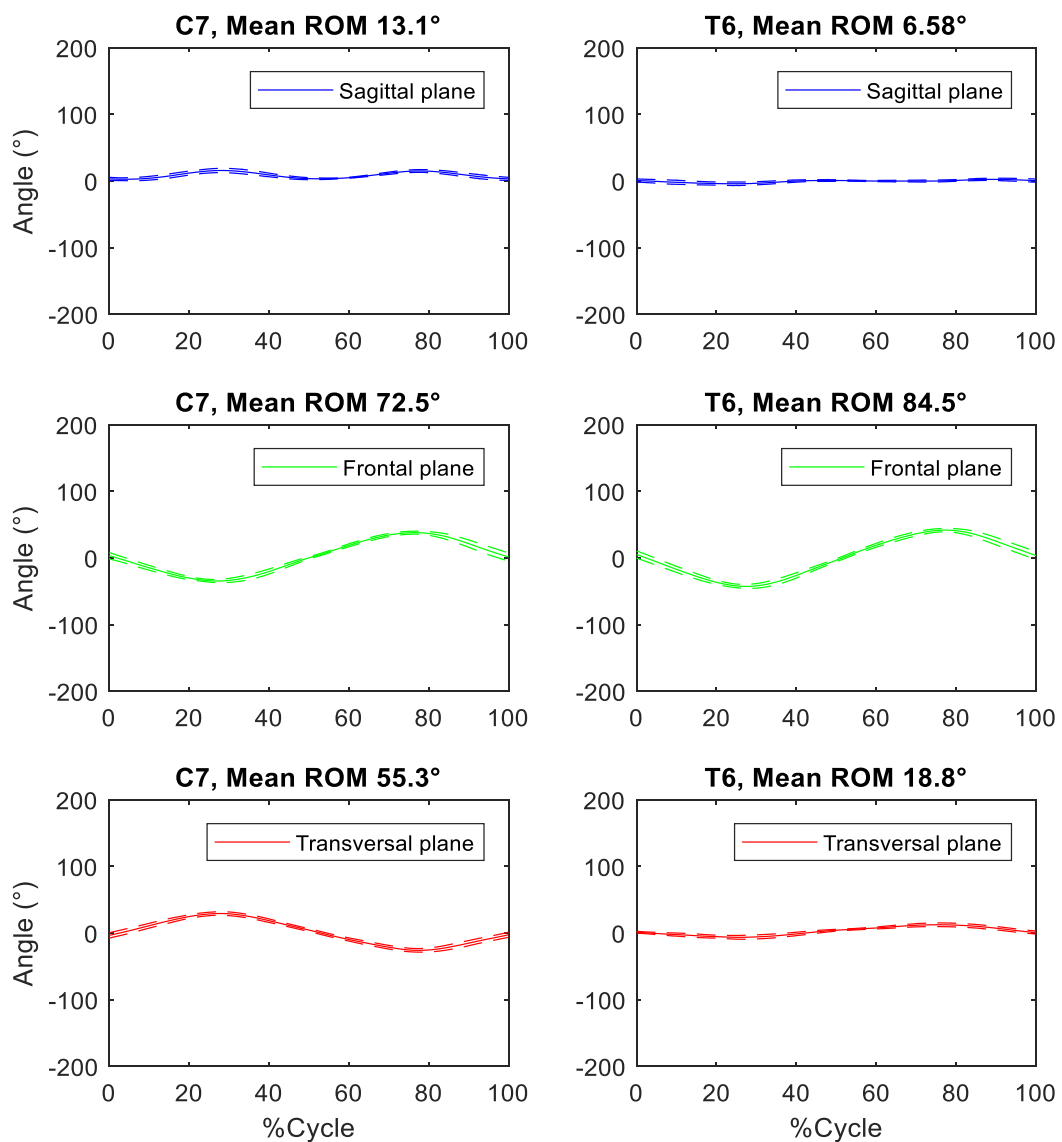


Fig. 4.3.1.1-3 Mean pattern and deviation of upper spinal segments in the three anatomical planes during Lateral Bending elementary exercise.

of the sensor during the movement of the column not related to the actual motion but to a movement of the sensor itself.

Lateral Bending in the Frontal Plane

In the lateral bending movement, it is again possible to confirm that the upper (Fig. 4.3.1.1-3) and lower (Fig. 4.3.1.1-4) segments of the spine have a greater ROM in the main plane of motion. It should be noted, however, that the C7 sensor also has an important motion in the transverse plane. The relative pattern reveals a right rotation when the subject was flexing on the right.

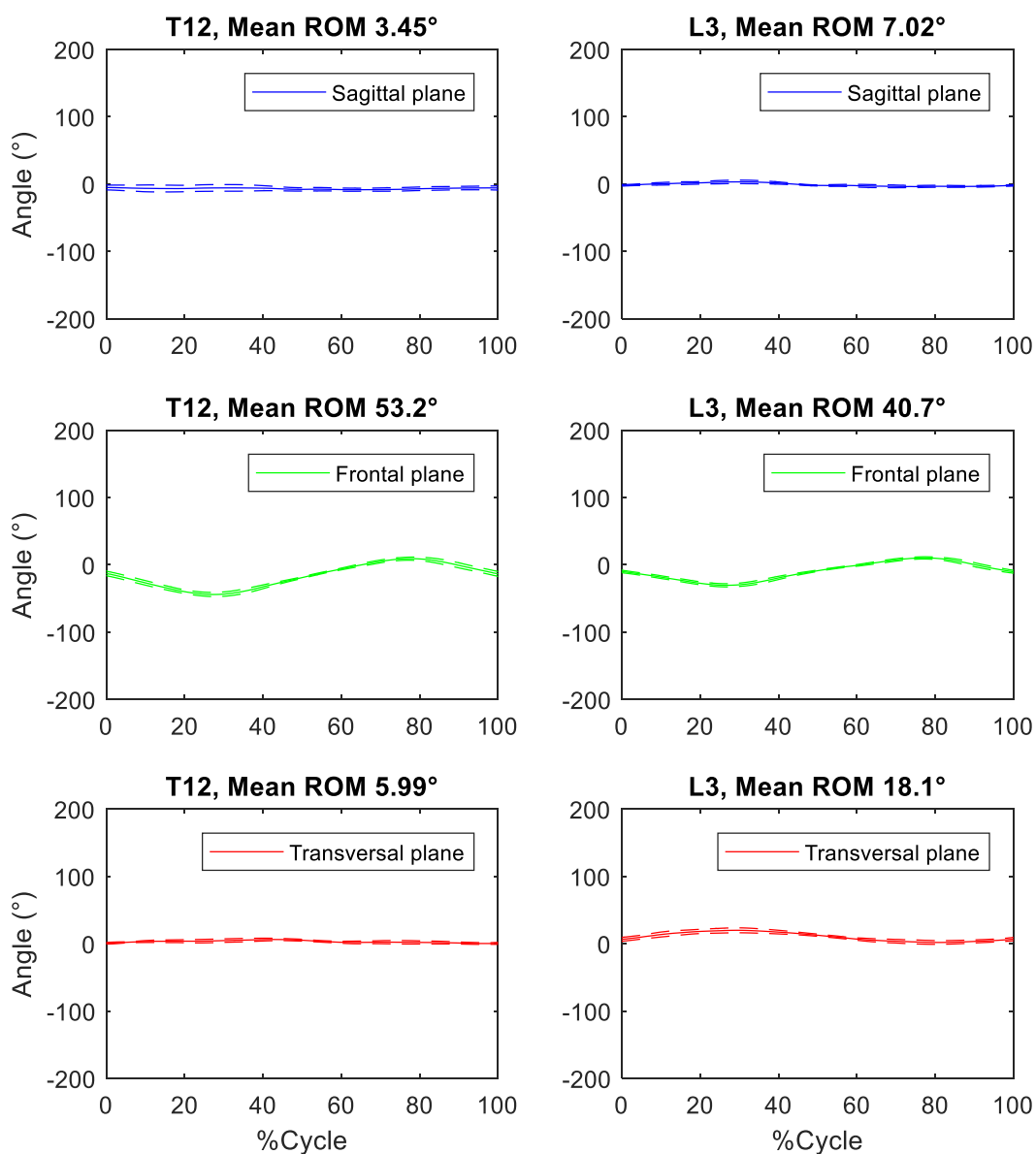


Fig. 4.3.1.1-4 Mean pattern and deviation of lower spinal segments in the three anatomical planes during Lateral Bending elementary exercise.

Axial Rotation in the Transversal Plane

Figs. 4.3.1.1-5 and 4.3.1.1-6 illustrate the trends in the angular displacements during the elementary movement of axial rotation. All segments have the highest ROM in the transversal plane, but with the exception of L3 segment, the others have values also in the other planes less negligible than those obtained for the other elementary movements tested. In fact, it seems that these oscillate significantly in the other planes as well. For example, looking at C7 segment in detail, a rotation of the trunk to the left involves an inclination of C7 on the left side and a

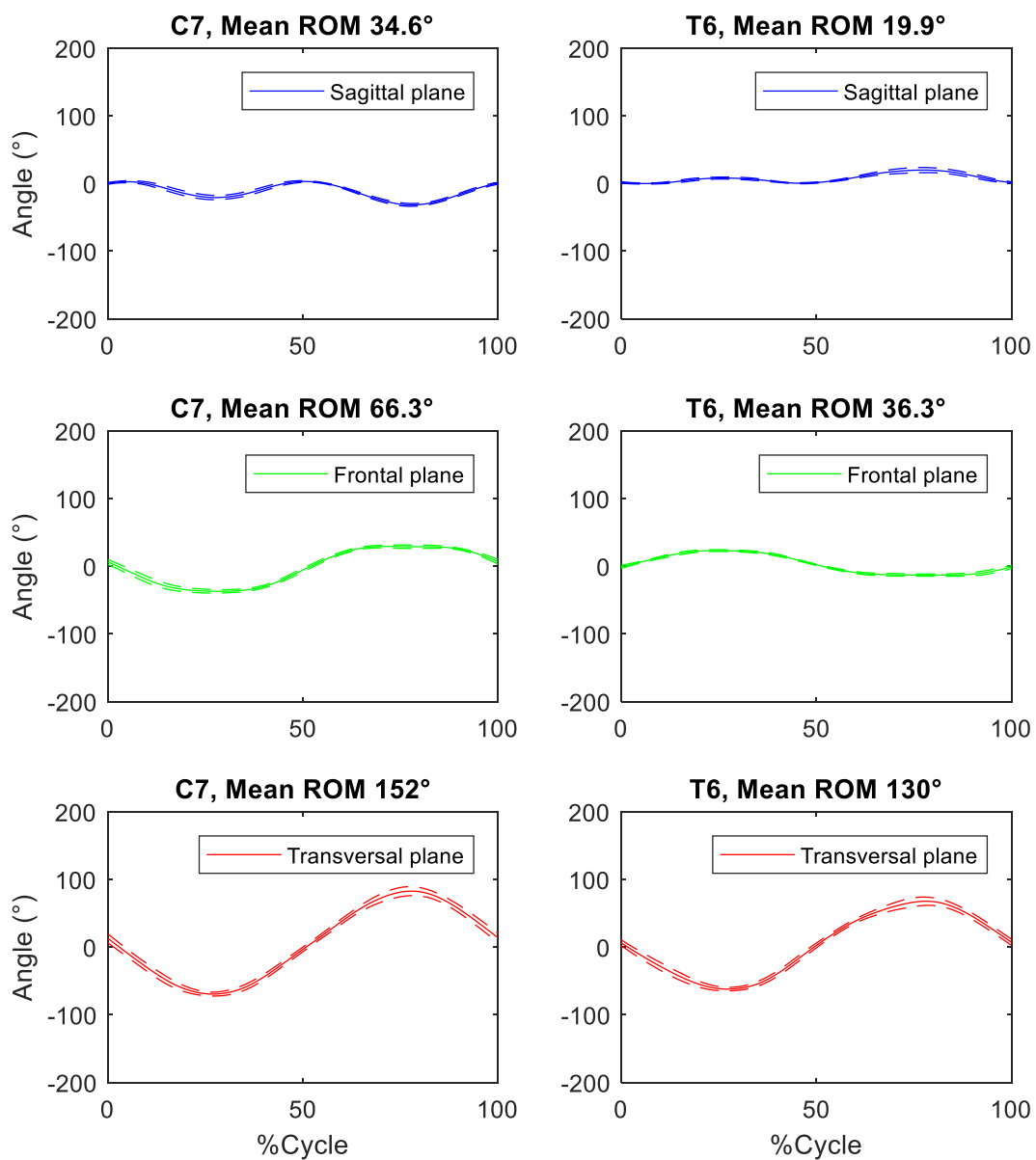


Fig. 4.3.1.1-5 Mean pattern and deviation of upper spinal segments in the three anatomical planes during Axial Rotation elementary exercise.

rotation to the right involves a lateralization to the right. In the sagittal plane is visible an oscillation of two complete cycles around the zero.

Looking at the totality of the spinal segments in this elementary exercise, it is possible to see that in the frontal plane the patterns tend to compensate each other. This compensation leads to no visual notice of a lateralisation of the trunk as a whole.

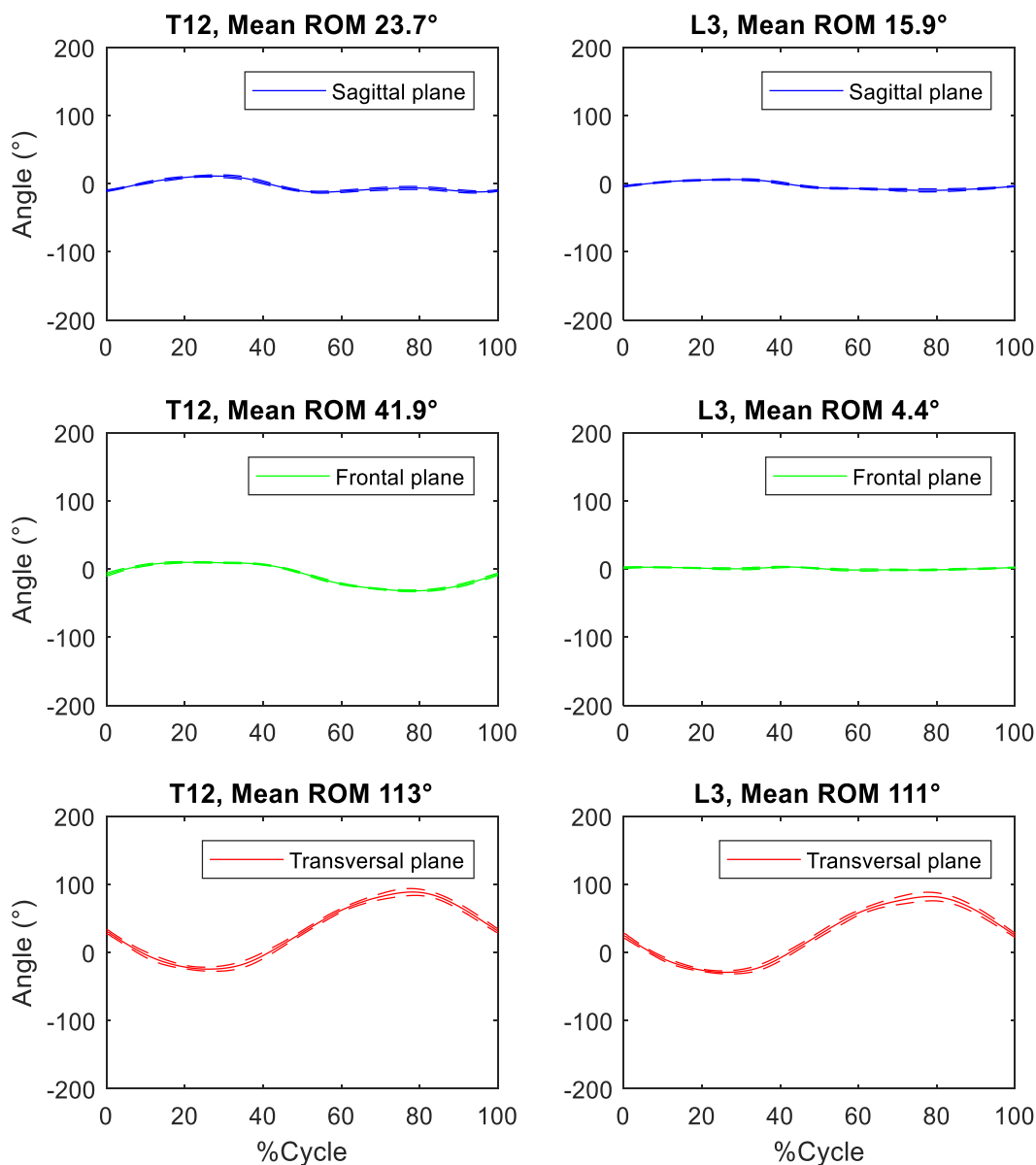


Fig. 4.3.1.1-6 Mean pattern and deviation of lower spinal segments in the three anatomical planes during Axial Rotation elementary exercise.

4.3.1.2 Sensor motion with respect to the neutral position of the Pelvis

In this other check, rather than describing the motion of each sensor with respect to its neutral position, it was described with respect to the neutral position of the sensor positioned on S1:

$${}^{S1}R_{Sen} = {}^N R_{S1}^{-1} \cdot {}^N R_{Sen} .$$

Flexion-Extension in the Sagittal Plane

Fig. 4.3.1.2-1 shows the trends of C7 and T6 segments with respect to the orientation of S1 sensor in neutral position. Also in this case, as it happened in the patterns in which the

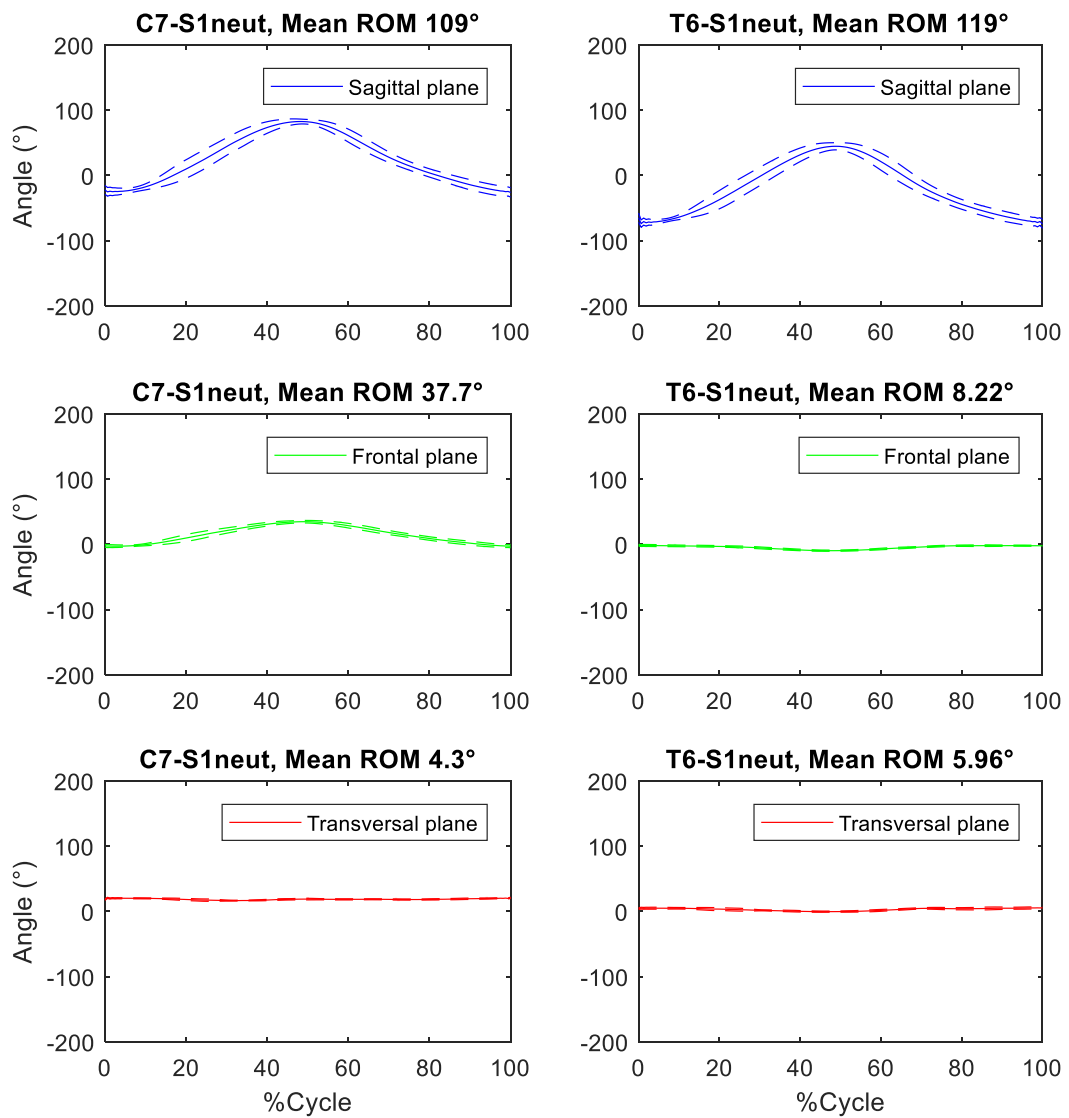


Fig. 4.3.1.2-1 Mean pattern and deviation of upper spinal segments in the three anatomical planes during Flexion-Extension elementary exercise.

orientation of each sensor was referred to its own in neutral position, the predominant motion is in the sagittal plane. In the transverse plane the patterns are almost completely flat and also in the frontal plane in reference to the T6 sensor. the C7 sensor, on the other hand, has a more marked motion in the frontal plane: the C7 sensor, as the maximum flexion is reached, tilts to the right with respect to the starting S1 sensor.

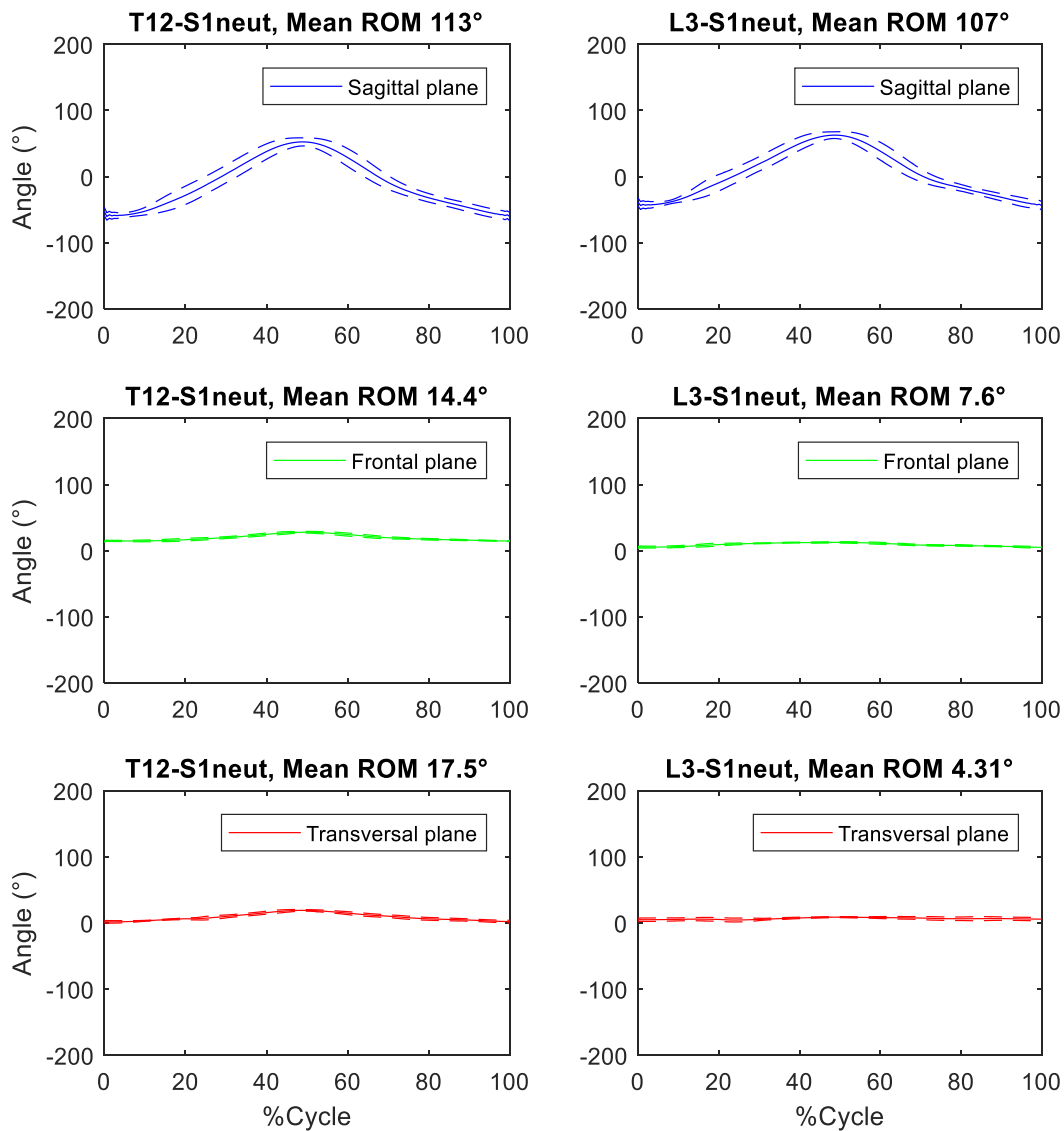


Fig. 4.3.1.2-2 Mean pattern and deviation of lower spinal segments in the three anatomical planes during Flexion-Extension elementary exercise.

Also the segments belonging to the lower region of the vertebral column (Fig. 4.3.1.2-2) have a motion that develops mainly in the sagittal plane. The T12 sensor in the frontal and transverse planes has peaks in lateral bending of axial rotation to the right or at the point of maximum bending. However, the peaks in question are certainly less accentuated than those obtained by

referring the orientation of T12 sensor to its neutral position (Fig. 4.3.1.1-2). As far as L3 sensor is concerned, it can be said that corresponding segment is less subject to oscillations in anatomical planes other than the main one than the others. The statement also takes into account the patterns of the same segment with respect to its neutral position (Fig. 4.3.1.1-2).

Lateral Bending in the Frontal Plane

In lateral bending (Figs. 4.3.1.2-3 and 4.3.1.2-4) the trends have the same peculiarities in the non-main planes of the motion of those obtained by referring the motion of each sensor with respect to its neutral position.

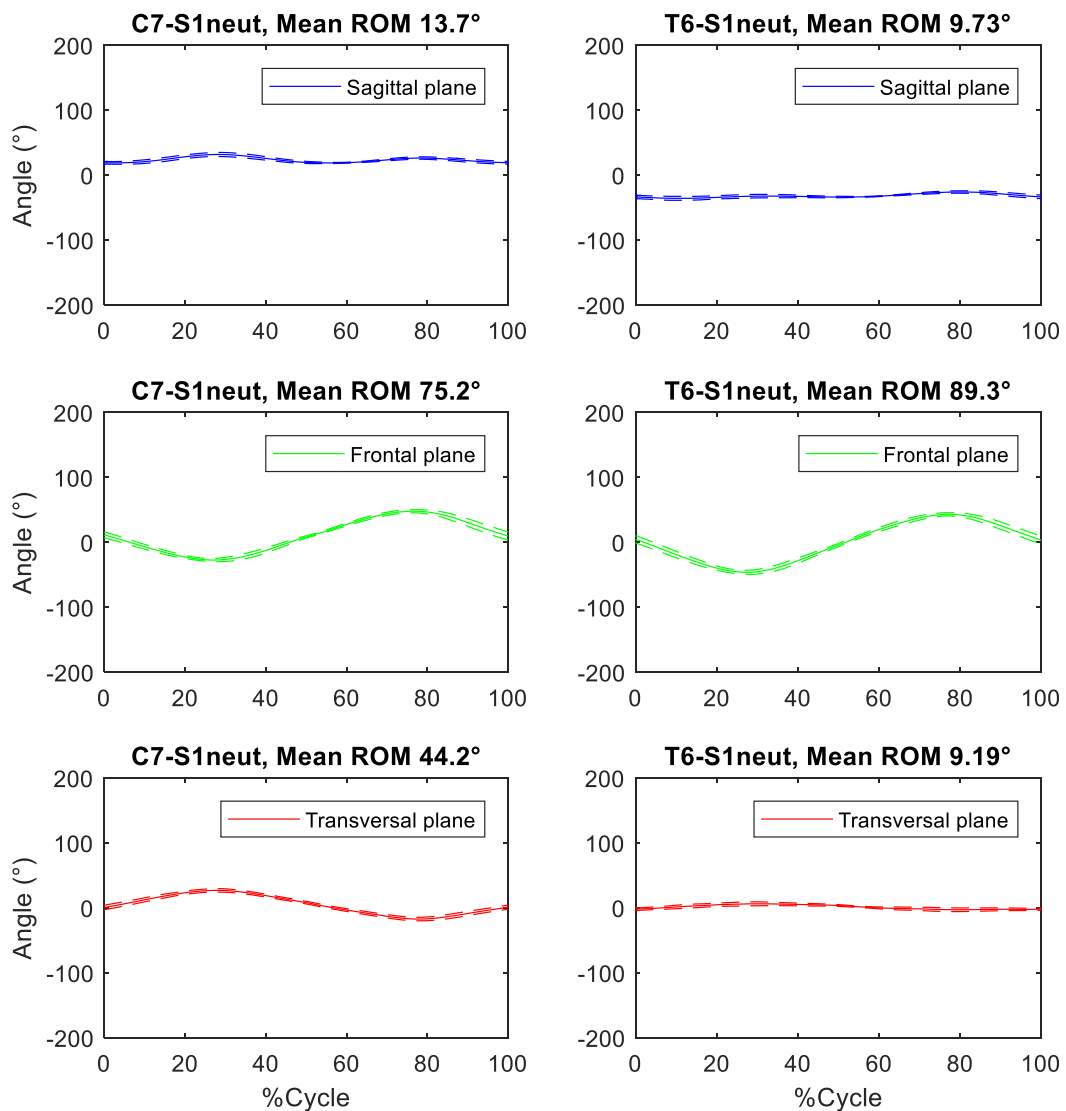


Fig. 4.3.1.2-3 Mean pattern and deviation of upper spinal segments in the three anatomical planes during Lateral Bending elementary exercise.

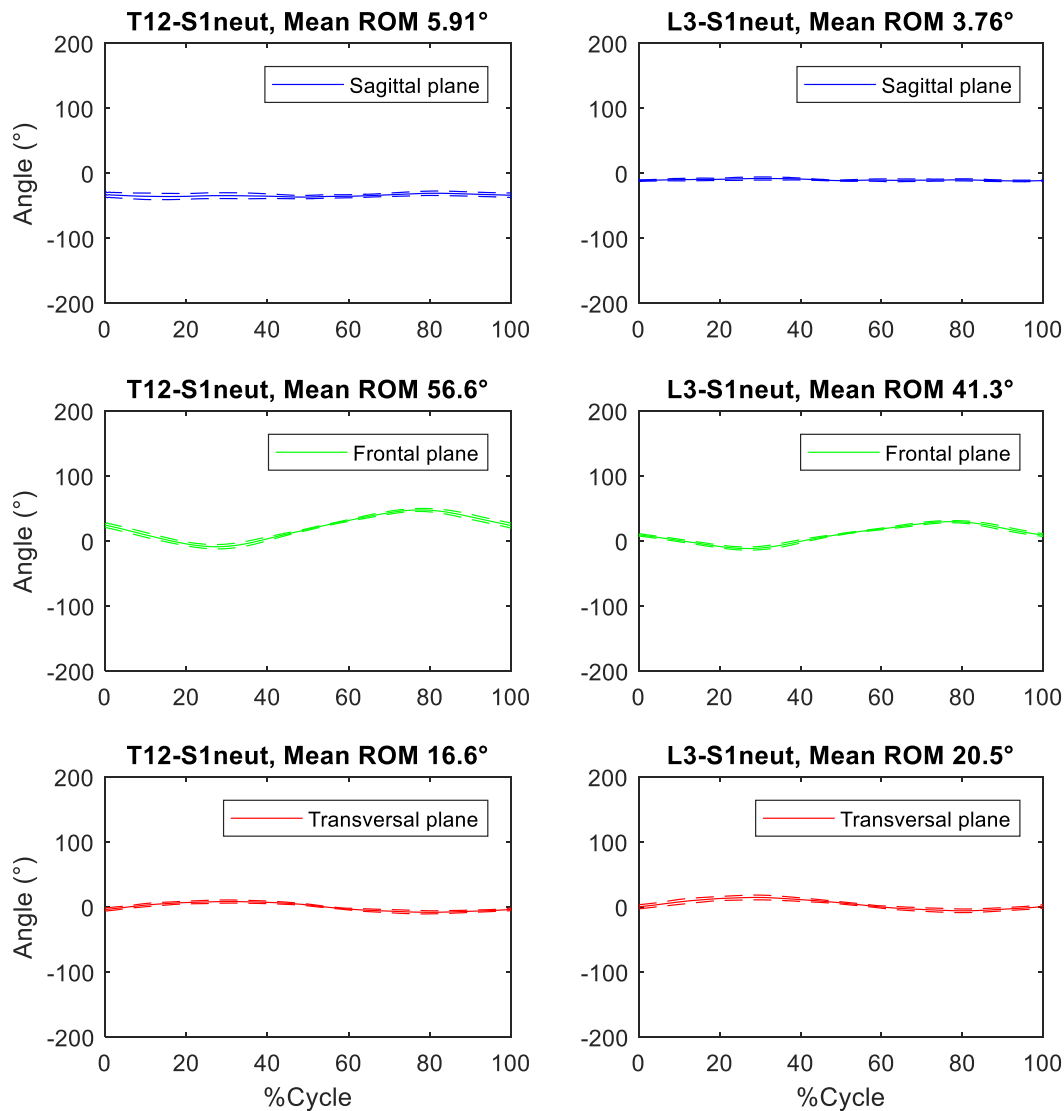


Fig. 4.3.1.2-4 Mean pattern and deviation of lower spinal segments in the three anatomical planes during Lateral Bending elementary exercise.

Axial Rotation in the Transversal Plane

Also for the axial rotation, the patterns obtained by referring the motion of each sensor with respect to the neutral position of the pelvis (Figs. 4.3.1.2-5 and 4.3.1.2-6) have the same characteristics of the previous verification. The slight differences are found in the ROMs.

At the beginning of the movement, when the subject is standing with the segments aligned, the sensor on C7 is flexed with respect to S1 (neutral position) by about 10°, tilted to the right and also rotate transversely. When the rotation peak on the left is reached, C7 is extended by a few

degrees and tilted to the left, while when the maximum rotation peak on the right is reached, C7 is flexed laterally to the right. Therefore, overall the pattern in the sagittal plane shows an oscillation around the zero value and two complete cycles are recognized. In the frontal plane, on the other hand, the segment bends towards the same side if the rotation. For the T6 level sensor in the sagittal plane, the same considerations as for C7 segment apply. In the frontal plane, however, the behaviour is the opposite, in other words that a rotation to the left

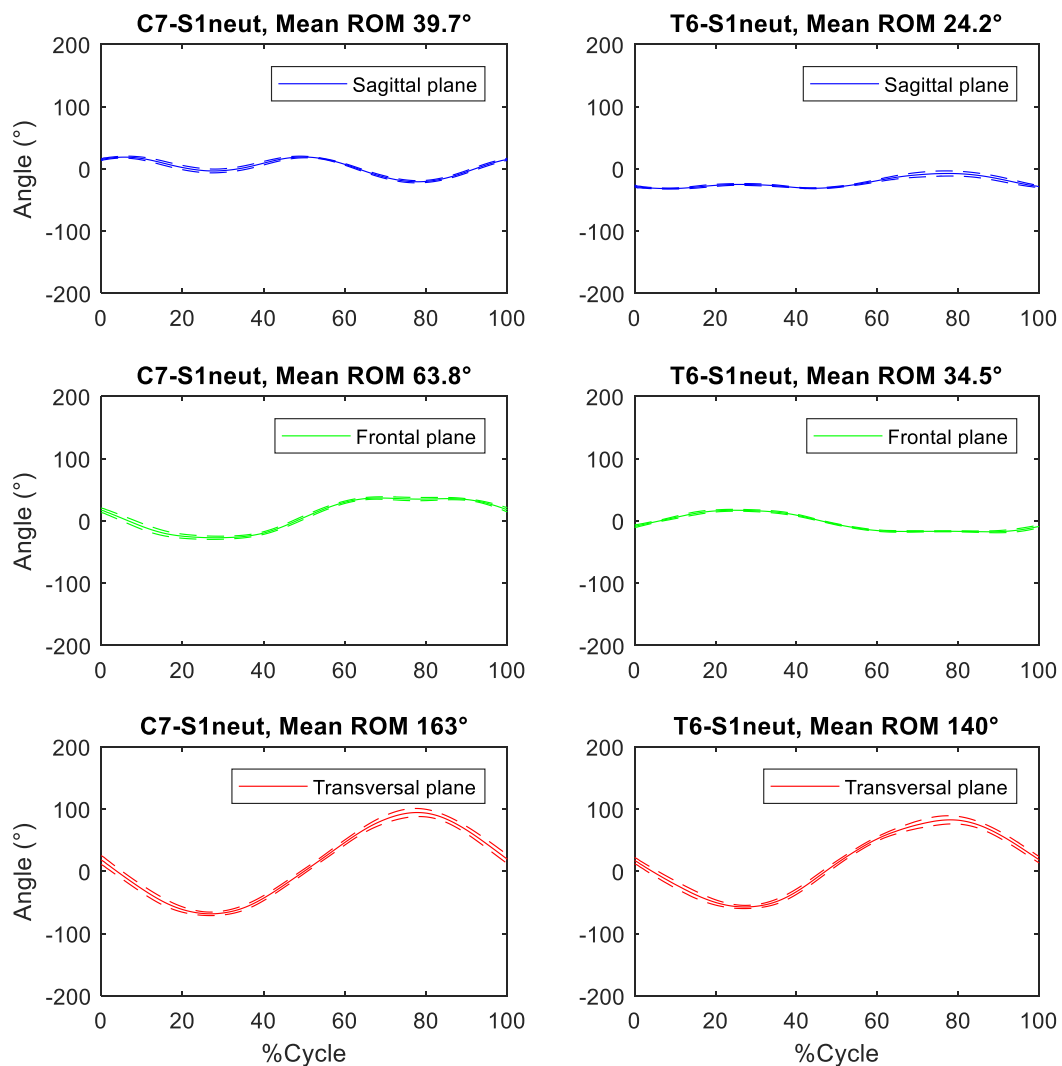


Fig. 4.3.1.2-5 Mean pattern and deviation of upper spinal segments in the three anatomical planes during Axial Rotation elementary exercise.

corresponds to a lateral flexion to the right and vice versa in the case of rotation to the right of the torso. In addition, in the neutral position, the T6 sensor is extended with respect to the pelvis.

T12 sensor in the frontal plane has the same behaviour described for T6 sensor, while in the sagittal plane it is possible to recognize only a complete cycle of flexion and extension during the whole movement. The phase of slight flexion occurs at the axial rotation on the left, while the extension occurs for the remaining part of the movement.

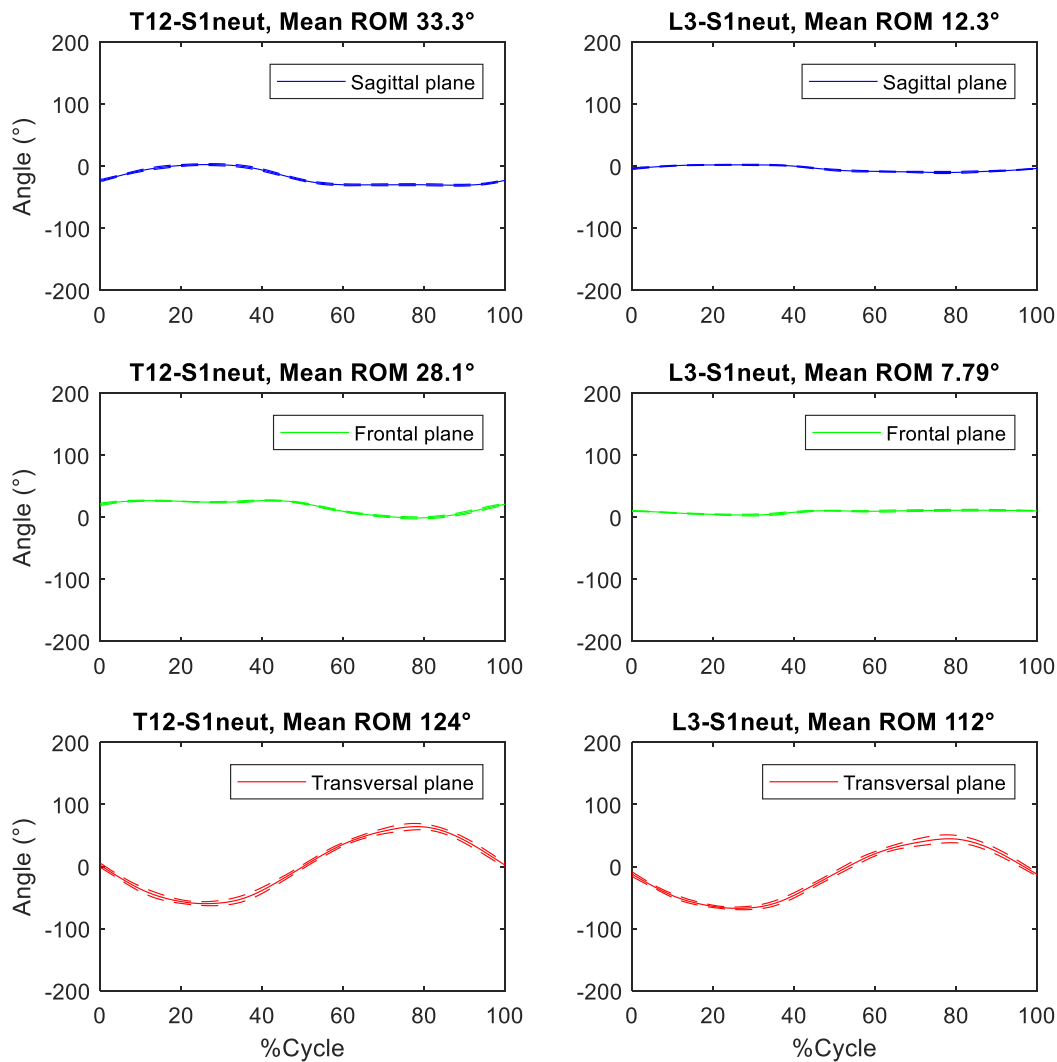


Fig. 4.3.1.2-6 Mean pattern and deviation of upper spinal segments in the three anatomical planes during Axial Rotation elementary exercise.

Finally, L3 is the segment most attached to S1 in the sagittal and frontal planes. This means that this segment is an active part of the axial rotation but whose component in the other planes is almost absent.

4.3.2 Walking Movement

During walking each body part plays an important role to ensure that the balance is maintained. Body movements depend from walking speed. In fact, as Crosbie et al. in 1997 affirmed, walking at higher speed caused a different pattern of the spine segments and pelvis and it increases their ROMs. In this work two different speeds were tested to verify whether inertial sensors can describe the movements with an acceptable level of uncertainty.

The subject was asked to walk over a 20 m path self-selected speed for a total of ten times. During processing phase, five of these were analysed in order to collect acquisitions in the same direction. When the indicator delimiting the path was reached, the subject impacted the right foot to the ground. To recognize the foot impact the acceleration X of the sensor at C7 vertebral level was analysed. The C7 vertebral level is subjected at major oscillations because it is the furthest point from where movement is generated: here the peaks are more distinguishable even without having to filter the signal (Fig. 4.3.2-1).

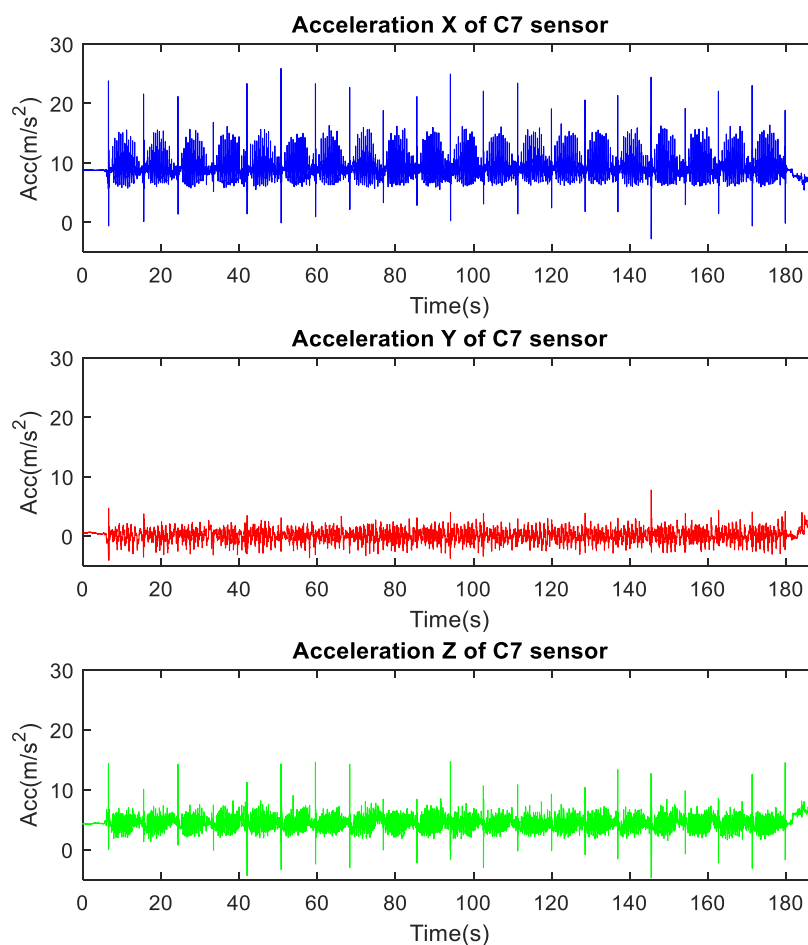


Fig. 4.3.2-1 Accelerations of sensor at C7 vertebral level during walking at comfortable walking speed.

Peak indices were identified to divide the entire data acquisition and analyse only one walking direction. Once it was done, gait cycles were identified using antero-posterior acceleration of T12 sensor level. In this case the signal was filtered choosing the right cut-off frequency. It was necessary show the power spectral density of acceleration Z of T12 sensor level (Fig. 4.3.2-2). The signal was filtered with a pass band filter (4th Butterworth) between 0.5 and 15 Hz for walking at comfortable speed while for walking at fast speed the cut-off frequencies are 0.5 and 13 Hz.

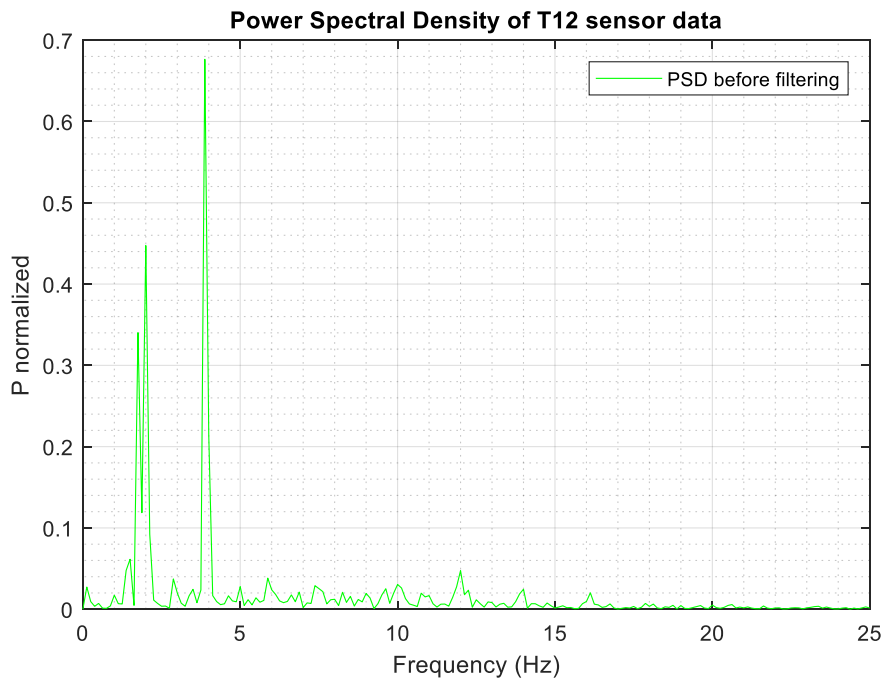


Fig. 4.3.2-2 Power spectral density of anterior-posterior acceleration of T12 sensor during walking at comfortable speed.

The subject was asked to walk at comfortable speed that was found to be equal to 1.39 m/s. Before starting the test, the subject was stationary for a few seconds like in the elementary movements' trials. In Fig. 4.3.2-3 is shown one gait cycle phases of right leg. Having made the path longer (with respect to first preliminary test Chapter 4.2), more steps, identified by an acceleration amplitude almost equal, can be considered for the calculation of the mean trends of spine angles. In other words, it was analysed only the gait cycles in the central portion of path. For each anatomical plane and for each gait cycle, spine angles were calculated. Then the mean patterns were obtained.

It was verified that two consecutive trends, related to two gait cycles of the right leg were actually contiguous.

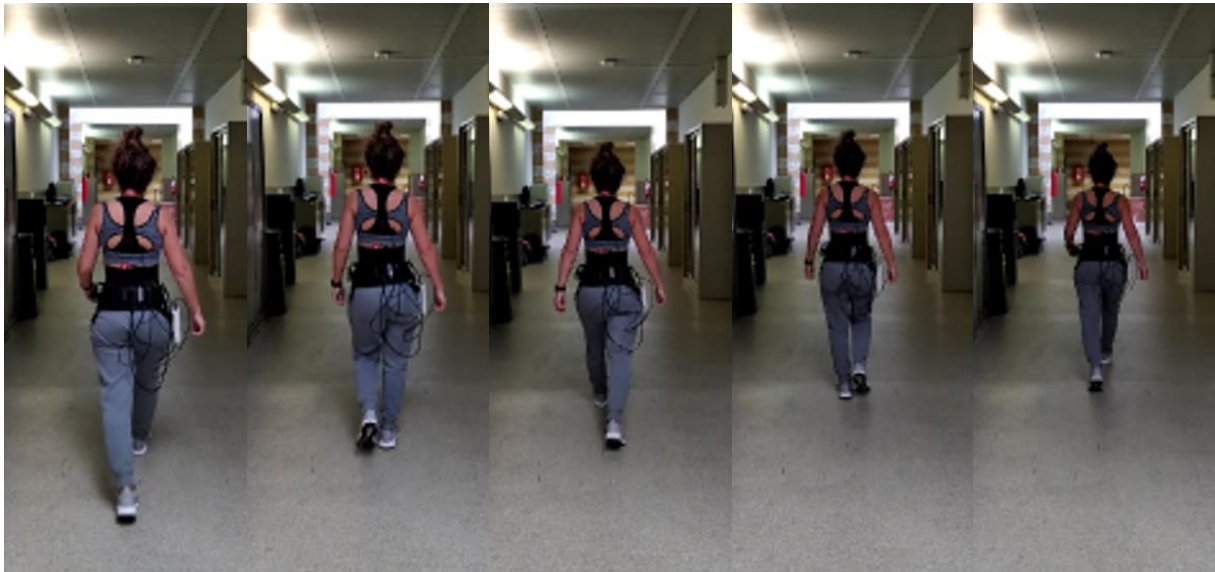


Fig. 4.3.2-3 Frame sequence of right gait cycle.

The mean trend and standard deviations of the trunk angles during gait cycle are shown in Figs. 4.3.2-4, 4.3.2-5, 4.3.2-6. In Tab. 4.3.2-1 ROMs and standard deviations are shown.

	ROM (SD) degree		
	Sagittal Plane	Frontal Plane	Transversal Plane
C7-T6	1.53 (0.67)	4.74 (2.53)	2.43 (1.50)
T6-T12	7.25 (2.82)	4.30 (0.81)	3.03 (2.72)
T12-L3	7.80 (3.58)	4.38 (1.23)	5.54 (2.62)
L3-S1	5.64 (1.94)	6.95 (1.57)	5.18 (1.22)
Pelvis	3.66 (2.22)	10.90 (6.33)	6.81 (4.82)

Tab. 4.3.2-1 ROMs in the three anatomical planes gait at comfortable speed.

The pelvis segment has a major ROM in the frontal and transversal planes compared to other segments, but it has also a higher dispersion. The segment in these two anatomical planes tends to have a motion that can favour the lower limbs to achieve the alternation of the gait phases. The lumbar segments in the frontal plane tend to bend mainly to the stance leg side. The ROM of the lower lumbar segment is greater than the other spinal segments because it is more influenced by the motion of the pelvis. In addition the different spinal segments flex towards the stance leg side to move the weight and allow the advancement of the contralateral leg.

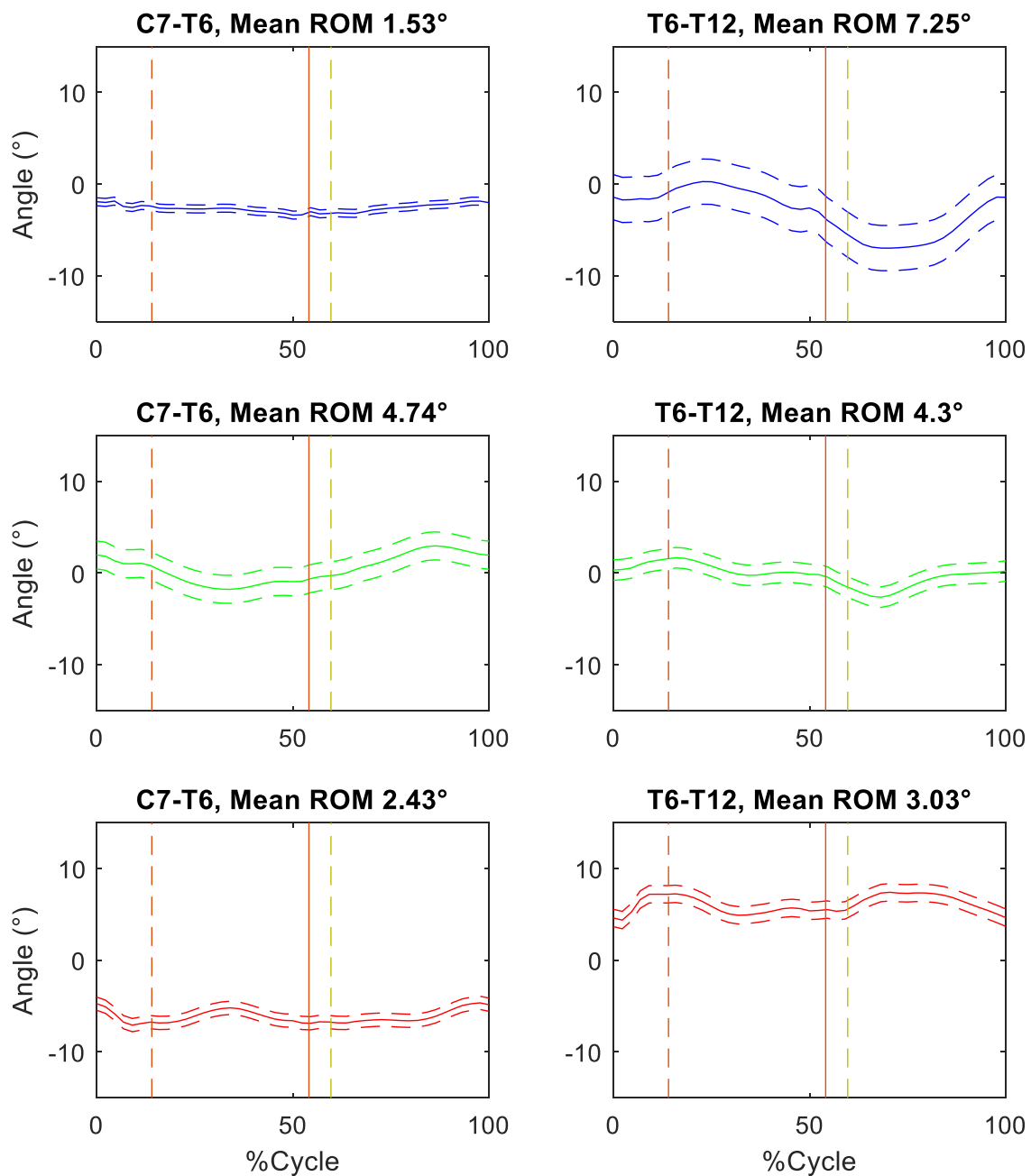


Fig. 4.3.2-4 Angle patterns of thoracic segments relative to right leg cycle at comfortable speed in the sagittal plane (up row), frontal plane (central row) and transversal plane (down row). The red continuous line represents the heel-strike of the left foot, the red dotted line represents the toe-off of the left foot and the yellow dotted line represents the toe-off of the right foot.

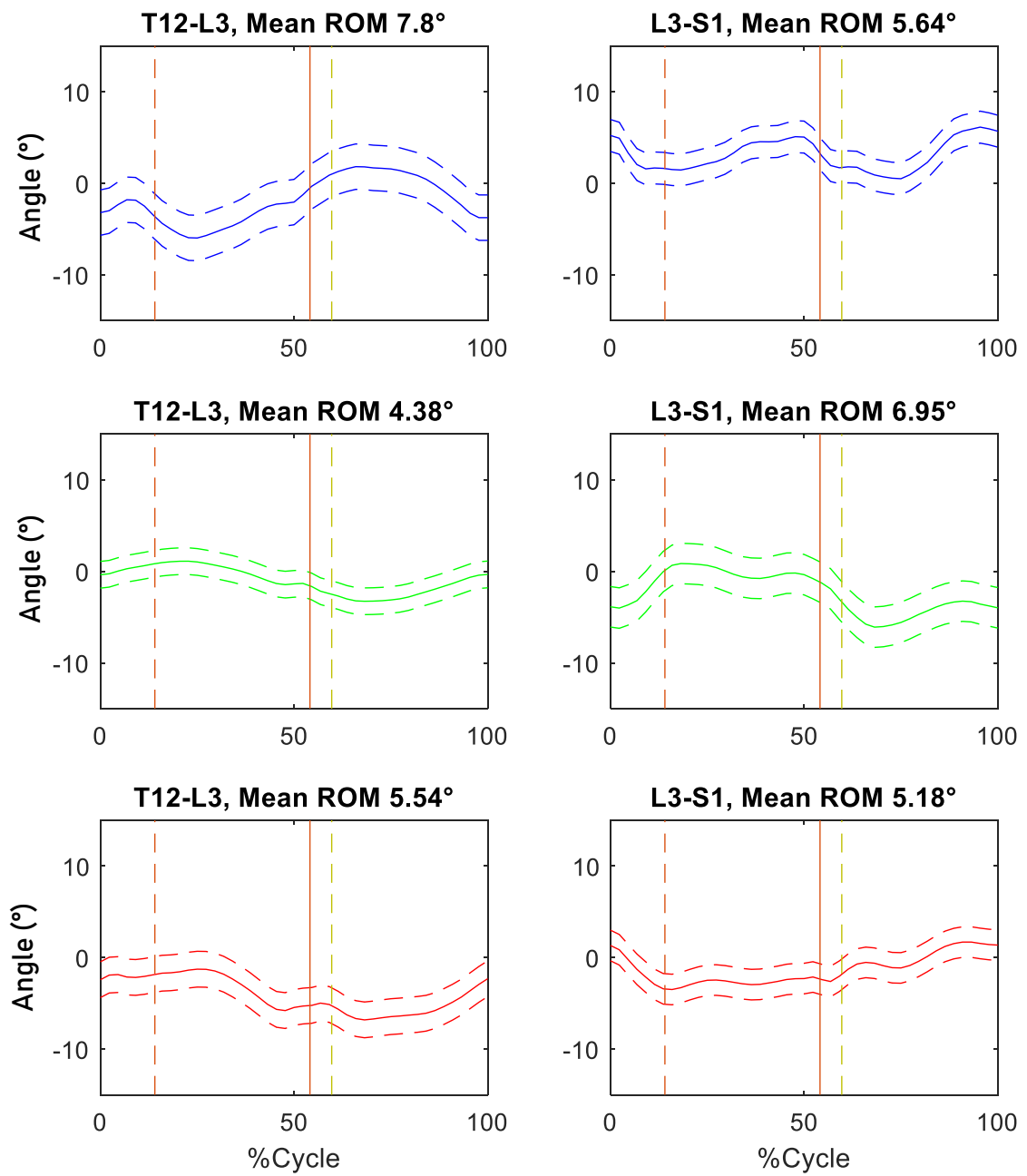


Fig. 4.3.2-5 Angle patterns of lumbar segments relative to right leg cycle at comfortable speed in the sagittal plane (up row), frontal plane (central row) and transversal plane (down row). The red continuous line represents the hell-strike of the left foot, the red dotted line represents the toe-off of the left foot and the yellow dotted line represents the toe-off of the right foot.

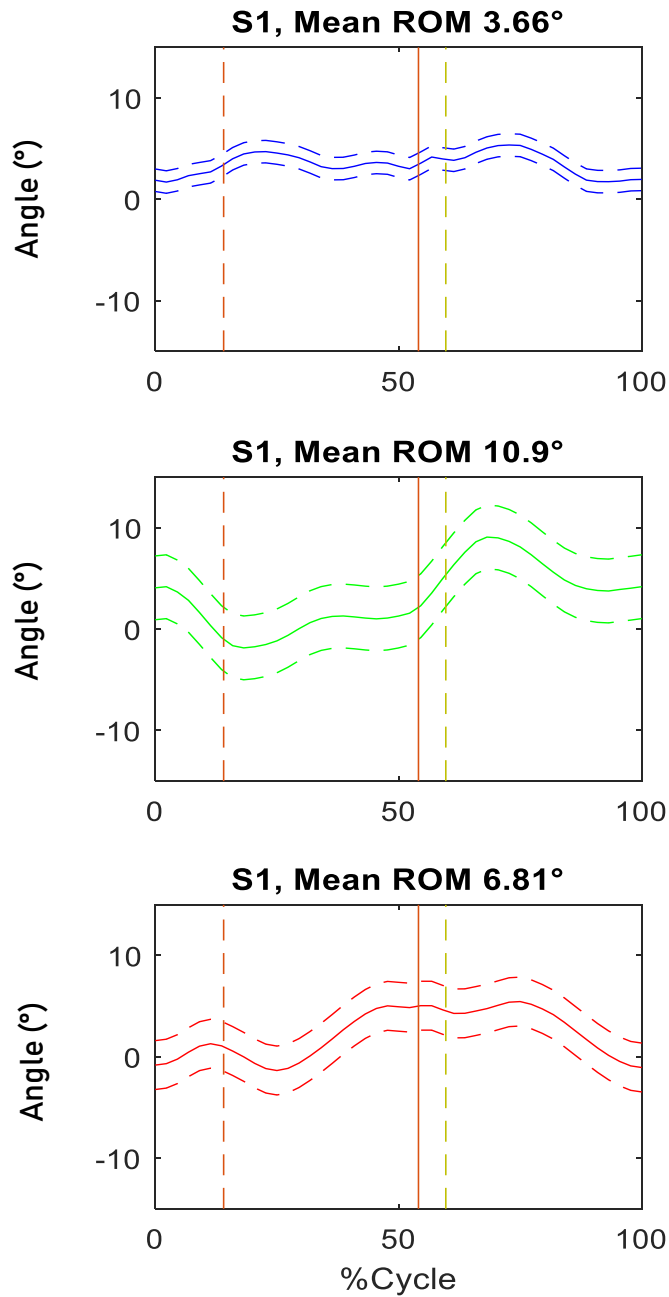


Fig. 4.3.2-6 Angle patterns of pelvis segment relative to right leg cycle at comfortable speed in the sagittal plane (up row), frontal plane (central row) and transversal plane (down row). The red continuous line represents the heel-strike of the left foot, the red dotted line represents the toe-off of the left foot and the yellow dotted line represents the toe-off of the right foot.

The walking at high speed was tested too. The self-selected high speed was found to be 1.65 m/s. It may be interesting to compare the angular patterns of the spine when the walking speed is different, as they may reveal the strategy with which the spinal segments respond to the step length increased. In Figs. 4.3.2-7, 4.3.2-8, 4.3.2-9 comparisons are shown. The most evident differences are in the frontal plane relative to C7-T6 segment. In fact, while in normal speed walking the segment is predominantly flexed to the left, in high speed walking the segment is flexed to the right.

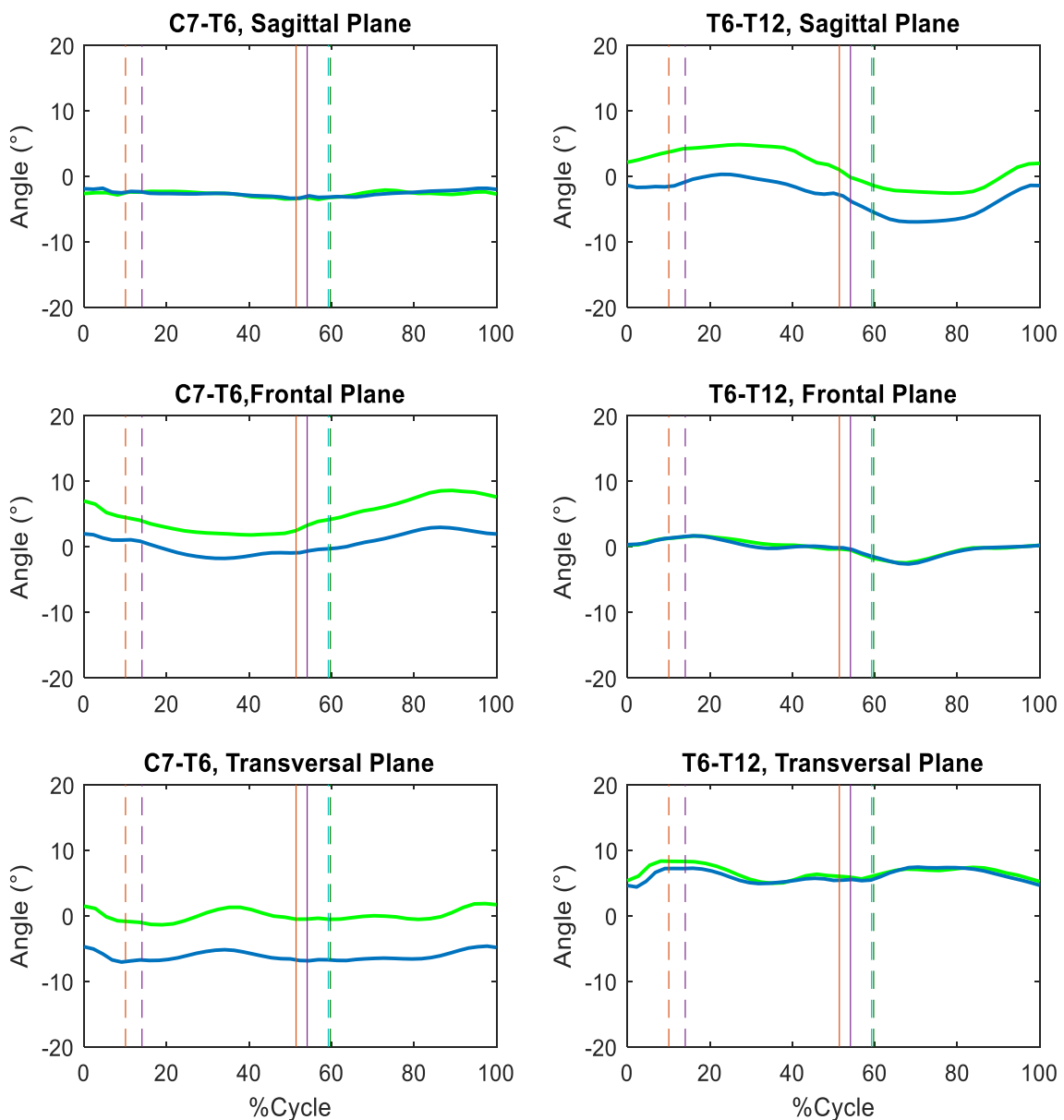


Fig. 4.3.2-7 High (green) and comfortable (blue) walking speed angles patterns comparison of thoracic segments relative to right leg cycle. For high walking speed the red continuous line represents the heel-strike of the left foot, the red dotted line represents the toe-off of the left foot and the green dotted line represents the toe-off of the right foot. For normal walking speed the purple continuous line represents the heel-strike of the left foot, the purple dotted line represents the toe-off of the left foot and the blue dotted line represents the toe-off of the right foot.

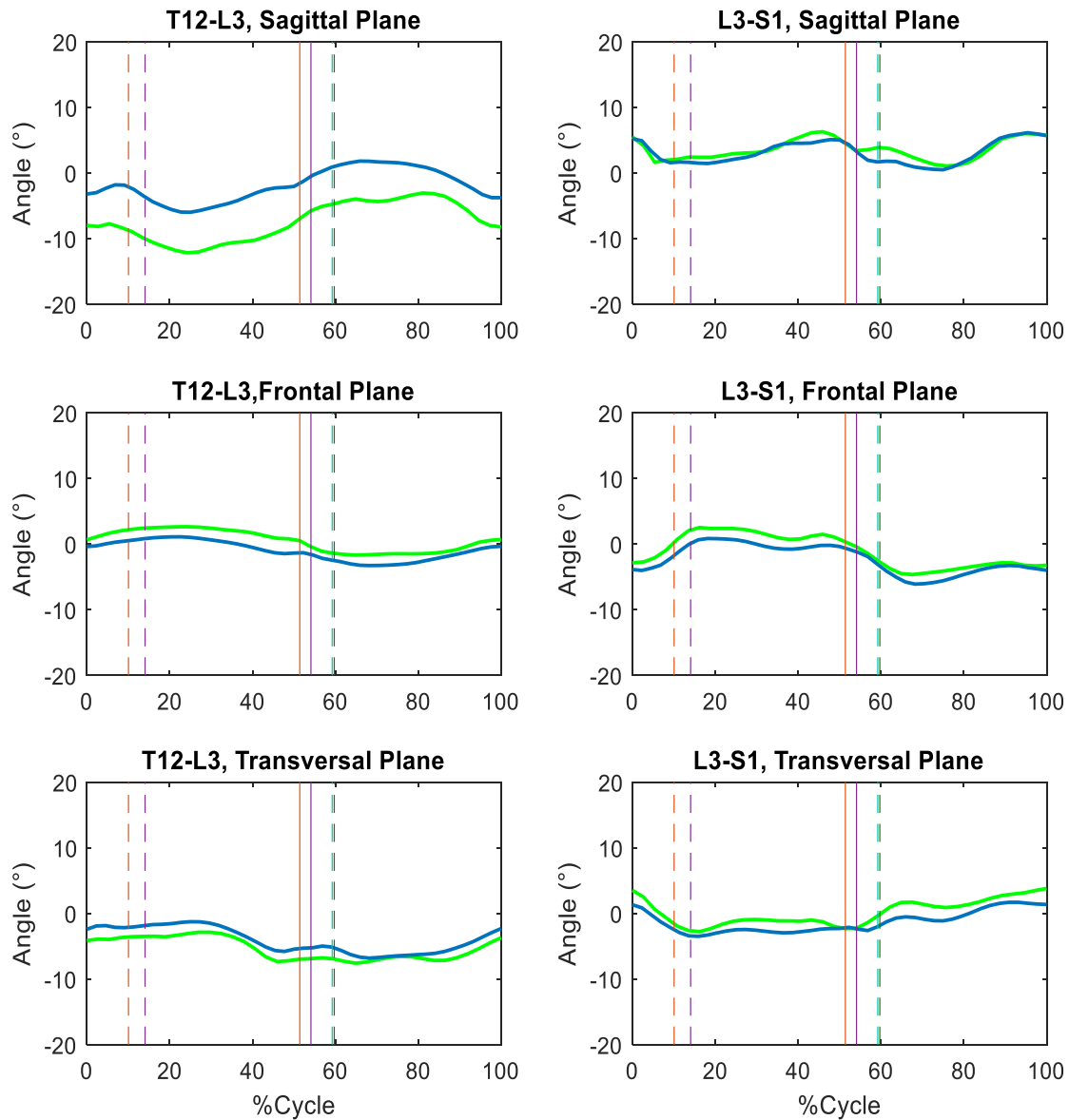


Fig. 4.3.2-8 High (green) and comfortable (blue) walking speed angles patterns comparison of lumbar segments relative to right leg cycle. For high walking speed the red continuous line represents the heel-strike of the left foot, the red dotted line represents the toe-off of the left foot and the green dotted line represents the toe-off of the right foot. For normal walking speed the purple continuous line represents the heel-strike of the left foot, the purple dotted line represents the toe-off of the left foot and the blue dotted line represents the toe-off of the right foot.

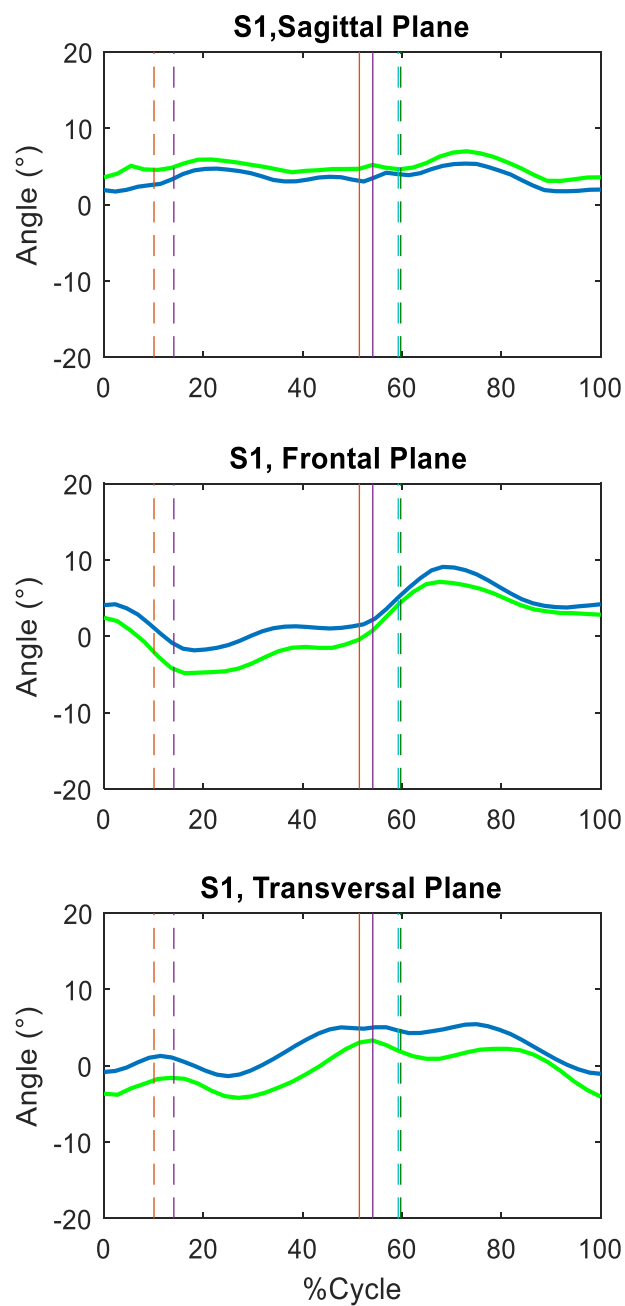


Fig. 4.3.2-9 High (green) and comfortable (blue) walking speed angles patterns comparison of pelvis segment relative to right leg cycle. For high walking speed the red continuous line represents the heel-strike of the left foot, the red dotted line represents the toe-off of the left foot and the green dotted line represents the toe-off of the right foot. For normal walking speed the purple continuous line represents the heel-strike of the left foot, the purple dotted line represents the toe-off of the left foot and the blue dotted line represents the toe-off of the right foot.

4.4 Preliminary Test with Spherical Joint Structure

During the examination of the elementary exercises some spinal segments had large movement outside the main plane of motion (Chapter 4 Section 3.1). A different definition of motion (Chapter 4 Section 3.1.1 and 3.1.2) was investigated to understand if these movements were reduced and that therefore the relative ROMs were due to a real movement and not to an error of the developed algorithm. The results obtained from that analysis actually showed a wider motion in the main plane of the elementary movement. Despite this, in some cases, the ROM values in the other planes were not entirely negligible. For this reason, a further analysis was made using only two sensors attached to two rods connected by a spherical joint. The spherical joint in fact allows to orient the two rods ensuring 3 DoF simulating a real condition applicable to the movements of the human body. As done in the preliminary test described in Chapter 4 Section 1, only two sensors were used, one positioned on the fixed base attached to a rod (fixed sensor) and the other attached to the rod that thanks to the spherical joint can assume different orientations in space (mobile sensor) (Fig. 4.4-1). Then the elementary movements of flexion-extension, lateral bending and axial rotation were proposed again. For each frame, the orientation of the mobile sensor was referred to that of the fixed sensor.

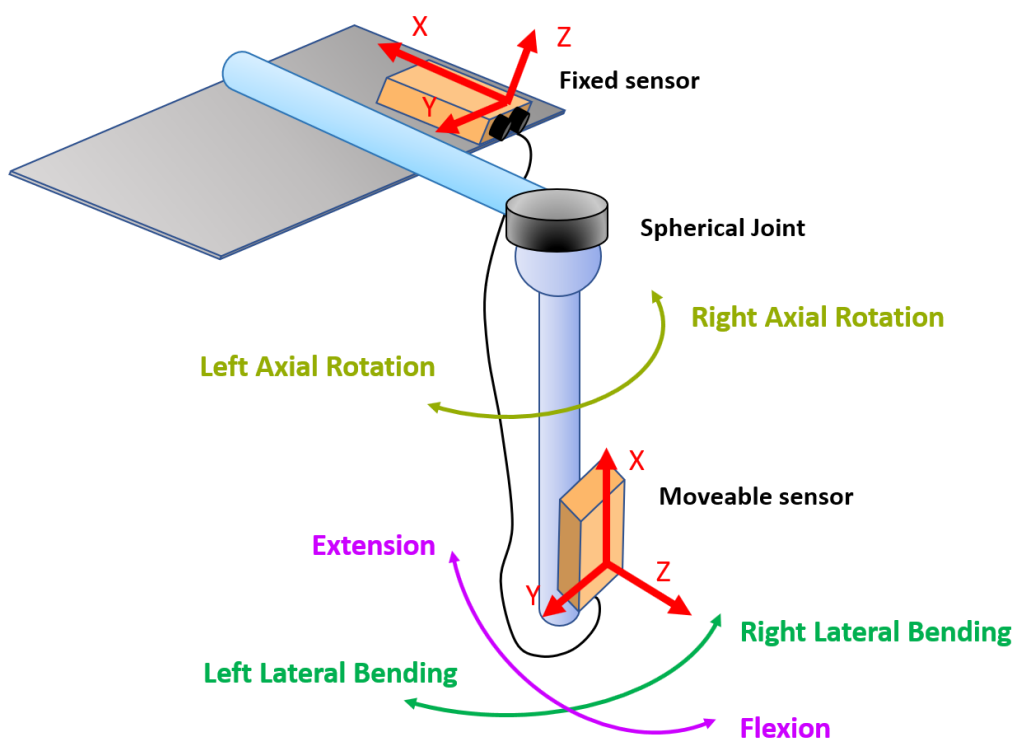


Fig. 4.4-1 Schematic representation of the instrumentation used and definition of the elementary movements tested.

Flexion-Extension in the Sagittal Plane

To evaluate the elementary flexion-extension movement, after having waited a few seconds from the start of the acquisition in order to extract the calibration data, the moving rod was moved back and forth (Fig. 4.4-1 movement described in purple) for a total of five repetitions. Care was taken to move the rod purely in the sagittal plane. The entire acquisition was segmented between two neutral positions. Then the rod from the vertical position was moved forward until it reached the maximum, it was returned to the neutral position and then moved backwards until it reached the maximum allowed again, and ending the movement by bringing the rod back vertically. The patterns and ROMs obtained in the three planes are shown in Fig. 4.4-2.

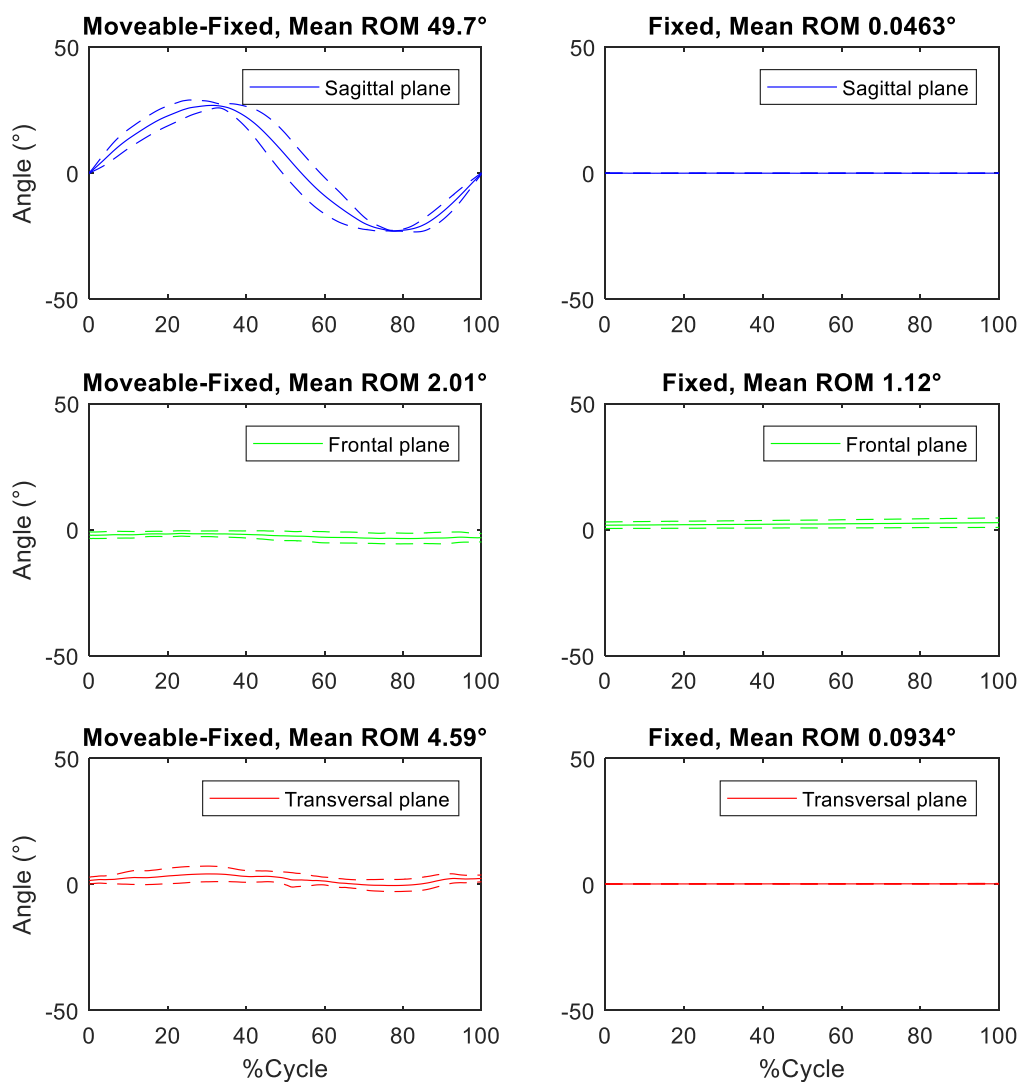


Fig. 4.4-2 Patterns and ROMs of the fixed sensor and of the mobile sensor with respect to the fixed one in the three anatomical planes during elementary exercise of Flexion-Extension.

As far as the fixed sensor is concerned, it is appreciable its staticity during the whole acquisition compared to the orientation assumed during the calibration phase. By shifting the attention to the mobile sensor, it can be seen that the main motion actually occurs in the sagittal plane. Even if the ROM value reached in the transverse plane is not so impressive, its pattern can be appreciated and it can be highlighted that, despite the use of instrumentation with a lower structural complexity than that which characterizes the spine, movements in the planes outside the main one of the motion are present. In this case, better sharpening the view, it seems that in bringing the rod in bending there is also a slight rotation to the right of the same, and that in bringing it in extension there is a slight rotation to the left.

Lateral Bending in the Frontal Plane

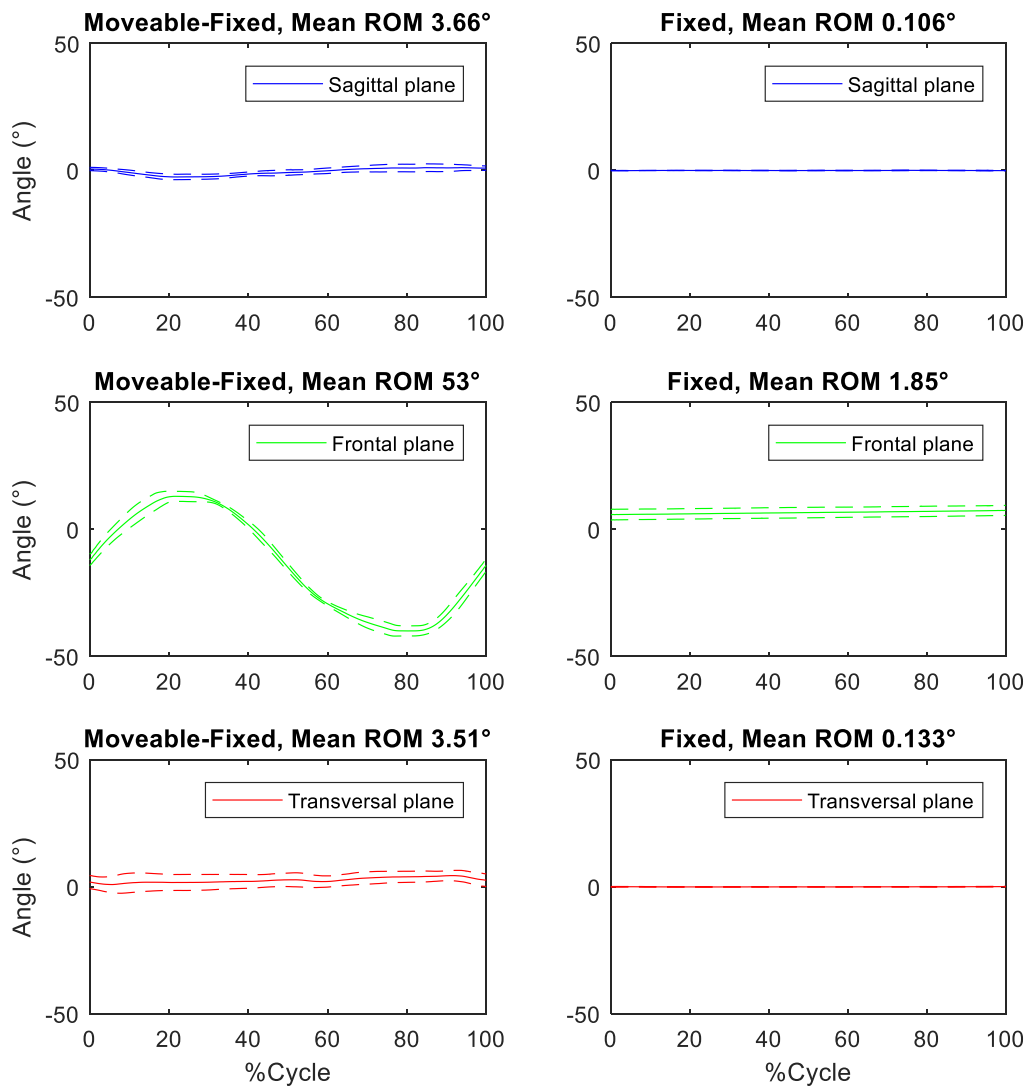


Fig. 4.4-3 Patterns and ROMs of the fixed sensor and of the mobile sensor with respect to the fixed one in the three anatomical planes during elementary exercise of Lateral Bending.

in this test, after having waited a few seconds, the rod was moved in the frontal plane, being careful not to make it oscillate in the other anatomical planes, with a first lateralization on the right that continues with an inclination on the left side (Fig. 4.4-1 movement described in green). In the post-processing phase, the acquisition was split between two vertical positions of the mobile rod. Fig. 4.4-3 shows the patterns and ROMs of the fixed sensor and of the mobile sensor with respect to the fixed one. The fixed sensor is characterized by negligible ROM and the patterns in the three anatomical planes are flat, indicating that the sensor remains in approximately the same starting position. The mobile sensor has the highest ROM in the frontal plane and the relative pattern has the shape of a sine wave. Even in this case, although the

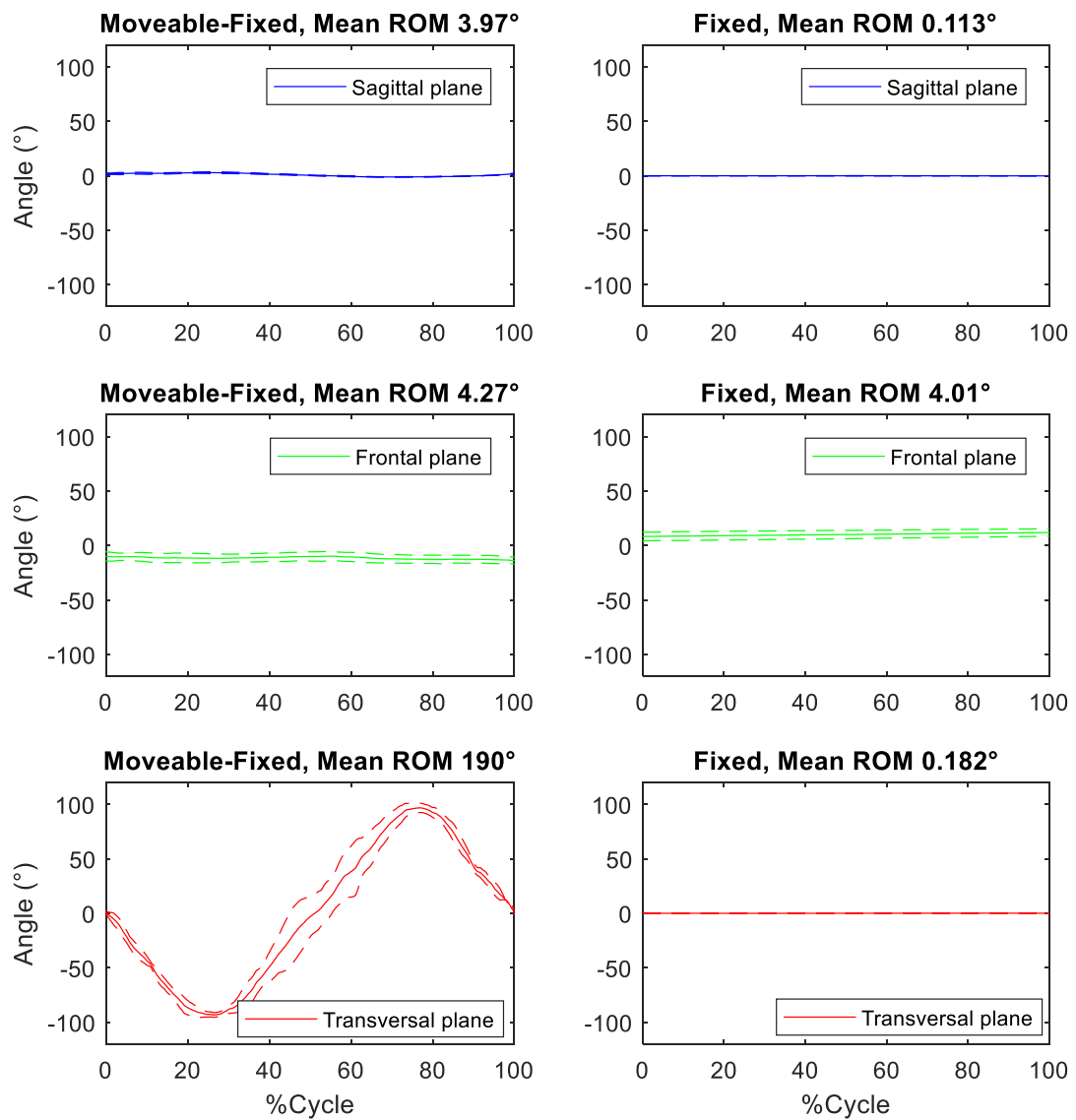


Fig. 4.4-4 Patterns and ROMs of the fixed sensor and of the mobile sensor with respect to the fixed one in the three anatomical planes during elementary exercise of Axial Rotation.

motion is mainly in the frontal plane, it can be seen small movements also in the sagittal and transversal plane.

Axial Rotation in the Transversal Plane

To obtain an axial movement, the moveable rod was rotated around its longitudinal axis. Then, from the vertical position, the rod was rotated to the left, and once returned to neutral position it was rotated to the right side (Fig. 4.4-1 movement described in acid yellow). As with the other tests, the acquisition was split between two vertical positions of the rod. The results obtained are visible in Fig. 4.4-4. It turns out that the mobile sensor has a wide movement in the transversal plane, as It should be, while in the other planes the ROM values reached are dictated by the small oscillations inevitable by manually moving the rod. It can be also appreciated that the fixed sensor remains in the same orientation throughout the cycle.

This test session was used to ensure that the algorithm applied to the detection of spinal angles is accurate and that the motion that some segments expressed in other planes had actually been detected and that it was not a processing error. From the results obtained here it is possible to affirm that a segment free to move with 3 DoF, even if the movement is performed in a predefined plane, presents oscillations also in the other anatomical planes. Therefore, it is correct to think a complex structure such as the spinal column during the execution of elementary movements can be characterized by wide movements even in planes different from the main one of the motion. The doubt arises, however, seeing that in some relative movements (motion of the upper segment compared to the motion of the lower segment) the ROM is widely greater in a plane that is not the main one of the motion. At this point, this result leads to think that either this behaviour is actually proper to some spinal segments or that in performing elementary movements in the three planes leads a displacement of the sensors that is expressed in these high ROMs values. The latter problem, however, would not affect the results obtained in angular kinematics during walking. Here, in fact, the slippage of the sensors by the movement itself is undoubtedly of little importance compared to that obtained in elementary movements.

4.5 Preliminary Test with Optitrack and Xsens

The test was performed with two Optitrack V120:Trio bars positioned at one end of the way traversed by recruited subject (Fig. 4.5-1). To make sure that the two bars are able to capture all markers placed on the spine for at least one gait cycle, they were tilted relative to the floor. The bars were placed at a distance of about 3 m and tilted to each other. Each bar has its own reference system:

- The z-axis is perpendicular to the bar and points toward the acquisition volume;
- The y-axis is perpendicular to the z-axis and points upwards;
- The x-axis is given by the cross product of the other two in order to create a right-handed triad.



Fig. 4.5-1 Location of the two V120:Trio bars.

The origin of the reference system described is located in the centre of the bar, that is in correspondence with the central camera (Fig. 4.5-2).

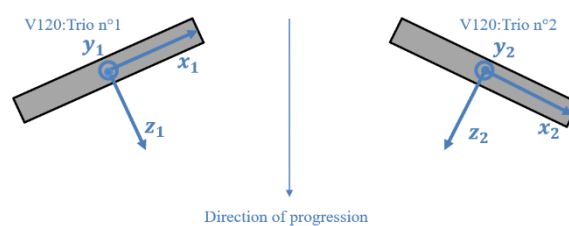


Fig. 4.5-2 Bars local reference frames.

With the aim to follow a straight line and in order to facilitate the subject involved to do this, a 6 m guide was drawn on the floor. Before performing the test with subject, the acquisition volume was identified in about 3 m in the middle of the total path (Fig. 4.5-3).

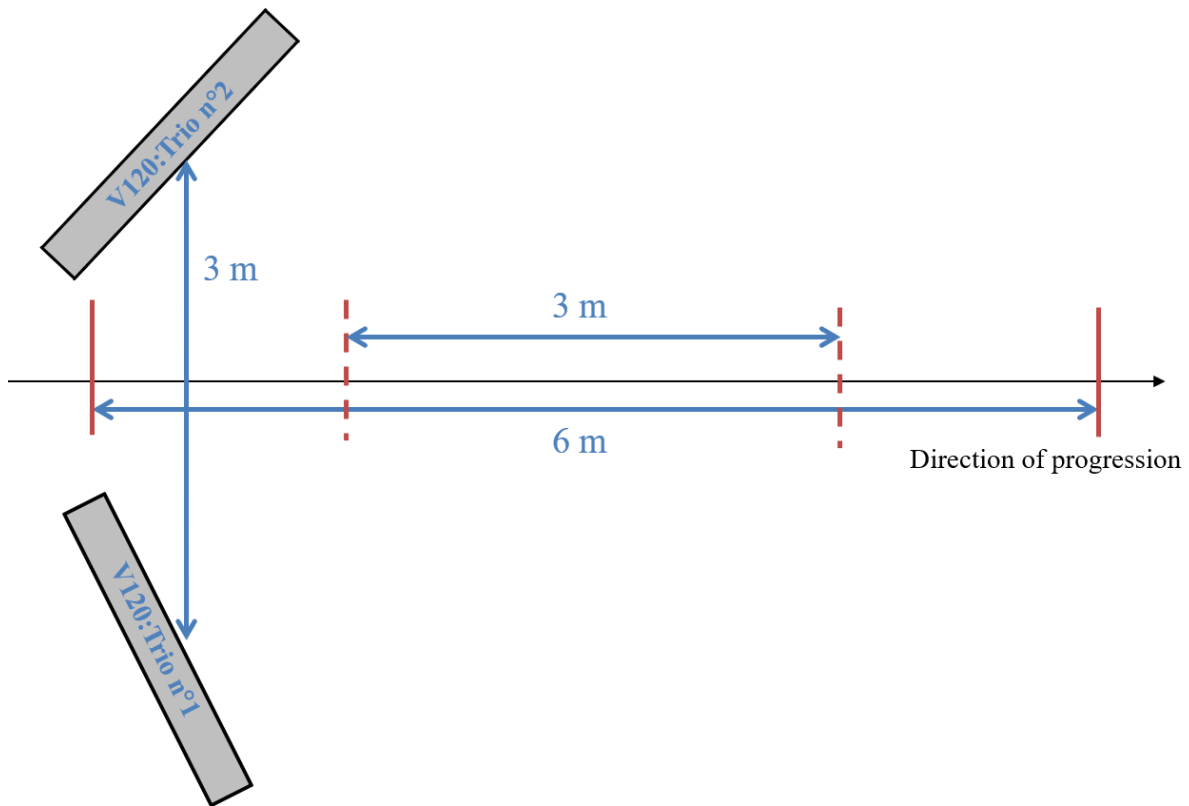


Fig. 4.5-3 Setting with distances.

Since each bar defines the coordinates of the markers in its own reference system, it was necessary to define a reference system attached to the laboratory. In this way it's possible obtain the transformation matrix necessary to switch the reference system of each bar into the laboratory reference system: each marker, even seen from different bars, will have the same coordinates.

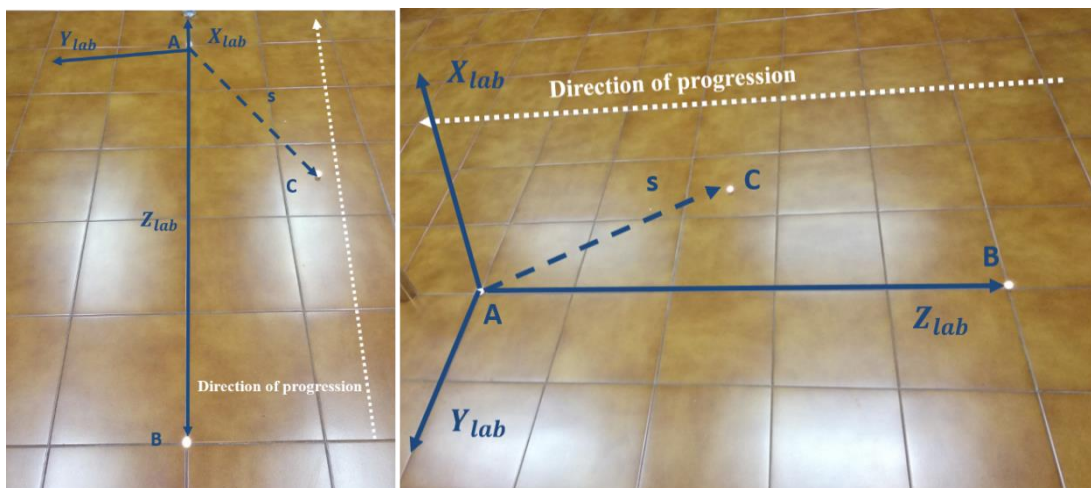


Fig. 4.5-4 Configuration of fixed markers for the creation of the transformation matrix.

In order to define the laboratory reference system, a static acquisition was carried out by placing three markers (A, B and C) on the floor in the configuration shown in Fig. 4.5-4: two of the three markers (A and B) were placed along the trajectory of the gait. The origin of the laboratory reference system is in A. the Z-axis (with direction opposite to the direction of the gait) was calculated as the distance of B from A; the support vector s was calculated as the distance of C from A. From the cross product of Z-axis and s , X-axis was obtained and it points upwards. Finally, from cross product of Z-axis and X-axis Y-axis was obtained. Fig. 4.5-4 shows the final configuration of the axes of the reference system attached to the laboratory.

Once the coordinates of markers A, B and C had been obtained, it was possible to construct the transformation matrix. The first three columns represent the coordinates of the triad in the local reference frame of the bar, while the fourth column represents the coordinates of the origin A in the reference system of the bar. For each of the two bars the transformation matrix is:

$${}^1M_{ABC} = \begin{bmatrix} x1_X & y1_X & z1_X & A1_X \\ x1_Y & y1_Y & z1_Y & A1_Y \\ x1_Z & y1_Z & z1_Z & A1_Z \\ 0 & 0 & 0 & 1 \end{bmatrix}$$

$${}^2M_{ABC} = \begin{bmatrix} x2_X & y2_X & z2_X & A2_X \\ x2_Y & y2_Y & z2_Y & A2_Y \\ x2_Z & y2_Z & z2_Z & A2_Z \\ 0 & 0 & 0 & 1 \end{bmatrix}$$

To ensure that these transformation matrices were correct, a fourth marker D was placed (Fig. 4.5-5). To make the new marker more recognizable than the others, it was placed at a different height with the help of a metal cylinder. The vector expressing the coordinates of D for each bar has been pre-multiplied for its transformation matrix: it has been verified that both products return an identical vector.

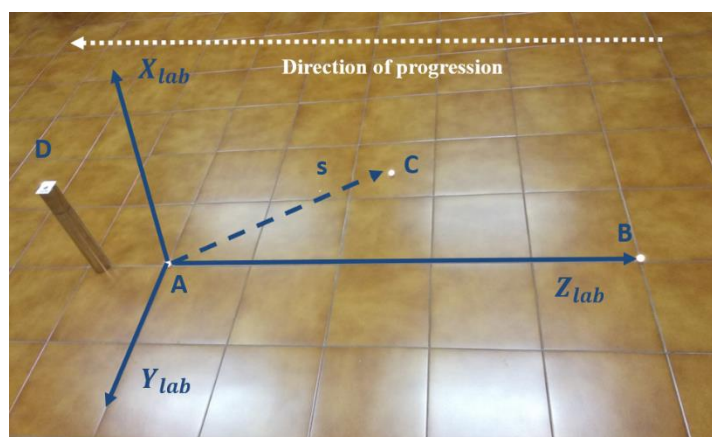


Fig. 4.5-5 Fixed markers placement.

During the dynamic acquisitions with the subject involved, it was asked to lift the right foot on witch an additional marker was placed. This movement allowed to synchronize the acquisitions not only of the two bars, but also the one with the inertial sensors. In fact, during the post-processing phase, the frame in which the marker on the right heel rises after hitting the ground represents the zero instant of the two bars. For Xsens the zero instant has been identified by the acceleration-X (vertical acceleration) of the sensor S1 (Fig. 4.5-6) closer to the ground: the impact of the heel to the ground generates an easily recognizable peak.

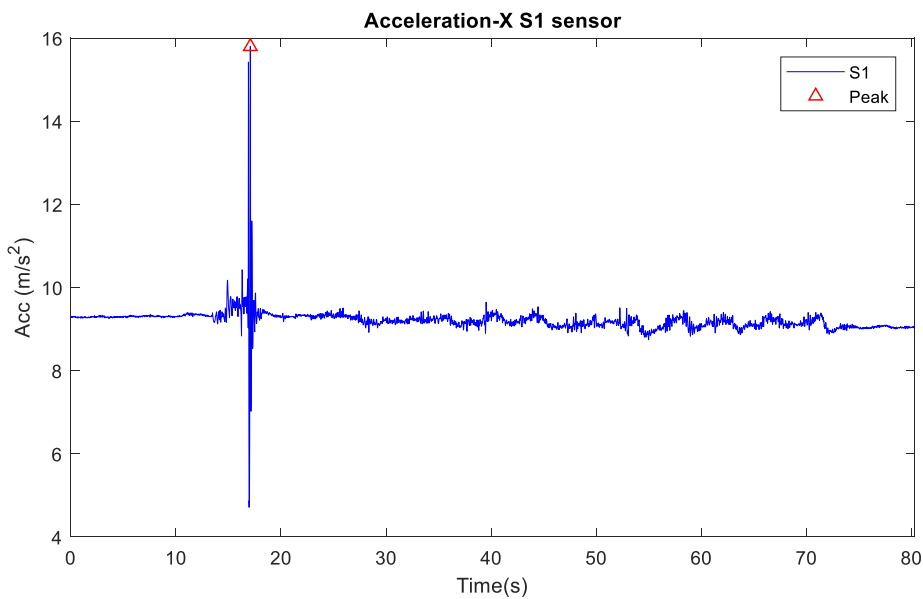


Fig. 4.5-6 Heel strike peek to synchronize Xsens and Optitrack systems.

The characteristics of the subject recruited for the test are reported in Tab. 4.5-1.

Subject gender	Age (years)	Height (cm)	Weight (kg)
Female	26	165	54

Tab. 4.5-1 Characteristics of subject recruited.

Three MTx sensors (Xsens, Technologies) were placed on the subject at S1, T12 and C7 level vertebrae (Fig. 4.5-7). The number of sensors used is lower than in previous test sessions. C7 and T12 sensors were fixed with double-sided adhesive tape and an elastic band was applied to the sensor at T12 level in order to improve adhesion during the execution of the movements. The sensor on the Pelvis (S1) has been placed in the special elastic band supplied by the Xsens Group.

Once the sensors were positioned, the markers were placed on them. At each vertebral level, therefore on each sensor, three markers (6 mm diameter) were fixed on the same plane. The three markers have been positioned to create a triad aligned with the reference system of the

sensor on which they are placed (Fig. 4.5-8), in order to obtain consistent data between the two measuring systems. In particular, the x-axis has been obtained by calculating the distance from marker 2 to marker 1; the support vector s is obtained by calculating the distance from marker 3 to marker 1; the cross product between the x-axis and s returns the z-axis; the y-axis is obtained from the cross product of z-axis and x-axis. The origin of the local reference system coincides with marker 1.

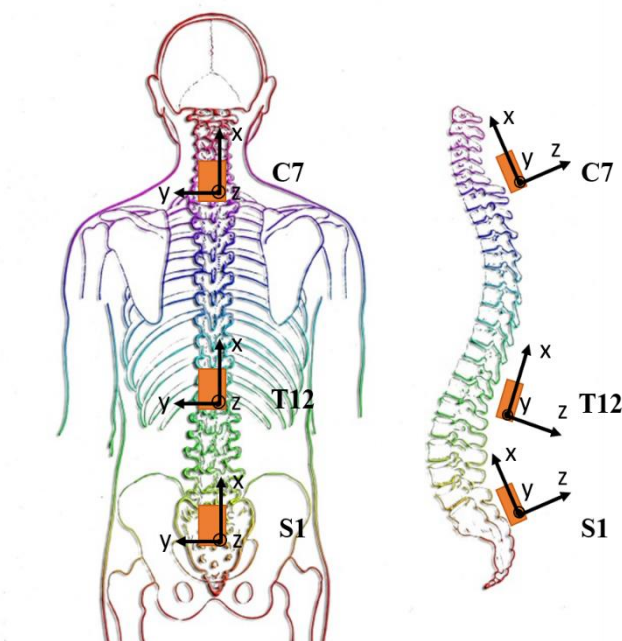


Fig. 4.5-7 Sensors location and orientation of local reference systems.

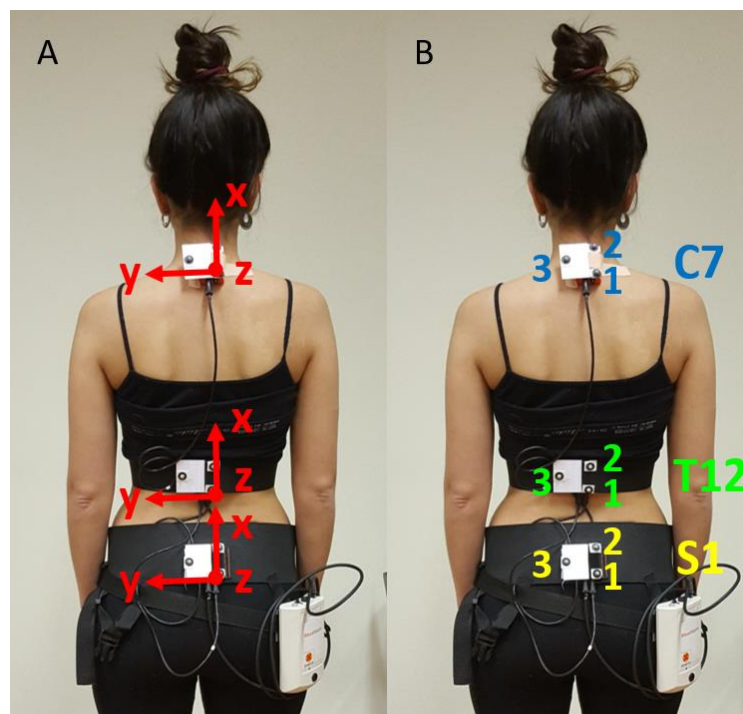


Fig. 4.5-8 B Markers placement and local reference systems created (A).

4.5.1 Elementary Movement: Lateral Bending

The subject was first asked to position himself with his back to the bars, in the acquisition volume of the cameras. Then, after starting the acquisition with both systems and impacting the right heel to the ground, the subject made a series of five elementary movements. The elementary movements chosen was the one in the frontal plane. The recruited subject was asked to perform the movement purely in the selected plane, starting to the right side, without reaching the maximum possible lateral flexion. This is to avoid the displacement of the sensors and markers, but also to avoid the oscillation of the column in other anatomical planes outside the frontal plane.

In the post-processing phase, the markers information from the two bars were combined in such way that there was no gap in the acquisition of markers coordinates. After this, the data was resampled because Optitrack adopted an acquisition frequency of 120 Hz, while for Xsens the sampling frequency was set to 50 Hz.

Before the dynamic movement begun, the subject was asked to remain upright for a few seconds. The data obtained in that acquisition section were used to define the calibration matrices of the three triad markers and the three inertial sensors.

The processing carried out on the matrices on the inertial sensors, described in the Chapter 3 Section 2, is the same as that used in the case of the matrices of the triad markers. The angles obtained with Tilt-Twist Method from inertial sensors were compared with Roll, Pitch and Yaw angles defined for Optitrack in the following way, according to the defined axis system:

$$Pitch = \text{atan2}\left(\frac{Z'_x}{Z'_z}\right)$$

$$Roll = \text{atan2}\left(\frac{-X'_y}{X'_x}\right)$$

$$Yaw = -\text{atan2}\left(\frac{-Z'_y}{Z'_z}\right)$$

The convention (Tab. 4.5.1-1) adopted to obtain the angles with Optitrack system is the same used in Xsens system.

	PITCH	ROLL	YAW
POSITIVE +	Flexion	Right	Right
NEGATIVE -	Extension	Left	Left

Tab. 4.5.1-1 Angles convention for Optitrack system.

The Roll, Pitch and Yaw angles were filtered using the Matlab routine *Curve Fitting Tool* and in particular, a Smoothing Spline was used for interpolation. In the Figs. 4.5.1-1,4.5.1-2,4.5.1-3 are shown examples of the result of the interpolation have been reported.

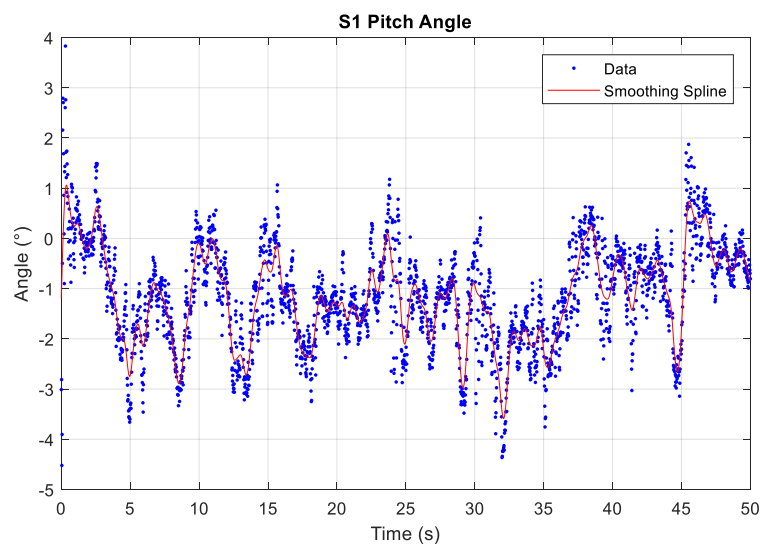


Fig. 4.5.1-1 Smoothing of S1 pitch angle.

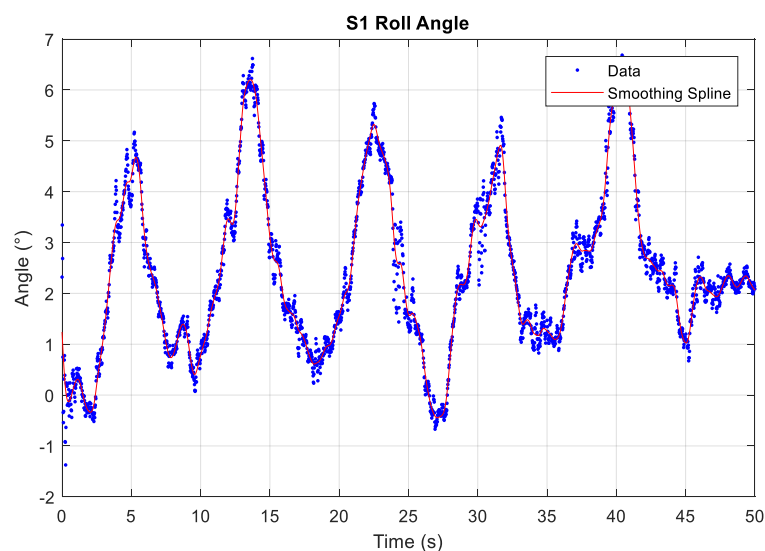


Fig. 4.5.1-2 Smoothing of S1 roll angle.

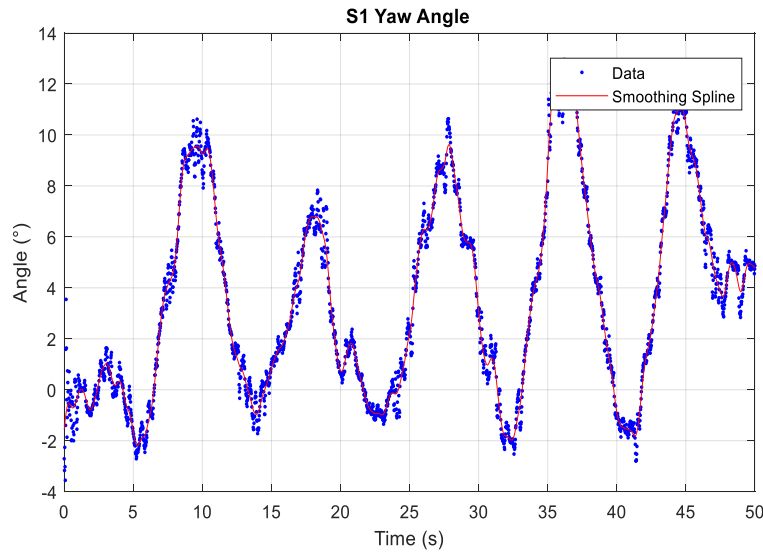


Fig. 4.5.1-3 Smoothing of S1 yaw angle.

Fig. 4.5.1-4 shows the movement patterns of C7 vertebra compared to the T12 vertebra detected by the two different measuring systems in the three planes. Visually from these graphs it is possible to notice that the patterns relative to the two measurement systems are very similar in the frontal and transversal planes, while in the sagittal plane there are some discrepancies. Moreover, in the frontal plane the Optitrack system pattern seems to be wider. Focusing on the pattern in the frontal plane, it is possible to recognize five complete movements: from the upright posture to positive lateral flexion (to the right side), from positive lateral flexion to upright posture, from upright posture to negative lateral flexion (left side) to return at upright posture. From these patterns it is possible to notice how a movement, even if executed in a specific plane, is accompanied by, more or less, wide movements in the other planes.

Fig. 4.5.1-5 shows the trends of the T12 vertebra compared to the Pelvis. Here again, in the sagittal plane, the two measurement systems return information that is not strictly consistent. In the frontal plane and in the transversal plane, on the other hand, the trends can be superimposed. In the transversal plane Optitrack pattern is slightly wider.

Finally, Fig. 4.5.1-6 shows the trend of the Pelvis with respect to its starting position, during lateral flexion movement. Unlike what happens in the other segments considered, the patterns are superimposed in all three anatomical planes.

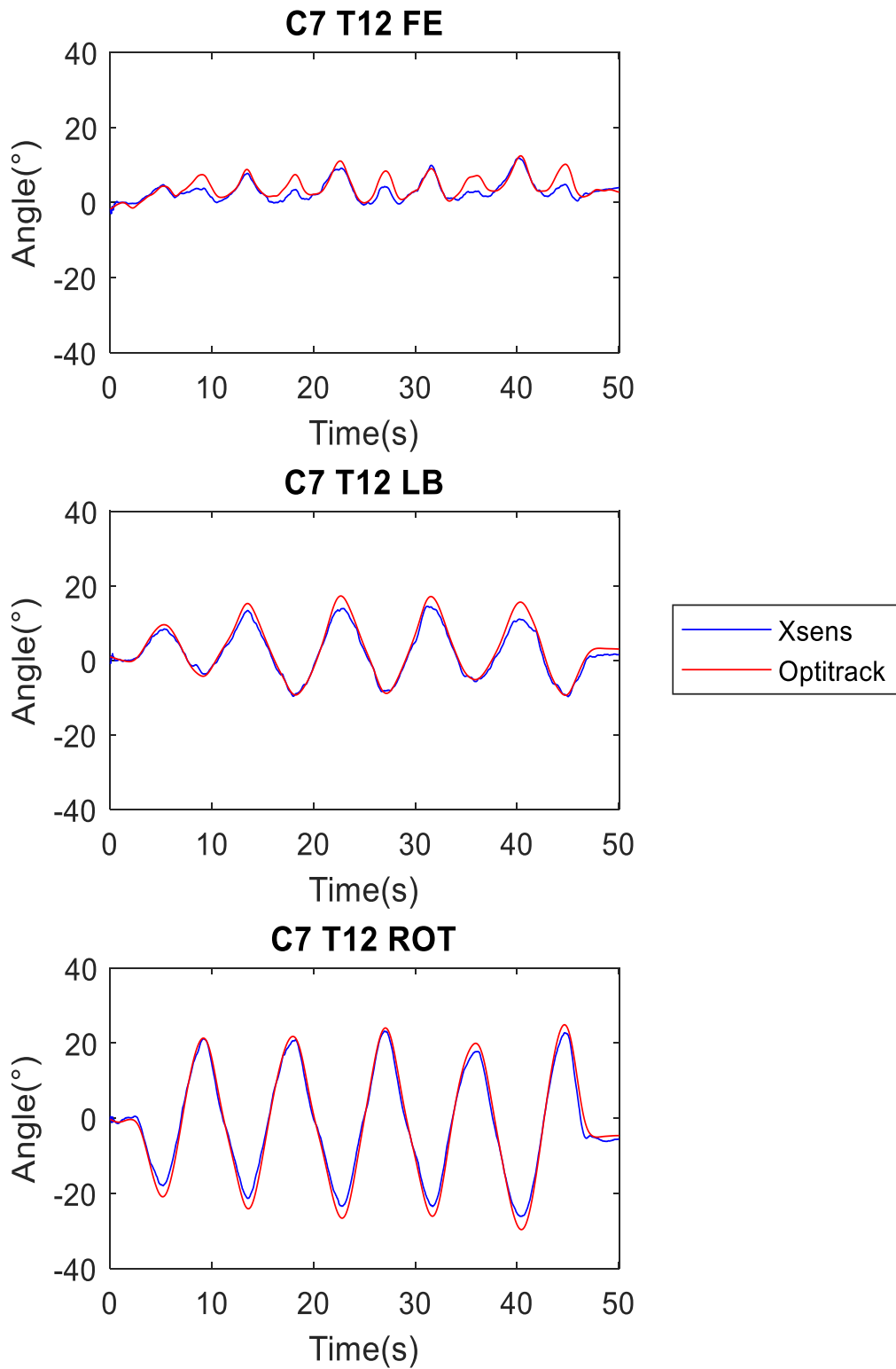


Fig. 4.5.1-4 Angles patterns of C7 vertebra compared to T12 vertebra during lateral bending.

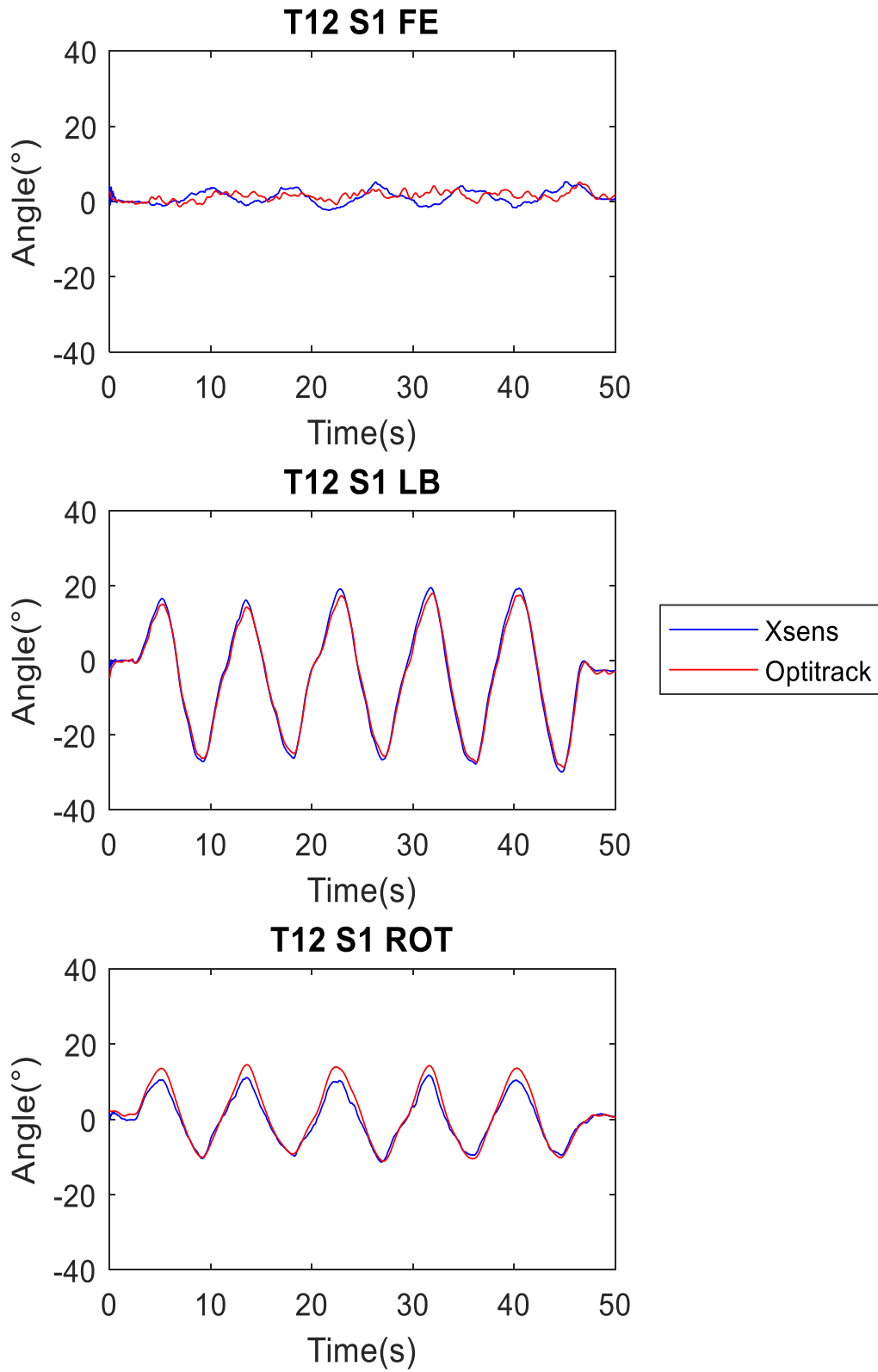


Fig. 4.5.1-5 Angles patterns of t12 vertebra with respect to Pelvis segment during lateral bending movement.

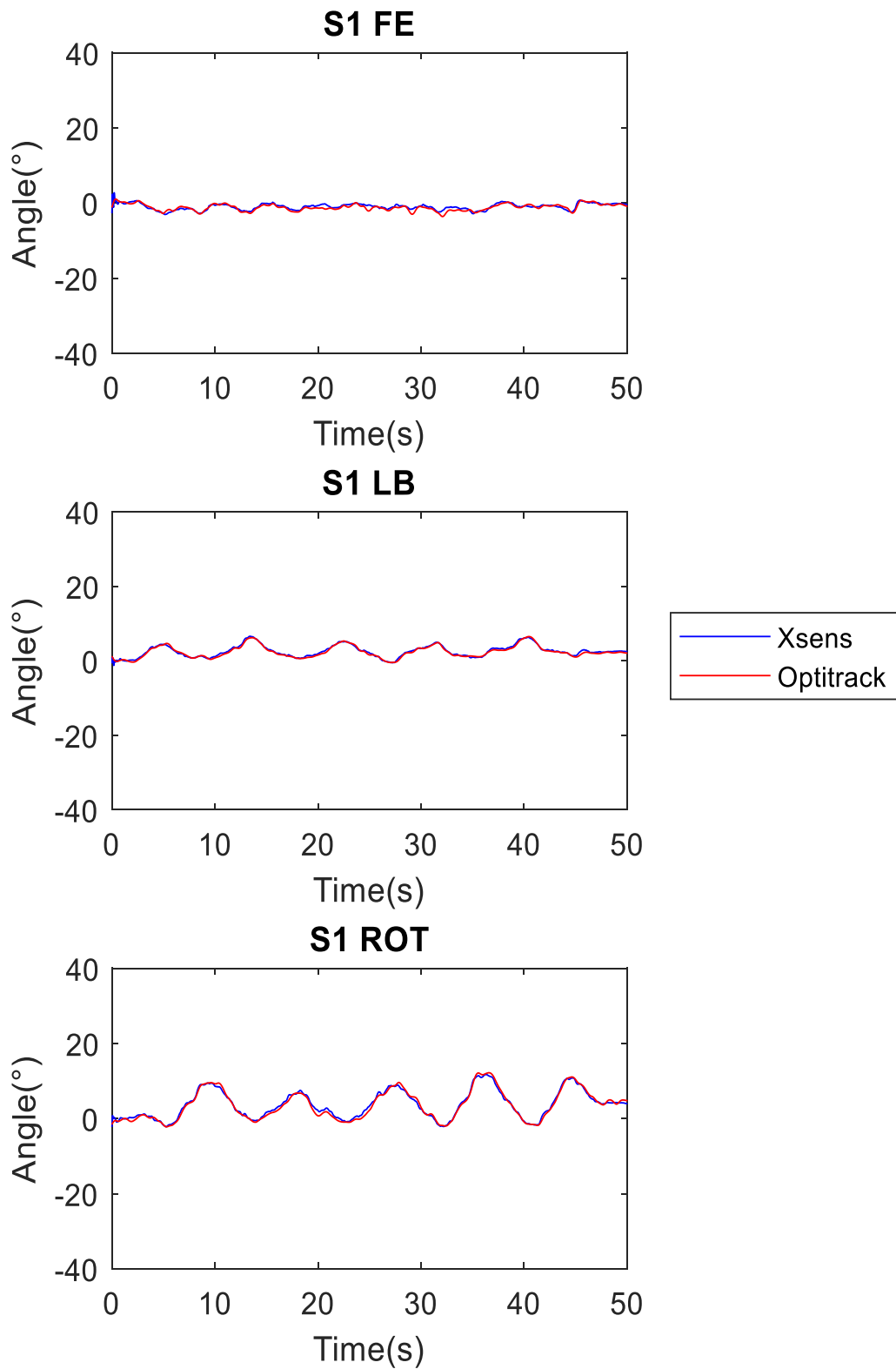


Fig. 4.5.1-6 Pelvis angles patterns during lateral bending.

Examining the results obtained in the sagittal plane, it can be deduced that the discrepancy in the patterns between C7-T12 are due to the more consistent oscillation of the cervical zone that causes a possible misalignment between the two reference systems attached to the C7 vertebra. The same reasoning can be associated with T12-S1 patterns, with the difference that the oscillation at T12 level is certainly less consistent than at C7 level. In fact, the patterns related to T12-S1 are less divergent than the patterns related to C7-T12. The consideration just made could explain the minor inconsistencies in the other two planes.

Tab. 4.5.1-2 shows the Range of Motions (ROMs) of the three segments considered in the three anatomical planes.

	C7-T12 ROM (°)			T12-S1 ROM (°)			S1 ROM (°)		
	Sagittal Plane	Frontal Plane	Transv Plane	Sagittal Plane	Frontal Plane	Transv Plane	Sagittal Plane	Frontal Plane	Transv Plane
Xsens	12.98	24.08	49.22	7.50	49.34	23.06	3.06	7.02	13.82
Optitrack	14.19	26.64	54.55	6.53	46.53	25.34	4.29	6.95	14.15
Difference	1.21	2.56	5.33	0.97	2.81	2.28	1.23	0.07	0.33

Tab. 4.5.1-2 Segments ROM obtained with the two measuring systems. The yellow row shows the difference between values corresponding to the spinal segment and the anatomical plane.

Analysing the ROMs in the frontal plane, the T12-S1 segment with respect to the Pelvis is the one that contributes most to the movement followed by the C7-T12 segment with respect to the T12-S1 segment. As already mentioned, it appears that C7 vertebra compared to T12 has a not negligible movement in the transversal plane, which is even greater than that in the main plane of movement. The same behaviour is found in the pelvic segment.

By looking at the differences between the two measurement systems, it is possible to confirm that the Xsens system is more reliable on the Pelvis than the other vertebral levels. It should be noted once again that the problem may be hidden in the structure used for the markers positioning.

4.5.2 Walking Movement

In this phase of the test it would correlate the angles of the spine to gait. As already done in the execution of the elementary movements, the subject was asked to position himself within the volume of the cameras, to lift the heel and hit the ground with the same. After this, the subject stood upright for a few seconds to obtain calibration data. The subject was then asked to reach the indicator at the beginning of the path traced on the floor and to follow it for 5 times giving is back to the cameras at a self-selected speed (0.93 m/s). Without interrupting the acquisition and once the 5 required executions had been completed, the subject was asked to repeat the 5 gaits but with higher speed.

In the post-processing phase, the acquisitions of the two measuring systems were synchronized, observing, in one case, the position of the marker on the heel and, in the other, the peak of the vertical acceleration of the sensor closest to the ground (S1).

After having expressed the coordinates of the markers in the same reference system, the information return from the two bars were combined in order to fill any gaps in the acquisition or to extend the visibility of the markers.

Fig. 4.5.2-1 shows the x coordinate of marker 1 of the triad in C7. It is visible how one bar can display the marker in question before the other and at the same time how the other bar can capture it up to a few samples later.

Since there are alternating phases in the gait where the markers are visible and phases in which the markers disappear because of the subject's exit from capture volume or because the walk is in direction if cameras, it was necessary recognize the sections of the acquisition where all markers are visible. In these sections gait cycles were identified using information of the antero-posterior acceleration of the inertial sensor at T12 level. The acceleration-Z signal has not been filtered to avoid additional lag that could compromise the synchronization of the two measuring systems.

Observing the acceleration-Z, it was found that among the samples in which all the markers were visible, only one gait cycle was recognized in the case of walking al comfortable speed (Fig. 4.5.2-2), while in the case of walking at higher speed, unfortunately, it was not possible to isolate only one gait cycle (Fig. 4.5.2-3).

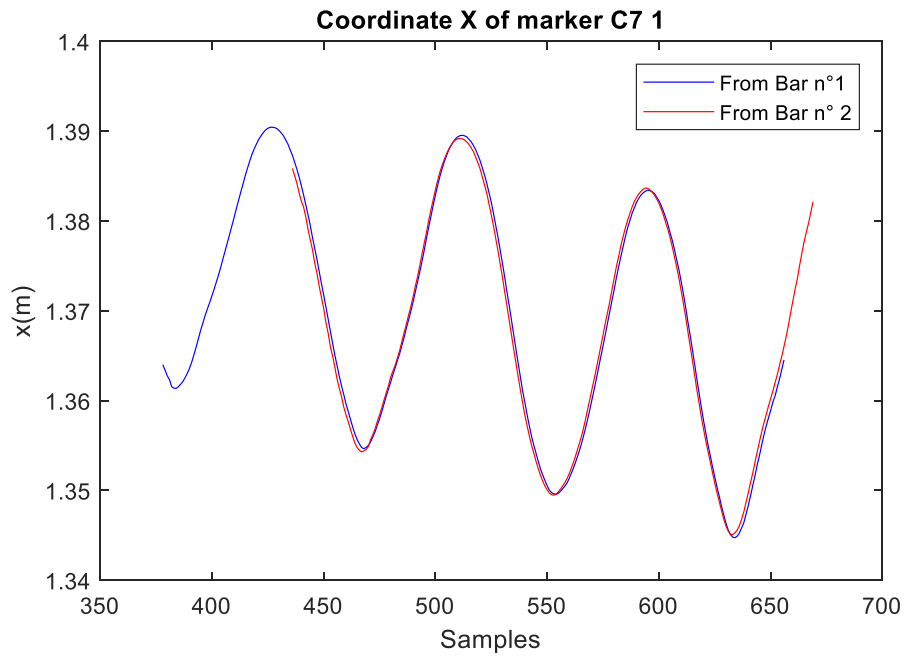


Fig. 4.5.2-1 X coordinate of marker number 1 belonging to C7 level triad.

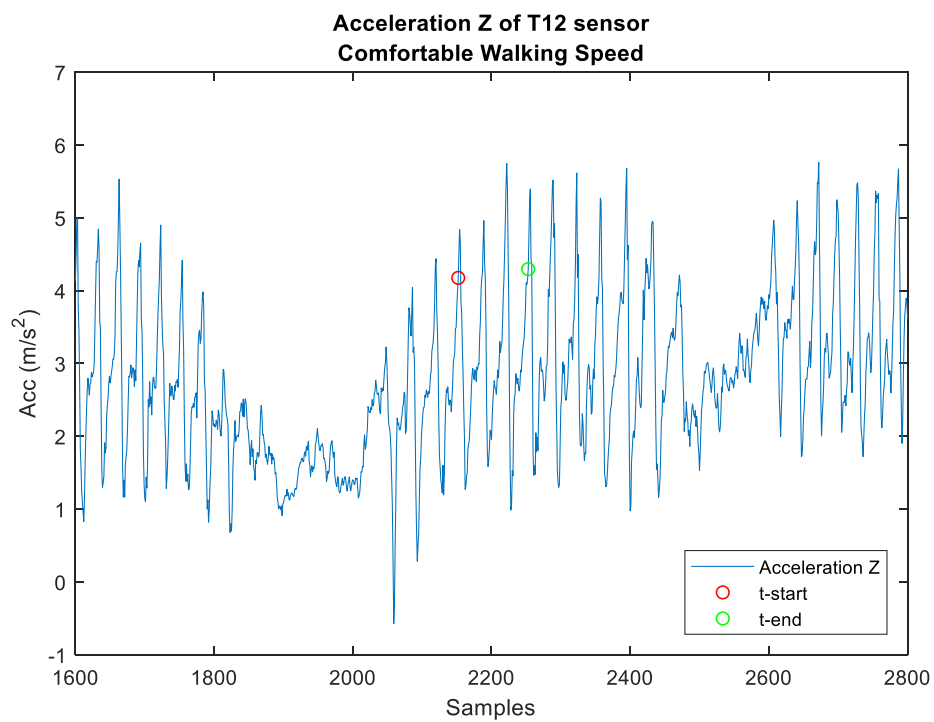


Fig. 4.5.2-2 Example of acceleration Z section (between the two red and green indicators) from which gait cycle can be extract.

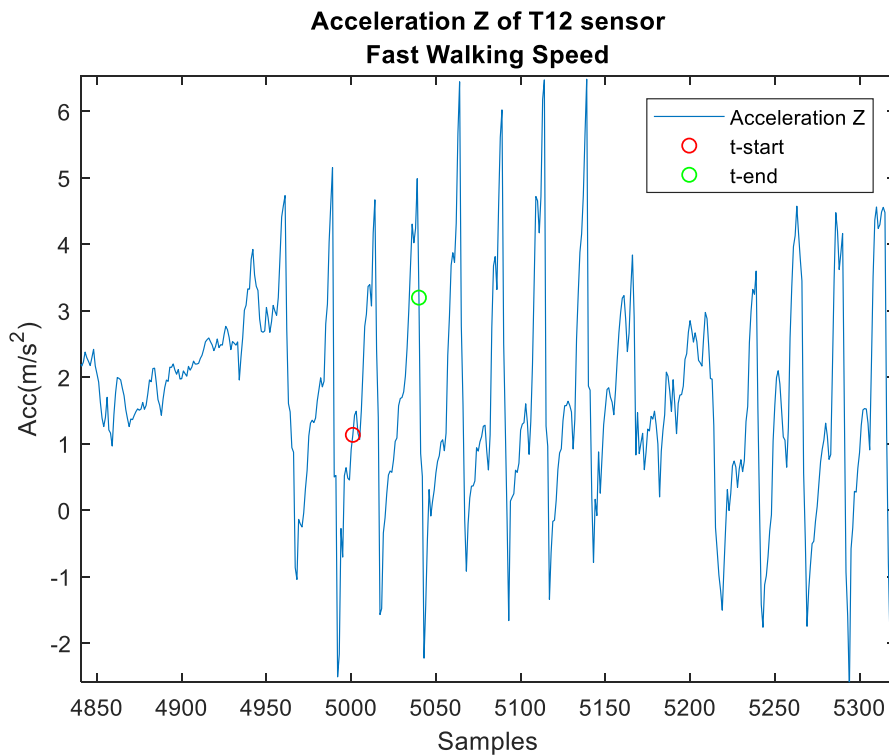


Fig. 4.5.2-3 Example of acceleration Z section (between the two red and green indicators) from which gait cycle cannot be extract.

The gait cycle identified in the walking at comfortable speed has been defined between two Heel-Strike (HS) of the same leg. In particular, the analysis of angular velocity around the vertical axis of the T12 sensor showed that the cycle is defined between two HSs of the right leg. The gait cycle can be defined by the following phases shown in Fig. 4.5.2-4.

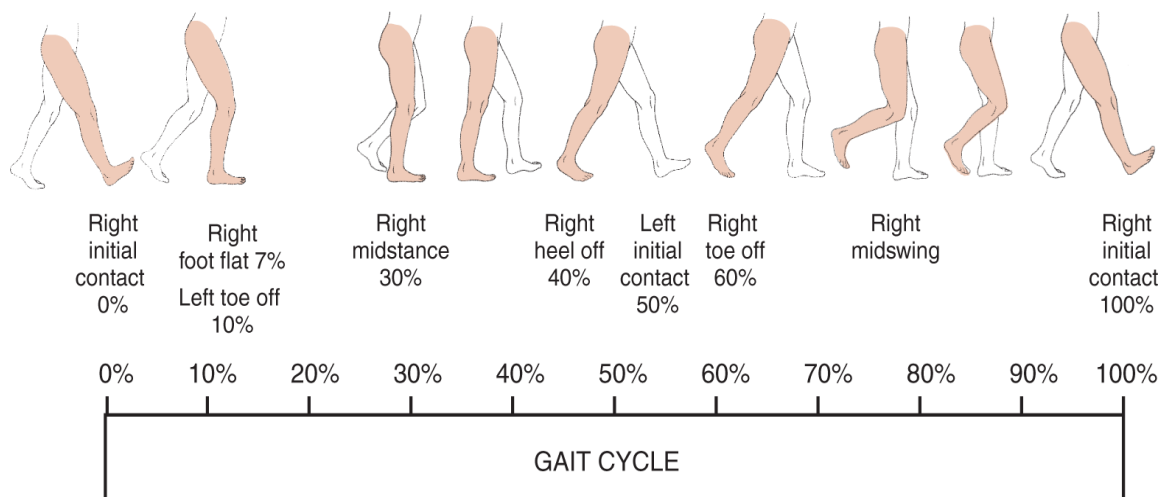


Fig. 4.5.2-4 Gait cycle definition between two consecutive toe-off of the same leg.

By calculating angles such as Roll, Pitch and Yaw in the case of the Optitrack system and using the Tilt-Twist Method in the case of the Xsens system, the average trends of the five gait cycle were obtained and shown in Figs. 4.5.2-5,4.5.2-6,4.5.2-7.

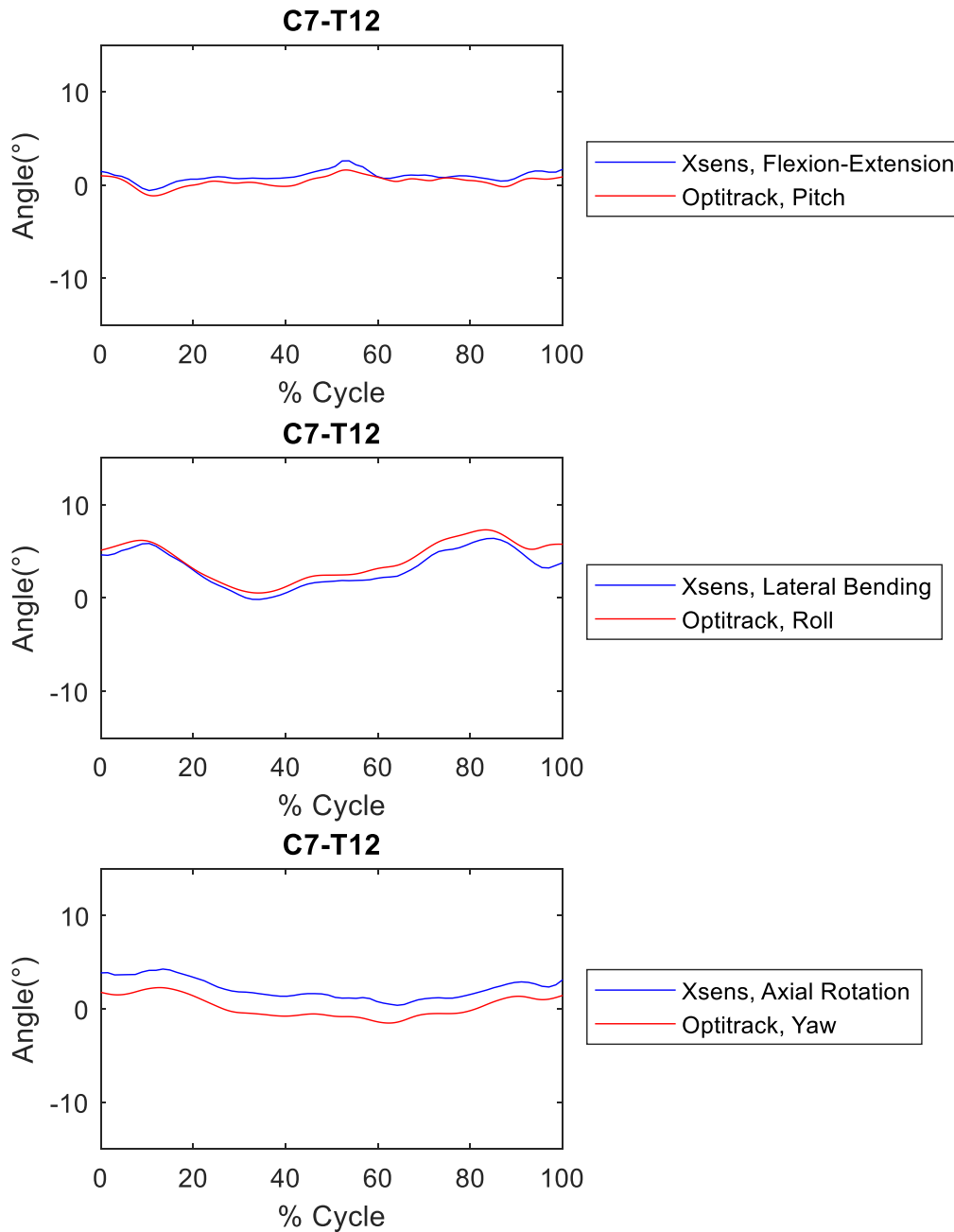


Fig. 4.5.2-5 Angles patterns of C7 vertebra compared to T12 vertebra during walking at comfortable speed (0.93 m/s).

Overall between the trends in the transversal plane of the two motion capture systems is visible a shift probably due to the non-optimal alignment of the reference systems.

For C7-T12 patterns (Fig. 4.5.2-5), the following considerations can be made:

- Sagittal plane: the triad attached to C7 vertebra, at the beginning of gait cycle (HS right leg) flexes with respect to the triad attached to T12 vertebra by about 1°; the flexion is reduced to a minimum at 10% of cycle where stance leg foot is completely flat; it increases and decreases again in the following phases; the maximum flexion (2-3°) is reached at 50% of the gait cycle (Pre-Swing phase);
- Frontal plane: for the entire gait cycle, C7 segment is flexed on the right side with respect to T12 segment. The maximum right bending is reached at 10% (loading response) and in the Mid-Swing phase. The slight decrease to the right, on the other hand, occurs in the terminal stance phase. Between 45% and 63% of the gait cycle, the pattern is flat and it represents the phase in which there is a stance leg switch;
- Transversal plane: the maximum right rotation is reached at 13% and 90% of the gait cycle. The maximum rotation on the left, with reference to the pattern obtained with optoelectronic system that for the inertial system pattern corresponds to a minimum rotation on the right, is in initial swing phase.

Examining the patterns between T12 and S1 (Fig. 4.5.2-6) it could see that:

- Sagittal plane: the triad attached to T12 vertebra is always flexed throughout the entire gait cycle compared to the S1 one; the maximum flexion is reached at 40% and 85% (Terminal stance and mid-swing phase), while the minimum flexions are 6% and 56% (loading response and pre-swing phases respectively);
- Frontal plane: in this plane, at the beginning of the cycle, that is the impact of the right heel on the ground, the T12-S1 segment is flexed on the left side to counterbalance the opposite lateralisation of the upper segment (C7-T12) and, as can be seen later, of the pelvic segment. Between 10 and 30% of gait cycle, which corresponds to the mid-stance phase, the lumbar segment is flexed on the stance leg side and reaches a maximum at 20%. Between 30 and 50%, on the other hand, the patterns are flat, indicating a stabilization phase that allows the transition to a flexion on the contralateral side. In fact, after 50%, the segment bends to the left, in other words it bends towards the contralateral side of the swing leg and reaches the maximum at 70%;
- Transversal plane: at right heel-strike, the lumbar segment rotates to the right of the pelvic segment. As gait cycle is completing, rotation is reduced to zero at the mid-stance phase. From here, the segment rotates to the left, reaching its maximum in the pre-swing phase. Subsequently, rotation reduces returning to the right at the end of the cycle.

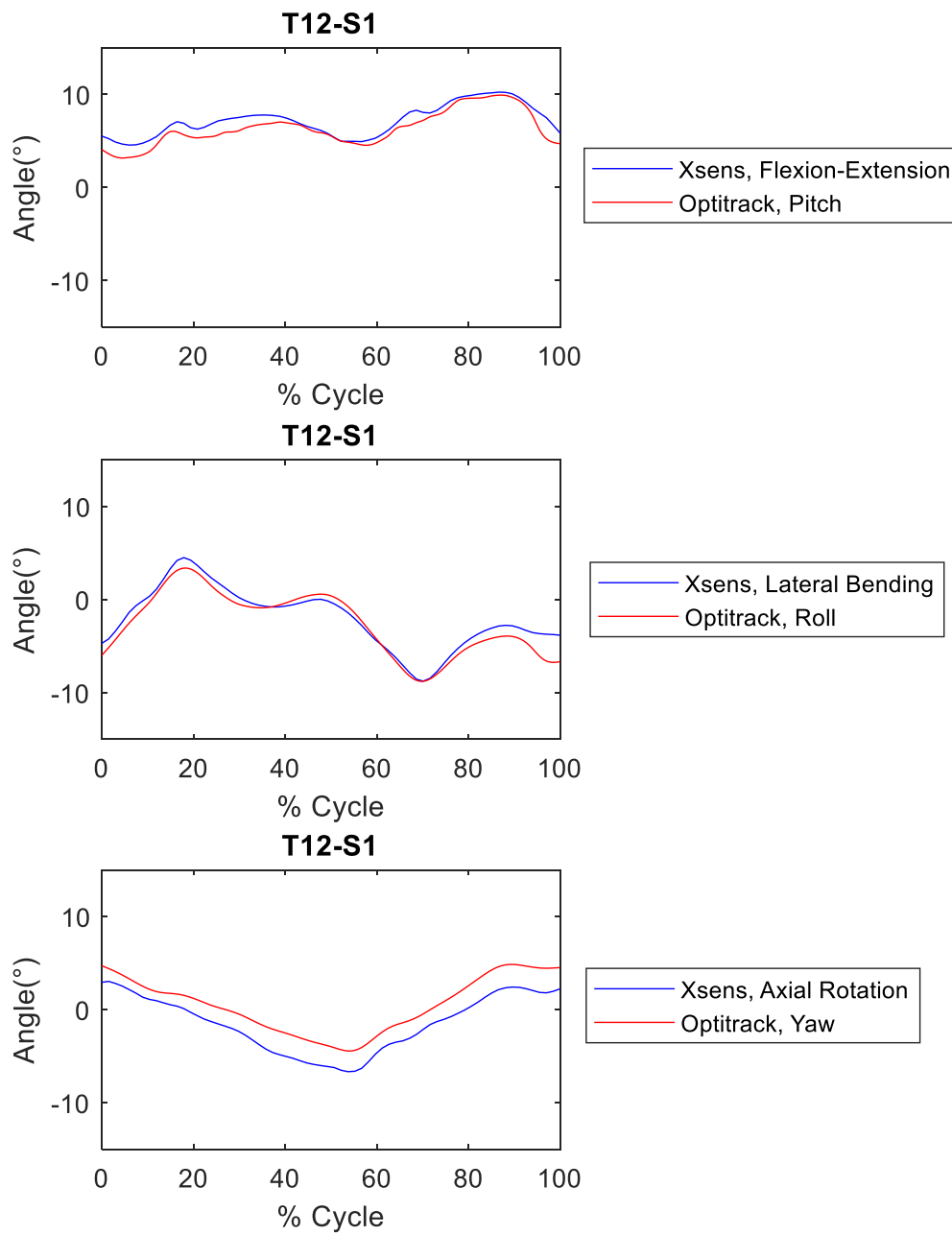


Fig. 4.5.2-6 Angles patterns of T12 vertebra compared to S1 vertebra during walking at comfortable speed (0.93 m/s).

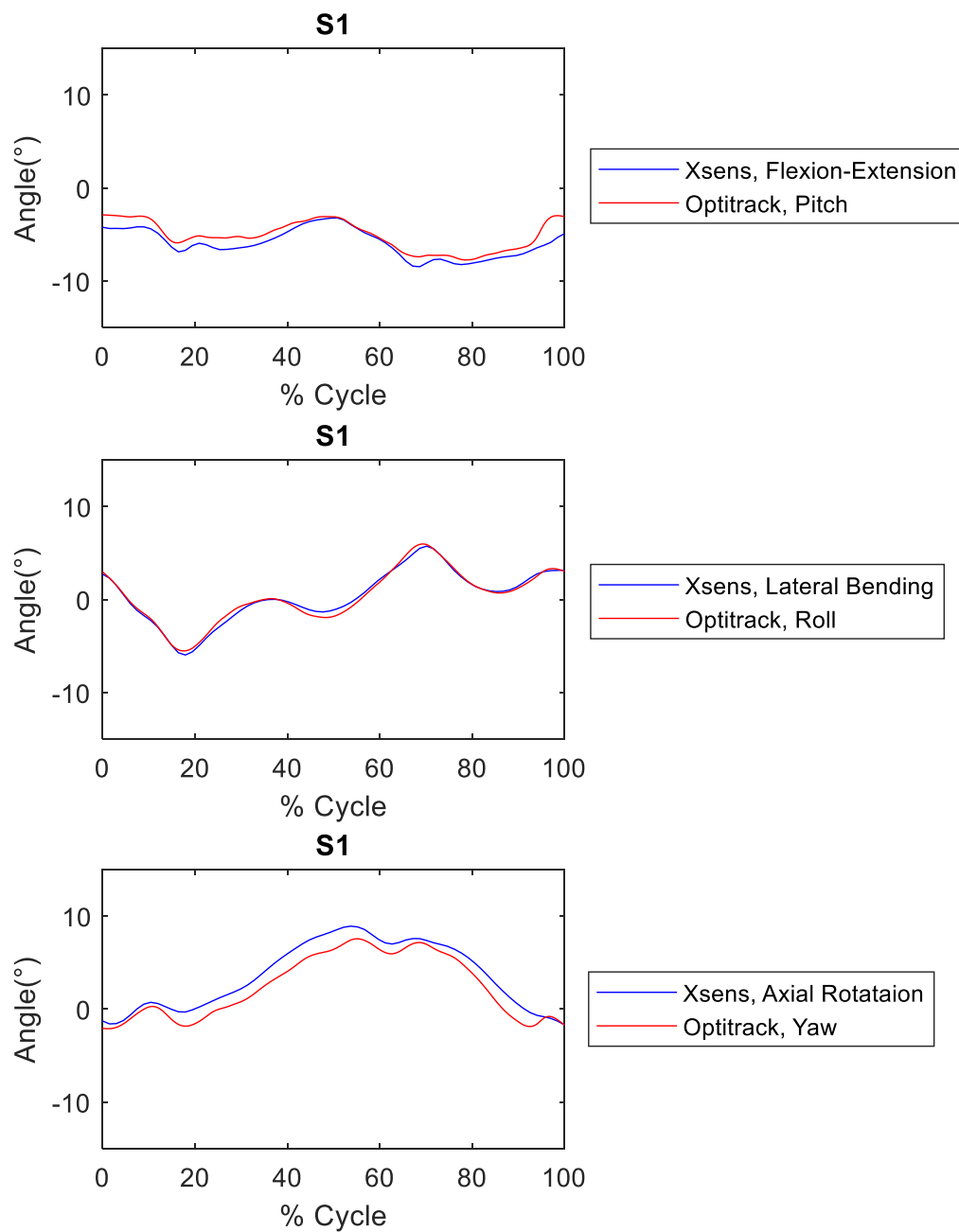


Fig. 4.5.2-7 Angles patterns of Pelvis segment during walking at comfortable speed (0.93 m/s).

The results obtained in the two systems for the Pelvis movement (Fig. 4.5.2-7) are certainly more overlapping than the other trends considered. It can be said that:

- Sagittal plane: the pelvis during waling is extended by a few degrees with respect to its resting orientation. The extension is maximum in the mid-stance and initial-swing phase, while it is reduced to a minimum in the middle of the step cycle;

- Frontal plane: at the beginning and end of the gait cycle (HS of the right foot) the segment tilts to the side of stance leg (right leg). This inclination is reduced until it cancels out and becomes negative. Negativity is an indication of a lateralisation to the left that reaches a maximum at 20% (Mid-stance phase). Throughout the terminal stance phase (30-50%) the trend fluctuates around the neutral position. As with the other segments examined, this transition phase allows the flexion to be converted on the opposite side, reaching a maximum at 70%. Basically, the pelvis bends towards the contralateral side of the stance leg;
- Transversal plane: when the right heel hits the ground, the pelvis promotes this movement by rotating to the left. Progressively, rotation is reduced and then becomes positive (rotation to the right). At 50% of gait cycle, corresponding to the left HS, pelvis reaches the maximum rotation value.

The ROMs during walking for the three segments considered are shown in Tab. 4.5.2-1. If differences between the two motion capture systems were considered, it's possible affirm that they are acceptable deviations. The greatest differences are found for T12-S1 segment in the frontal plane (1.10°) and in the transverse plane (1.07°).

	C7-T12 ROM (°)			T12-S1 ROM (°)			S1 ROM (°)		
	Sagittal Plane	Frontal Plane	Transv Plane	Sagittal Plane	Frontal Plane	Transv Plane	Sagittal Plane	Frontal Plane	Transv Plane
Xsens	3.18	6.55	3.88	5.68	13.26	9.70	5.26	11.71	10.62
Optitrack	2.77	6.77	3.80	6.75	12.16	9.30	4.76	11.50	9.76
Difference	0.41	0.22	0.08	1.07	1.10	0.40	0.50	0.21	0.86

Tab. 4.5.2-1 Segments ROM obtained with the two measuring systems. The yellow row shows the difference between values corresponding to the spinal segment and the anatomical plane.

From ROM values it is possible to notice how in the sagittal plane the segment subjected to the greatest oscillation during the whole gait cycle is the lumbar segment. This value is almost equal to the pelvic segment. Also in the frontal plane it is the segment T12-S1 to be characterized by the greatest ROM followed by the pelvic segment. If transversal plane is observed, the pelvic segment has a ROM that exceeds, even if slightly, that of the pelvis. From these values it can be deduced that the spine regions most mobile are those belonging to its lower part, while the movement of the thoracic segment is damped by the effect of the other segments. After all, this lower mobility of the upper body part of the spine is justified by the fact that the head must be subject to small fluctuations so as not to intercede with the intrinsic mechanisms for maintaining balance.

By comparing the Optitrack motion capture system with the Xsens motion capture system during the execution of elementary lateral flexion movements, it was possible firstly to consolidate the convention defined during the calculation of the angles with Tilt-Twist Method; secondly, also considering the trends during walking, it was possible to confirm that the Tilt-Twist Method returns angles that well describe the movements in a joint, freeing the angles obtained from rotations sequence.

During walking, the results obtained with Xsens system are comparable and superimposable to those obtained with gold-standard technique. The exception is the patterns of the C7-T12 segment in the transverse plane. The measurements system in fact return the same patterns if their shape is evaluated, but there is a shift between the two of about 2° . This could be related to the structure on which the three markers were placed, which during the dynamic movement, may have moved transversely from its initial orientation. Also in the T12-S1 segment in the transversal plane it is visible a gap between the two trends equal to approximately 1.5° to which the same conclusion can be reached. As far as S1 segment is concerned, at the beginning of the cycle there is no gap in the transversal plane, but at the maximum peak the misalignment between the two is once again about 1.5° .

5. Test on Healthy Subjects

5.1 Material and Methods

5.1.1 Participants

In order to evaluate the angular patterns of the spine and the ROMs of its segments on a greater number of individuals, twelve were recruited: six females and six males. The subjects did not present any neurological or muscular disorders. None of them had spinal deformities such as scoliosis. The sample was made up of young boys and girls who were informed about how to perform the tests and gave their written consent before starting the trial. In Tab. 5.1.1-1 anthropometric characteristics of subjects were shown.

N°	Gender	Age (years)	Mass (kg)	Height (cm)	BMI (kg/m ²)	S (cm)	B (cm)	T (cm)	C (cm)	G (cm)	Cav (cm)
1	F	26	54	165	19.8	35	54	60	46	56	75
2	F	27	68	172	23.0	36	62	62	48	47	80
3	F	26	45	153	19.2	37	49	54	43	40	69
4	F	24	43	152	18.6	35	45	58	50	38	68
5	F	26	60	155	25.0	38	50	53	44	46	70
6	F	25	54	157	21.9	37	53	57	52	48	75
Avg (SD)		25.7 (1.03)	54 (9.32)	159.0 (7.87)	21.3 (2.49)	36.3 (1.21)	52.2 (5.78)	57.3 (3.44)	47.2 (3.49)	48.8 (6.40)	72.8 (4.62)
7	M	25	70	174	23.1	45	57	58	51	50	79
8	M	26	82	181	25.0	44	57	70	53	50	83
9	M	26	75	175	24.5	43	59	62	46	53	81
10	M	25	77	173	25.7	42	55	69	45	51	73
11	M	25	82	182	24.8	44	60	66	52	50	84
12	M	24	82	188	23.2	44	54	66	54	53	81
Avg (SD)		25.2 (0.75)	78 (4.94)	178.8 (5.85)	24.4 (1.03)	43.7 (1.03)	57.0 (2.28)	65.2 (4.49)	50.2 (3.76)	51.2 (1.47)	80.2 (3.92)

Tab. 5.1.1-1 Anthropometrics characteristics of subjects involved in the experimentation. S: distance between Acromions; B: distance between Acromion and wrist; T: distance between sternum aspects and pubis; C: distance between hip and knee; G: distance between knee and ground; Cav: distance between pubis and the ground.

5.1.2 Protocol

The subjects were equipped with five MTx sensors (Xsens Technologies) positioned at the vertebral levels C7, T6, T12, L3, S1. The sensors at T12 and L3 levels were positioned in a different orientation from the others as done in the preliminary tests. The sensors were attached to the skin of the subjects with double-sided adhesive tape (Fig. 5.1.2-1). To ensure better adhesion to the L3 and T12 vertebral levels, specially designed elastic bands were used. The sensor at S1 level was positioned using the elastic band supplied by the Xsens group.

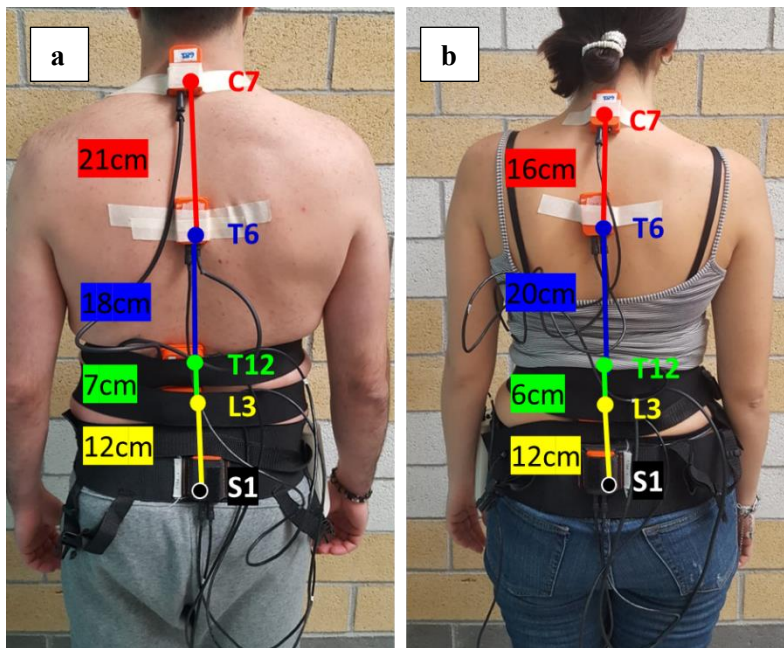


Fig. 5.1.2-1 Example of rachis segmentation adopted for both genders (**a** male subject, **b** female subject).

The subjects were asked to walk along a 20 m long path delimited by two indicators placed on the floor. When the indicators were reached, the subjects impacted one foot on the ground so as to be able to segment the signals and analyse in the post-processing phase only the paths performed in a single direction. The 20 m path was crossed five times (considering both directions) and then three of these were analysed to extract trunk angles.

Each subject was asked to perform three tests each with different characteristics. For the first two tests, a metronome was used to mark the step frequency. In particular, in the first test, both for male and female subjects, a frequency of 1.5 steps/s was set. In this way the subjects were guided to walk at slow speed (Öberg, 1993). When performing the second test, the step frequency was set to 2.0 steps/s, then in a second to realize a complete gait cycle. This last set frequency allows them to walk at normal speed (Öberg, 1993). The third test differs from the

other two because the metronome was not used and therefore the subjects were asked to walk at a speed that was comfortable for them.

The choice of having the subjects walk slowly was made with the prospect of testing the system on elderly subjects suffering from Parkinson's disease. This subjects category, in fact, due to neurological condition, perform a more uncertain walk, less controlled. Therefore, reducing walking speed, oscillations, especially those affecting the head, are reduced and the vestibular system is able to process the information and maintain balance.

All tests were carried out with barefoot subjects. Before each test starting the subjects were made to hear the rhythm of the metronome so that they could synchronize the impact of each heel to each sound emitted by the metronome. Moreover, once the acquisitions were started, for about 7 s the subjects remained standing to extract the calibration data.

5.1.3 Signal Processing and Data Analysis

From each sensor, Excel file was obtained containing, at each sample time, information on acceleration, angular velocity and magnetic field along X, Y and Z axes and the elements of the orientation matrix of the sensor in the global reference system. The sample range for the calibration data (100 samples) was extracted from the acquisition part where the subject remained stationary. From this range, the acceleration-Y values of each sensor were averaged in order to identify which rotation matrices sensors had to be rotate by 90° (sensors on T12 and L3 vertebral levels). The rotation matrix was manipulated as described in Chapter 3 Section 2. In order to be able to recognize the impacts of the foot on the ground when the indicators on the floor were reached, the acceleration along X-axis was evaluated. Since the oscillation that occurs at this vertebral level varies from subject to subject, it was necessary to evaluate also the acceleration of the same sensor along the Y and Z axes. Once these peaks were recognized, it was possible to segment the entire acquisition by discriminating between the two directions of travel. For each acquisition section in the same identified direction, the acceleration-Z of the sensor at T12 level was evaluated (Chapter 3 Section 3). Acceleration-Z and angular velocity-Y were filtered with a 4th Butterworth bandpass filter between 0.5 and 15 Hz. From the acceleration signal it was possible to define the gait cycle between two successive heel-strikes of the same foot; by the angular velocity it was possible to isolate the gait cycles relative to the right leg. For each subject and for each speed tested 36 gait cycles of right leg were obtained. Thanks to the acceleration-Z of the T12 sensor, it was possible extract the speed at which each subject performed the test (Tabs. 5.1.3-1, 5.1.3-2).

Female subjects	Walking at 1.5 steps/s		Walking at 2.0 steps/s		Walking at comfortable speed	
	Speed (m/s)	Step frequency (steps/s)	Speed (m/s)	Step frequency (steps/s)	Speed (m/s)	Step frequency (steps/s)
Subject#1	0.78	1.36	1.26	1.95	1.23	1.85
Subject#2	0.95	1.56	1.31	1.97	1.08	1.78
Subject#3	0.67	1.41	1.00	1.96	0.94	1.79
Subject#4	0.98	1.56	1.30	1.95	1.25	1.94
Subject#5	0.94	1.41	1.35	2.02	1.28	1.93
Subject#6	0.77	1.38	1.27	1.97	1.20	1.86
Mean (SD)	0.85 (0.13)	1.45 (0.09)	1.25 (0.13)	1.97 (0.03)	1.16 (0.13)	1.86 (0.07)

Tab. 5.1.3-1 Subjects velocities and cadence during the three different trials. The last row indicates the mean (SD) velocities and step frequencies over female subjects.

Male subjects	Walking at 1.5 steps/s		Walking at 2.0 steps/s		Walking at comfortable speed	
	Speed (m/s)	Step frequency (steps/s)	Speed (m/s)	Step frequency (steps/s)	Speed (m/s)	Step frequency (steps/s)
Subject#1	0.91	1.51	1.29	2.00	1.22	1.83
Subject#2	0.99	1.53	1.56	2.10	1.14	1.72
Subject#3	1.06	1.59	1.46	1.90	1.18	1.76
Subject#4	0.91	1.49	1.35	2.09	1.19	1.96
Subject#5	1.06	1.54	1.28	1.86	1.27	1.78
Subject#6	1.08	1.51	1.50	1.95	1.31	1.83
Mean (SD)	1.00 (0.08)	1.53 (0.04)	1.41 (0.12)	1.98 (0.10)	1.22 (0.13)	1.81 (0.08)

Tab. 5.1.3-2 Subjects velocities and cadence during the three different trials. The last row indicates the mean (SD) velocities and step frequencies over male subjects.

From each subject, for each test, the angles of each spinal segment with respect to one below were calculated. Then it was possible to obtain the trends of the angles during walking. For each subject, the average pattern and the ROM of each segment were obtained. These in turn were mediated among all subjects belonging to the same sexual gender, obtaining the mean pattern and the mean ROM for each type of gait examined.

In general, these tests were used to study the relative angular motion of the spinal segments during different walking conditions. This is to investigate differences in patterns and ROMs as test conditions vary. In addition, the aim was to keep the two gender groups separate so as to identify the intrinsic differences between them. Then determine the gender effect on the kinematics of spinal segments during walking and, in particular, which intersegmental motion and which anatomical plane is most affected by it. In a second moment different types of gait were compared considering the overall movement of each spinal segment both keeping separated the data of males and females and considering the totality of the sample recruited. A further analysis was conducted to assess the differences in the overall motion of the column in the three anatomical planes. To obtain all this information, a One-Way ANOVA analysis was carried out on the ROM values, setting a level of significance equal to 0.05. One-Way ANOVA is based on a linear model whose purpose is to identify if different groups have a common mean.

5.2 Results

5.2.1 Walking at 1.5 steps/s

Fig 5.2.1-1 shows the average trends of the segments belonging to the thoracic segment of the spine in three anatomical planes. The upper thoracic segment in the sagittal plane shows a little oscillating trend along the whole gait cycle, in fact its average ROM (Tab. 5.2.1-1) is 1.80° (SD 1.79°). The C7-T6 segment tends to be extended. In the frontal plane, however, the segment shows an oscillation around a negative mean value as well as in the transversal plane. This means that on average the women analysed tend to flex the upper thoracic segment compared to the lower thoracic segment slightly to the left as is the case of rotation. The lower thoracic segment

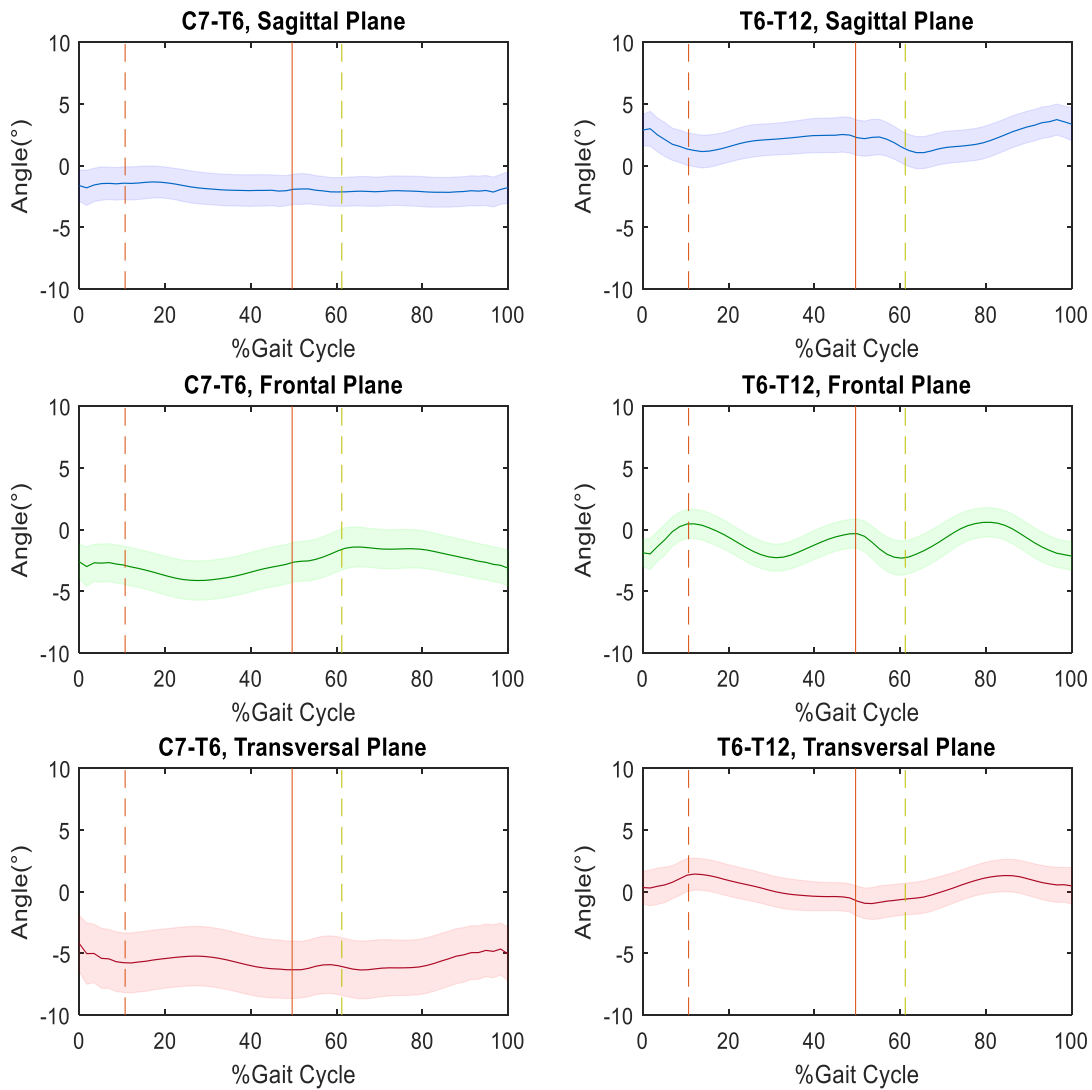


Figure 5.2.1-1 Angles patterns of thoracic segments during walking at slow speed for female subjects.

shows higher average oscillations. Analysing the pattern in the frontal plane, it results that at the first TO (left leg) the segment bends towards the stance leg (right leg); on the contrary, at the TO of the right foot, the segment bends on the left side.

The segments belonging to the lumbar spine (Fig. 5.2.1-2), in the frontal plane tend to bend on the stance leg side. In the transverse plane, the upper lumbar segment reaches an average ROM of 6.53°, comparable to that in the frontal plane (Tab. 5.2.1-1).

Finally, the pelvic segment (Fig. 5.2.1-3), in the frontal plane, bends and rotates on opposite side of the stance leg. In the frontal plane the maximum flexion on the left side is reached in the mid-stance phase while the maximum flexion on the right side is at 70% of the cycle. In general, the greatest dispersion occurs in the sagittal and transversal planes. In the frontal plane,

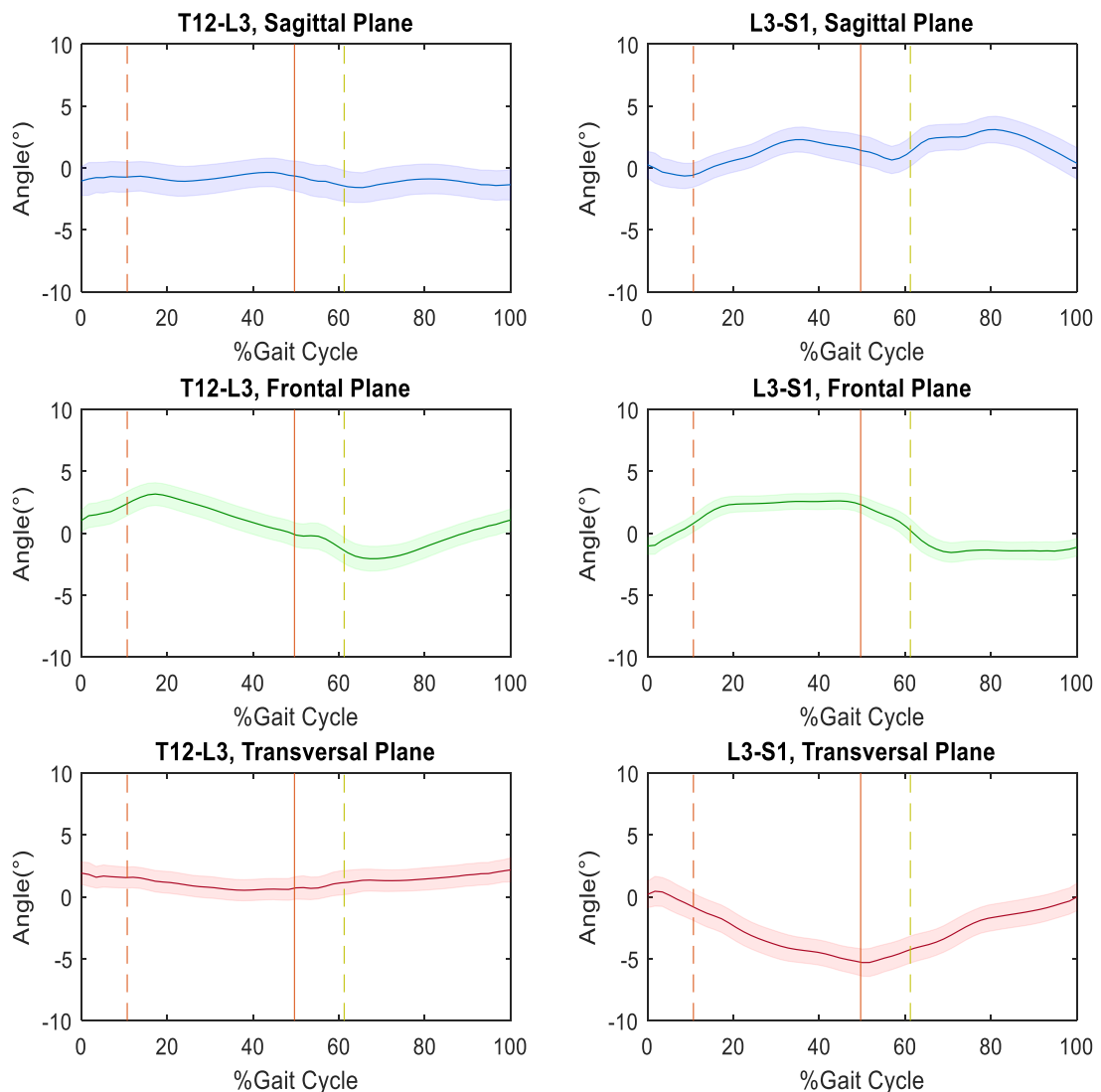


Figure 5.2.1-2 Angles patterns of lumbar segments during walking at slow speed for female subjects.

dispersion decreases as pelvis is approached. This could be explained by considering that the movement of the pelvis is a consequence of the lower limbs' movement. As a higher vertebral level is considered, it is plausible to think that everyone has his own segments movement due to a series of factors, first of all his own strategy in maintaining balance during movement execution. By shifting the focus to the ROMs achieved in the three planes (Tab. 5.2.1-1), pelvis shows higher values especially when referring to those in the frontal and transversal planes. It is also possible to notice that in the sagittal plane the average values tend to decrease in higher vertebral levels considered.

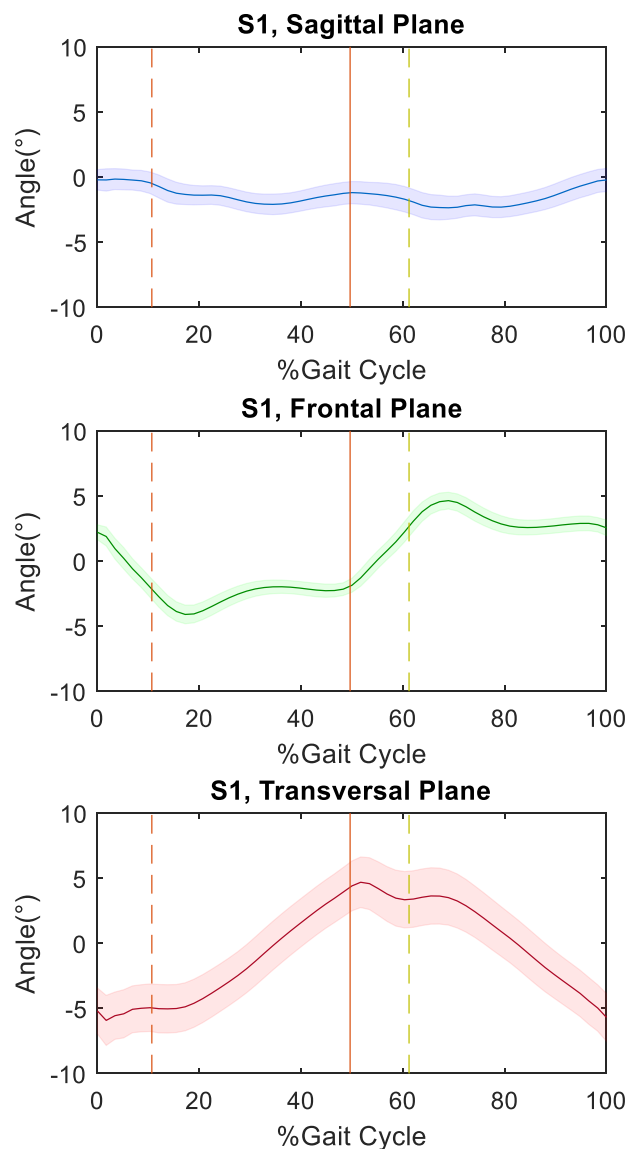


Figure 5.2.1-3 Angles patterns of pelvis segment during walking at slow speed for female subjects.

	Sagittal Plane		Frontal Plane		Transversal Plane	
	Avg ROM (°)	Avg SD (°)	Avg ROM (°)	Avg SD (°)	Avg ROM (°)	Avg SD (°)
C7-T6	1.80	1.79	3.31	1.57	2.72	1.41
T6-T12	3.79	1.74	4.46	1.78	4.63	1.85
T12-L3	3.65	1.90	5.36	3.40	2.69	1.17
L3-S1	5.82	1.76	6.54	2.62	6.53	5.09
S1	4.14	1.81	9.18	2.86	11.53	3.66

Tab. 5.2.1-1 ROMs (SD) for female subjects during walking at slow speed.

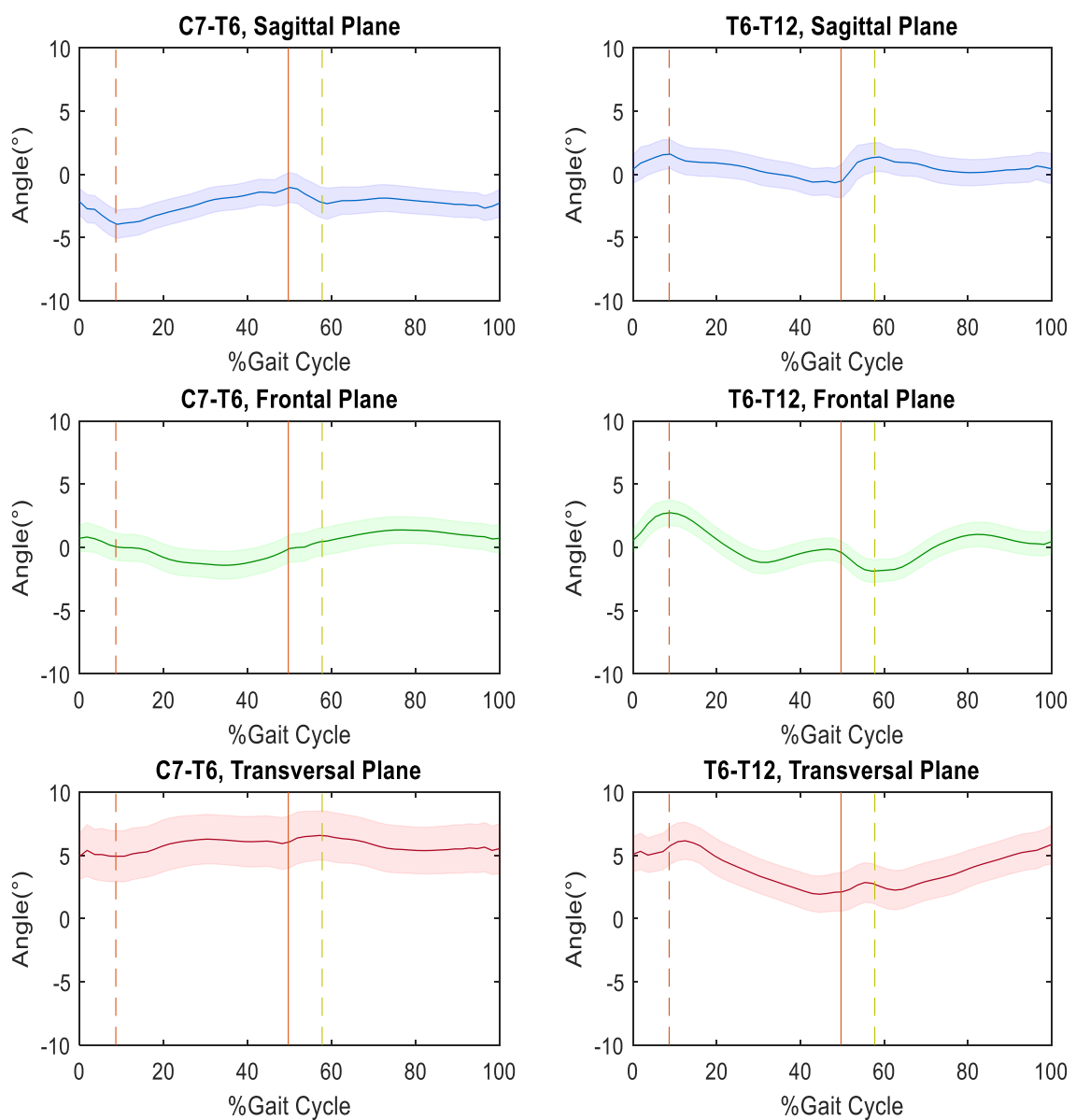


Fig. 5.2.1-4 Angles patterns of thoracic segments during walking at slow speed for male subjects.

For men the same considerations can be made, noting however that upper thoracic segment (Fig. 5.2.1-4) in the sagittal plane has a greater amplitude oscillation than in woman. The lumbar segments (Fig. 5.2.1-5) in the frontal plane, on the other hand, show less movement than women of the order 2° for lower lumbar segment. This could be consequence of the pelvic motion (Fig. 5.2.1-6) to which L3-S1 segment is referred. In fact, for men the pelvis reaches (Tab. 5.2.1-2) in the frontal plane a ROM of about 6° , 3° less than that reached in women. It could be connected to the set speed or to the proper conformation that characterizes the sex.

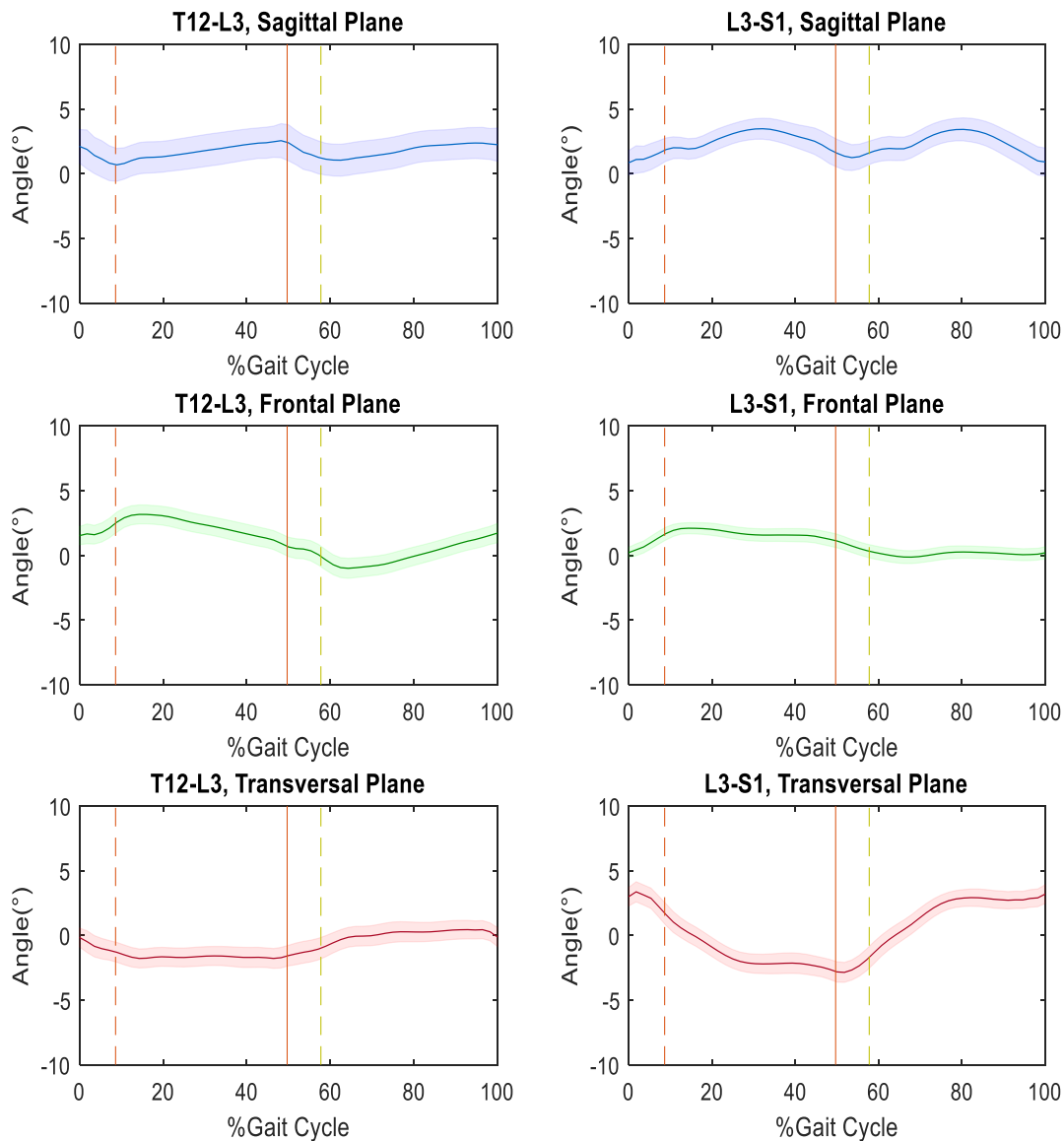


Fig. 5.2.1-5 Angles patterns of lumbar segments during walking at slow speed for male subjects.

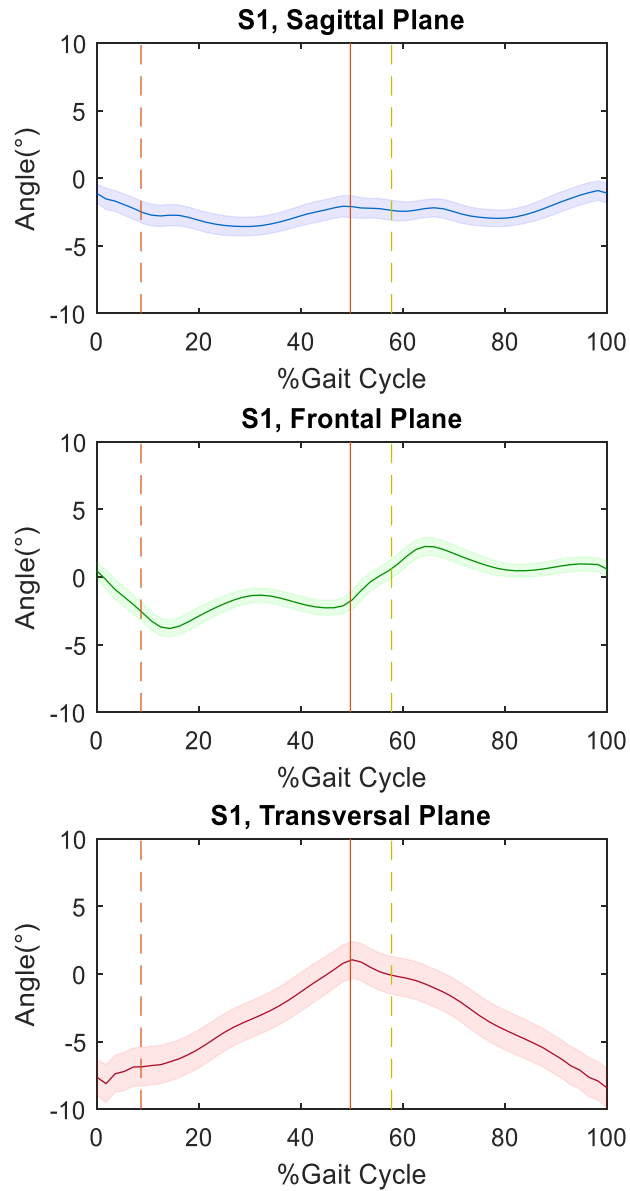


Fig. 5.2.1-6 Angles patterns of pelvis segment during walking at slow speed for male subjects.

	Sagittal Plane		Frontal Plane		Transversal Plane	
	Avg ROM (°)	Avg SD (°)	Avg ROM (°)	Avg SD (°)	Avg ROM (°)	Avg SD (°)
C7-T6	3.99	2.38	2.94	1.00	3.22	1.56
T6-T12	3.92	1.46	4.78	1.86	5.49	3.23
T12-L3	4.40	2.28	4.41	1.97	3.00	1.23
L3-S1	4.79	2.34	3.26	1.41	7.05	2.26
S1	3.99	2.38	2.94	1.00	3.22	1.56

Tab. 5.2.1-2 ROMs (SD) for male subjects during walking at slow speed.

Segment	C7-T16		T6-T12		T12-L3		L3-S1		S1	
Gender	M	F	M	F	M	F	M	F	M	F
ROM (SD) ^o Sagittal plane	3.88 (2.38)	1.80 (1.79)	3.92 (1.46)	3.79 (1.74)	4.40 (2.28)	3.65 (1.90)	4.79 (2.34)	5.82 (1.76)	3.58 (1.23)	4.14 (1.81)
p-value	0.05*		0.89		0.55		0.41		0.54	
ROM (SD) ^o Frontal plane	2.94 (1.00)	3.31 (1.57)	4.78 (1.86)	4.46 (1.78)	4.41 (1.97)	5.36 (3.40)	3.26 (1.41)	6.54 (2.62)	6.30 (2.08)	9.18 (2.86)
p-value	0.82		0.35		0.56		0.02*		0.07	
ROM (SD) ^o Transversal plane	3.22 (1.56)	2.72 (1.41)	5.49 (3.23)	4.63 (1.85)	3.00 (1.23)	2.69 (1.17)	7.05 (2.26)	6.53 (5.09)	6.96 (3.73)	11.53 (3.66)
p-value	0.66		0.59		0.67		0.83		0.48	

Tab. 5.2.1-3 Comparison of gender using the average ROM in the three planes of each segment related to slow walking speed. Those with statistical differences (ANOVA) are indicated with *.

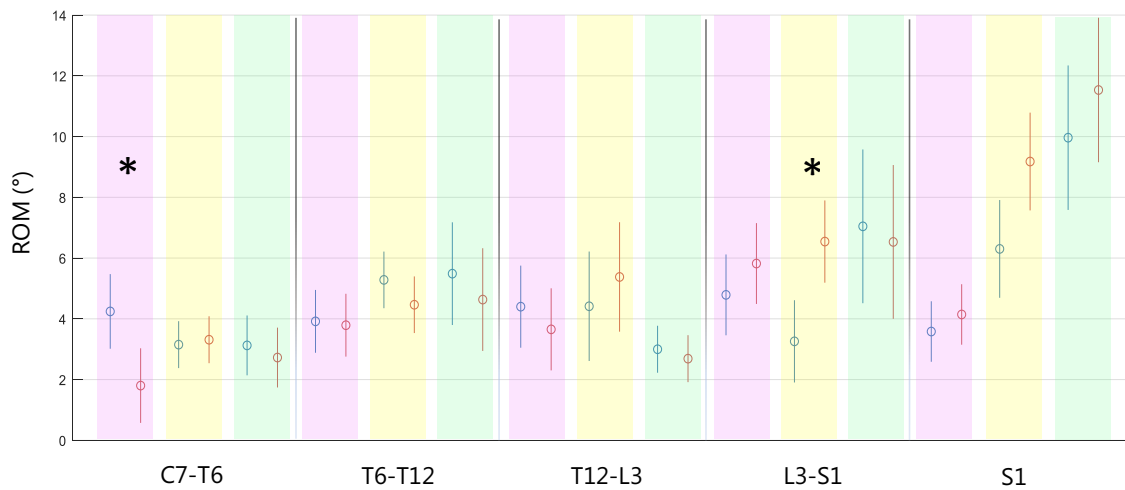


Fig. 5.2.1-7 Comparison of gender using the average ROM in the three planes of each segment related to slow walking speed. Those with statistical differences (ANOVA) are indicated with *. The purple areas identify the sagittal plane, the yellow areas the frontal plane and the green areas the transversal plane. For each area the ROMs of the male group (blue) and the ROMs of the female group (magenta) are reported.

Fig. 5.2.1-7 and Tab. 5.2.1-3 show the two statistical differences between the two genders. One of these is found in the motion of the lumbar segment in the frontal plane. Here the female sex shows a higher ROM than that found in male subjects. The p-value relative to the upper thoracic in the sagittal plane is equal to 0.05 which is indicative of a strong difference between the motion of the same between males and females. Overall, the females group has a higher ROM than males at the lower region spine level that affects the lower lumbar and pelvic segments mainly in the frontal plane. Observing the upper part of the spinal column, males have a predominant motion.

5.2.2 Walking at 2.0 steps/s

Figs. 5.2.2-1, 5.2.2-2, 5.2.2-3 show the average angle trends in women during normal step frequency walking (1.25 m/s mean speed). It is possible to notice differences from the patterns obtained during slow walking (0.85 m/s mean speed). Referring to the thoracic segments of the spine (Fig. 5.2.2-1) it is easy to notice that the dispersions in the three planes for both segments are reduced. In addition, the T6-T12 segment in the frontal plane in the terminal stance phase has a flatter profile. In the sagittal plane however, the T6-T12 segment oscillates with lower ROM around a value slightly higher than 0° and more frequently. Analysing the ROMs in Tab. 5.2.2-1, it is possible to notice that, in general, the values reached are greater than those relative to the slow walking.

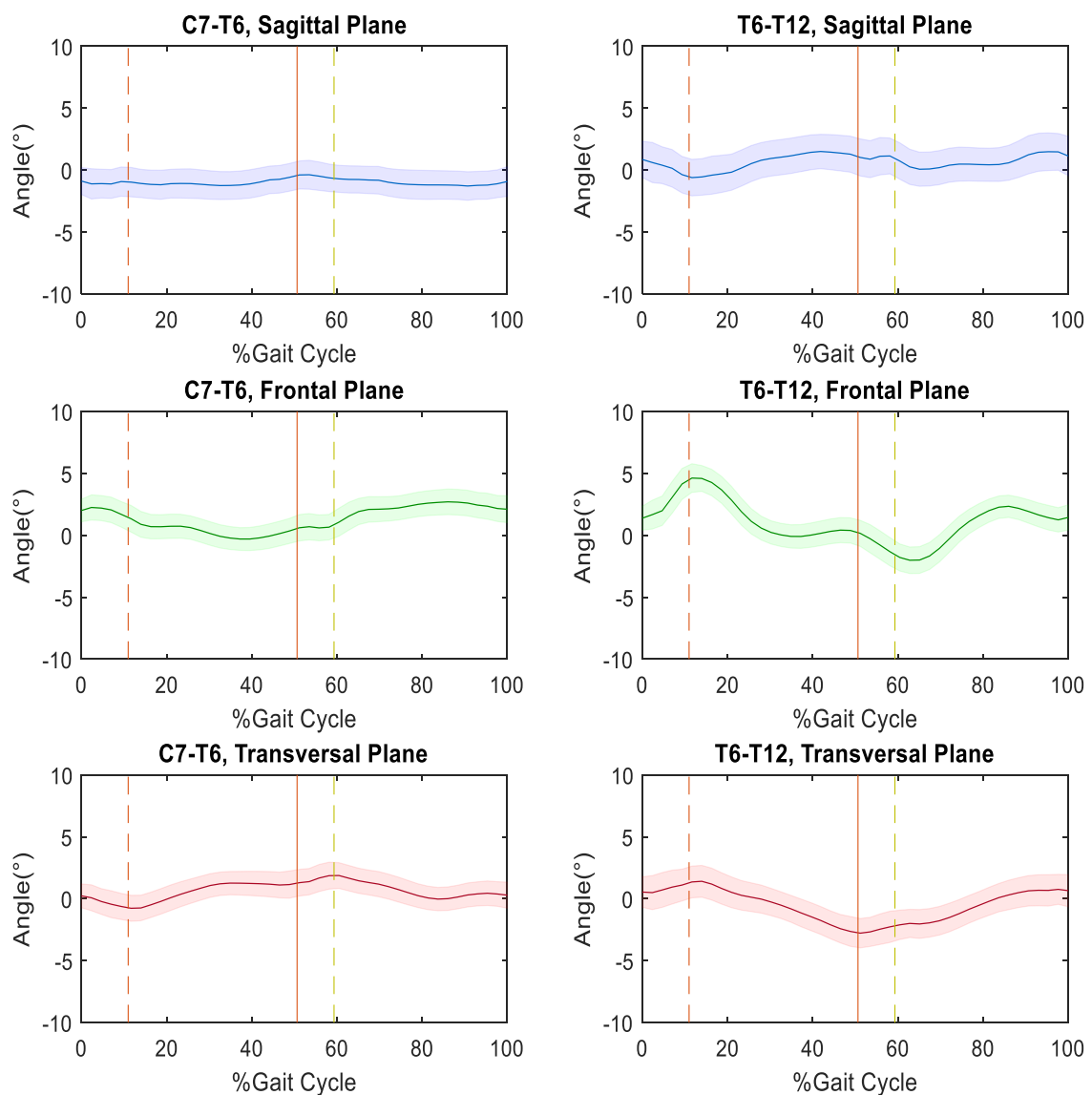


Fig. 5.2.2-1 Angles patterns of thoracic segments during walking at normal speed for female subjects.

Also the lumbar segments show a different angular profile (Fig. 5.2.2-2), but less evident than those the other segments considered.

For the pelvis (Fig. 5.2.2-3) the profiles are rather overlapping except for a slight increase in ROM.

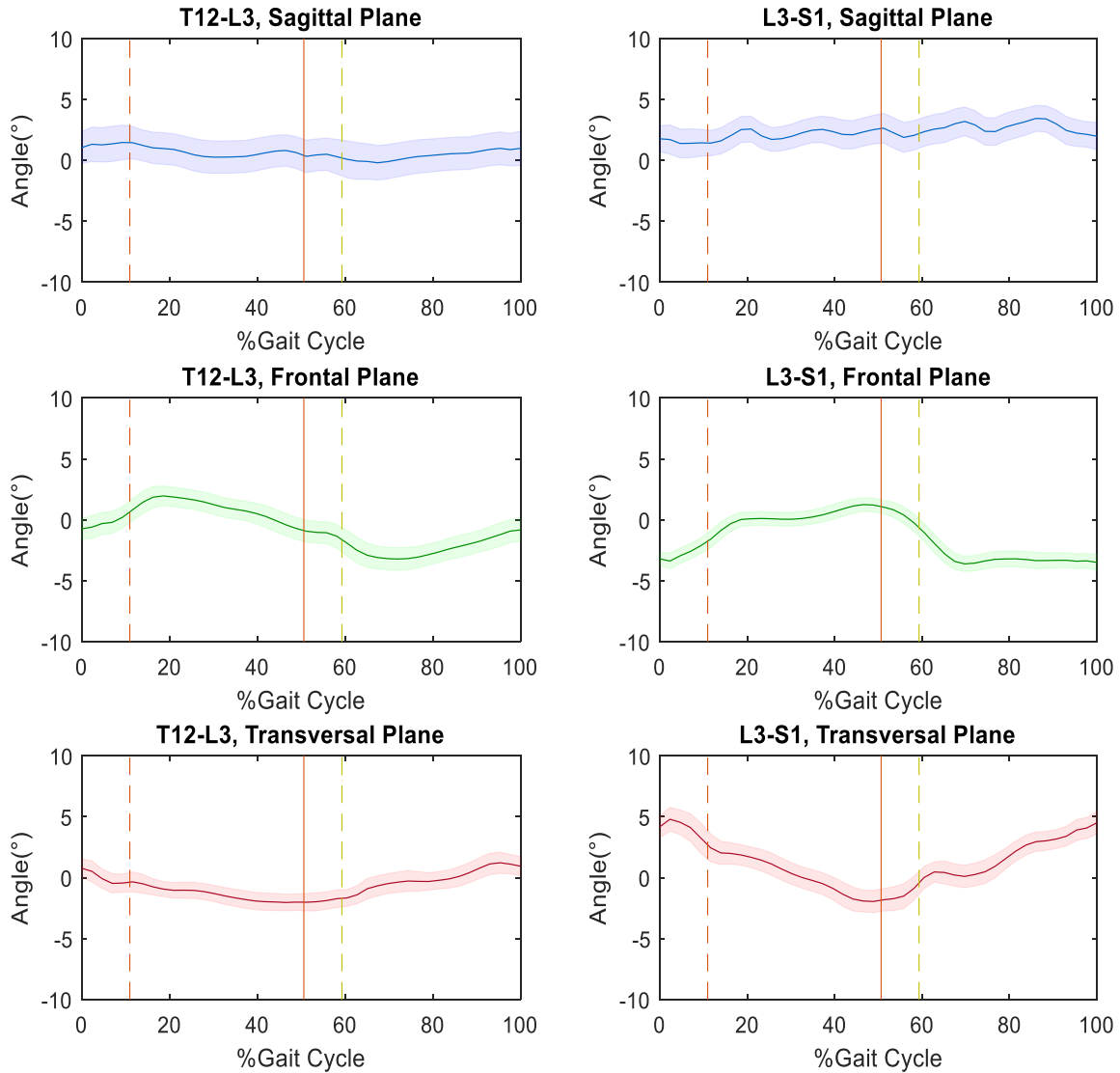


Fig. 5.2.2-2 Angles patterns of lumbar segments during walking at normal speed for female subjects.

	Sagittal Plane		Frontal Plane		Transversal Plane	
	Avg ROM (°)	Avg SD (°)	Avg ROM (°)	Avg SD (°)	Avg ROM (°)	Avg SD (°)
C7-T6	2.08	0.87	3.49	1.65	3.33	1.57
T6-T12	4.30	3.31	7.26	3.40	5.43	1.25
T12-L3	4.31	3.18	5.32	3.48	4.64	3.09
L3-S1	5.45	1.66	6.90	3.51	7.98	4.10
S1	4.64	2.41	10.53	3.49	10.27	4.24

Tab. 5.2.2-1 ROMs (SD) for female subjects during walking at normal speed.

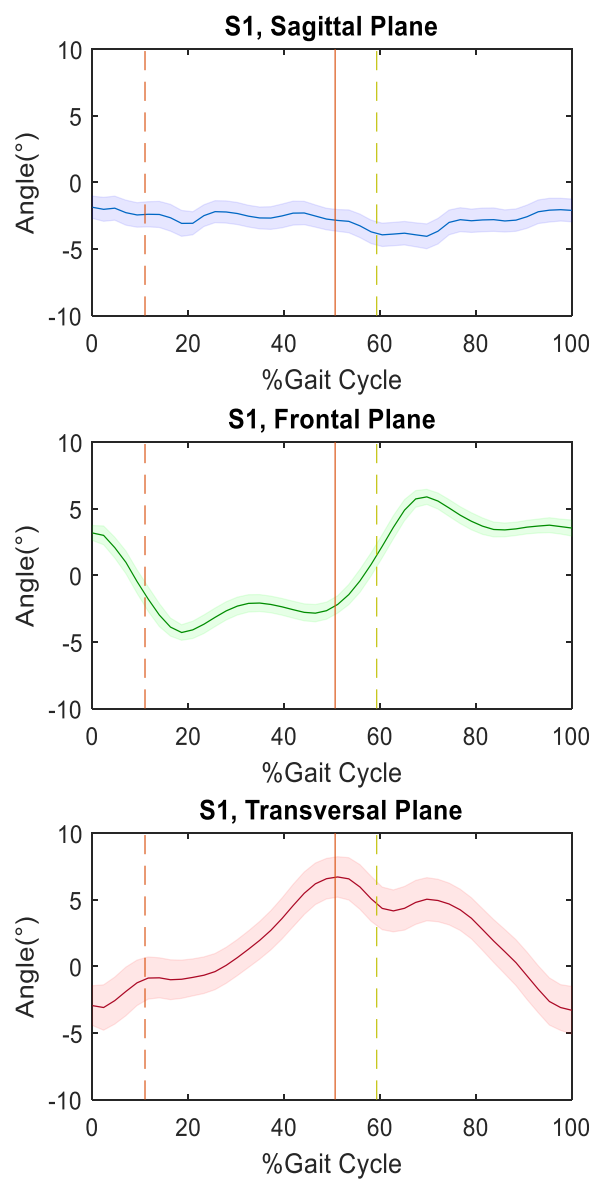


Fig. 5.2.2.-3 Angles patterns of pelvis segment during walking at normal speed for female subjects.

For males the patterns shown in Fig 5.2.2-4, 5.2.2-5, 5.2.2-6 and ROMs in Tab. 5.2.2-2 are obtained relative to fast walking speed (1.41 m/s mean speed). Also for males, an increase in speed leads to an increase in the ROM of the spinal segments. As for woman, the segment that most shows a different pattern in the frontal plane is the T6-T12 segment.

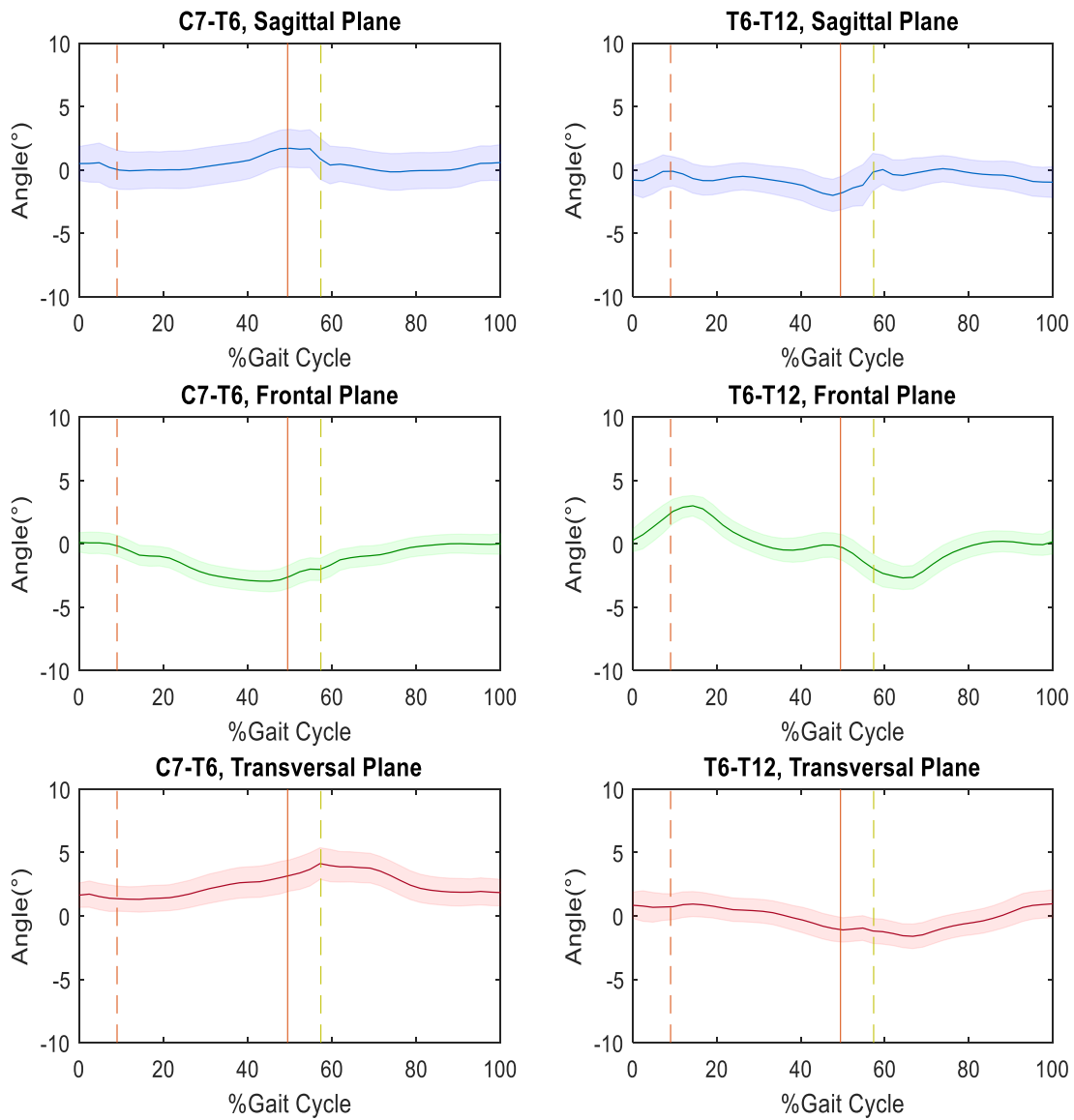


Fig. 5.2.2.-4 Angles patterns of thoracic segments during walking at high speed for male subjects.

	Sagittal Plane		Frontal Plane		Transversal Plane	
	Avg ROM (°)	Avg SD (°)	Avg ROM (°)	Avg SD (°)	Avg ROM (°)	Avg SD (°)
C7-T6	3.71	2.14	3.71	0.79	3.50	2.02
T6-T12	3.52	1.68	5.91	2.36	4.28	1.81
T12-L3	4.42	2.02	3.98	2.17	4.85	2.93
L3-S1	4.40	1.88	2.83	1.11	7.83	3.98
S1	3.64	1.41	6.99	2.65	8.70	4.82

Tab. 5.2.2-2 ROMs (SD) for male subjects during walking at normal speed.

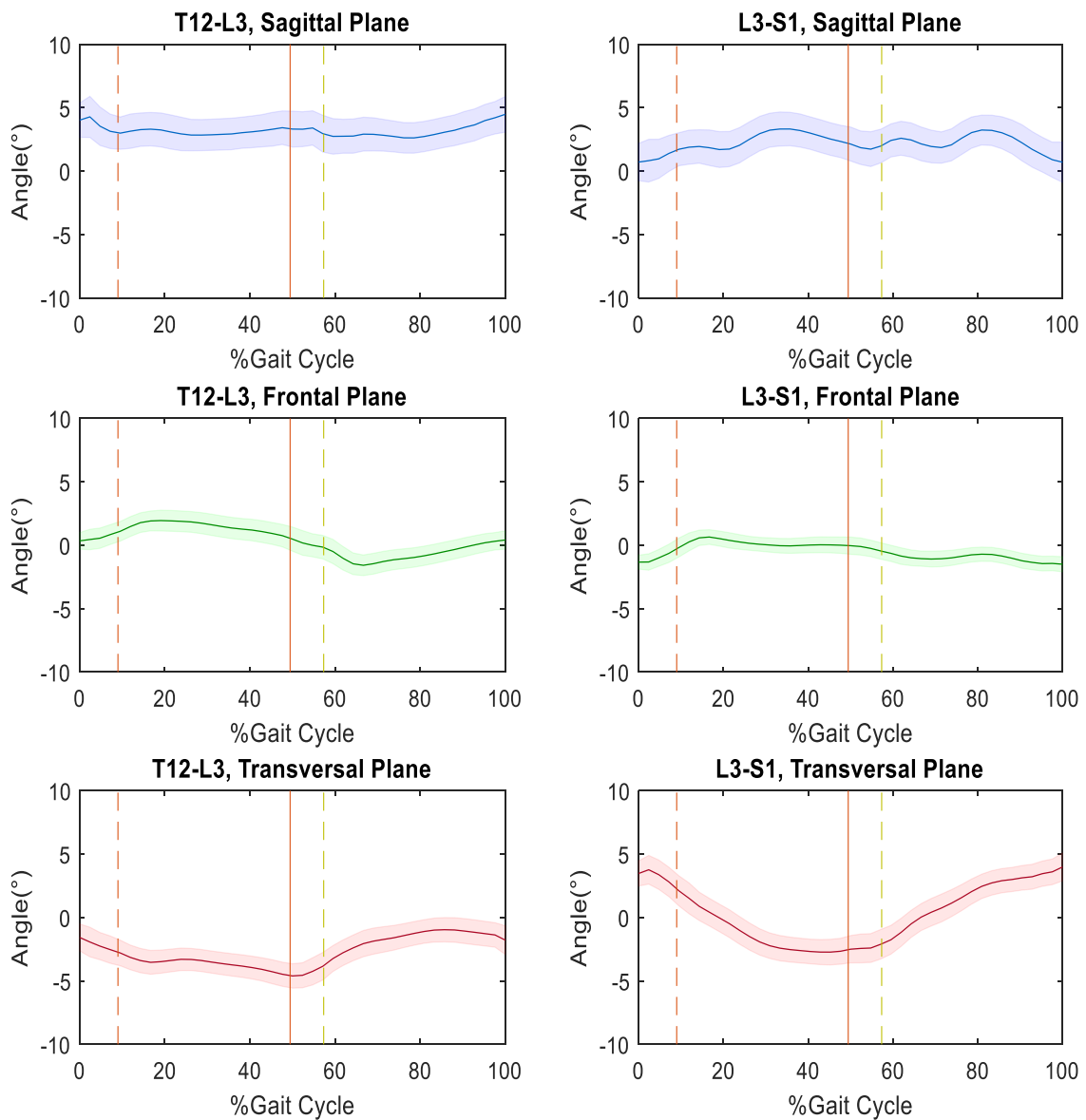


Fig. 5.2.2.-5 Angles patterns of lumbar segments during walking at normal speed for male subjects.

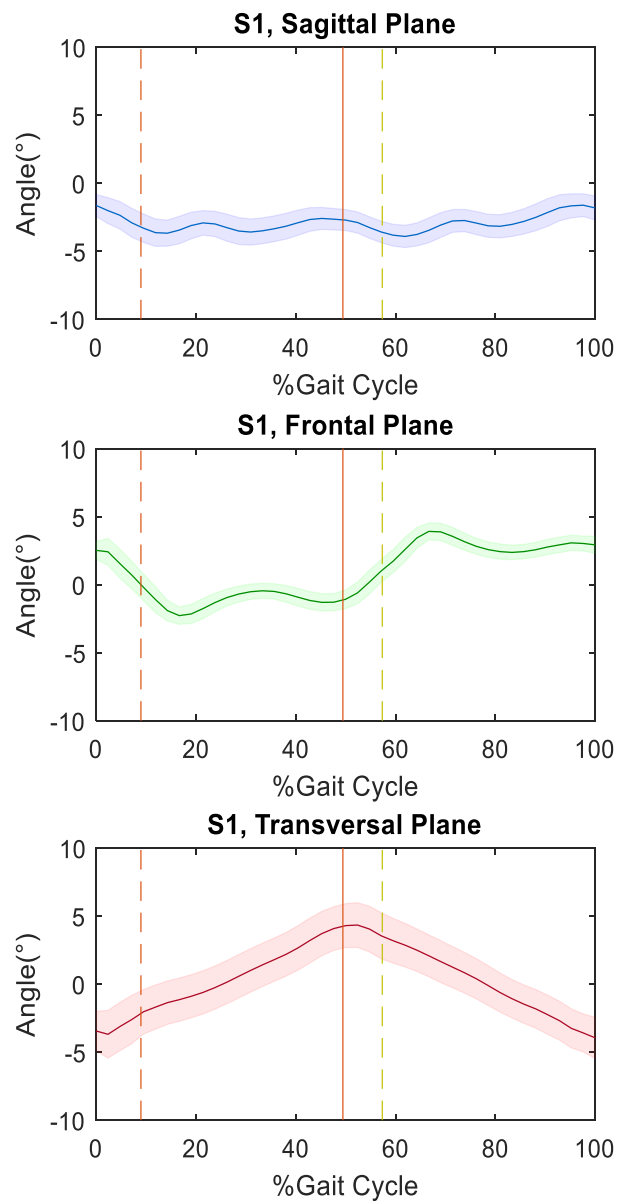


Fig. 5.2.2-6 Angles patterns of lumbar segments during walking at normal speed for male subjects.

Segment	C7-T16		T6-T12		T12-L3		L3-S1		S1	
Gender	M	F	M	F	M	F	M	F	M	F
ROM (SD) ^o Sagittal plane	3.71 (2.14)	2.08 (0.87)	3.52 (1.68)	4.30 (3.31)	4.42 (2.02)	4.31 (3.18)	4.40 (1.88)	5.45 (1.66)	3.64 (1.41)	4.64 (2.41)
p-value	0.12		0.62		0.94		0.33		0.40	
ROM (SD) ^o Frontal plane	3.71 (0.79)	3.49 (1.65)	5.91 (2.36)	7.26 (3.40)	3.98 (2.17)	5.32 (3.48)	2.83 (1.11)	6.90 (3.51)	6.99 (2.65)	10.53 (3.49)
p-value	0.77		0.44		0.44		0.02*		0.08	
ROM (SD) ^o Transversal plane	3.50 (1.68)	4.30 (3.31)	4.28 (1.81)	5.43 (1.25)	4.85 (2.93)	4.64 (3.09)	7.83 (3.98)	7.98 (4.10)	8.70 (4.82)	10.27 (4.24)
p-value	0.87		0.23		0.91		0.95		0.57	

Tab. 5.2.2-3 Comparison of gender using the average ROM in the three planes of each segment related to normal walking speed. Those with statistical differences (ANOVA) are indicated with *.

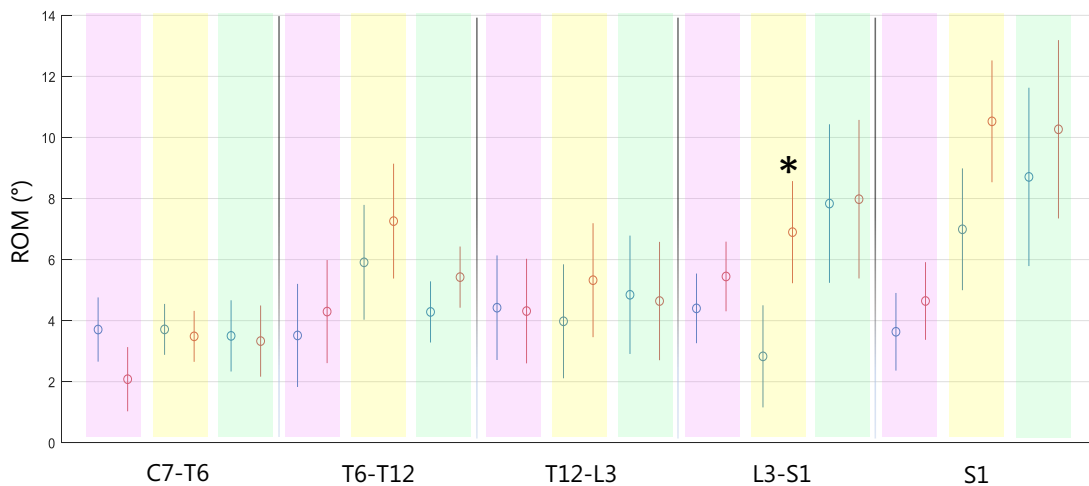


Fig. 5.2.2-7 Comparison of gender using the average ROM in the three planes of each segment related to normal walking speed. Those with statistical differences (ANOVA) are indicated with *. The purple areas identify the sagittal plane, the yellow areas the frontal plane and the green areas the transversal plane. For each area the ROMs of the male group (blue) and the ROMs of the female group (magenta) are reported.

The Fig. 5.2.2-7 and Tab. 5.2.2-3 give similar information obtained from slow waling speed, but the only statistical difference observed is relative to the lower lumbar segment in the frontal plane. In this type of gait, however, the p-value of the thoracic segment in the sagittal plane (p-value= 0.12) is greater than that belonging to slow trial. Another easily visible difference is related to the motion in the frontal plane of T6-T12 segment: the average ROM that characterizes the female gender is greater than that of man.

5.2.3 Walking at comfortable speed

Finally, the walk at comfortable speed selected by the single subject was tested. This is to analyse the movement in its naturalness without being bound to a set speed.

In Figs. 5.2.3-1, 5.2.3-2, 5.2.3-3 are shown the mean patterns of female subjects, while in Tab. 5.2.3-1 ROMs during walking at comfortable walking speed (1.16 m/s mean value) are shown.

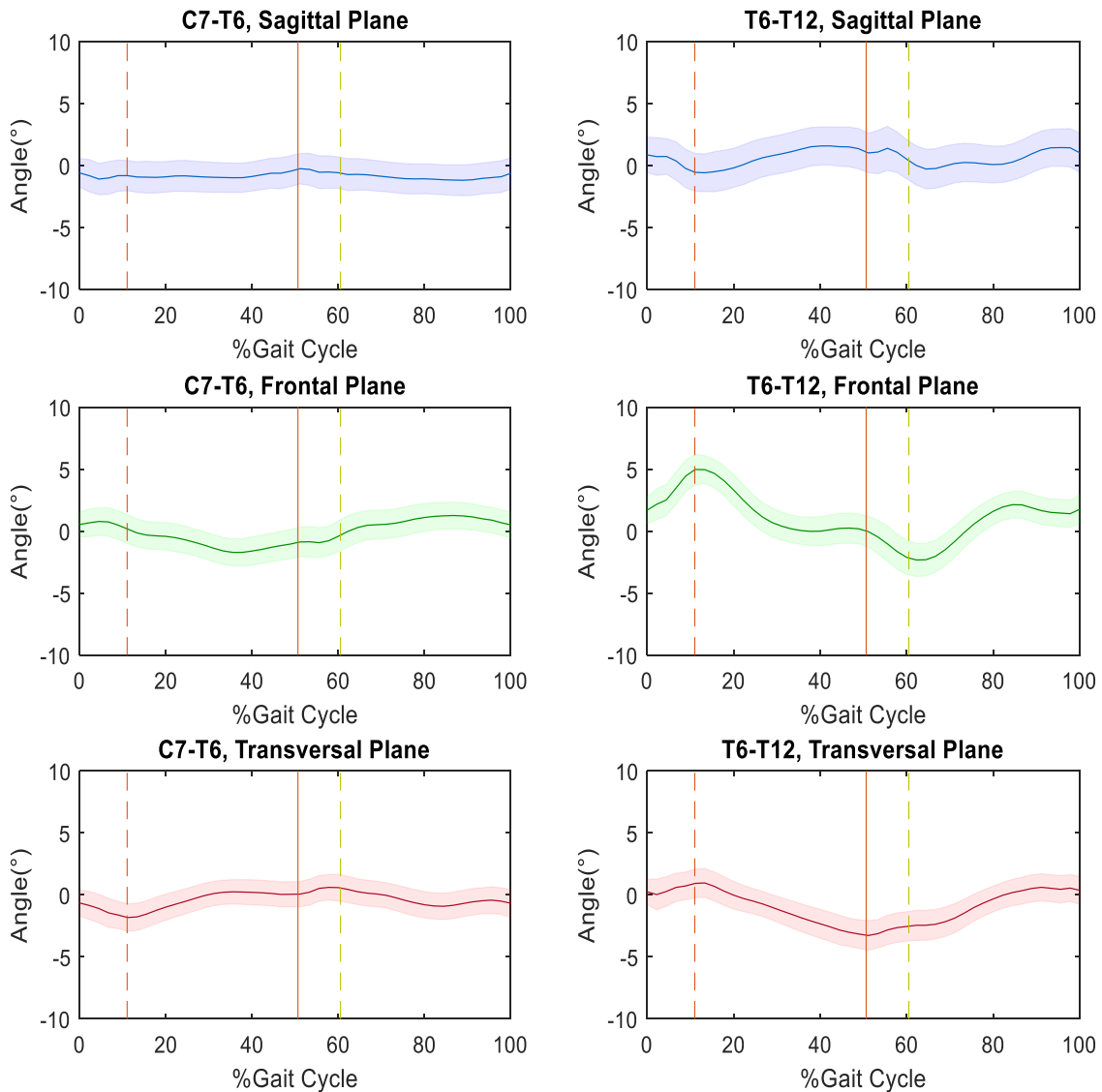


Fig. 5.2.3-5.2-1 Angles patterns of thoracic segments during walking at comfortable speed for female subjects.

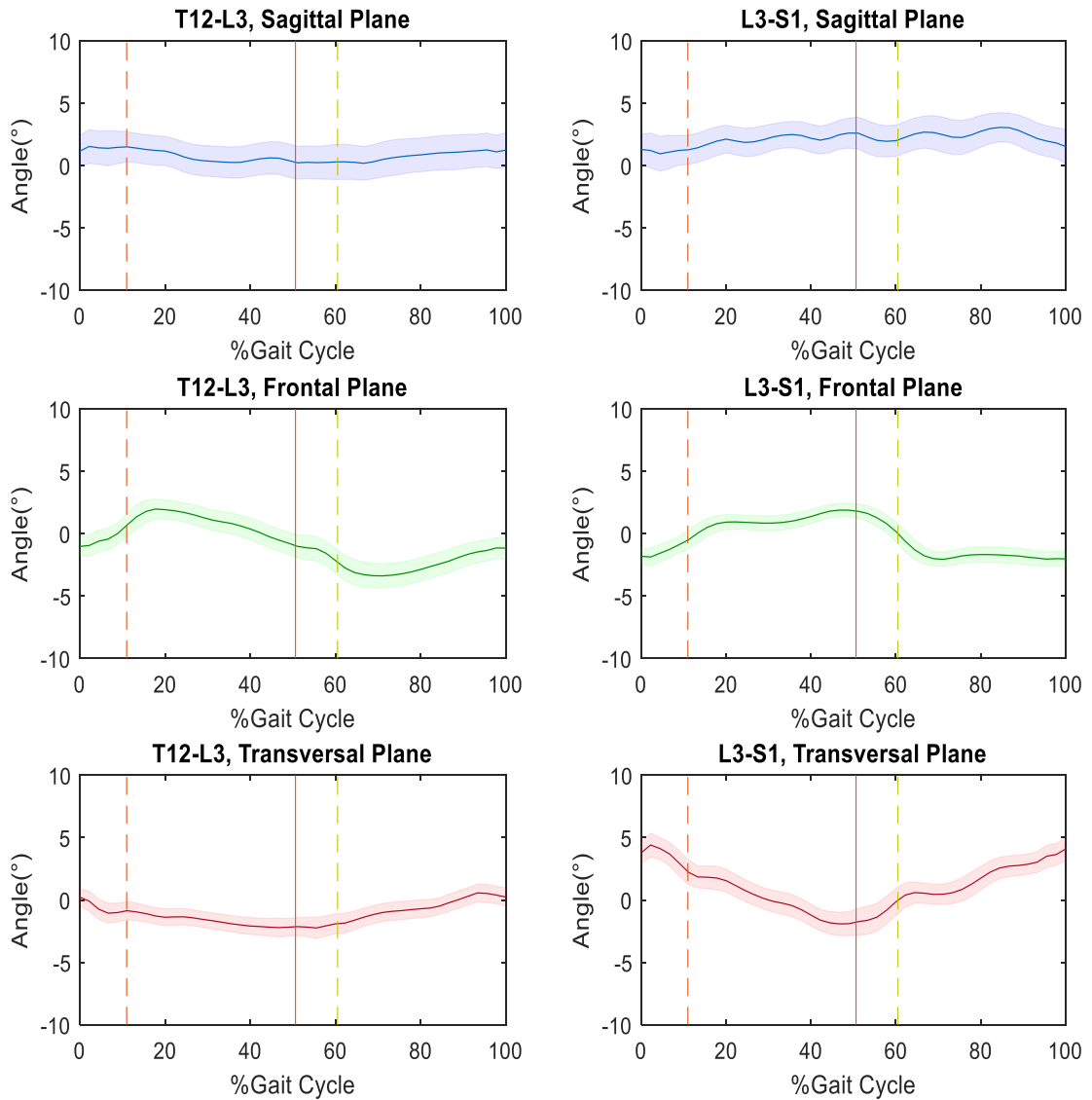


Fig. 5.2.3-5.2-2 Angles patterns of lumbar segments during walking at comfortable speed for female subjects.

	Sagittal Plane		Frontal Plane		Transversal Plane	
	Avg ROM (°)	Avg SD (°)	Avg ROM (°)	Avg SD (°)	Avg ROM (°)	Avg SD (°)
C7-T6	2.16	1.24	3.43	1.60	3.44	1.53
T6-T12	4.23	3.28	7.85	4.22	5.59	1.16
T12-L3	3.92	3.20	5.45	3.80	4.36	3.09
L3-S1	5.19	1.71	6.15	2.80	7.42	3.92
S1	7.17	2.02	10.19	3.41	9.66	4.63

Tab. 5.2.3-1 ROMs (SD) for female subjects during walking at comfortable speed.

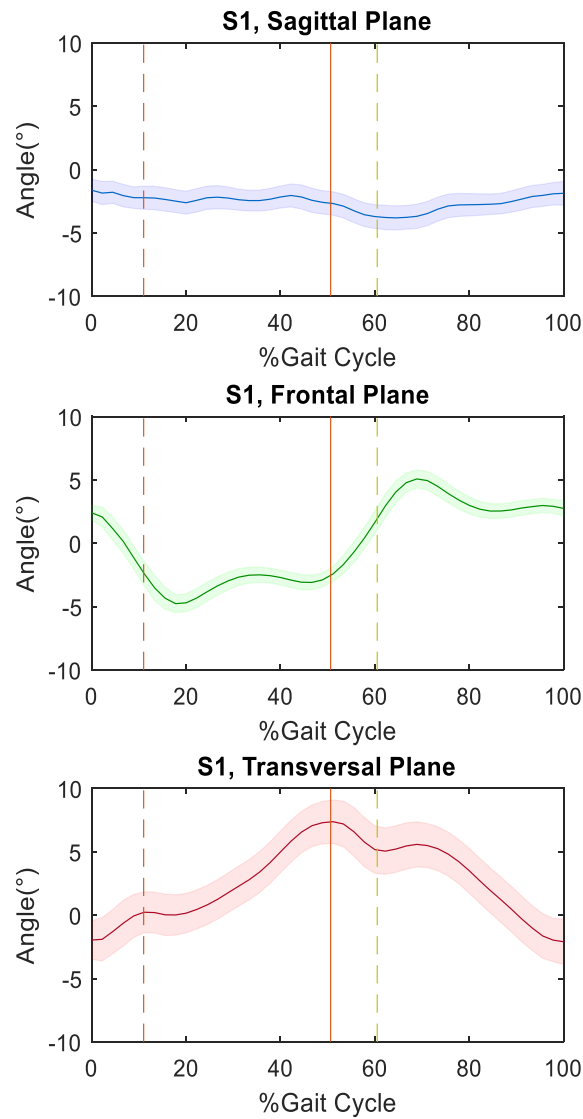


Fig. 5.2.3-3 Angles patterns of lumbar segments during walking at comfortable speed for female subjects.

	Sagittal Plane		Frontal Plane		Transversal Plane	
	Avg ROM (°)	Avg SD (°)	Avg ROM (°)	Avg SD (°)	Avg ROM (°)	Avg SD (°)
C7-T6	3.67	1.63	3.67	0.61	2.81	1.54
T6-T12	3.88	1.61	6.36	1.34	5.10	2.42
T12-L3	4.63	2.30	4.33	2.10	4.00	1.33
L3-S1	5.27	2.32	3.19	1.23	7.45	2.61
S1	3.38	1.18	7.39	2.02	9.55	5.99

Tab. 5.2.3-2 ROMs (SD) for male subjects during walking at comfortable speed.

In Figs. 5.2.3-4, 5.2.3-5, 5.2.3-6 are shown the mean patterns of male subjects, while in Tab. 5.2.3-2 ROMs during walking at comfortable walking speed (1.22 m/s mean value) are shown.

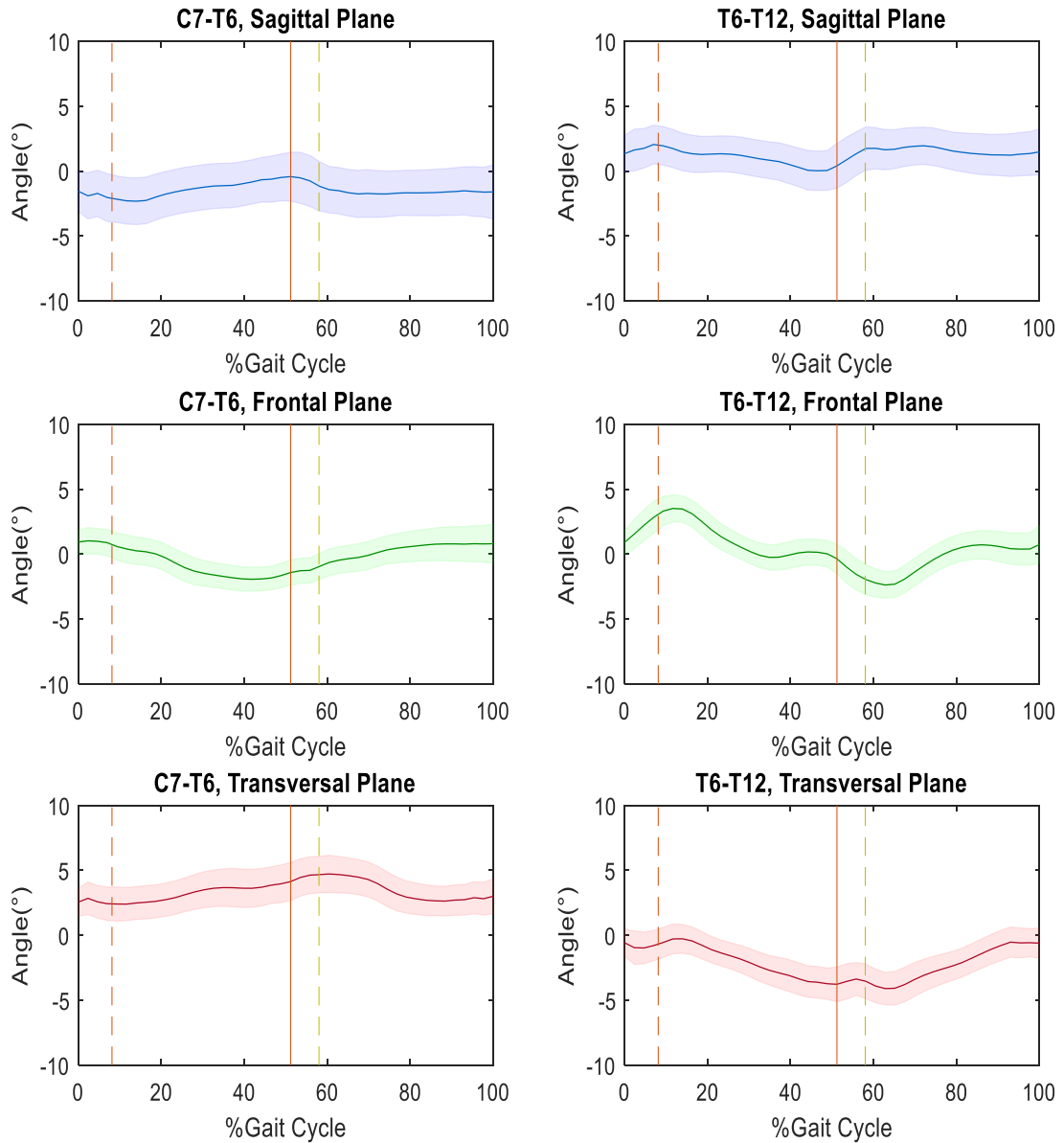


Fig. 5.2.3-3 Angles patterns of thoracic segments during walking at comfortable speed for male subjects.

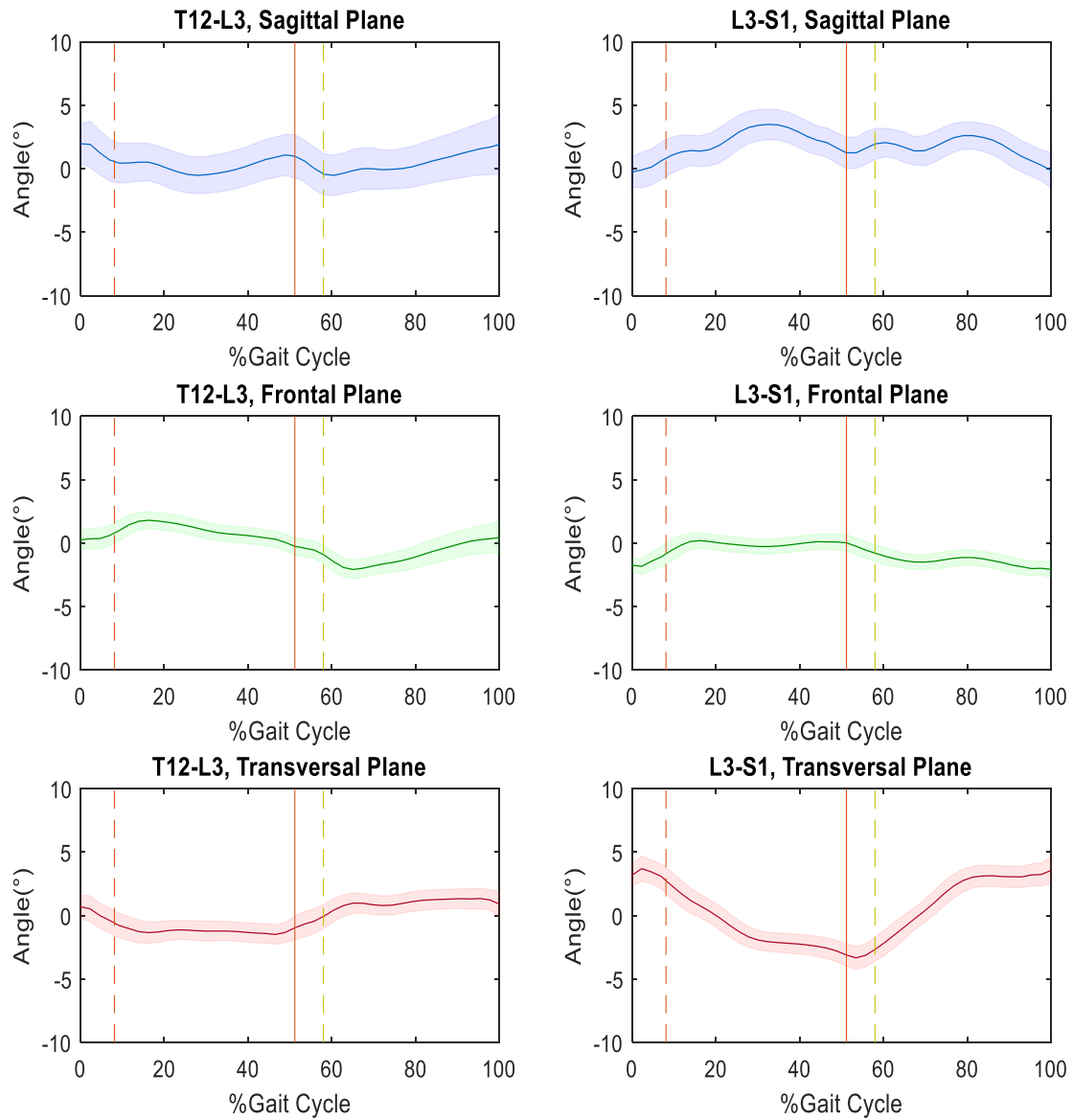


Fig. 5.2.3-4 Angles patterns of lumbar segments during walking at comfortable speed for male subjects.

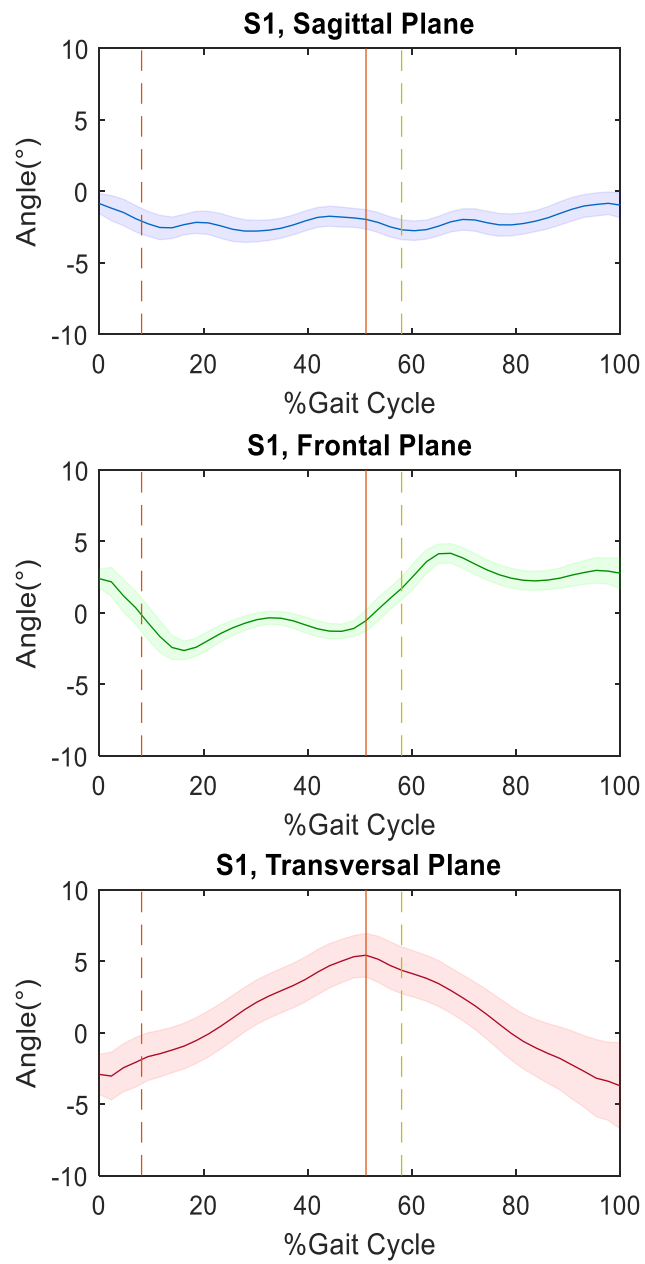


Fig. 5.2.3-5 Angles patterns of pelvis segment during walking at comfortable speed for male subjects.

Segment	C7-T16		T6-T12		T12-L3		L3-S1		S1	
Gender	M	F	M	F	M	F	M	F	M	F
ROM (SD) ^o Sagittal plane	3.64 (1.63)	2.16 (1.24)	3.88 (1.61)	4.23 (3.28)	4.63 (2.30)	3.92 (3.20)	5.27 (2.32)	5.19 (1.71)	3.38 (1.18)	4.17 (2.02)
p-value	0.13		0.84		0.67		0.95		0.43	
ROM (SD) ^o Frontal plane	3.67 (0.61)	3.43 (1.90)	6.36 (1.34)	7.85 (4.22)	4.33 (2.10)	5.45 (3.80)	3.19 (1.23)	6.15 (2.80)	7.39 (1.23)	10.2 (3.41)
p-value	0.73		0.43		0.54		0.04*		0.11	
ROM (SD) ^o Transversal plane	2.81 (1.54)	3.44 (1.53)	5.10 (2.42)	5.59 (1.16)	4.00 (1.33)	4.36 (3.09)	7.45 (2.61)	7.42 (3.92)	9.55 (5.99)	9.66 (4.63)
p-value	0.56		0.65		0.80		0.99		0.97	

Tab. 5.2.3-3 Comparison of gender using the average ROM in the three planes of each segment related to comfortable walking speed. Those with statistical differences (ANOVA) are indicated with *.

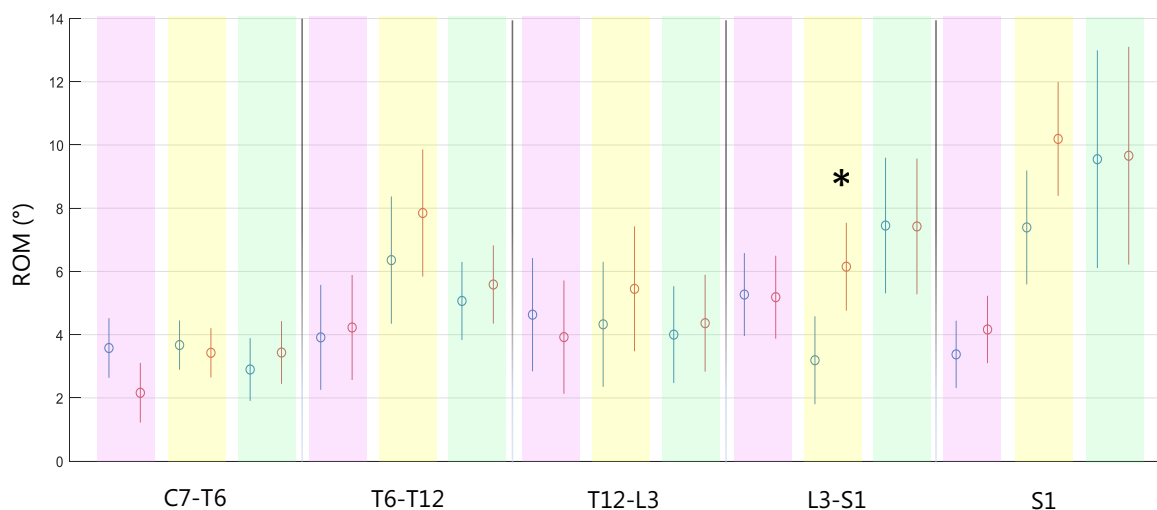


Fig. 5.2.3-6 Comparison of gender using the average ROM in the three planes of each segment related to comfortable walking speed. Those with statistical differences (ANOVA) are indicated with *. The purple areas identify the sagittal plane, the yellow areas the frontal plane and the green areas the transversal plane. For each area the ROMs of the male group (blue) and the ROMs of the female group (magenta) are reported.

In the self-selected speed walking trial, once again, the only statistical difference (data shown in Tab. 5.2.3-3 and Fig. 5.2.3-7) between the spinal segment analysed and the sex of the sample of the subjects is for the L3-S1 segment in the frontal plane. As in the case of walking at normal speed (step frequency equal to 2 steps/s), women show greater movement at all spinal segments and in the frontal plane except for the upper thoracic segment.

5.3 Discussion

During the three different types of gait examined, it appears that the gender effect affects the motion of the lower lumbar region of the spine in the frontal plane, but not in the remaining segments (with the exception of the upper thoracic segment in the sagittal plane during gait with a step frequency set at 1.5 steps/s). It seems that the males are generally more rigid than females, especially at lumbar region and pelvis.

For each group, the differences in the overall motion of each segment obtained under the three different test conditions were evaluated. In the meantime, for neither of the two groups significant differences were found between the three types of path. About Fig. 5.3-1 male subjects during walking at comfortable speed have higher ROM in the pelvis, lower lumbar segment and lower thoracic segment than that obtained in the two testes in which the metronome was used to dictate the step frequency. In the other segments, therefore, in the upper lumbar segment and in the upper thoracic segment, it is the gait at a 2 steps/s that has the highest ROM. According to Crosbie, et al. (1997), an increase in speed should correspond to an increase in ROM that in this case does not occur, and it seems that there is not a well-defined relationship between these two variables. In conclusion, it is possible to say that for males, the walking speed has an effect on the spinal column motion, which is not very marked.

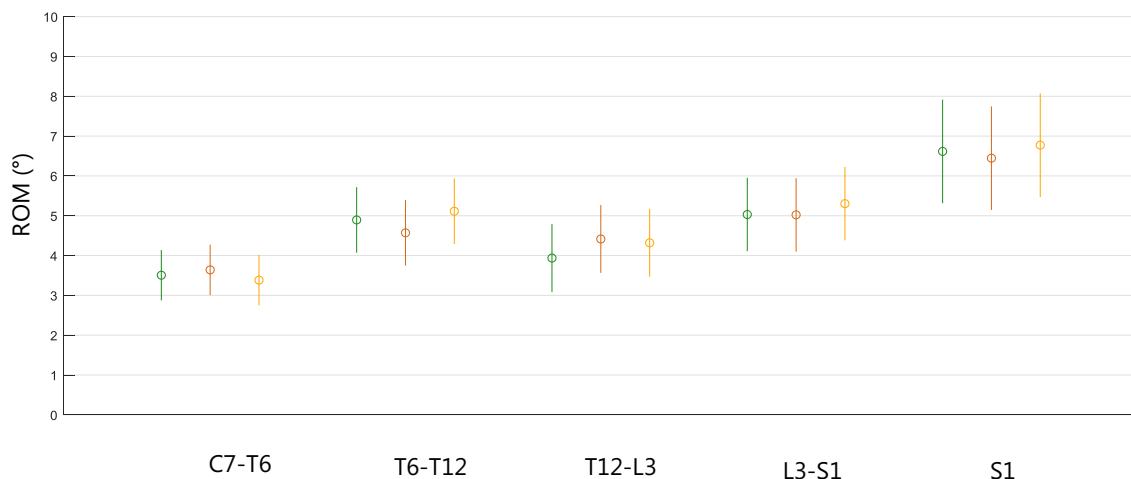


Fig. 5.3-1 Comparison of different gait conditions in male subjects. Those with statistical differences (ANOVA) are indicated with *. The green bars indicate walking at 1.5 steps/s; the red bars represent walking at 2.0 steps/s; the yellow bars represent the walking at comfortable speed.

By observing the Fig. 5.3-2 it is possible to analyse the motion of the spinal segments of the female sex in the different walking conditions tested.

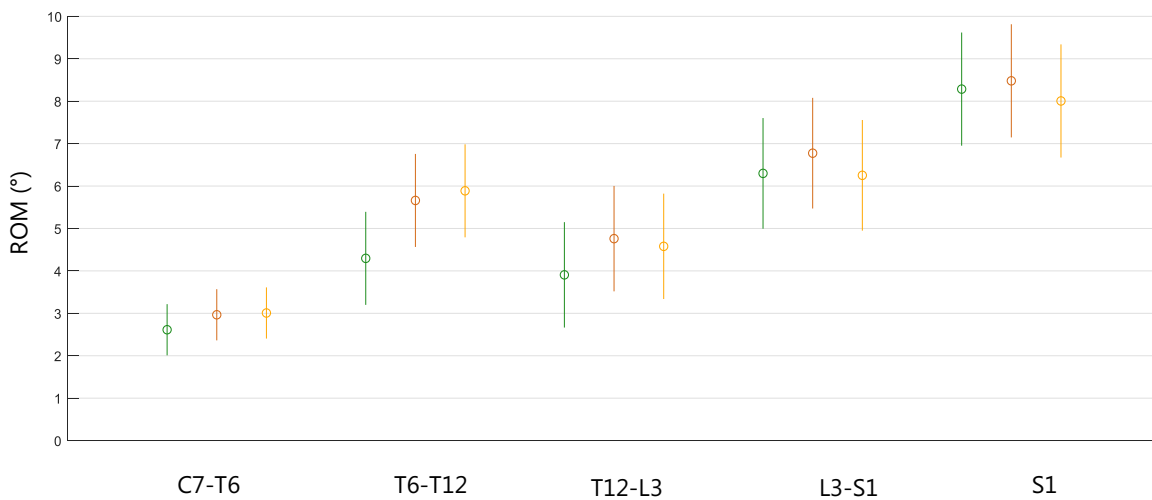


Fig. 5.3-2 Comparison of different gait conditions in female subjects. Those with statistical differences (ANOVA) are indicated with *. The green bars indicate walking at 1.5 steps/s; the red bars represent walking at 2.0 steps/s; the yellow bars represent the walking at comfortable speed.

In group composed of female subjects, the segment most affect by speed variation is the T6-T12 (p-value= 0.17). In addition, regarding this segment and C7-T6 segment, the 2 steps/s cadence does not show the greatest overall movement compared to the other speeds tested. In fact, this is used for walking at self-selected speed. Apart from this, it can be said that at low speed walking there is a movement of all lower segments except for the L3-S1 and pelvis segments. Here it is the self-selected speed gait that has the least motion.

The purpose of this thesis was to investigate the kinematics of the spine during walk using inertial sensors. This, from the bibliographic analysis conducted, does not seem to have been investigated by other authors, who were mainly interested in testing inertial systems in elementary movements such as flexion-extension, lateral bending and axial rotation, or other movements not of interest in this thesis. Furthermore, with the approach adopted, the relative motion between two adjacent and consecutive spine segments was investigated and not their absolute motion.

Since the spine represents a complex structure made up of many small joints, its representation with motion capture system is rather complicated. Therefore, based on the various segmentations found in the literature and medical knowledge, a compromise was found between the complexity of spine representation and the number of sensors that can be positioned taking into account their numerical availability and the size by which they are characterized. The developed model is composed by four spine segments, separating the thoracic and lumbar

regions, plus the pelvis described by a three-dimensional motion. More in detail, the aim is to analyse the various parts of the trunk in helping to maintain balance during locomotion.

The results obtained from the tests carried out on healthy subjects were compared with those obtained in the literature. Comparisons were made trying to associate the results of groups with similar characteristics. For example, in Leardini, et al. (2011), were shown the patterns of the entire sample of 5 males and 5 females, but also those of a single male subject (25 years, height 173 cm, mass 63 kg, BMI 21.0 kg/m²). The first comparison concerns precisely the patterns of the single subject with one of the sample recruited in this work. In this regard, a male subject was chosen whose anthropometric characteristics were similar to those of the subject described in Leardini, et al. (2011): 25 years, height 174 cm, mass 70 kg, BMI 23.1 kg/m².

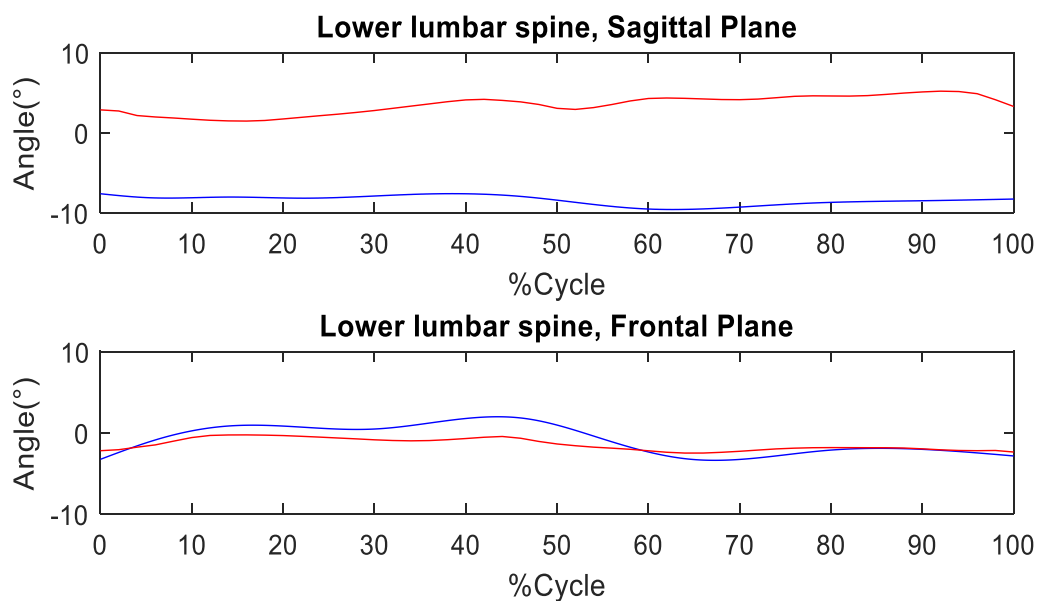


Fig. 5.3-3 Pattern of the lower lumbar segment in the sagittal and frontal plane of a single subject: in red is represented the trend of the thesis subject (comfortable walking speed) and in blue is represented the trend of the subject recruited in Leardini, et al. (2011).

In Fig. 5.3-3 it results that in the frontal plane the two subjects have a very different trend. In fact, between the two there is a shift of about 10°. The ROM between the two deviates by 0.84° (Leardini 2.9°, Thesis 3.74°). In the frontal plane it is possible to recognize more or less the same trend even if in Leardini the average ROM is 5.5° while in Thesis it is 2.24°.

In Fig. 5.3-4 the trends as in the previous case are quite different. In the sagittal plane it results that the thesis subject has a pattern that oscillates around zero value while Leardini subject has a trend that oscillates around a negative value. The average ROMs deviate by about 1.5° with a higher value in the Thesis subject. Also in the frontal plane the patterns differ and this could also be due to a different positioning of the markers/sensors. In fact, even though the motion is

described more or less in the same way, it is possible that the landmarks are not perfectly coincident and that therefore they are expressed in a different pattern.

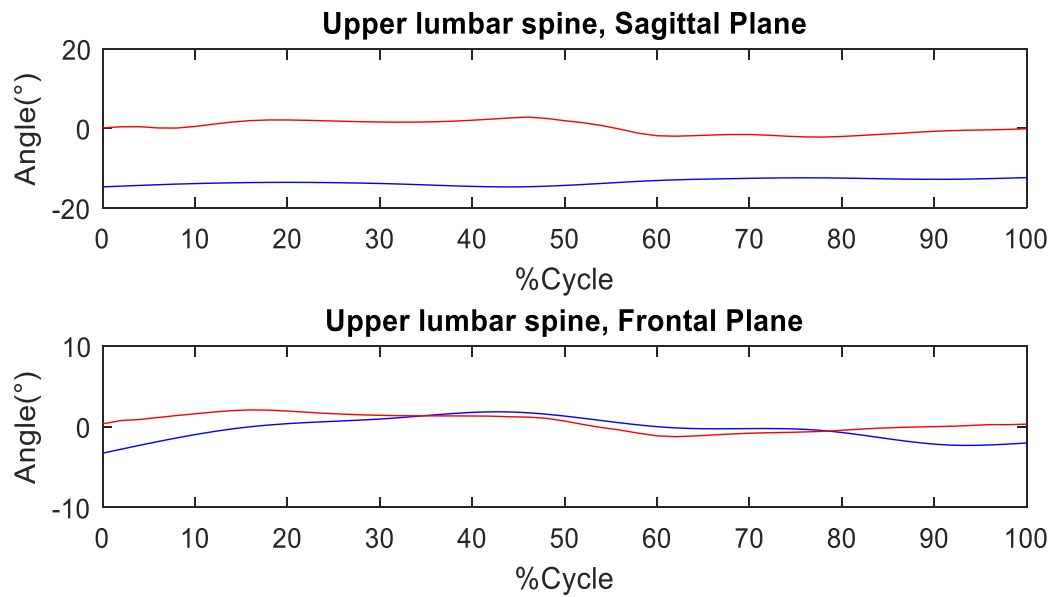


Fig. 5.3-4 Pattern of the upper lumbar segment in the sagittal and frontal plane of a single subject: in red is represented the trend of the thesis subject (comfortable walking speed) and in blue is represented the trend of the subject recruited in Leardini, et al. (2011).

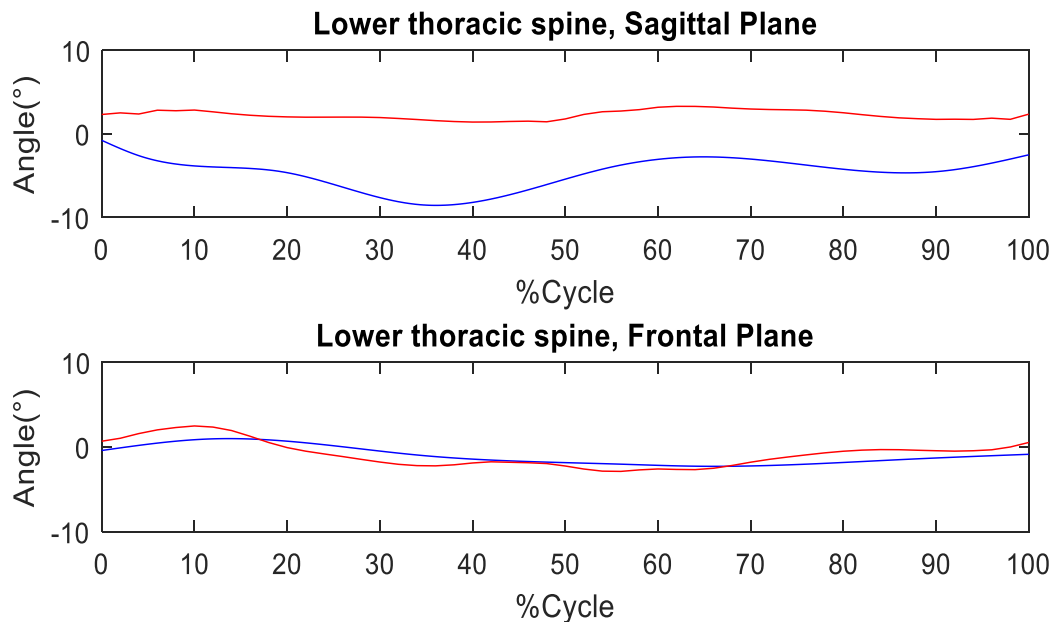


Fig. 5.3-5 Pattern of the lower thoracic segment in the sagittal and frontal plane of a single subject: in red is represented the trend of the thesis subject (comfortable walking speed) and in blue is represented the trend of the subject recruited in Leardini, et al. (2011).

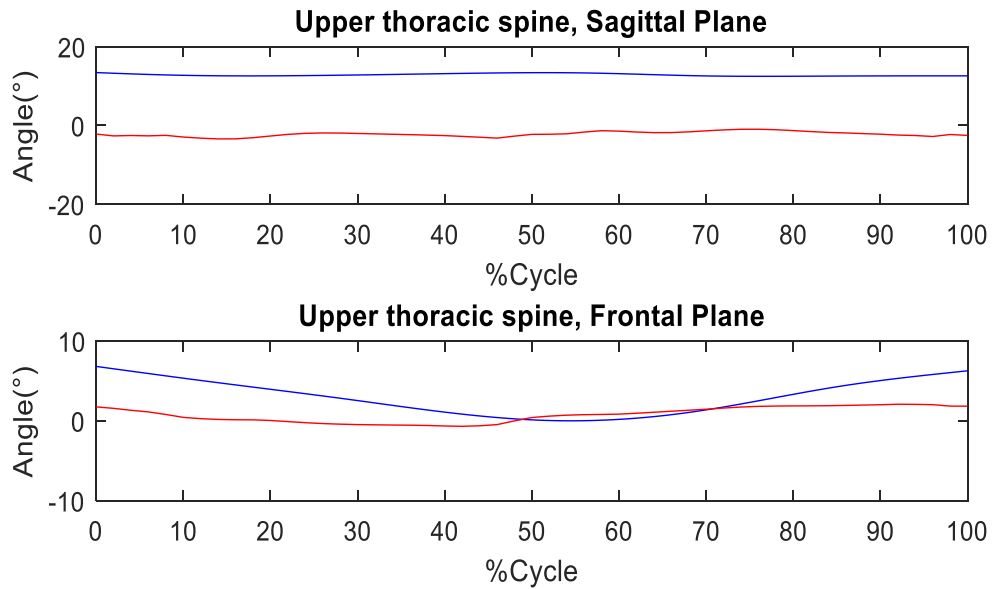


Fig. 5.3-6 Pattern of the upper thoracic segment in the sagittal and frontal plane of a single subject: in red is represented the trend of the thesis subject (comfortable walking speed) and in blue is represented the trend of the subject recruited in Leardini, et al. (2011).

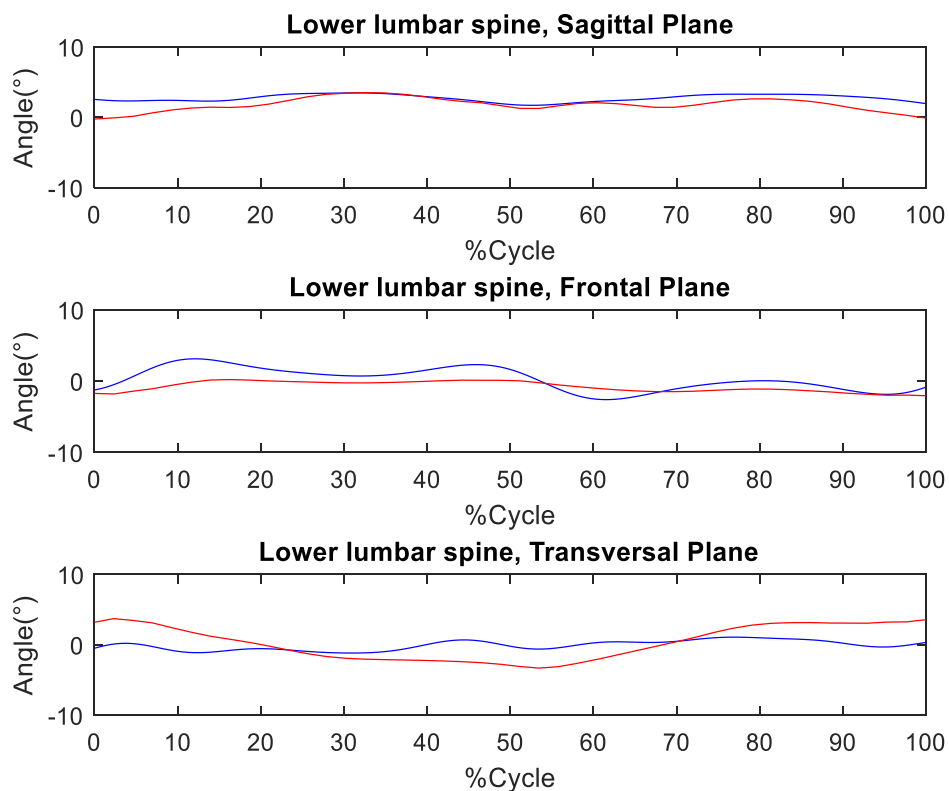


Fig. 5.3-7 Pattern of the lower lumbar segment in the sagittal, frontal and transverse plane. In red is represented the trend of the thesis male subjects (comfortable walking speed) and in blue is represented the trend of the subjects recruited in Needham, et al. (2015).

Figs. 5.3-5 and 5.3-6 show the trends of the thoracic segments. Unlike what happened for the description of the lumbar zone, here the landmarks used in the two approaches are different. In

this thesis, to represent the lower thoracic segment, the sensor was placed on T6 while in Leardini the landmark was at the T8/T9 vertebra. Also in the case of the upper thoracic segment, there are different landmarks: C7 for the thesis model and T2 for the model developed in Leardini, et al. (2011).

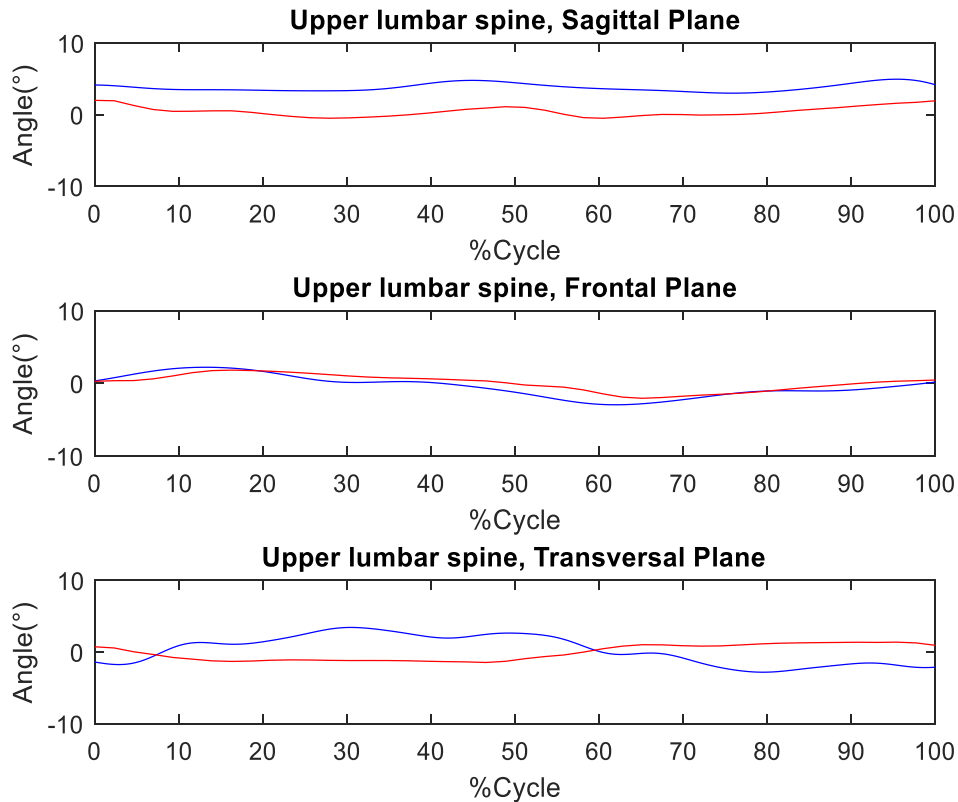


Fig. 5.3-8 Pattern of the upper lumbar segment in the sagittal, frontal and transverse plane. In red is represented the trend of the thesis male subjects (comfortable walking speed) and in blue is represented the trend of the subjects recruited in Needham, et al. (2015).

In Needham, et al. (2015) the sample of subjects was composed by ten males. For this reason, the average pattern of these was compared with the average pattern of the six males recruited in the thesis. It is possible to compare the patterns of the lower lumbar segment in three planes (Fig. 5.3-7) and that of the upper lumbar segment (Fig. 5.3-8). In the latter case, in Needham the motion is described between the T8 and L3 vertebrae, while in the thesis it is described between T12 and L3. The patterns of the lower lumbar segment in the sagittal plane seem to coincide at multiple points even if complete overlap is not reached. More marked differences in this plane occur at the beginning and end of the gait cycle (HS right foot). The patterns in the frontal plane have the same profile but in Needham the average ROM reached is 6.50° while in the thesis it is 3.19° . In the transversal plane, the profiles are very different. For the upper lumbar segment in the sagittal plane the two testes report approximately the same profile even if there is a shift of about 3° . In the frontal plane the patterns are rather superimposed even if in

the one relative to the thesis the lateral flexion peaks are slightly postponed. This is probably dictated by a different landmark: it would seem that the vertebral level higher up T8 flexes temporally before the vertebra T6 and this is in agreement with Ceccato, et al. (2009) that the curvature originates from a top-down approach.

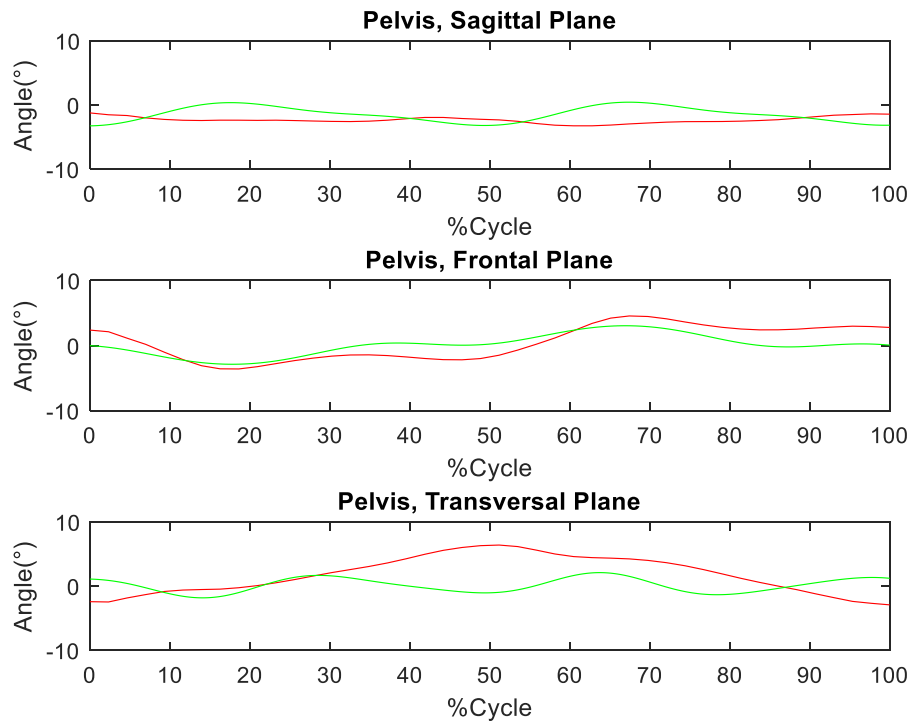


Fig. 5.3-9 Pattern of the Pelvis segment in the sagittal, frontal and transverse. In red is represented the trend of the thesis subjects (comfortable walking speed) and in green is represented the trend of the subjects recruited in Crosbie, et al. (1997).

The last comparison was made between the entire sample of subjects, then both males and females, recruited to obtain patterns in this work and the mixed sample of Crosbie, et al. (1997) and Leardini, et al. (2011) works. The comparison on pelvic patterns (Fig. 5.3-9) can only be done considering the work of Crosbie, et al. (1997) in which 50 male and 58 female subjects with an average age of about 45 years old were recruited. In the sagittal plane and in the transverse plane the patterns differ from each other, but in the frontal plane some similarities can be accepted. In fact, the lateral peaks on the right and left correspond to the same percentages of gait cycle: at about 15% there is the lateral flexion peak on the left and at about 65% there is the flexion peak on the right.

Examining the patterns of the lower lumbar segment (Fig. 5.3-10) in the frontal plane it is possible to notice that this time the patterns obtained by the 10 subjects (5 males and 5 females) in the study of Leardini, et al. (2011) and by the 12 subjects (6 males and 6 females) recruited in this thesis have more or less the same trend. The average ROMs differ by about 2° (6.7° in

Leardini and 4.67° in Thesis). The motion trend found in Crosbie's work appears different also because the movement is described in different way from the previous. Crosbie, et al. (1997) in fact defines the lumbar segment between T12 and L5.

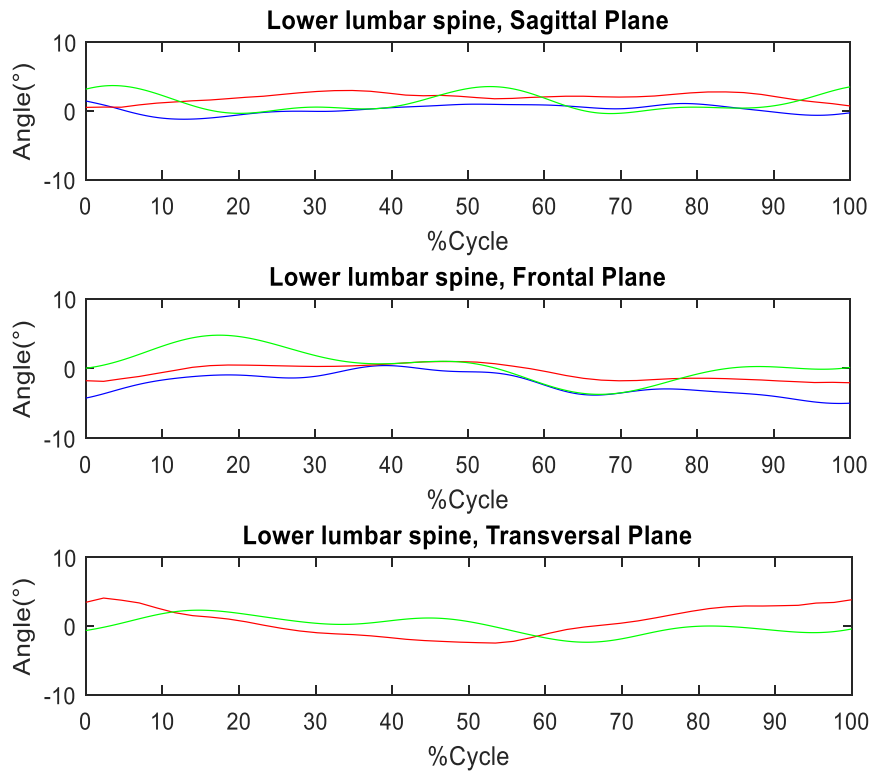


Fig. 5.3-10 Pattern of the lower lumbar segment in the sagittal, frontal and transverse. In red is represented the trend of the thesis subjects (comfortable walking speed), in green is represented the trend of the subjects recruited in Crosbie, et al. (1997) and in blue the pattern of subjects recruited in Leardini, et al. (2011).

In Fig. 3.5-11 are shown the comparisons in the three anatomical planes of the upper lumbar segment obtained in three works. This time in the frontal plane there are fewer similarities between the pattern obtained from Leardini's work and the pattern obtained in this thesis. In Fig. 3.5-12 instead is represented the trend of the lower thoracic segment that for the present work is defined between T6 and T12, while Leardini's segment between T8/T9 and L1 and in Crosbie's segment between T6 and T12. Only the Crosbie pattern is slightly shifted to the right, probably due to the different definition of the adopted motion. In the remaining two, peaks are at the same phases of gait cycle. The average ROM found in Leardini is equal to 4.4° while in the present study it is equal to 7.1° .

In Fig. 5.3-13 is possible to observe the comparison between the patterns of the upper thoracic segment. In the sagittal plane both patterns present few oscillations. In addition, the shift between the two is evident. Even if the frontal plane there are no relevant similarities. This diversity can be associated once again with the different segment definition. In fact, Leardini

defines an upper thoracic segment from T2 to T8/T9 while in the present thesis the segment extends from C7 to T6.

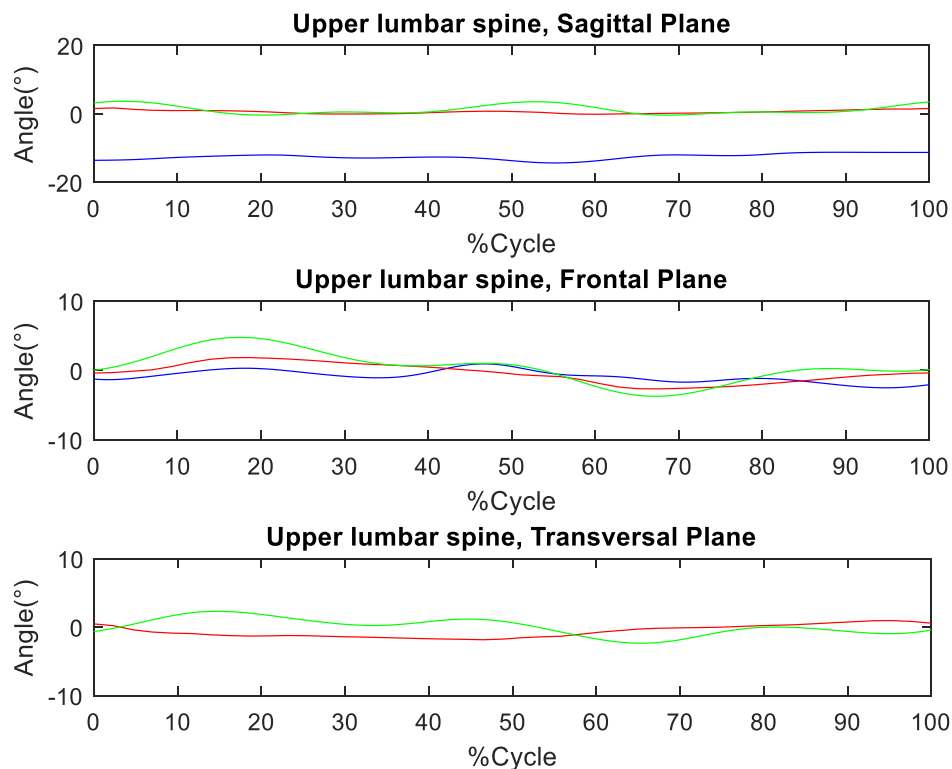


Fig. 5.3-11 Pattern of the upper lumbar segment in the sagittal, frontal and transverse. In red is represented the trend of the thesis subjects (comfortable walking speed), in green is represented the trend of the subjects recruited in Crosbie, et al. (1997) and in blue the pattern of subjects recruited in Leardini, et al. (2011).

From the comparisons made with the trends of the spinal segments found in literature in relation to locomotion, it appears that few similarities can be found. Surely, in some cases, the most agreeable patterns are found in the frontal plane. The differences are due to several factors, first of all the different motion capture system (inertial sensor system and optoelectronic system). Other possible divergences can be hidden in the variability of the landmarks between one study and another, in the age of the subjects and also in the speed. This in fact influences the trends of the angular kinematics of the column, but in Leardini's study this information is not reported.

Gathering more information, then applying this spinal segmentation model to more subjects, could create a basis of measurements on which to determine how the various segments contribute to the complete trunk motion. They could also be a reference on which to establish and quantify the impairment of an unhealthy subject. In fact, the model could be applied in the neurological field, for example in verifying trunk control in Parkinsonian subjects, in the orthopaedic field and in rehabilitation. It is important to underline that a modification of the

trunk mass distribution affects the gait patterns, that is to say that a change in the trunk inclination disturbs its kinematics.

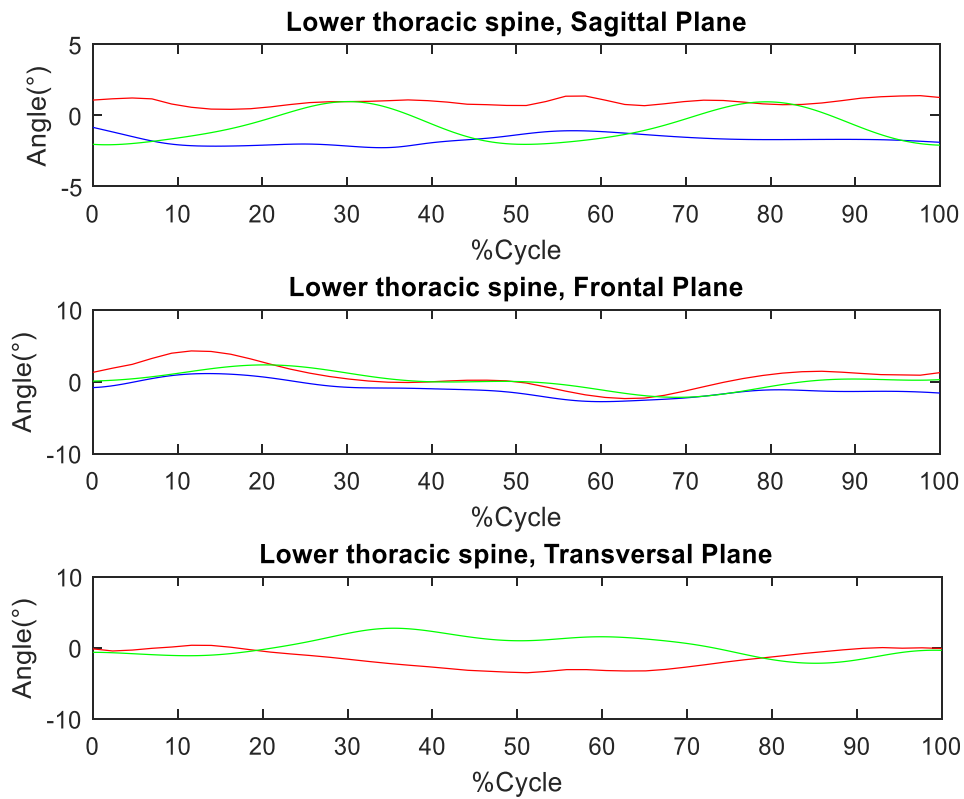


Fig. 5.3-12 Pattern of the lower thoracic segment in the sagittal, frontal and transverse. In red is represented the trend of the thesis subjects (comfortable walking speed), in green is represented the trend of the subjects recruited in Crosbie, et al. (1997) and in blue the pattern of subjects recruited in Leardini, et al. (2011).

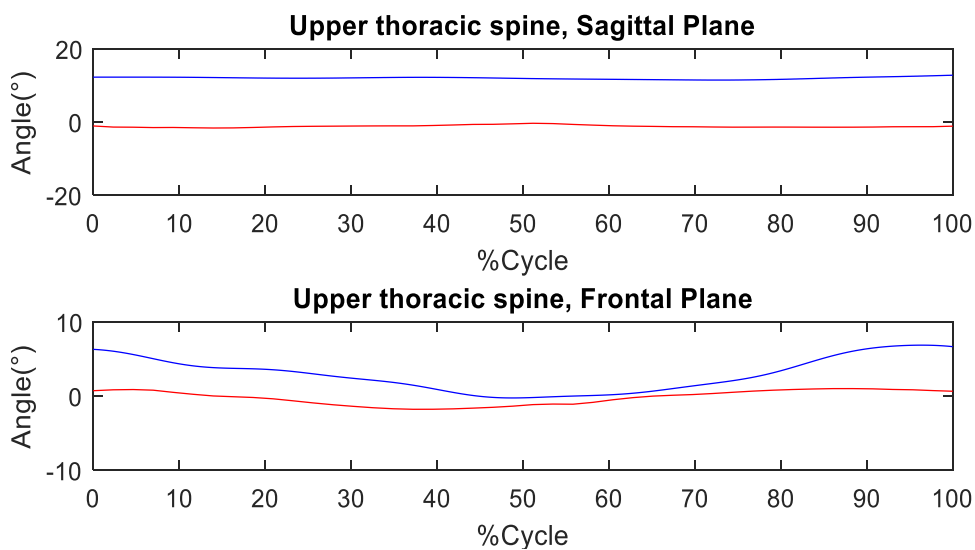


Fig. 5.3-13 Pattern of the upper thoracic segment in the sagittal, frontal and transverse. In red is represented the trend of the thesis subjects (comfortable walking speed), in blue the pattern of subjects recruited in Leardini, et al. (2011).

References

- Alqhtani, R.S., et al. 2016.** Investigation the contribution of the upper and lower lumbar spine, relative to hip motion, in everyday tasks. *Manual Therapy*. 2016, Vol. 21, 268-273.
- . **2015.** Reliability of an accelerometer-based system for quantifying multiregional spinal range of motion. *Journal of Manipulative and Physiological Therapeutics*. 2015, Vol. 38, 4.
- Asher, Anna. 2018.** Anatomy of the Ligaments in the Spine. *verywellhealth*. [Online] 14 October 2018. <https://www.verywellhealth.com/spinal-ligament-anatomy-296462>.
- Bauer, C.M., et al. 2015.** Concurrent validity and reliability of a novel wireless inertial measurement system to assess trunk movement. *Journal of Electromyography and Kinesiology*. 2015, Vol. 25, 782-790.
- Brindwell, K. M. and Dewald, R. L. 1997.** *The textbook of spinal surgery*. Philadelphia : Lippincott-Raven, 1997.
- Cafolla, D., Chen, I-M. and Ceccarelli, M. 2015.** An experimental characterization of human torso motion. *Front. Mech: Eng*. 2015, Vol. 10 (4), 311-325.
- Calais-German, B. 1991.** *The Anatomy of Movement*. Seattle : Eastland Press, 1991.
- Ceccato, J.C., et al. 2009.** Comparison of trunk activity during gait initiation and walking in humans. *PLoS ONE*. 2009, Vol. 4 (12).
- Comparison of Different Motion Capture Setups for Gait Analysis Validation of spatio-temporal parameters estimation. Panero, E., et al. 2018.* 2018.
- Crawford, N.R., Yamaguchi, G.T., Dickman, C.A. 1999.** A new technique for determining 3D joint angles: tilt/twist method. *Clinical Biomechanics*. 1999, Vol. 14, 153-165.
- Crosbie, J., Vachalathiti, R. and Smith, R. 1997.** Age, gender and speed effects on spinal kinematics during walking. *Gait & Posture*. 1997, Vol. 5, 13-20.
- . **1997.** Patterns of spinal motion during walking. *Gait & Posture*. 1997, Vol. 5, 6-12.
- Cyron, B. M., Hutton, W. C., and Stott, J.R. 1979.** Spodylolyis: the shearing stiffness of the lumbar intervertebral joint. *Acta Orthop Belg*. 1979, Vol. 45 (4), 459-469.
- El Fagoun, A.B., Schwab, F., Gamez, L., Champain, N., Skalli, W., and Farcy, J.P. 2005.** Center of gravity and radiographic posture analysis: a preliminary review of adult volunteers and adult patients affected by scoliosis. *Spine*. 2005, Vol. 30 (13), 1535-1540.
- Friego, C., et al. 2003.** The upper body segmental movements during walking by young females. *Clinical Biomechanics*. 2003, Vol. 18, 419-425.
- Goodvin, C., et al. 2006.** Development of a real-time three-dimensional spinal motion measurement system for clinical practice. *Med Bio Eng Comput*. 2006, Vol. 44, 1061-1075.
- Hajibozorgi, M. and Arjmand, N. 2016.** Sagittal range of motion of the thoracic spine using inertial tracking device and effect of measurement errors on model predictions. *Journal of Biomechanics*. 2016, Vol. 49, 913-918.

- Jacquelin, Perry. 1992.** *Gait Analysis Normal and Pathological Function.* 1992.
- Leardini, A., et al. 2011.** Multi-segment trunk kinematics during locomotion and elementary exercises. *Clinical Biomechanics.* 2011, Vol. 26, 562-571.
- Magee, D.J. 1987.** *Orthopedic Physical Assessment.* Philadelphia : W.B.Saunders Company, 1987.
- Maslivec, A., et al. 2018.** Mechanisms of head stability during gait initiation in young and older women: a neuro-mechanical analysis. *Journal of Electromyography and Kinesiology.* 2018.
- Mow, V.C., Hayes, Wilson C. 1991.** *Basic Orthopedic Biomechanics.* New York : Raven Press, 1991.
- Needham, R., et al. 2015.** Multi-segment kinematic model to assess three-dimensional movement of the spine and back during gait. *Prosthetics and Orthotics International.* 2015, 1-12.
- Öberg, T., Karsiznia, A., Öberg, k. 1993.** Basic gait parameters: Reference data for normal subjects, 10-79 years of age. *Journal of Rehabilitation Research and Development.* 1993, Vol. 30, 2, 210-223.
- Pope, M. H. 1991.** *Occupational low back pain: assessment, treatment, and prevention.* St. Louis : Mosby Year Book, 1991.
- Quantitative assessment of the motion of the lumbar spine and pelvis with wearable inertial sensors.* **Chhikara, A., et al. 2010.** 2010. International Conference on Body Sensor Networks.
- Real-time representation of the human spine with absolute orientation sensors.* **Antonya, C., Butnariu, S. and Ponza, C. 2016.** Phuket, Thailand : s.n., 2016. 14th International Conference on Control, Automation, Robotics & Vision.
- Rozumalski, A., et al. 2008.** The in vivo three-dimensional motion of the human lumbar spine during gait. *Gait & Posture.* 2008.
- Schall, M.C. Jr, et al. 2015.** A comparison of instrumentation methods to estimate thoracolumbar motion in field-based occupational studies. *Applied Ergonomics.* 2015, Vol. 48, 224-231.
- Schwab, F., Lafage, V., Boyce, R., Skalli, W., and Farcy, J.P. 2006.** Gravity line analysis in adult volunteers: age-related correlation with spinal parameters, pelvic parameters, and foot position. *Spine.* 2006, Vol. 31 (25), E959-967.
- Syczewska, M., Oberg, T. and Karlsson, D. 1999.** Segmental movements of the spine during treadmill walking with normal speed. *Clinica Biomechanics.* 1999, Vol. 14, 384-388.
- Todd, D. T. 1997.** *A comprehensive investigation of an artificial intervertebral disc from the lumbar spine in the sagittal plane.* Iowa City : Unpublished Master's Thesis, The University of Iowa, 1997.
- Voloshin, A., and Worsk, J. 1982.** An in vivo study of low back pain and shock absorption in the human locomotor system. *J Biomech.* 1982, Vol. 15 (1), 21-27.

White, A. A., 3rd and Panjabi, M. M. 1978. The basic kinematics of the human spine. A review of past and current knowledge. *Spine*. 1978, Vol. 3 (1), 12-20.

Wong, W.Y. and Wong, M.S. 2008. Trunk posture monitoring with inertial sensors. *Eur Spine J*. 2008.

Xsens. 2000. [Online] 2000. <https://www.xsens.com/fascination-motion-capture/>.

—. XM-B User Manual.

Ringraziamenti

Le persone da ringraziare sono molteplici, chi per un motivo, chi per un altro. Inizio con la parte accademica e quindi ringrazio la professoressa Laura Gastaldi per l'argomento assegnatomi, per avermi fatto scoprire quanto lavoro, quanta dedizione e quanti espedienti si celino dietro una sperimentazione. Un immenso "Grazie" va ad Elisa Digo per essere stata sempre presente, per avermi aiutata quando ogni mio piccolo dubbio mi attanagliava, per aver avuto la pazienza di risolvere assieme qualsiasi problema presentatosi, non in ultimo per essersi prestata a farmi da cavia. A questo proposito sono veramente grata a tutte le persone, amici, conoscenti e non, che hanno accettato di prendere parte alla tesi mettendo a disposizione il proprio corpo per il bene della scienza, o meglio, per essersi fatti intenerire dai miei "Per favore, per favore!". C'è chi lo ha fatto una sola volta e chi molteplici volte come Betty, ma soprattutto Nunzia, togliendo del tempo ai loro impegni qualsiasi essi fossero.

Ringrazio le nuove e le amicizie storiche per avermi distolto dai preoccupanti momenti di stallo, chi come Olga con la scoperta di nuovi mercatini o con i vecchi Spritz di "Carmen", chi come Arkida con i caffè e le cene. Tutti voi avete saputo rassicurarmi con un "Ma vedrai che si risolve tutto", e siete stati partecipi dei miei passi avanti.

Grazie Marisa per essere un porto sicuro, per il tuo senso di unione e per aver sborsato ogni volta per due. C'era un gioco che facevamo da piccole: per ogni bacio che mi davi, io dovevo restituirte. Per fortuna adesso non ho più quel senso del dovere così marcato, ma un giorno, e dico uno, per la tua gioia, mi sentirai dire "Lascia, pago io". Ringrazio Giovanni per le cassette colme di verdura che hanno salvato i periodi di carestia di questi anni da fuori sede. Michelona, io ti ringrazio per la tua sopportazione quando divento appositamente infantile per fare il carico di affetto prima di andarmene via e ritrovarti poi sempre più cresciuta.

Grazie mamma e papà per avermi permesso con il vostro sostegno economico, con non poche difficoltà, di andare via, andare lontano da quella che è la realtà del nostro paese. Ogni chilometro che mettevo tra di noi sembrava trasformarsi in un pizzico di libertà in più, libertà che comunque non mi avete mai negato, ma che ad un certo punto sembrava non bastarmi. Sono sempre stata taciturna con voi, a volte mi infastidivo per niente. Così come è successo con Michelona, la distanza è stato il punto cardine della mia apertura verso di voi e ogni anno che passa crescono in me le tipiche preoccupazioni della figlia lontana. Spero di avervi reso fieri finora, ma soprattutto spero che i nostri sacrifici, seppur differenti, abbiano un risvolto positivo.

Mi scuso con tutti quelli che hanno dovuto leggere tutte queste frasi a volte melanconiche, ma non potevo lasciarmi sfuggire un'occasione come questa. Ringrazio infine tutti quelli che sono fisicamente qui a festeggiare con me questo giorno memorabile e tutti quelli che lo sono almeno con il pensiero.

Vi voglio bene tutti!